NANCY Université – Institut National Polytechnique de Lorraine

Ecole Doctorale « Informatique –Automatique – Electrotechnique – Electronique – Mathématiques »
Département de Formation Doctorale « Electrotechnique– Electronique »

THESE

Présentée à

L'Institut National Polytechnique de Lorraine

En vue de l'obtention du titre de

DOCTEUR de l'INPL
Spécialité : Génie Electrique

par

Panarit SETHAKUL

Ingénieur de l'Université de Wuppertal (Allemagne)

RESEAUX ELECTRIQUES ET FILTRAGE DES HARMONIQUES MISE EN ŒUVRE ET METHODE D'ETUDE

Soutenue publiquement le 13 novembre 2009 devant la commission d'examen

Membres du Jury :

Président :	LOUIS Jean-Paul
Rapporteurs :	FAUCHER Jean
	MACHMOUM Mohamed
Examinateurs :	DAVAT Bernard
	MEIBODY-TABAR Farid

Thèse préparée au Groupe de Recherche en Electronique et Electrotechnique de Nancy

Préambule

Ce document présente une partie des travaux de recherche que nous avons réalisés dans le cadre de l'Institut d'Innovation Franco-Taïlandais (IIFT ou plus communément TFII pour Thai-French Innovation Institute).

Existant depuis 1990, cet institut comprend plusieurs départements (Corrosion, Energie, Métrologie, Productique, Soudure, Technologies électronique et électrique) collaborant chacun avec un ou plusieurs centres techniques ou universités et plusieurs industriels.

Pour le département des Technologies électronique et électrique, c'est l'Institut National Polytechnique de Lorraine (INPL) qui depuis une dizaine d'années nous apporte une aide en parallèle avec le support d'industriels comme Schneider Thailand Limited.

La collaboration avec l'INPL a permis au travers d'un Programme d'Action Intégré (PAI France-Thaïlande 2003-2005) du Ministère des Affaires Etrangères français et de son homologue thaïlandais de développer la formation de Master et de Doctorat ainsi que la recherche dans le domaine du génie électrique. Un Programme Hubert Curien (PHC 2009-2010) est actuellement destiné à développer des travaux de recherche autour de la pile à combustible.

Ayant assuré la direction du département des Technologies électronique et électrique de 1994 à 1995 puis la direction de l'IIFT (alors CIFT pour Centre d'Innovation Franco-Thaïlandais avant de devenir Institut) de 1996 à 2008, j'occupe actuellement les fonctions de doyen de la Faculty of Technical Education. Pendant toutes ces années, je me suis investi dans le développement d'enseignements et de travaux de recherche dans le domaine des réseaux électriques et de la qualité de l'énergie électrique. Ce manuscrit de thèse présente les travaux que nous avons réalisés dans ce domaine

La collaboration et les travaux réalisés à l'IIFT s'effectuent en anglais ou en thaïlandais. Cette thèse a donc été rédigée en anglais et le présent manuscrit comporte un résumé étendu en français placé au début de la thèse. Ce résumé reprend l'introduction et la conclusion de la thèse et décrit les quatre chapitres qui la composent. De plus, dans le texte en anglais, les figures et tables comportent toute une légende en anglais et en français.

Remerciements

Tout d'abord, je voudrais exprimer ma gratitude à mon directeur de thèse le Professeur Bernard Davat pour son inestimable soutien et ses encouragements. Son entrain et ses conseils m'ont aidé durant ce travail de thèse.

Je voudrais aussi remercier sincèrement le Président de la *King Mongkut's University of Technology North Bangkok* (KMUTNB), le Prof. Teravuti Boonyasopon et le Dr. Jean-Pierre Delsol qui fut le directeur général adjoint du *Thai-French Innovation Centre* (TFIC) pour m'avoir aider à initier ces travaux de recherche et pour l'aide financière apportée.

Je suis très reconnaissant envers l'*Electricity Generating Authority of Thailand* (EGAT) qui m'a fourni les informations concernant la ligne CCHT 300/600 MW reliant la Thaïlande à la Malaisie, soulignant ainsi l'intérêt que porte cette entreprise à diffuser ses connaissances vers le milieu académique.

Je remercie aussi les personnels du *Thai-French Innovation Institute* (TFII), du KMUTNB et du Groupe de Recherches en Electronique et Electrotechnique de Nancy (GREEN) qui m'ont assuré un environnement de travail plaisant et source d'inspirations lors de nombreuses discussions : Professeur Farid Meibody-Tabar, Professeur-associé Phatiphat Thounthong, Monsieur Sakda Somkun et Monsieur Wattana Kaewmanee.

Je voudrais enfin remercier tous ceux qui ont contribué à cette thèse.

Preface

This document presents a part of the research work we have done within the frame of the Thai-French Innovation Institute (TFII) which is located and supported by the King's Monkut University of Technology North Bangkok (KMUTNB).

Created in 1990, this institute contains different departments (Corrosion, Energy, Metrology, Automation, Welding, Electronic and Electrical Technology) which develop collaboration with technical centers, universities and industries.

The department of Electronic and Electrical Technology have close relationship for about ten years with the *Institut National Polytechnique de Lorraine* (INPL) and also with industries such as Schneider Thailand Limited.

The collaboration with INPL gives us the possibility to participate to two French-Thai research programs. The first one, a *Programme d'Action Intégré* (PAI France-Thaïlande 2003-2005) from the French and Thai Ministries of Foreign Affairs has the goal to develop Research and Master and Doctorate curriculum in Electrical Engineering. The second one within the *Hubert Curien* program (PHC 2009-2010) actually develops research works in the field of fuel cells. Former director of the department of Electronic and Electrical Technology (1994-1995) and of the TFII (1996-2008), I am actually the Dean of the Faculty of Technical Education of KMUTNB. During all these years I was involved in teaching and research on electrical network and quality of electrical energy. This thesis presents the works we have done in this field.

The teaching and research work at TFII are done in English or in Thai. It is why this thesis is written in English. It is preceded by an extended summary in French containing the introduction and conclusion of the thesis and a description of the different chapters. Furthermore all legends of figures and tables are both in English and in French.

Acknowledgments

Sommaire

Résumé de la thèse

Introduction

La qualité de la distribution d'énergie électrique et la stabilité des réseaux électriques est un problème de plus en plus important en raison de la croissance du nombre de charges non linéaires utilisées dans l'industrie [1]. La distorsion des ondes de tension peut créer des dysfonctionnements dans différents secteurs comme les industries utilisant des automates, les systèmes de communication, les aéroports ou les hôpitaux. Outre les perturbations sur les charges alimentées, les systèmes de puissance peuvent créer des harmoniques et les interconnections à courant continu haute tension (CCHT) sont connues pour les perturbations qu'elles apportent.

Les liaisons CCHT sont intéressantes d'un point de vue économique, par rapport aux connexions classiques en alternatif, pour des puissances importantes transitant sur de longues distances [2], [3]. Un exemple récent de ce type d'installation est la liaison CCHT commencée en 1997 entre la Thaïlande et la Malaisie. Il s'agit d'une liaison 300/600 MW d'une longueur de 110 km. Comme un convertisseur est présent à chaque extrémité de la liaison continue, de nombreux harmoniques sont générés vers les deux réseaux alternatifs, harmoniques qui nécessitent un traitement spécifique.

La solution la plus simple de réduction des harmoniques consiste à utiliser un filtre passif. Accordé sur certaines fréquences, celui-ci crée un chemin basse impédance où les harmoniques sont piégés. Un filtre étant associé à une gamme de fréquence, c'est un ensemble de filtres qui est nécessaire pour éliminer les harmoniques dans une gamme de fréquences étendue.

Une autre solution consiste à utiliser un filtre actif. Celui-ci peut être placé tant côté continu qu'alternatif [4]. Le premier filtre actif pour liaison CCHT a été installé par Siemens en 1998 dans le cadre d'une expérimentation réalisée au Danemark [3]. Depuis plus de quatorze filtres actifs pour station CCHT ont été installés au niveau mondial et couvrent une gamme de puissance de 0,6 à 22 MVA. Le principe du filtre actif est de générer un jeu

d'harmoniques de même amplitude mais opposés aux harmoniques que l'on veut supprimer. Les harmoniques devant être générés par le filtre pouvant évoluer dans le temps, le filtre actif est un convertisseur de puissance contrôlé par des techniques de type MLI (Modulation de Largeur d'Impulsion) définies par des processeurs numériques comme les DSP (Digital Signal Processeur), [5]. La structure et le contrôle des filtres actifs sont encore l'objet de travaux de recherche et cette thèse détaille le fonctionnement, le contrôle de ces filtres actifs et présente un prototype réalisé par l'auteur.

D'autres méthodes peuvent être aussi utilisées comme par exemple les déphasages introduits par des transformateurs. Le déphasage classique utilisé est le déphasage de 30° introduit par les connexions en étoile et en triangle de deux enroulements secondaires. Ce type d'enroulements est en particulier utilisé dans les redresseurs dodécaphasés qui réduisent de façon importante les harmoniques injectés sur le réseau [6].

Cette thèse comporte quatre chapitres. Le premier est consacré à la production, au transport et à la distribution de l'électricité en Thaïlande.

Le deuxième chapitre s'intéresse aux liaisons CCHT, la liaison 300/600 MW entre la Thaïlande et la Malaisie permettant d'illustrer ce type de dispositif.

Le troisième chapitre concerne la qualité de l'énergie électrique en termes d'harmoniques, tant du côté des sources que des solutions que l'on peut apporter. Les techniques de déphasage ou de filtrage actif sont alors détaillées, ainsi que des exemples de réalisation de filtre actif.

Le quatrième chapitre propose une méthode de modélisation des convertisseurs à indice de pulsation élevé comme par exemple les redresseurs dodécaphasés utilisés dans les liaisons CCHT. Cette méthode est basée sur une solution exacte du problème d'état [7-8]. En utilisant des propriétés de symétrie temporelle, l'étude du fonctionnement sur une période peut se réduire à l'étude de seulement deux séquences de fonctionnement. Le modèle ainsi développé donne des informations sur le fonctionnement du système tant dans le domaine fréquentiel que temporel.

Chapitre 1 - Production, transport et distribution de l'électricité en Thaïlande

Le premier chapitre est consacré à la production, au transport et à la distribution de l'électricité en Thaïlande.

La Thaïlande a suivi une évolution que l'on retrouve dans de nombreux pays. Dans les années soixante, les producteurs et distributeurs sont regroupés dans une compagnie d'état, seule capable de faire face aux énormes investissement nécessaires pour moderniser le réseau et les moyens de production. L'une des originalités de la Thaïlande est d'avoir, dès le début, séparé les activités de production et de transport, de la distribution.

Durant ces dix dernières années, ces compagnies publiques sont l'objet de programmes de privatisation, en particulier des moyens de production.

Comme dans de nombreux pays [9], les années 90 ont vu le développement de règlements concernant les harmoniques et le phénomène de flicker.

Marché de l'électricité en Thaïlande

La principale société en charge de la production et du transport de l'électricité en Thaïlande est l'EGAT (*Electricity Generating Authority of Thailand*, [10]). D'autres producteurs vendent de l'électricité à l'EGAT et sont selon leur taille qualifiés de producteurs indépendants ((*Independent Power Producers*, IPP) ou de petits producteurs (*Small Power Producers*, SPP). L'électricité produite est transportée par le réseau géré par l'EGAT et est distribuée par la MEA (*Metropolitan Electricity Authority*) dans la région de Bangkok et par la PEA (*Provincial Electricity Authority*) dans les autres parties de la Thaïlande. Le marché de l'électricité est dirigé par un organisme l'EPPO (*Energy Policy and Planning Office*) dépendant directement du Ministère de l'Energie (figure I).

L'EGAT a été créée le 1er mai 1969 sous la responsabilité du Ministère de l'Energie et a regroupé les activités de trois entreprises d'état qui se partageaient précédemment le marché de la production et du transport de l'électricité YEA (Yanhee Electricity Authority), LA (Lignite Authority) et NEA (Northeast Electricity Authority).
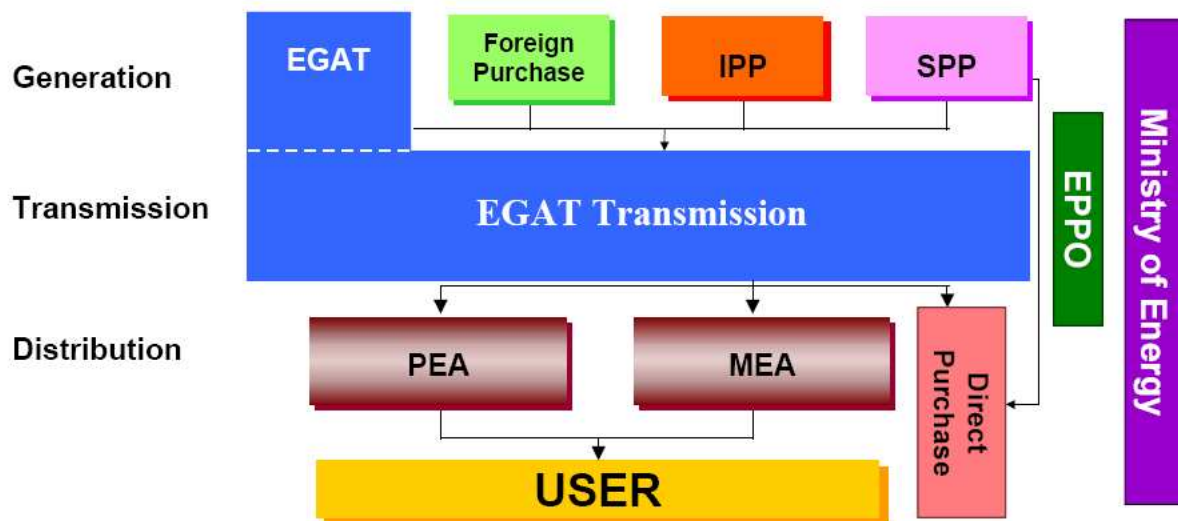
Figure I. Structure du marché de l'électricité en Thaïlande [11].

Les missions de l'EGAT étaient d'une part de générer, acquérir et transmettre l'électricité aux distributeurs MEA et PEA et d'autre part de promouvoir la production et l'usage de l'électricité sous toutes ses formes. A ce cahier des charges concernant l'électricité s'est ajoutée la nécessité de promouvoir l'utilisation du lignite, obligation liée à l'existence de mines importantes dans le nord de la Thaïlande (Mae Moh) et dont la production est destinée majoritairement à l'alimentation de centrales thermiques.

L'ambition de l'EGAT était de devenir la principale entreprise de production et de transport de l'électricité pour les pays de l'ASEAN[1].

EGAT gère une capacité de production de près de 28 000 MW pour une production annuelle de 117 000 GWh[2]. 59 % de cette capacité proviennent de centrales appartenant à EGAT, le reste de producteurs privés ou des pays voisins (figure II). Un nouvel opérateur

---

[1] L'ASEAN est l'association des pays du sud-est asiatique. Créée le 8 août 1967 par l'Indonésie, la Malaisie, les Philippines, Singapour et la Thaïlande, elle a été rejointe par Brunei (1984), le Vietnam (1995), le Laos (1997), la Birmanie (1997) et le Cambodge (1999). Cette association régionale couvre 4,5 millions de km², occupés par une population de 500 millions d'habitants.

[2] Année fiscale 2003, octobre 2002 – septembre 2003.

RATCH apparaît sur cette figure. Il a été créé en 2000 lors de la privatisation de centrales de production d'EGAT.
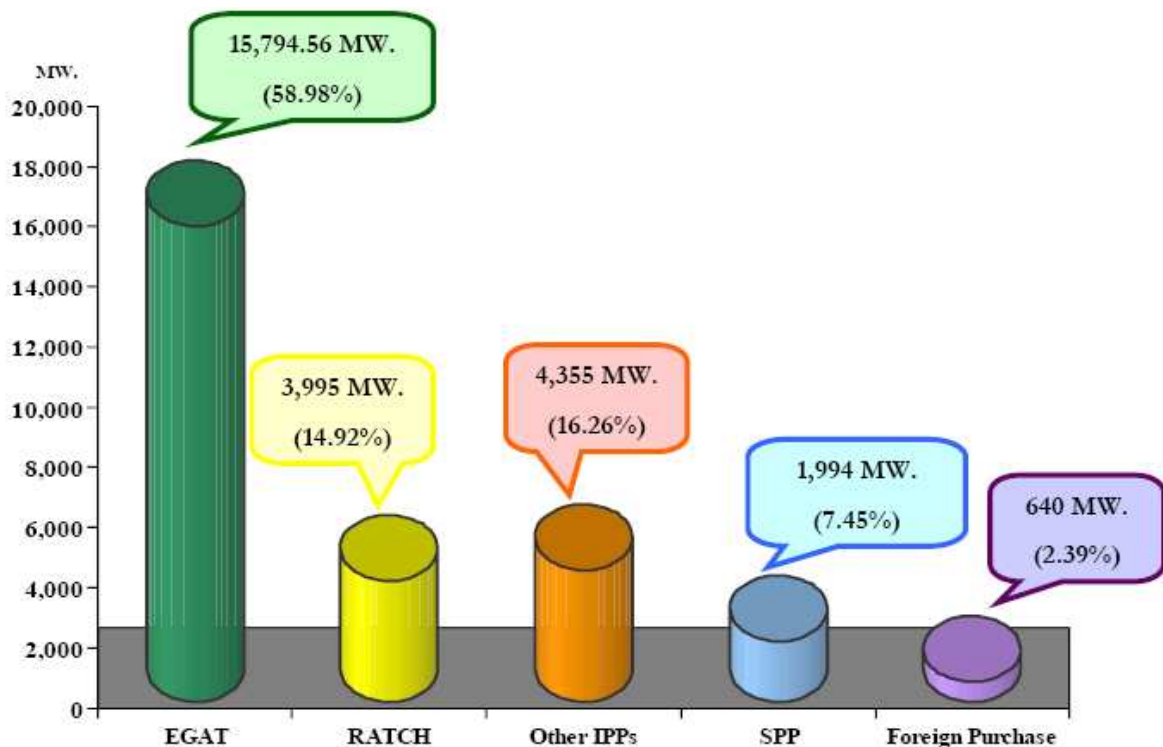
Figure II. Capacité de production d'électricité en avril 2005 [11].

La capacité actuelle est suffisante et le maximum de la production (ou de la consommation) qui a lieu entre mars et mai lors de la saison chaude est encore loin de la capacité de production maximale (figure III). Malgré tout, l'augmentation de la production moyenne est de 6 à 7 % par an ce qui nécessite de nouveaux investissements chaque année (la capacité de production devrait être de 35 000 MW en 2010, [11]).

Cette croissance a encouragé la Thaïlande à signer des accords de fourniture d'électricité avec ses voisins. Des accords ont été ainsi signés dès 1993 avec le Laos (possibilité de fournir 1 500 MW dès 2000 et 3 000 MW en 2006) et avec la Chine (possibilité de fournir 1 500 MW à l'horizon 2013 et 3 000 MW en 2018). Avec d'autres pays comme la Birmanie et le Cambodge des accords de fourniture à moyen terme ont été signés (au-delà de 2010) sachant qu'entre temps, c'est la Thaïlande qui supplée à un manque d'électricité dans ces deux pays.
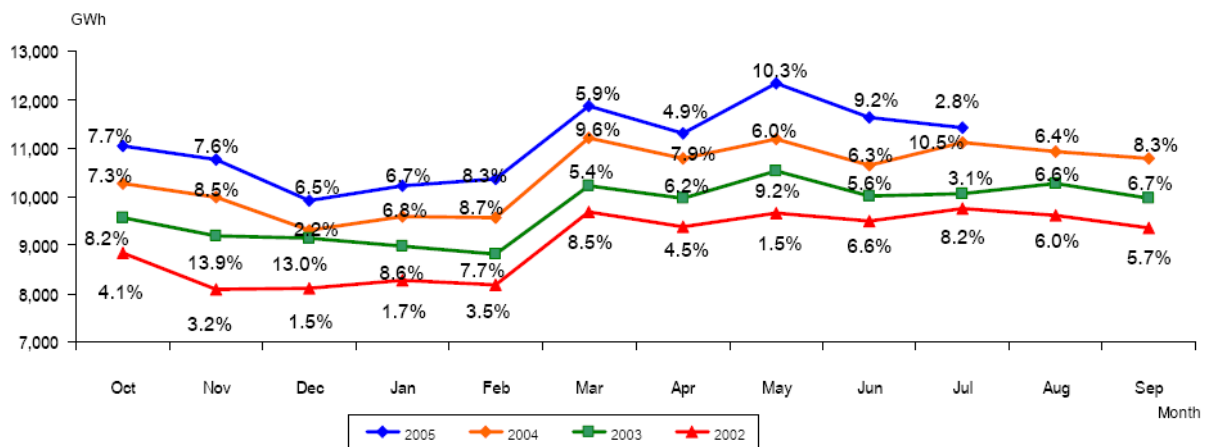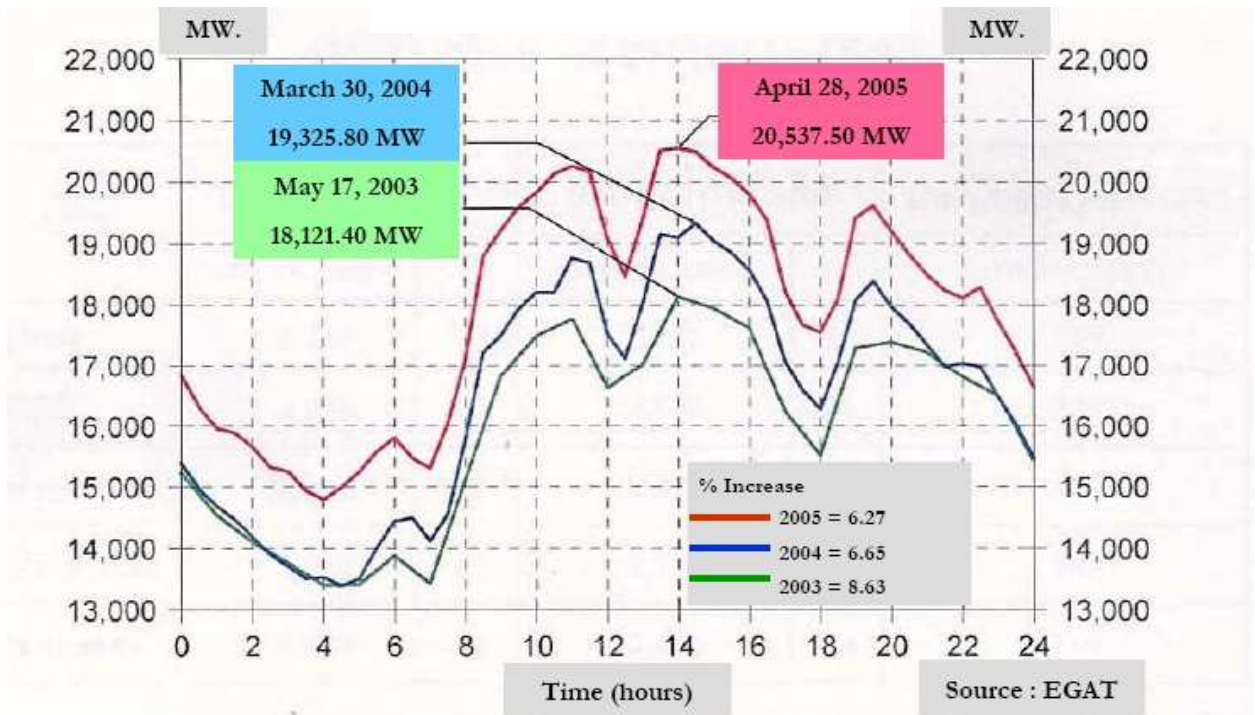
Figure III. Maximum de production (en haut) et production mensuelle (en bas)[3] [11].

La production est diversifiée mais essaie d'utiliser au maximum les ressources locales : gaz naturel, lignite et hydroélectricité qui sont à l'origine de plus de 85 % de l'électricité produite (figure IV). La production de base est obtenue à l'aide de centrales thermiques classiques, les ajustements étant réalisés à l'aide de turbines à gaz, de barrages ou même de groupes diesel. Les principales centrales thermiques sont dispersées sur l'ensemble du territoire en fonction des ressources et des besoins en consommation (figures V et VI).

---

[3] Les nombres sur les courbes correspondent à l'accroissement par rapport à l'année précédente.
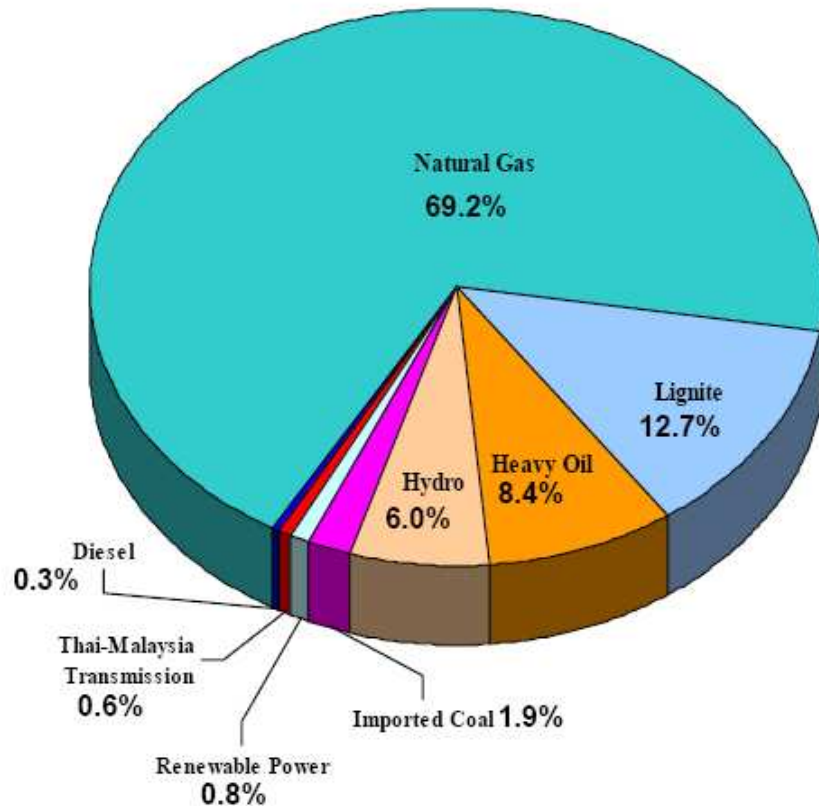
Figure IV. Production par type d'énergie primaire [11].

La centrale de Bang Pakong située au sud de Bangkok est actuellement la plus moderne et la plus importante de Thaïlande. Elle a une capacité de production d'un peu moins de 4 000 MW. Son développement a accompagné la découverte de gaz naturel dans le Golfe de Thaïlande. Cette centrale est la vitrine de l'EGAT. 70 % de la production sont obtenus à l'aide de générateurs utilisant de la vapeur, les autres 30 % par des générateurs fonctionnant en cycle combiné. Elle peut utiliser soit du gaz naturel, soit du pétrole. Le refroidissement des générateurs utilise de l'hydrogène fabriqué sur place. La capacité de production est de 45 m^3 par heure et cette unité alimente aussi les installations de refroidissement d'autres centrales de la région de Bangkok. Un centre de formation destiné à la Thaïlande et aux pays voisins est attaché à cette centrale.

La capacité de production hydroélectrique représente 6 % de la capacité totale et concerne des unités situées dans les régions ouest, nord-ouest et nord-est de la Thaïlande. Ces unités sont en général de petites puissances (entre 6 et 40 MW) à l'exception notable de la centrale de pompage de 500 MW de Lam Takhong (province de Nakhom Ratchasima, nord-est de la

Thaïlande) et du barrage « au fil de l'eau[4] » de 136 MW de Pak Mun (province d'Ubon Ratchathani, nord-est de la Thaïlande) et construit sur la rivière Mun, un affluent du Mékong.

1. Bang Pakong
2. Mae Moh
3. South Bangkok
4. Wang Noi
5. Nam Phong
6. Nong Chok
7. Sai Noi
8. North Bangkok
9. Surat Thani
10. Lan Krabue
11. Ratchaburi
12. Mae Hong Son
13. Krabi
14. Surat Thani
15. Thap Sakae

Figure V. Localisation des principales centrales d'EGAT [12].

Les énergies renouvelables sont assez peu représentées dans les capacités de production et correspondent pour l'essentiel à des projets d'expérimentation de l'EGAT :

- Réalisation d'une centrale de 300 kW utilisant l'énergie géothermique qui est opérationnelle depuis 1989 ;

- Installation de 70 kW de panneaux solaires sur 62 sites en 2000 ;

- Installation de 6 éoliennes de 150 kW sur l'île de Phuket en 1996.

---

[4] Utilisant la force du courant et non une chute d'eau.

a) 3680 MW, Bang Prakong Power Plant,
Chachoengsao province

d) 710 MW, Nam Phong Power Plant,
Khon Kaen province

b) 2625 MW, Mae Moh Power Plant,
Lampang province

e) 2024 MW, Wang Noi Power plant,
Ayutthaya province

c) 2288 MW, South Bangkok Power
Plant, Samut Prakan province

f) 743.8 MW, Bhumibol Hydro Electric
Dam, Tak province

Figure VI. Centrales thermiques et barrage d'EGAT [12].

EGAT a la responsabilité du transport de l'électricité. Le réseau de plus de 28 000 km recouvre l'ensemble du territoire national et possède trois niveaux de tension 500 kV, 230 kV et 115 kV. Le réseau est géré à partir d'un centre national de contrôle situé à Bangkok et de cinq centres régionaux qui divisent le pays en cinq zones (la capitale et les régions Sud, Centre, Nord et Nord-Est).

Le réseau est interconnecté avec les pays voisins. Les principales liaisons actuelles sont avec le Laos (115 et 230 kV, [13]) et la Malaisie (115, 132 kV et 300 kV en courant continu haute tension, CCHT, [14-15]). Une ligne CCHT à 500 kV est en projet avec la Chine [16].

EGAT délivre l'électricité qu'elle produit et la production des producteurs indépendants à deux entreprises d'état qui réalisent la distribution. La première MEA (Metropolitan Electricity Authority) est en charge de l'agglomération de Bangkok et utilise de l'ordre de 35 % de la production. La deuxième PEA (Provincial Electricity Authority) distribue dans les différentes provinces thaïlandaises de l'ordre de 63 % de la production. Ces entreprises de distribution de l'électricité dépendent du Ministère de l'Intérieur et ont été créées en 1958 pour MEA et en 1960 pour PEA.

Lors de sa création, MEA produisait une partie de l'électricité consommée dans l'agglomération de Bangkok. Dès 1961, cette activité de production a été transférée à Yanhee Electricity Authority, l'une des trois entités à l'origine d'EGAT. Depuis cette date, MEA ne s'occupe plus que de la distribution. Le réseau comporte 13 stations où arrivent les lignes haute tension et comporte un maillage basé sur 122 sous-stations. Le principe utilisé pour la distribution aux particuliers est l'existence d'un réseau à 12 ou 24 kV sur lequel sont placés à intervalles plus ou moins réguliers des transformateurs sur lesquels sont connectés les utilisateurs en 220-380 V.

PEA de son côté s'occupe du reste de la Thaïlande soit de l'ordre de 99 % de la surface du pays. Depuis sa création, elle s'est attachée à amener l'électricité dans les zones rurales les plus reculées et a joué et joue encore un rôle important dans la politique nationale de développement.

A la suite des décisions gouvernementales de privatisation du marché de l'électricité destinées à accroître la participation des investisseurs privés dans ce domaine, deux nouvelles compagnies ont été créées en 1992 et 2000.

La première EGCO (Electricity Generating Public Company) est née de la cession par EGAT de la centrale de Rayong (1 200 MW) puis plus tard de celle de Khanon (750 MW). EGAT est le principal actionnaire de cette société, sa participation étant passée de 40,7 % à l'origine à 25,8 % aujourd'hui.

La deuxième RATCH (Ratchaburi Electricity Generating Holding Public Company) Limited a regroupé les moyens de production de la province de Ratchaburi (de l'ordre de 4 000 MW) située au sud de Bangkok. EGAT possède aujourd'hui 45 % de cette société.

A terme ce sont toutes les centrales de production qui ont vocation à être privatisées, EGAT ne conservant que la tache d'opérateur du réseau et de lien entre producteurs et consommateurs d'électricité.

Qualité de l'électricité

Le développement de la consommation industrielle et l'existence de consommateurs risquant de polluer le réseau électrique ont conduit EGAT et les distributeurs MEA et PEA à réfléchir aux problèmes de la pollution du réseau. Un conseil dédié à ce problème a ainsi été créé en 1995. Celui-ci s'est inspiré des travaux déjà réalisés dans les autres pays industrialisés.

C'est ainsi que différents documents ont été rédigés. Ils correspondent à des recommandations diffusées auprès des clients, afin d'obtenir leurs réactions. Aujourd'hui ces recommandations sont en train de devenir des normes.

Les premiers documents officiels datent de 1998 sur les harmoniques [18] et la fluctuation de la tension [19].

Pour les harmoniques, les recommandations sont à plusieurs niveaux et concernent :

- Les niveaux de courant admissibles pour les harmoniques ;
- Le taux de distorsion en tension ;
- Les équipements et en particulier les convertisseurs statiques.

Les niveaux de courant admissibles en fonction du rang de l'harmonique sont définis dans la table I et dépendent de la tension au point de raccordement. De même, le taux de distorsion harmonique en tension dépend du niveau de tension (table II).

Pour les équipements, les normes proposées dépendent de leur puissance et de la tension au point de raccordement. En monophasé, les règles définies dans les tables I et II ne s'appliquent pas pour les convertisseurs statiques qui ne dépassent pas une puissance de 5

kVA en 220 V et 7,5 kVA en 415 V sous réserve de ne produire que des harmoniques de rang impair. En triphasé, la régulation dépend du niveau de tension (table III).

Voltage (kV)	Rang de l'harmonique et courant limite (A$_{rms}$)																		
	2	3	4	5	6	7	8	9	10	11	12	13	14	15	16	17	18	19
0 - 400	48	34	22	56	11	40	9	8	7	19	6	16	5	5	5	6	4	6
11 et 12	13	8	6	10	4	8	3	3	3	7	2	6	2	2	2	2	1	1
22, 24 et 33	11	7	5	9	4	6	3	2	2	6	2	5	2	1	1	2	1	1
69	8.8	5.9	4.3	7.3	3.3	4.9	2.3	1.6	1.6	4.9	1.6	4.3	1.6	1	1	1.6	1	1
115 et après	5	4	3	4	2	3	1	1	1	3	1	3	1	1	1	1	1	1

Table I. Limites des courants harmoniques au point de connexion au réseau.

Voltage (kV)	Distorsion totale en tension (%)	Distorsion en tension par rang d'harmonique (%)	
		Rang impair	Rang pair
0 - 400	5	4	2
11, 12, 22 et 24	4	3	1,75
33	3	2	1
69	2,45	1,63	0,82
115 et après	1,5	1	0,5

Table II. Limites de la distorsion en tension au point de connexion au réseau.

Voltage (kV)	Convertisseur triphasé			Gradateur triphasé	
	3-pulse (kVA)	6-pulse (kVA)	12-pulse (kVA)	6 thyristors (kVA)	3 thyristors 3 diodes (kVA)
0 - 400	8	12	-	14	10
11 et 12	85	130	250	150	100

Table III. Puissance maximale des convertisseurs en fonction du niveau de tension.

Ces limites correspondent à l'ensemble des convertisseurs connectés à un même point de raccordement et non à chaque convertisseur pris un par un. Dans le cas de plusieurs convertisseurs, des facteurs de coïncidence permettent de tenir compte du fait qu'ils ne

fonctionnent pas toujours en même temps ou que les courants absorbés ne sont pas systématiquement en phase (table IV). Au delà de ces limites, le problème doit être résolu au cas par cas et se pose différemment selon que l'on à affaire à une installation déjà en fonctionnement ou en projet.

Catégorie	Mode de commande du convertisseur	Facteur multiplicatif
1	Convertisseur non contrôlé	0,9
2	Convertisseur commandé utilisé plusieurs fois par jour	0,75
3	Convertisseur commandé utilisé de temps en temps ou causant des harmoniques au démarrage	0,6 quand moins de 3 convertisseurs sont utilisés 0,5 pour plus de 4 convertisseurs

Table IV. Coefficient de pondération lors de la connexion au même point de plusieurs convertisseurs.

Pour les creux de tension, l'objectif de la directive [19] est d'éviter les creux de tension susceptibles de gêner les autres utilisateurs. On considère ainsi trois niveaux de fluctuation en tension au point de connexion selon la valeur relative de la fluctuation créée par la charge par rapport à la puissance nominale du réseau exprimée en kVA :

- Si la fluctuation en valeur relative est inférieure à 0,002, le dispositif considéré peut être connecté sans précaution au réseau ;

- Si la fluctuation relative est comprise entre 0,002 et 0,03, le dispositif peut être connecté au réseau sous réserve de ne pas dépasser les limites données sur la figure VII. Sur cette figure, si la fluctuation apparaît de façon régulière le terme Pst[5] vaut 1 et la limite est donnée par la courbe 2. dans le cas contraire, le Pst est égal à 0,5 et la limite est donnée par la courbe 1.

---

[5] Facteur de sévérité à court terme, le Pst permet d'évaluer la sévérité du phénomène de flicker dans les temps courts (10 minutes).

- Si la fluctuation relative est supérieure à 0,03, le dispositif ne peut être connecté et doit être amélioré.
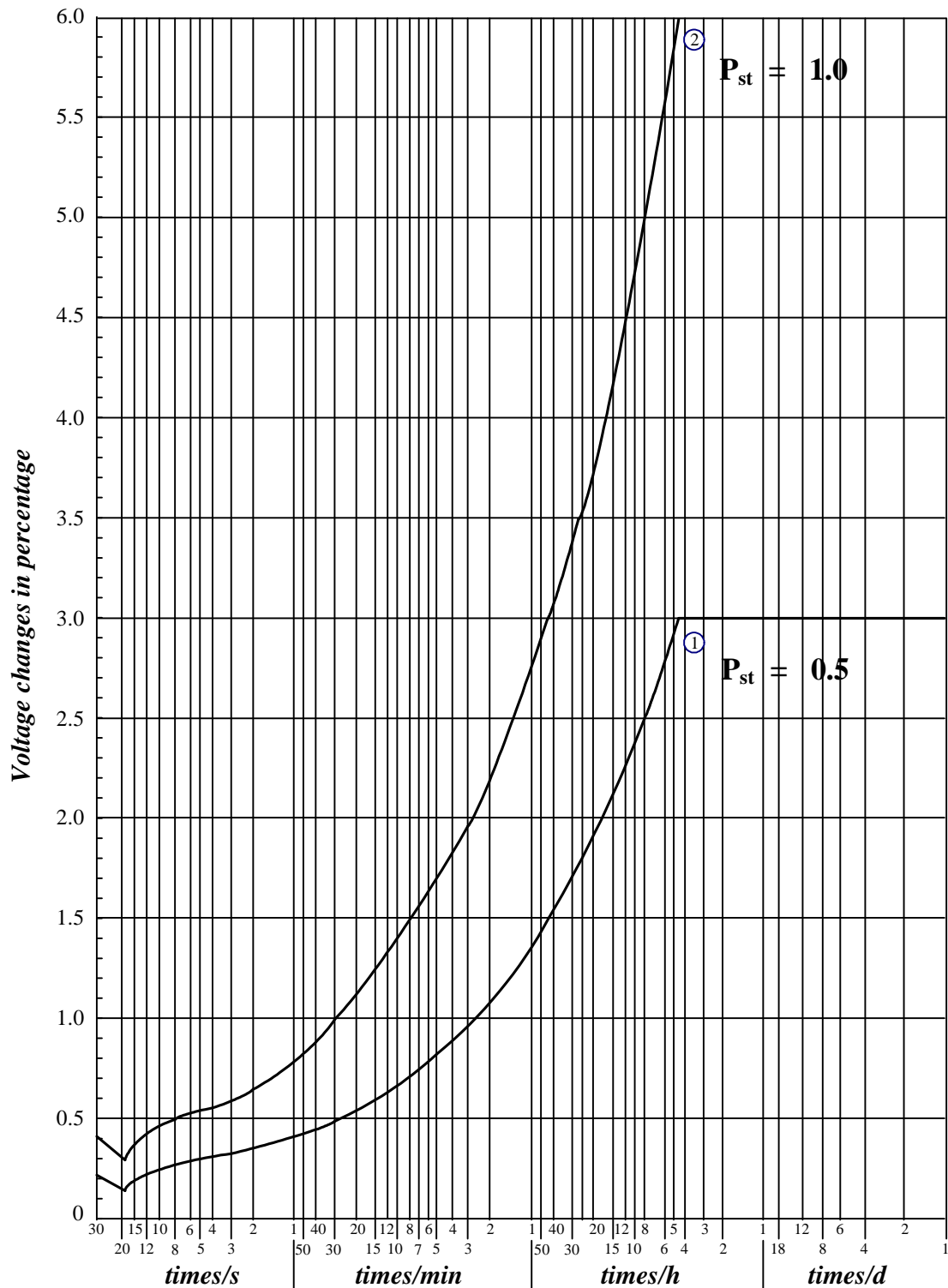
Figure VII. Fluctuation relative acceptée en fonction du nombre de fluctuations de tension par unité de temps (seconde, minute, heure et jour).

Plusieurs méthodes existent pour améliorer une charge :

- Améliorer son fonctionnement de façon à ne pas faire fonctionner en même temps plusieurs moteurs, ou limiter les variations de tension et la durée de fonctionnement de certaines charges ;

- Améliorer les caractéristiques de la charge;

- Installer des équipements afin de limiter les ondulations de tension.

L'annexe 1 donne un exemple de calcul dans le cas d'un moteur électrique démarrant quinze fois par heure.

Chapitre 2 - Liaison CCHT Thaïlande – Malaisie

Le deuxième chapitre s'intéresse aux liaisons à courant continu haute tension (CCHT). Le principe de ces liaisons est tout d'abord décrit avant de détailler la liaison entre les réseaux électriques de Thaïlande et de Malaisie. Cette liaison dont la construction a été lancée en 1997 est opérationnelle depuis 2001. Première interconnexion entre deux pays de l'ASEAN celle-ci représente une première dans le projet d'intégration des différents réseaux de cette région (projet d'un *Asean Power Grid*).

Dans la première partie de ce chapitre, les différents types d'interconnexion sont décrits. Ceux-ci diffèrent principalement par le nombre de connexions physiques entre les convertisseurs placés aux deux extrémités de la liaison CCHT et par l'existence ou non de possibilités de conduction par le sol. Les figures VIII et IX illustrent deux exemples de modes de connexion dits unipolaire ou bipolaire, les différents modes de connexion envisageables étant présentés dans le chapitre 2 dans les figures 2.5 à 2.10[6].
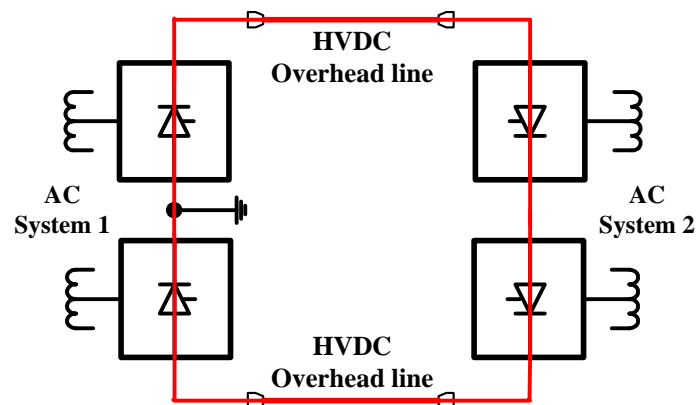
Figure VIII. Liaison bipolaire équilibrée.

La deuxième partie du chapitre est ensuite consacrée au contrôle de la liaison CCHT [21], contrôle réalisé de façon indépendante sur les deux convertisseurs placés aux extrémités et assurant la liaison entre l'étage continu et chacun des réseaux alternatifs (figure X).

---

[6] Les figures 2.n sont des figures du chapitre 2 rédigé en anglais et se trouvent dans les pages 19 à 68 du manuscrit.
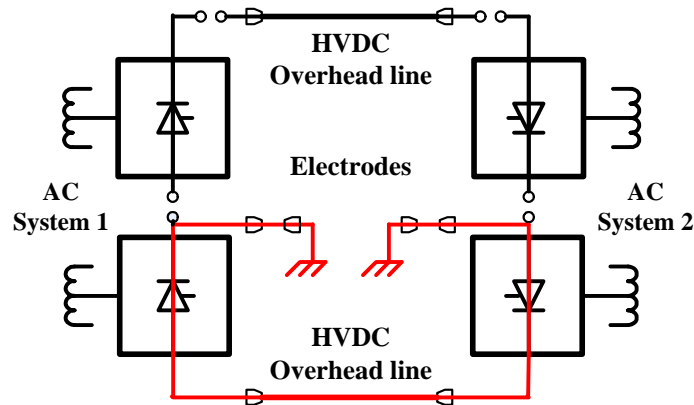
Figure IX. Structure bipolaire avec retour par le sol lors de l'ouverture d'une des lignes aériennes.
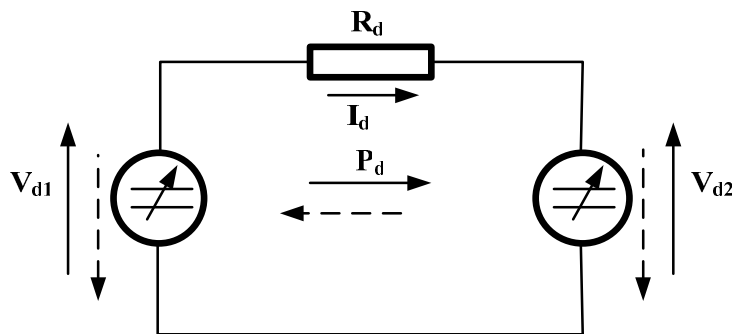
Figure X. Schéma équivalent simplifié d'une liaison CCHT.

Les principaux objectifs de ce contrôle sont, outre d'éviter tout problème de commutation pour le convertisseur fonctionnant en onduleur, de limiter d'une part le courant continu et d'autre part la consommation de réactif. Cela signifie qu'il s'agit d'avoir la tension continue la plus importante possible (afin de limiter le courant) et l'angle de retard à l'amorçage le plus faible possible (afin d'avoir la tension la plus grande et de limiter la consommation de réactif). Le risque de dysfonctionnement du convertisseur fonctionnant en onduleur est limité en imposant l'angle de retard à l'amorçage. Cela revient à imposer la tension du côté de l'onduleur, le courant étant imposé du côté fonctionnant en redresseur.

On aboutit ainsi à un mode de contrôle (figure XI) où l'on distingue deux trajectoires de fonctionnement pour chacun des convertisseurs correspondant principalement à un fonctionnement à angle de retard à l'amorçage imposé auquel est adjoint un mode de fonctionnement à courant constant en cas de décroissance de la tension sur l'un des réseaux alternatifs. Les principales boucles de régulation sont ensuite décrites, contrôle du courant

pour le convertisseur fonctionnant en redresseur (figure XII) et contrôle de l'angle de retard à l'amorçage pour celui fonctionnant en onduleur (figure XIII).
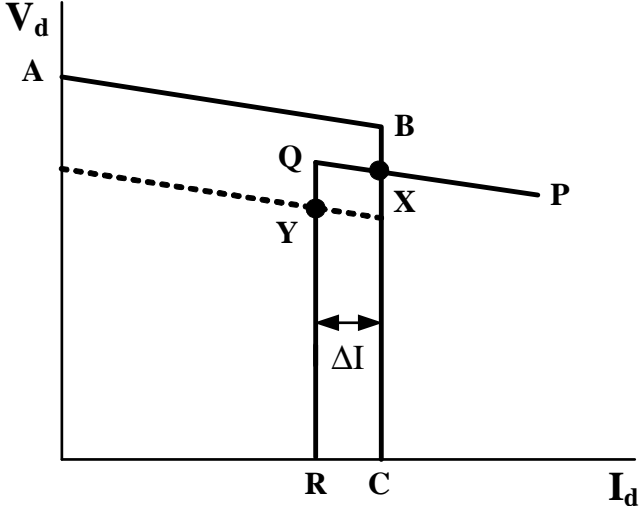
Figure XI. Caractéristique simplifiée Vd-Id.
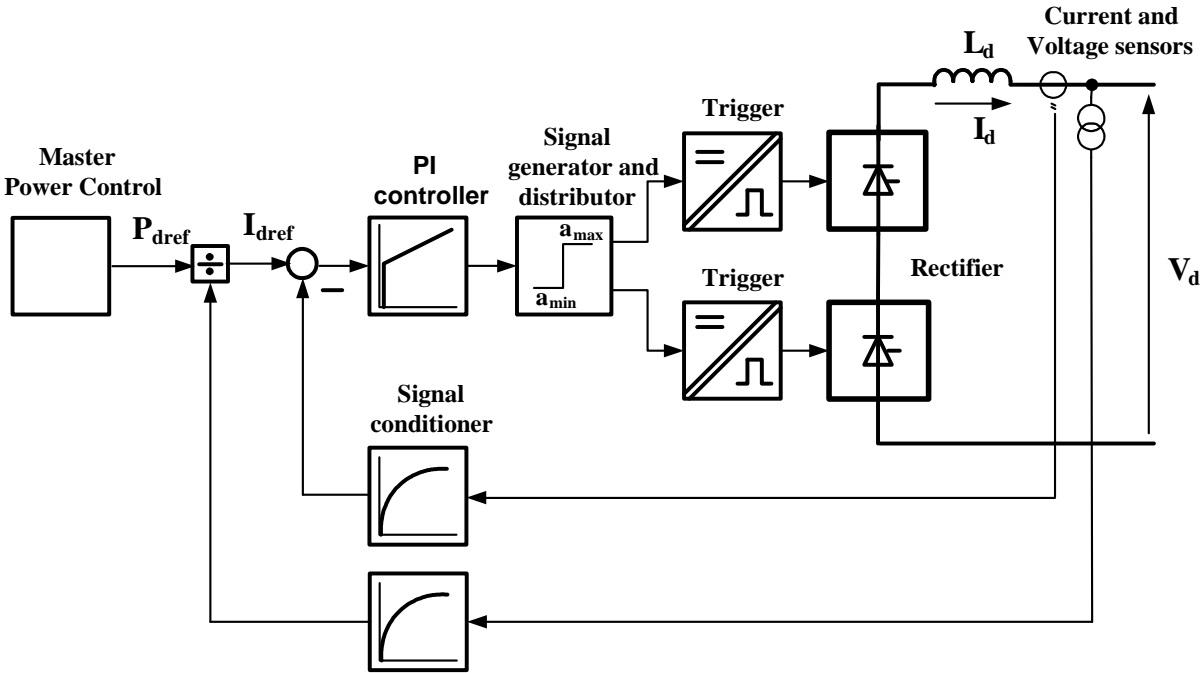
Figure XII. Boucle de régulation du courant côté redresseur (contrôle à courant constant).
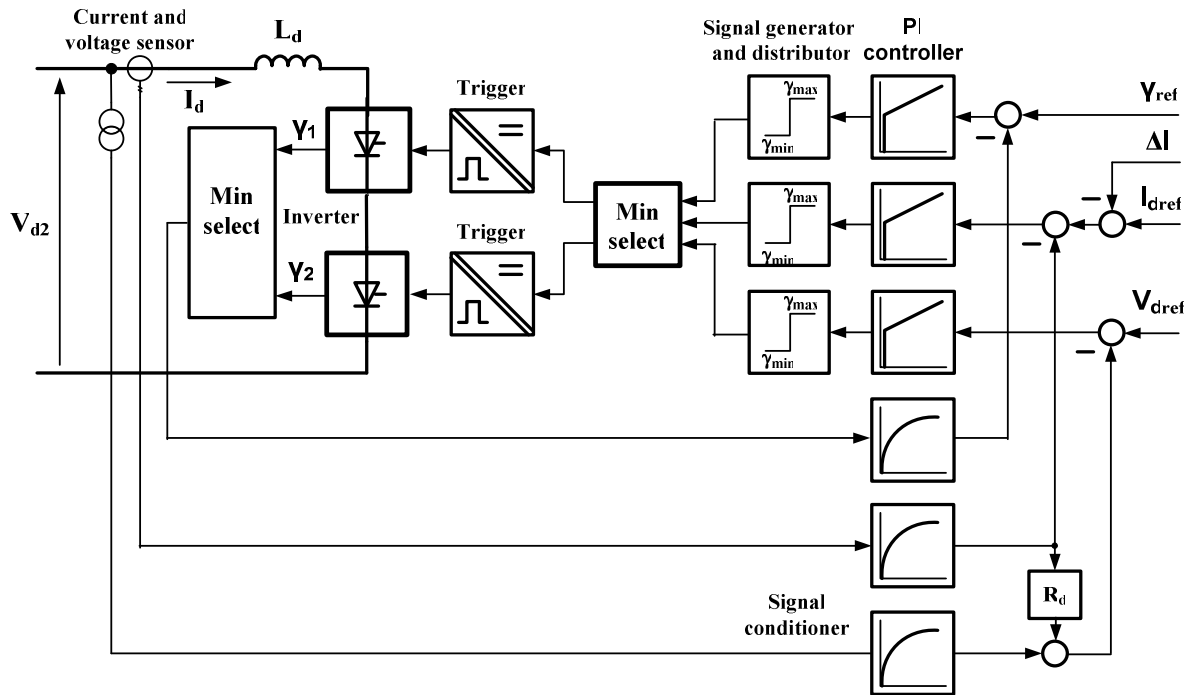
Figure XIII. Contrôle de l'angle gamma côté onduleur.

La troisième partie, la plus importante de ce chapitre, décrit en détail la liaison CCHT entre la Thaïlande et la Malaisie. Il s'agit tout d'abord de rappeler l'historique de cette liaison qui a fait suite à une première connexion en alternatif des réseaux de ces deux pays. Dès 1982, une partie du réseau thaïlandais pouvait être isolée du reste du pays et alimentée par la Malaisie (80 MW en 132/115 V, [25]).

L'augmentation des besoins d'échange a conduit naturellement à envisager une liaison CCHT qui permettait des échanges plus importants tout en assurant un fonctionnement découplé des deux réseaux électriques. Celle-ci est a été conçue de type bipolaire avec une capacité de transfert de 60 à 600 MW. Elle fonctionne actuellement selon un mode unipolaire (figures 2.21 à 2.24), sa capacité de transfert actuelle étant limitée à 300 MW avec une surcapacité de 450 MW pendant une dizaine de minutes.

Le schéma de ce dispositif est représenté sur la figure XIV, les principales caractéristiques de cette liaison CCHT étant détaillées dans la table V.
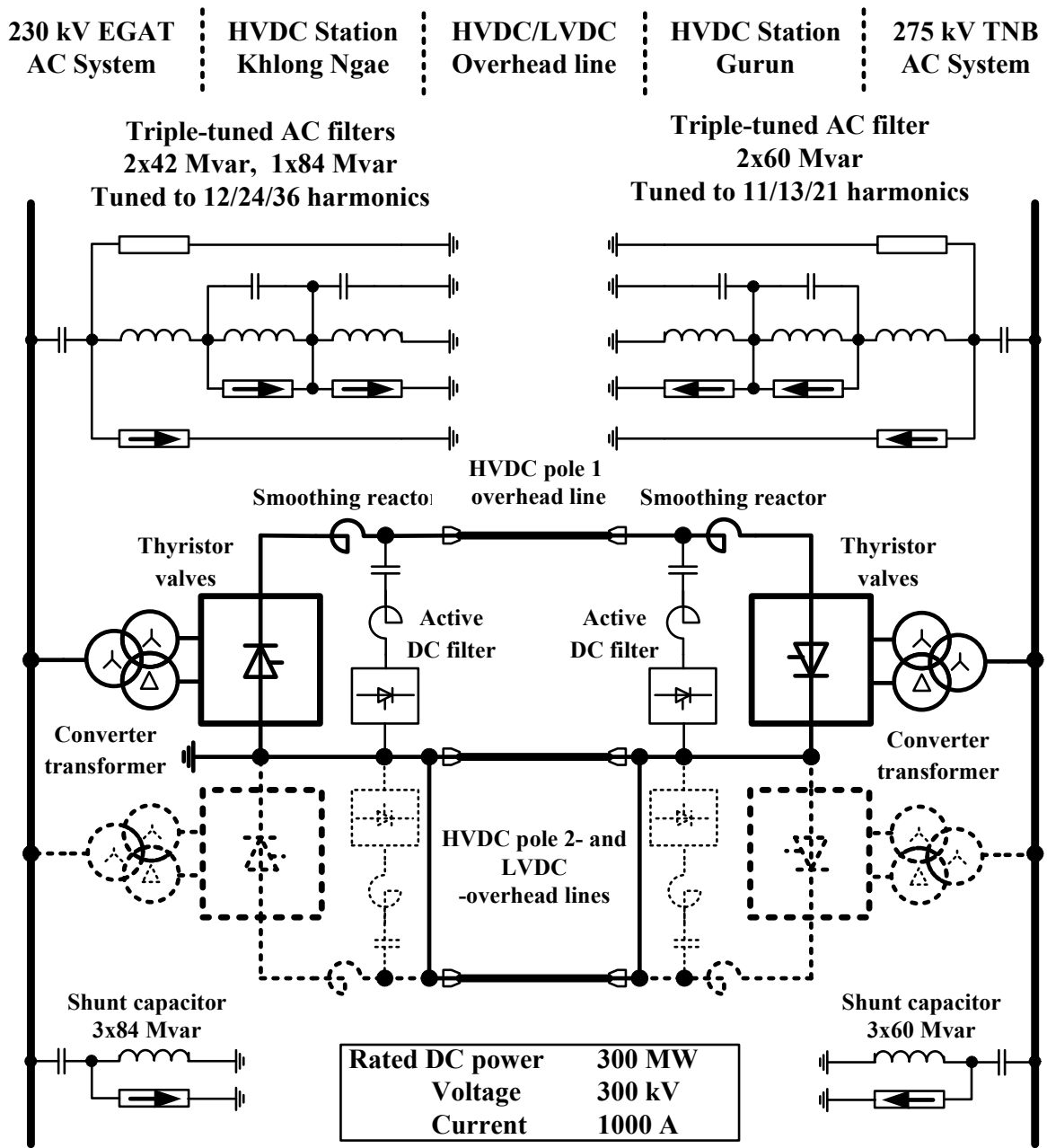
Figure XIV. Schéma de principe de la liaison CCHT en mode de fonctionnement unipolaire [26].

Caractéristiques de la liaison CCHT		
Puissance nominale en mode de fonctionnement unipolaire	**300**	**MW**
Puissance de surcharge (10 mn)	**450**	**MW**
Puissance minimale	**30**	**MW**
Courant continu nominal	**1000**	**A**
Courant de surcharge (10 mn)	**1562**	**A**
Courant minimal à 300 kV	**100**	**A**
Tension nominale	**300**	**kV**
Tension maximale	**308**	**kV**
Tension minimale	**292**	**kV**

Table V. Principales caractéristiques de la liaison CCHT [23].

Une vingtaine de pages est ensuite consacrée à la description des différents constituants de cette ligne CCHT. Outre les données techniques correspondant à ces différents éléments, de nombreuses photos accompagnent ces données : bâtiment accueillant le convertisseur AC-DC (figure 2.26), disjoncteurs côté alternatif (figure 2.27), filtres accordés et capacitifs côté alternatif (figure 2.27), transformateur triphasé dodécaphasé (figures 2.31 et 2.32), interrupteurs de puissance (figures 2.33 et 2.34), système de refroidissement des interrupteurs (figure 2.35), inductance de lissage (figure 2.36), filtre de l'étage continu (figure 2.37), disjoncteur de l'étage continu (figure 2.38) et ligne à courant continu (figure 2.39).

La figure XV donne quelques exemples des photos présentées dans le chapitre 2. Il s'agit ici du transformateur alimentant les redresseurs, réalisé à partir de trois transformateurs monophasés comportant chacun deux enroulements secondaires. Le choix de cette structure représentée sur la figure XVI a été effectué en partie pour des raisons de difficulté de transport d'une structure triphasée unique.

Les autres composants représentés sur la figure XV sont d'une part les interrupteurs où chaque valve est constituée par la mise en série de 48 thyristors élémentaires et d'autre part les éléments de filtrage des harmoniques placés tant côté alternatif que continu.

a) Transformateurs monophasés

b) Connexions des transformateurs dans le hall des redresseurs

c) Section des redresseurs

d) Valve élémentaire de 48 thyristors

e) Filtre côté alternatif

f) Filtre côté continu

EGAT site de Khlong Ngae, Songkla [25]

Figure XV. Quelques composants de la liaison CCHT.
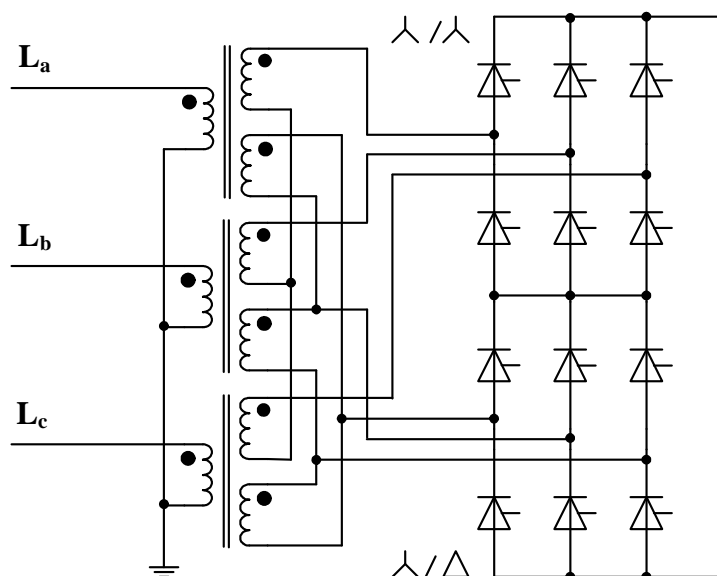
Figure XVI. Schéma de connexion des trois transformateurs monophasés.

Le chapitre se termine par la présentation du diagramme de contrôle du système (figure 2.40) sur lequel on retrouve les principes de base définis sur la figure XI.

Le bon fonctionnement de la commande du dispositif est illustré par quelques résultats expérimentaux (ou de simulation pour les derniers) permettant de montrer la réponse du système à des échelons de courant entre 920 et 1000 A (figure 2.41), à des échelons de tension entre 240 et 300 kV (figure 2.42) ou lors d'un démarrage (figures 2.43 et 2.44).

Chapitre 3 - Qualité de l'électricité et harmoniques

La qualité de l'électricité est l'objet du troisième chapitre. Son amélioration passe par l'élimination des harmoniques en traitant les sources à l'aide de solutions classiques basées sur des déphasages introduits par des connexions de bobinages de transformateur ou par des filtres passifs ou à l'aide de méthodes plus sophistiquées telle que l'utilisation de filtre actif. Le filtre actif réalisé dès 2003 par l'auteur (premier dispositif réalisé en Thaïlande utilisant un DSP) est détaillé dans ce chapitre.

La qualité de l'énergie électrique concerne les fournisseurs d'électricité, les utilisateurs et les fabricants de tout dispositif devant être connecté sur le réseau électrique. Au départ on incluait sous ce terme de nombreux phénomènes allant des creux ou des fluctuations de la tension, aux harmoniques. Cette qualité de l'énergie électrique est devenue problématique avec le développement croissant des convertisseurs de puissance qui, en apportant une souplesse de réglage de l'amplitude ou de la forme des ondes électriques, à partir du seul aiguillage du courant entre des branches adjacentes d'un convertisseur, induisent des harmoniques dont le niveau peut être important. Chaque famille de convertisseurs (redresseurs commutés par le réseau, convertisseurs DC-DC ou DC-AC à modulation, cycloconvertisseurs…) apporte son lot d'harmoniques dont les rangs et les amplitudes dépendent du mode de conversion réalisé et des fréquences de commutation des interrupteurs.

Les conséquences des harmoniques sont connues. Sur le réseau électrique lui-même, on peut voir apparaître des phénomènes de résonance, une augmentation des pertes, un vieillissement prématuré d'isolant, des interférences avec la commande de dispositifs ou des organes de sécurité… On peut aussi avoir des interférences avec les systèmes de communication ou de téléphonie.

Afin de quantifier les niveaux d'harmoniques, différents termes ont été définis : taux de distorsion harmonique, facteur de crête, facteur de puissance, coefficient de déclassement…, termes faisant l'objet de normalisation au niveau international.

Les méthodes permettant de réduire les harmoniques sont de différentes natures. La première méthode consiste à utiliser des déphasages introduits par des couplages différents d'enroulements de transformateurs. On réalise ainsi des systèmes à indice de pulsation 12, 24 ou même 48 en introduisant des déphasages respectivement de 30°, 15° et 7,5°.

La deuxième méthode limite les harmoniques au moyen de filtres passifs accordés sur une fréquence, plusieurs fréquences ou une gamme de fréquences. Ces filtres présentent aux harmoniques que l'on veut supprimer des chemins à faible impédance détournant ainsi les harmoniques du réseau d'alimentation.

La troisième méthode, plus récente, s'appuie sur des convertisseurs statiques auxiliaires que l'on appelle filtre actif. L'utilisation de convertisseurs permet de compenser globalement les harmoniques et de faire face à toute modification due à la charge alimentée. Pour cela des techniques de modulation sont utilisées afin de s'adapter en temps réel à toute modification des harmoniques que l'on désire compenser. Les structures de ces filtres actifs sont de nature série, parallèle ou hybride selon que l'on se contente de supprimer les harmoniques ou bien de compenser aussi le réactif.

L'auteur ayant au cours de ce travail de thèse réalisé un filtre actif de structure parallèle, la modélisation d'un tel filtre est détaillée ainsi que la structure de contrôle utilisée. Ce filtre est constitué d'un onduleur à IGBT placé en parallèle sur la charge non linéaire alimentée (figure XVII).
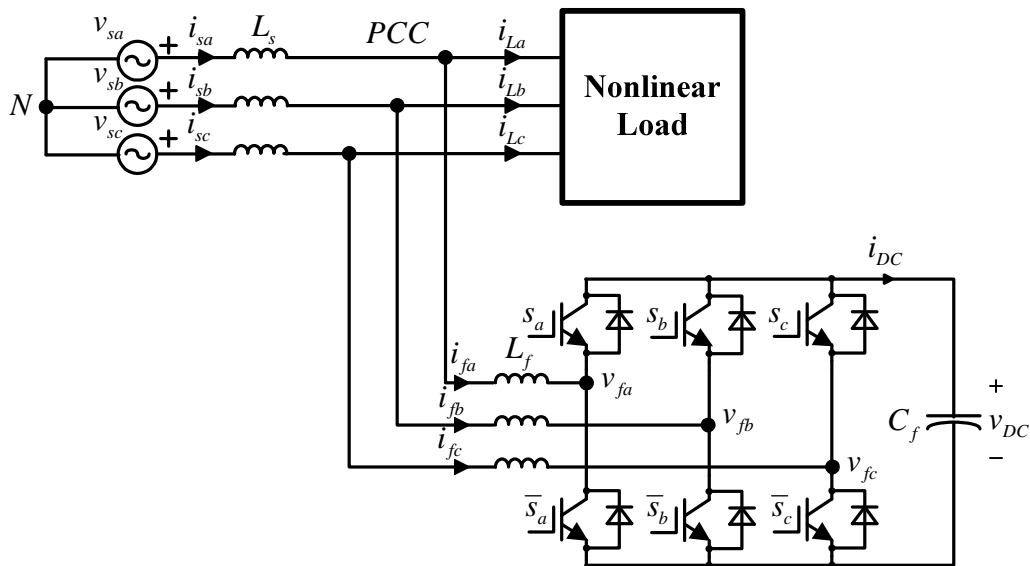
Figure XVII. Onduleur de tension utilisé comme filtre actif parallèle.

La méthode utilisée pour déterminer les références des harmoniques à compenser est dite de la puissance réactive instantanée [42], la structure du système de contrôle comportant à la

fois la détermination des références de courant devant s'opposer aux harmoniques et un contrôle de la tension aux bornes de la capacité du filtre actif.

Afin de vérifier le bon fonctionnement du filtre actif, différentes charges non linéaires sont utilisées. La première est un redresseur triphasé classique à diodes (figure XVIII). La deuxième comporte la première charge, à laquelle on a adjoint un redresseur monophasé placé sur deux phases du réseau (figure XIX). On a ainsi dans le premier cas une charge non linéaire mais équilibrée alors que dans le deuxième cas, cet équilibre est rompu.
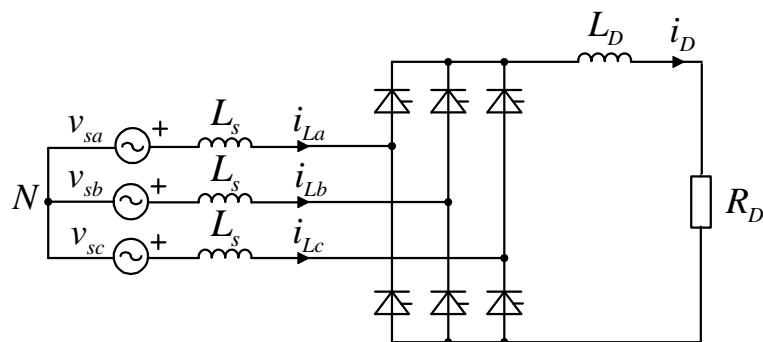
Figure XVIII. Redresseur contrôlé d'indice de pulsation 6 (ou hexaphasé).
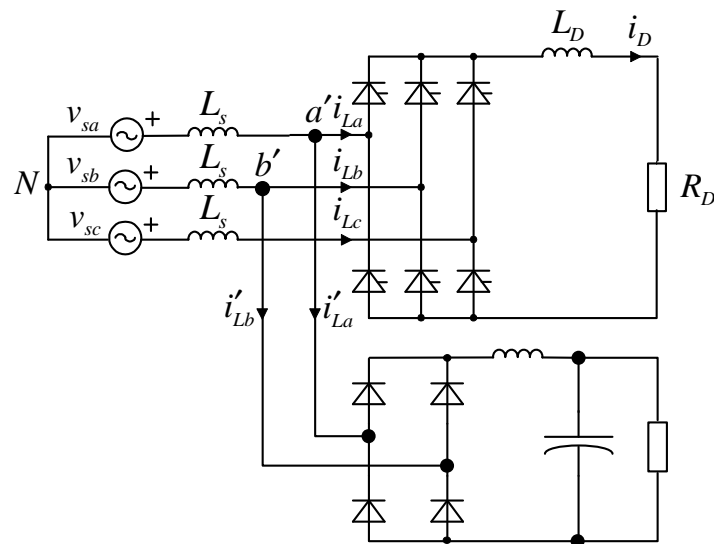
Figure XIX. Redresseur hexaphasé et redresseur monophasé.

Des résultats de simulation permettent d'illustrer le calcul des courants dans le cas de charges équilibrées (figures 3.17 et 3.18[7]) et déséquilibrées (figures 3.20 et 3.21). L'influence

---

[7] Les figures 3.n sont des figures du chapitre 3 rédigé en anglais et se trouvent dans les pages 69 à 122 du manuscrit.

de la fréquence de coupure du filtre permettant le calcul du spectre harmonique est ensuite soulignée par différents résultats de simulation qui montrent que le problème est plus difficile à résoudre lorsque la charge est déséquilibrée (figures 3.22 à 3.24). Le calcul de l'inductance et de la capacité du filtre actif en fonction des paramètres retenus comme la fréquence de découpage ou l'ondulation de courant tolérée permet de définir les éléments qui le composent.

Les différents éléments du filtre actif définis, des résultats de simulation soulignent son bon fonctionnement dans le cas de charges équilibrées (figures 3.26 et 3.27) et déséquilibrées (figures 3.28 et 3.29). La figure XX donne un exemple des résultats de simulation présentés au chapitre 3.
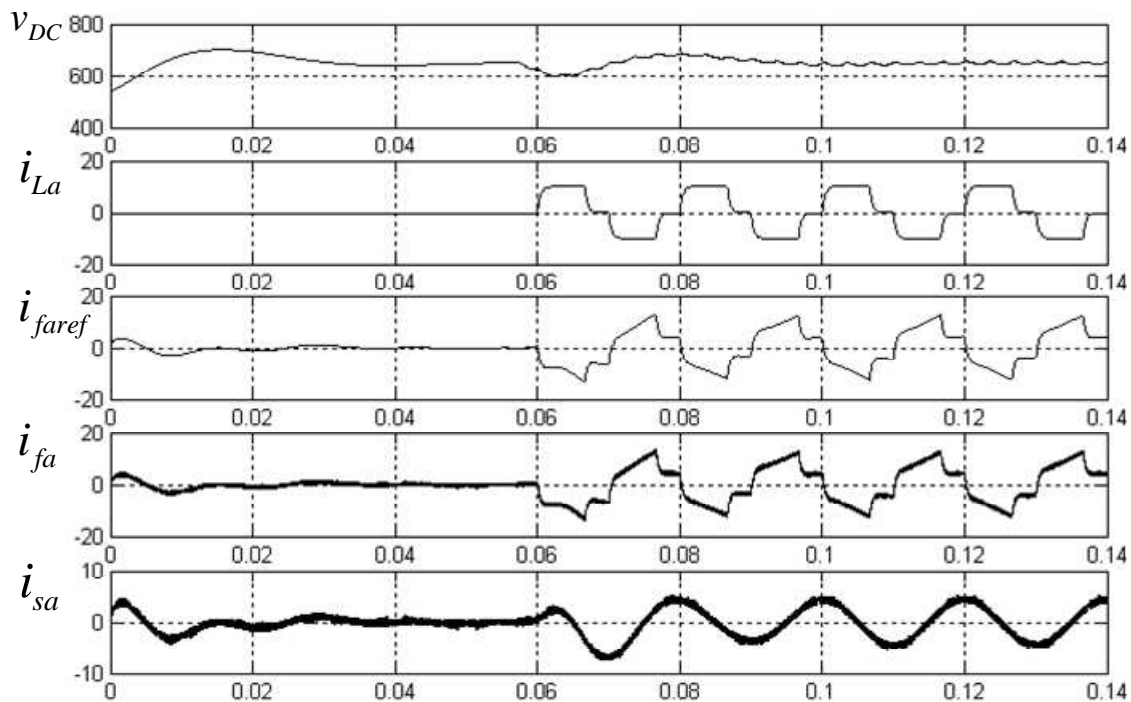
Figure XX. Réponse du filtre à un échelon de charge $i_{La} = i_{Lmax} = 12,5\,A$ ($\alpha = 0$).

Le filtre actif ainsi dimensionné a été construit, le contrôle étant réalisé à partir d'un TMS320F243 (figures XXI et XXII). Les interrupteurs utilisés sont des modules IGBT 1000 V - 50 A fonctionnant à une fréquence de découpage moyenne de 25 kHz. Différents résultats expérimentaux, formes d'onde et analyses harmoniques, soulignent le bon comportement du filtre. Deux types de charge équilibrée ont été retenus pour les essais expérimentaux. Elles sont toutes deux constituées de pont de diodes triphasés, l'étage continu étant pour la première résistif (avec la possibilité de faire varier brutalement la charge de 135 Ω à 45 Ω) et pour la

deuxième de type L-C-R. Avec la première charge il s'est agi de montrer les capacités de réagir à des variations importantes du courant de charge lors de variation brutale de la résistance. Pour la deuxième charge, pour laquelle les formes d'onde sont assez perturbées, il a été montré la forte amélioration du THD en courant qui passe d'une valeur proche de 60 % à moins de 7 %.
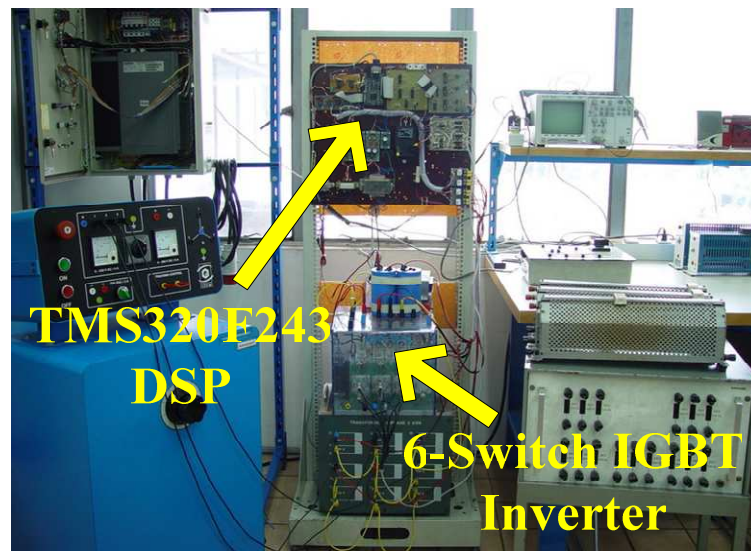
Figure XXI. Circuits de puissance et de contrôle du filtre actif.
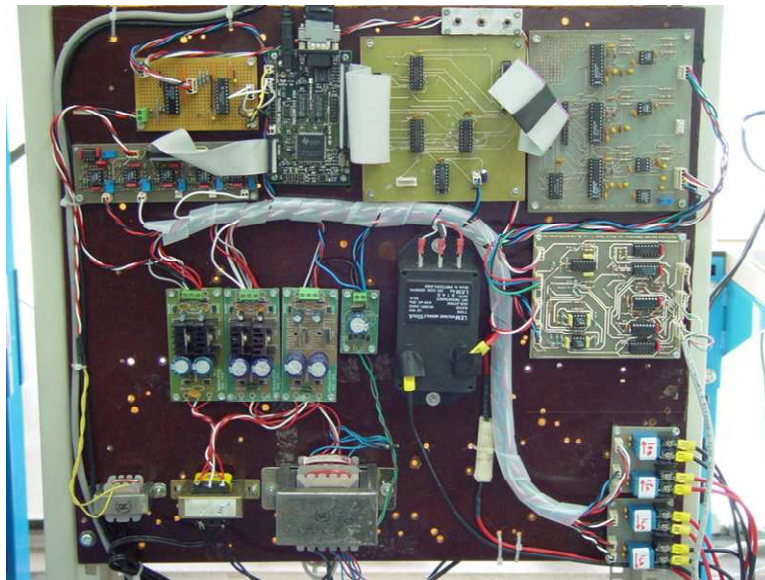
Figure XXII. DSP TMS320F243 avec ses circuits auxiliaires (convertisseur digital-analogique, détection de passage par zéro, contrôleur de courant et capteurs).

Chapitre 4 - Modélisation des convertisseurs à indice de pulsation élevé

Le quatrième chapitre propose une méthode de modélisation des convertisseurs à indice de pulsation élevé. Ces convertisseurs sont l'une des solutions utilisées pour réduire les harmoniques injectées sur le réseau. Cette solution présente de nombreux avantages par rapport aux techniques de filtrage passif ou actif en particulier en forte puissance.

Des logiciels de simulation classiques peuvent être utilisés, comme Matlab/Simulink ou SPICE, pour étudier le fonctionnement en régime permanent de tels convertisseurs. Les durées des simulations sont souvent importantes et celles-ci échouent parfois pour des raisons de stabilité numérique. De plus, les méthodes aux valeurs moyennes ne sont pas non plus d'un grand secours dès lors que l'on s'intéresse au problème d'harmoniques.

C'est donc une méthode de modélisation analytique qui est proposée pour l'étude en régime permanent de ces convertisseurs et qui permet de déterminer les différentes grandeurs tant côté continu qu'alternatif. Pour cela, on considère le plus petit intervalle de temps sur lequel apparaissent les séquences élémentaires de fonctionnement. Cette méthode a déjà été présentée pour l'étude d'un onduleur [55] et d'un redresseur [56]. Elle est ici généralisée à l'étude d'un convertisseur d'indice de pulsation p, pour lequel la largeur de l'intervalle d'étude sera réduite à $2 \cdot \pi / p$ [7-8].

A partir de la résolution du problème sur cet intervalle, les différentes grandeurs sont ensuite définies sur une période. Pour les redresseurs à indice de pulsation p, sur l'intervalle d'étude considéré, le problème se limite à l'étude de deux séquences élémentaires, une séquence de commutation et une séquence dite entre commutations.

L'utilisation d'une représentation complexe des grandeurs triphasées permet d'obtenir simplement les grandeurs côté alternatif à partir de la résolution du problème sur l'intervalle réduit.

Après la définition de la transformation de grandeurs triphasées définies en instantané en grandeurs complexes :

$$\overline{X} = \begin{bmatrix} \overline{x} \\ \overline{x}^* \end{bmatrix} = \frac{1}{\sqrt{3}} \cdot \begin{bmatrix} 1 & a & a^2 \\ 1 & a^2 & a \end{bmatrix} \cdot \begin{bmatrix} x_a \\ x_b \\ x_c \end{bmatrix} = K_s \cdot X \qquad (I)$$

il est rappelé les différentes propriétés classiques d'un redresseur alimenté à partir d'un réseau triphasé et présentant un indice de pulsation p :

- l'indice de pulsation est un multiple de 3 ;
- les harmoniques côté continu sont de pulsation $p \cdot \omega$ où ω est la pulsation du réseau triphasé ;
- les harmoniques côté alternatif sont de rang $k \cdot p \pm 1$. A partir de cette dernière propriété, il est démontré que dans le plan complexe, toute grandeur triphasée connue sur un intervalle de largeur $2 \cdot \pi / p$ est obtenue sur l'intervalle suivant par une rotation angulaire de $2 \cdot \pi / p$.

La modélisation d'un convertisseur dodécaphasé (figure XXIII) est ensuite présentée en utilisant la méthode proposée. La puissance de la modélisation en complexe apparaît dans un premier temps lorsque le fonctionnement du redresseur est supposé idéal (courant continu constant et commutation instantanée). A partir du diagramme de conduction des deux redresseurs de la figure XXIV, on obtient aisément les valeurs des différents courants sur les deux premiers intervalles élémentaires puis sur toute la période.
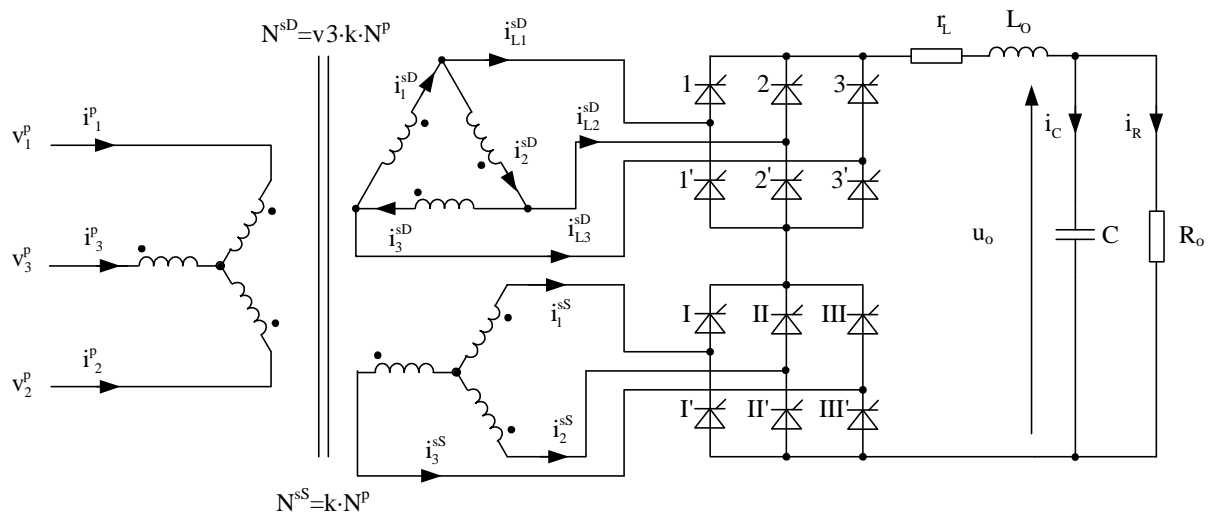
Figure XXIII. Schéma du redresseur dodécaphasé.
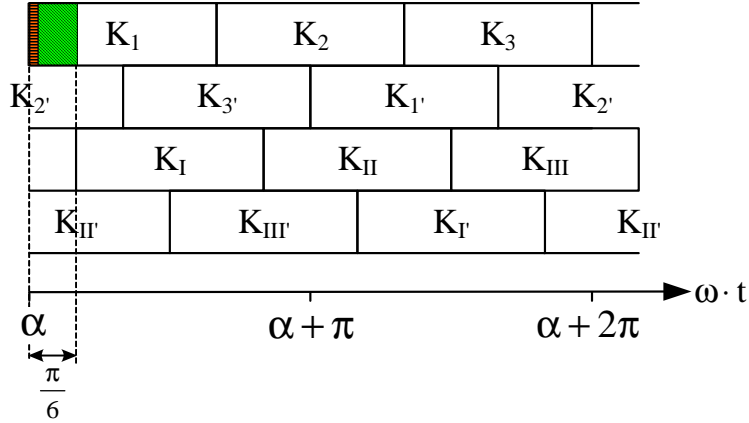
Figure XXIV. Diagramme de conduction des deux redresseurs.

On obtient ainsi sur l'intervalle $\left[0, \dfrac{\pi}{6}\right]$ suivant l'amorçage de l'interrupteur K_1 :

$$\overline{i^{sS}} = \frac{I}{\sqrt{3}} \cdot \left(-a + a^2\right) = -j \cdot I$$

$$\overline{i_L^{sD}} = \frac{I}{\sqrt{3}} \cdot \left(1 - a\right) = -a^2 \cdot \overline{i^{sS}} \tag{II}$$

$$\overline{i^{sD}} = \frac{\overline{i_L^{sD}}}{1 - a^2} = -\frac{I}{\sqrt{3}} \cdot a = -\frac{a^2}{1 - a^2} \cdot \overline{i^{sS}} = \frac{1}{\sqrt{3}} \cdot e^{j\frac{\pi}{6}} \cdot \overline{i^{sS}}$$

soit pour le courant primaire :

$$\overline{i^p} = k \cdot \frac{I}{\sqrt{3}} \cdot \left[-a + a^2 - \sqrt{3} \cdot a\right] = -k \cdot I \cdot \left(a + j\right)$$

$$= k \cdot \left(1 + e^{j\frac{\pi}{6}}\right) \cdot \overline{i^{sS}} = k \cdot \sqrt{2 + \sqrt{3}} \cdot e^{j\frac{\pi}{12}} \cdot \overline{i^{sS}} \tag{III}$$

On remarque que la connaissance du courant $\overline{i^{sS}}$ permet d'obtenir les autres courants (figure XXV). De son côté, le courant complexe $\overline{i^p}$ conduit au calcul des courants primaires :

$$i_1^p = \frac{2}{\sqrt{3}} \cdot \operatorname{Re}\left(\overline{i^p}\right) = k \cdot I \cdot \frac{1}{\sqrt{3}}$$

$$i_2^p = \frac{2}{\sqrt{3}} \cdot \operatorname{Re}\left(a^2 \cdot \overline{i^p}\right) = -k \cdot I \cdot \left(1 + \frac{2}{\sqrt{3}}\right) \tag{IV}$$

$$i_2^p = \frac{2}{\sqrt{3}} \cdot \operatorname{Re}\left(a \cdot \overline{i^p}\right) = k \cdot I \cdot \left(1 + \frac{1}{\sqrt{3}}\right)$$

XXXI
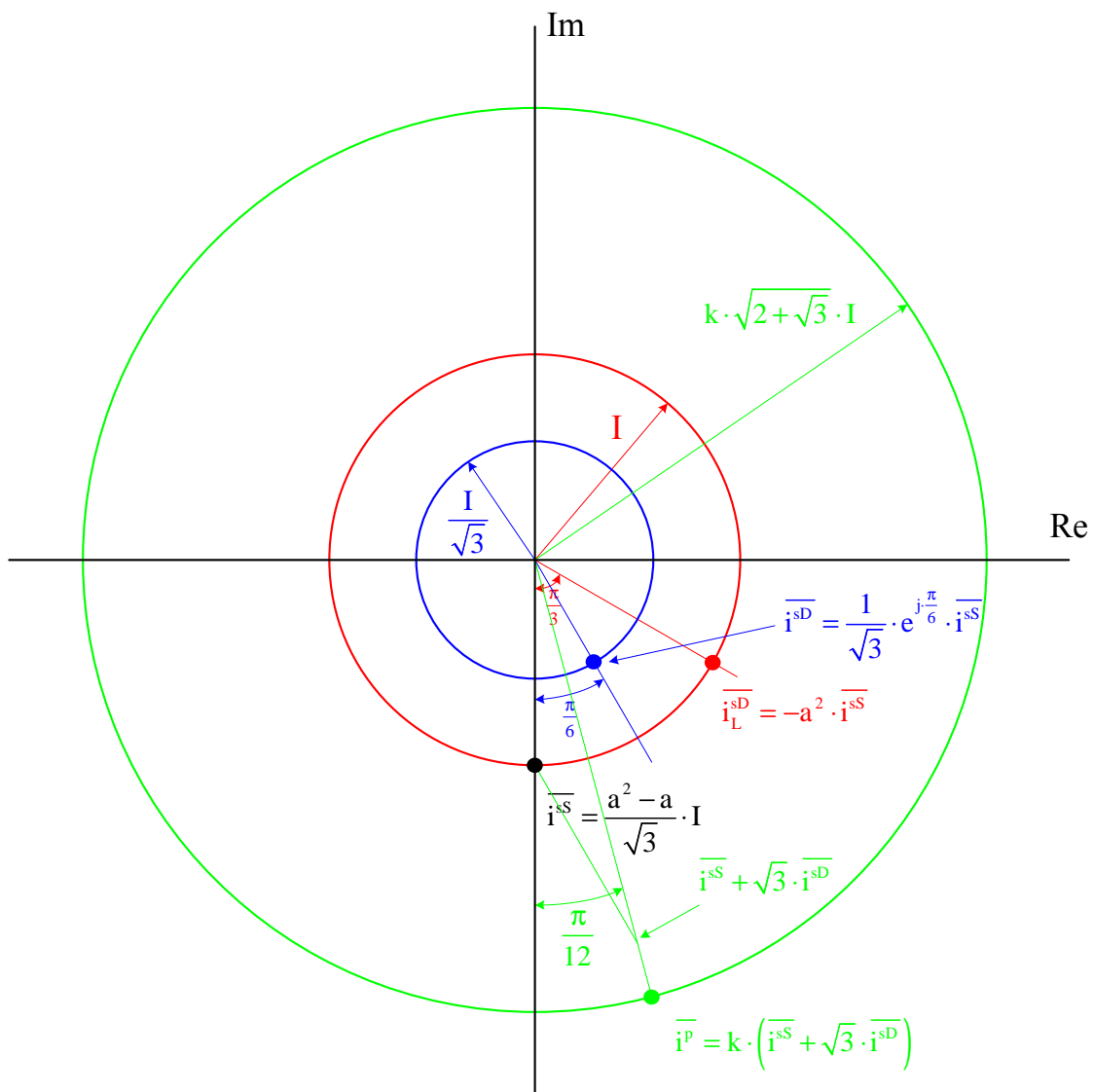
Figure XXV. Courants complexes sur l'intervalle $\left[0, \dfrac{\pi}{6}\right]$.

On peut calculer de la même façon le courant $\overline{i^p}$ sur l'intervalle $\left[\dfrac{\pi}{6}, \dfrac{\pi}{3}\right]$ et en déduire l'expression des courants primaires :

$$i_1^p = \frac{2}{\sqrt{3}} \cdot \mathrm{Re}\left(\overline{i^p}\right) = k \cdot I \cdot \left(2 + \sqrt{3}\right)$$

$$i_2^p = \frac{2}{\sqrt{3}} \cdot \mathrm{Re}\left(a^2 \cdot \overline{i^p}\right) = -k \cdot I \cdot \left(1 + \sqrt{3}\right) \tag{V}$$

$$i_3^p = \frac{2}{\sqrt{3}} \cdot \mathrm{Re}\left(a \cdot \overline{i^p}\right) = -k \cdot I$$

La connaissance des courants sur $1/6^{\text{ème}}$ ème de période permet de les calculer sur la période en utilisant la relation suivante [55] :

$$i_n^p\left(\omega \cdot t + \frac{\pi}{3}\right) = -i_{n+1}^p(\omega \cdot t) \tag{VI}$$

On obtient ainsi les courants représentés sur la figure XXVI.
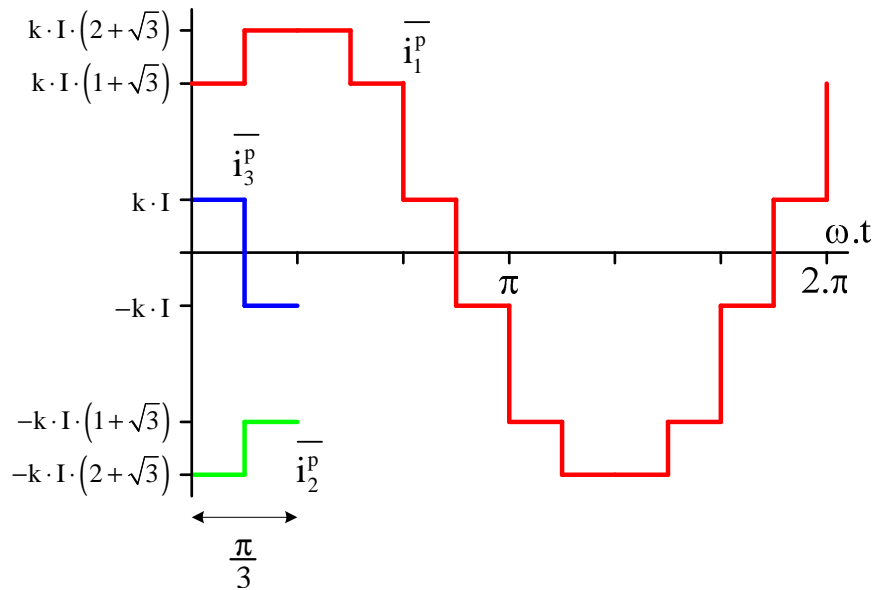
Figure XXVI. Courant dans la phase 1 du primaire (l'origine du temps correspond à l'amorçage du thyristor K_1).

Dans un deuxième temps, c'est la simulation du fonctionnement de l'ensemble du transformateur et des deux redresseurs qui est effectuée sur un intervalle de 30° (l'indice de pulsation est de 12). Deux séquences sont ainsi modélisées, une séquence de commutation et une séquence entre commutations.

Pour la séquence de commutation (figure XXVII), on aboutit au système d'équations différentielles :

$$\frac{d}{dt} X_1 = A_1 \cdot X_1 \tag{VII}$$

XXXIII

où :
$$X_1 = \begin{bmatrix} i_1^{sD} \\ \overline{I^p} \\ i_L \\ v_C \\ e^{j \cdot \omega \cdot t} \\ e^{-j \cdot \omega \cdot t} \end{bmatrix}$$
(VIII)
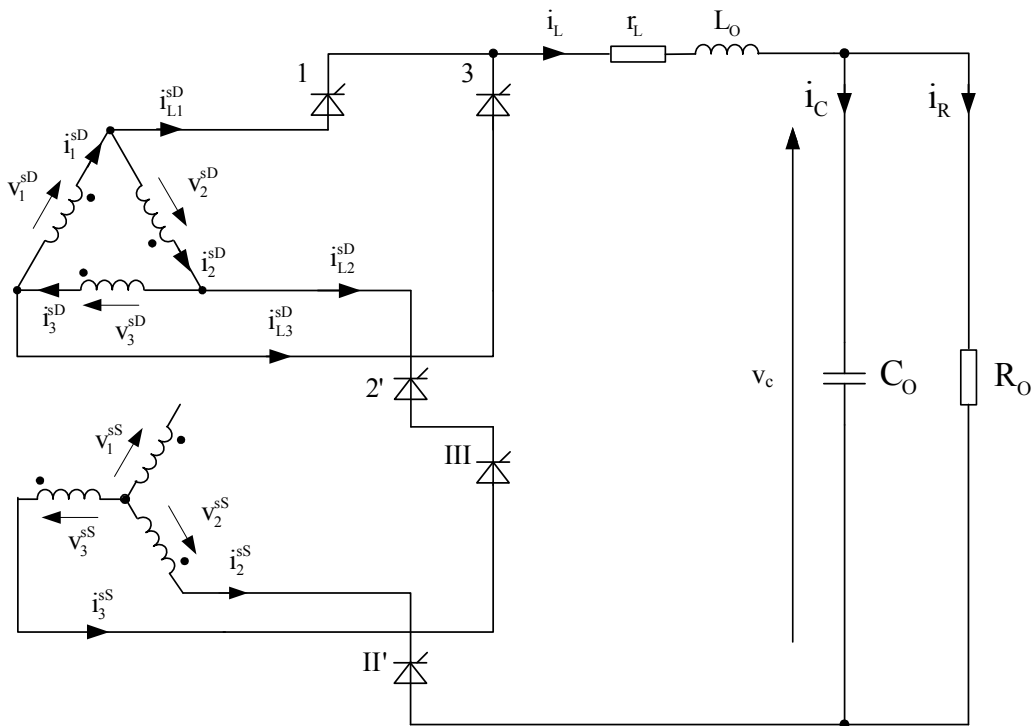
Figure XXVII. Schéma au secondaire lors de la commutation.

Ce système d'équations comporte sept variables d'état :

- i_1^{sD}, le courant dans un des enroulements secondaires concernés par la commutation ;

- Les deux composantes du courant primaire complexe $\overline{I^p}$;

- i_L, le courant dans l'inductance de l'étage continu ;

- v_C, la tension aux bornes de la capacité de l'étage continu ;

- Les termes $e^{j \cdot \omega \cdot t}$ et $e^{-j \cdot \omega \cdot t}$ qui permettent de faire entrer les termes sources (tension d'alimentation du réseau alternatif) dans le vecteur d'état et d'obtenir ainsi une solution analytique simple de l'équation différentielle :

$$X_1(t) = e^{A_1 \cdot (t-t_0)} \cdot X_1(t_0) \tag{IX}$$

où t_0 est l'instant d'amorçage de l'interrupteur K_1.

Pour la séquence entre commutations (figure XXVIII), tous les courants au secondaire peuvent être déduits du courant dans l'inductance.
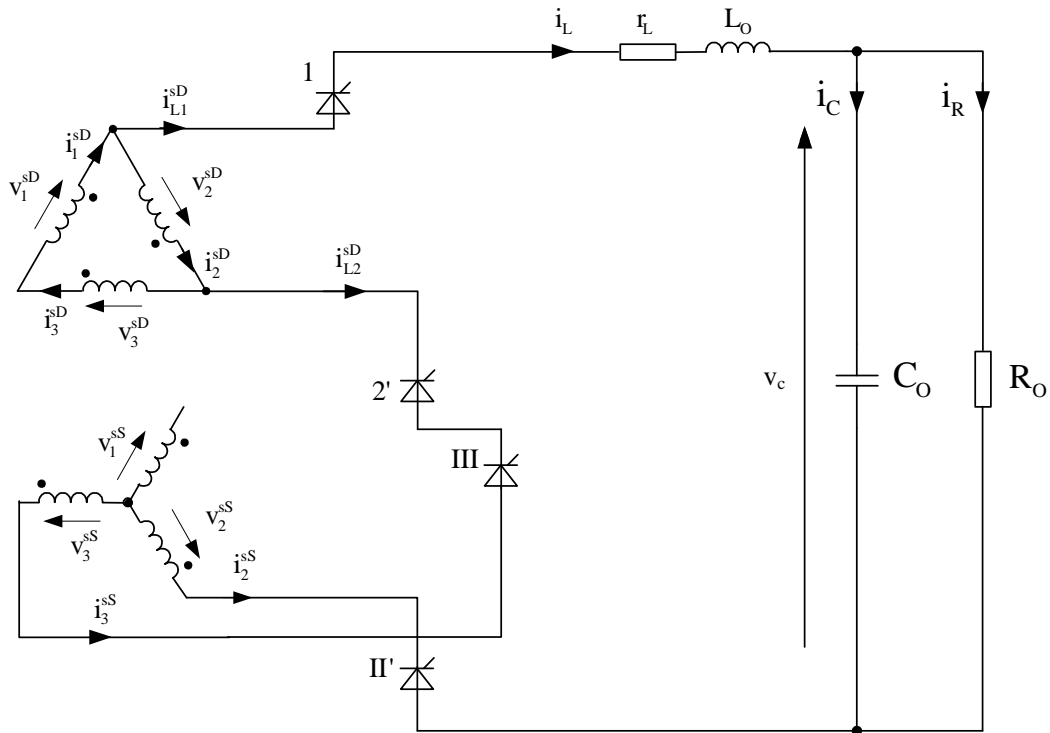
Figure XXVIII. Schéma au secondaire en dehors des commutations.

Le système d'équations différentielles ne comporte plus que six variables d'état, le courant i_1^{sD}, étant maintenant lié à i_L :

$$\frac{d}{dt}X_2 = A_2 X_2 \tag{X}$$

où :

$$X_2 = \begin{bmatrix} \overline{I^p} \\ i_L \\ v_C \\ e^{j \cdot \omega \cdot t} \\ e^{-j \cdot \omega \cdot t} \end{bmatrix} \tag{XI}$$

et :

$$X_2(t) = e^{A_2 \cdot (t-t_1)} X_2(t_1) \tag{XII}$$

où t_1 est l'instant de fin de commutation (instant de blocage de l'interrupteur K_3), le vecteur d'état initial $X_2(t_1)$ étant obtenu en supprimant l'élément i_1^{sD} du vecteur d'état final de la séquence précédente :

$$X_2(t_1) = N_1 \cdot X_1(t_1) = N_1 \cdot e^{A(t_1-t_0)} X_1(t_0) \tag{XIII}$$

où :

$$N_1 = \begin{bmatrix} 0 & 1 & 0 & 0 & 0 & 0 & 0 \\ 0 & 0 & 1 & 0 & 0 & 0 & 0 \\ 0 & 0 & 0 & 1 & 0 & 0 & 0 \\ 0 & 0 & 0 & 0 & 1 & 0 & 0 \\ 0 & 0 & 0 & 0 & 0 & 1 & 0 \\ 0 & 0 & 0 & 0 & 0 & 0 & 1 \end{bmatrix} \tag{XIV}$$

La résolution analytique des deux systèmes d'équations différentielles nécessite de connaître les valeurs initiales des variables au début de la séquence de commutation ainsi que la durée de cette séquence. On a ainsi quatre inconnues liées par quatre relations :

- pour le courant primaire complexe $\overline{I^p}$, il suffit d'écrire que le courant à la fin de l'intervalle d'étude est déduit de sa valeur initiale par une rotation de $\pi/6$ (redresseur dodécaphasé) :

$$\overline{i^p}(t_0) \cdot e^{j \cdot \frac{\pi}{6}} = G_1 \cdot e^{A_2 \cdot \left(\frac{1}{12 \cdot f} - T_C\right)} \cdot N_1 \cdot e^{A_1 \cdot T_C} \cdot X_1(t_0)$$
$$\overline{i^p}(t_0)^* \cdot e^{-j \cdot \frac{\pi}{6}} = G_2 \cdot e^{A_2 \cdot \left(\frac{1}{12 \cdot f} - T_C\right)} \cdot N_1 \cdot e^{A_1 \cdot T_C} \cdot X_1(t_0) \tag{XV}$$

où :

$$G_1 = \begin{bmatrix} 1 & 0 & 0 & 0 & 0 & 0 \end{bmatrix}$$
$$G_2 = \begin{bmatrix} 0 & 1 & 0 & 0 & 0 & 0 \end{bmatrix} \tag{XVI}$$

- pour le courant dans l'inductance et la tension aux bornes de la capacité, ce sont les valeurs initiales et finales au niveau de l'intervalle d'étude qui sont égales :

$$i_L(t_0) = G_3 \cdot e^{A_2 \cdot \left(\frac{1}{12 \cdot f} - T_C\right)} \cdot N_1 \cdot e^{A_1 \cdot T_C} \cdot X_1(t_0)$$
$$v_C(t_0) = G_4 \cdot e^{A_2 \cdot \left(\frac{1}{12 \cdot f} - T_C\right)} \cdot N_1 \cdot e^{A_1 \cdot T_C} \cdot X_1(t_0) \tag{XVII}$$

où :

$$G_3 = \begin{bmatrix} 0 & 0 & 1 & 0 & 0 & 0 \end{bmatrix}$$
$$G_4 = \begin{bmatrix} 0 & 0 & 0 & 1 & 0 & 0 \end{bmatrix}$$
(XVIII)

- la durée de la commutation est obtenue en écrivant que le thyristor K_3 de la figure XXVII se bloque lorsque le courant i_{L1}^{sD} est égal au courant i_L. On a alors la relation suivante :

$$\overline{i_1^{sD}} = \frac{2}{\sqrt{3}} \cdot Re\left(\overline{i^{sD}}\right) = \frac{2}{\sqrt{3}} \cdot Re\left(-\frac{1}{\sqrt{3}} \cdot a \cdot i_L\right) = \frac{1}{3} \cdot i_L$$
(XIX)

soit :

$$M_1 e^{A_1 \cdot T_C} \cdot X_1(t_0) = 0$$
(XX)

où :

$$M_1 = \begin{bmatrix} 1 & 0 & 0 & -\dfrac{1}{3} & 0 & 0 & 0 \end{bmatrix}$$
(XXI)

Ces relations définissent un système d'équations non linéaires que l'on peut résoudre à l'aide de la méthode de Raphson-Newton. Cette méthode nécessite le calcul d'une fonction jacobienne qui est effectué de façon analytique à partir des relations entre grandeurs inconnues.

Deux exemples de simulation, correspondant à des angles de retard à l'amorçage différents, sont ensuite présentés où les différentes grandeurs sur une période sont déduites des calculs effectués sur l'intervalle élémentaire de 30°. Les figures XXIX à XXXI illustrent les résultats obtenus pour un angle de retard à l'amorçage de 40°.
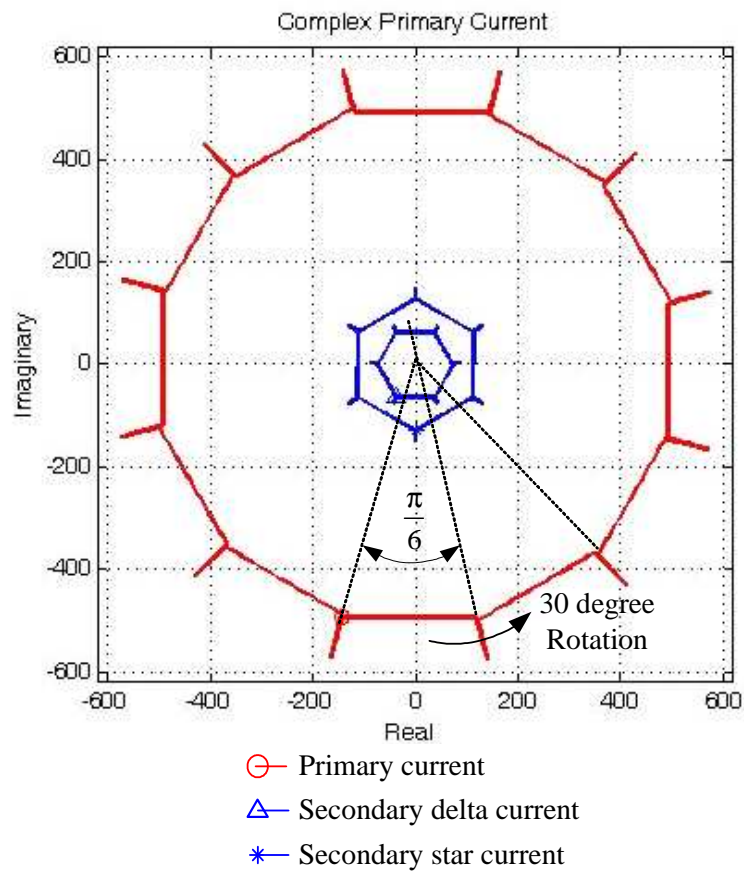
Figure XXIX. Trajectoire du courant dans le plan complexe pour $\alpha = 40°$.
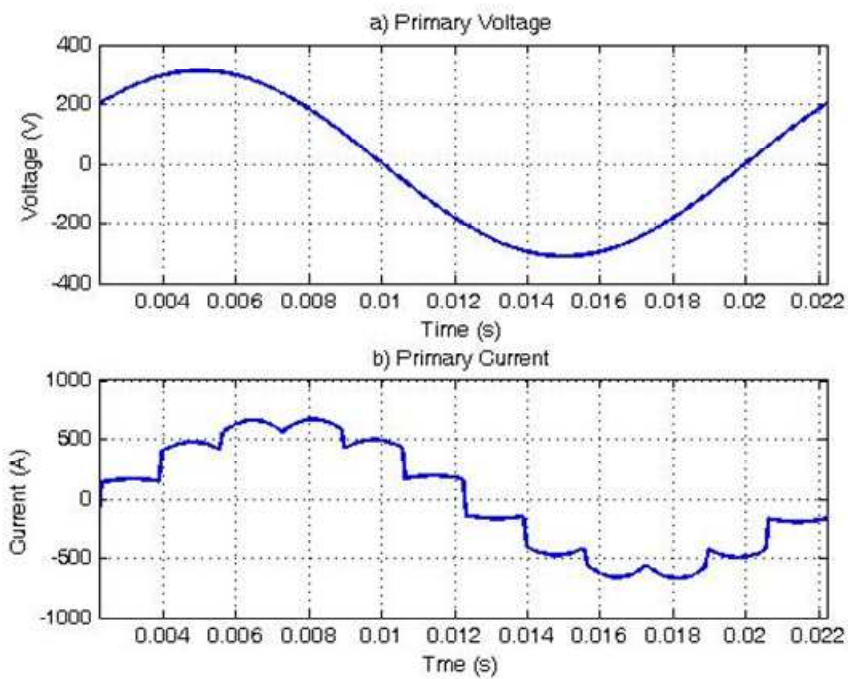
Figure XXX. Tension et courant au primaire du transformateur ($\alpha = 40°$).
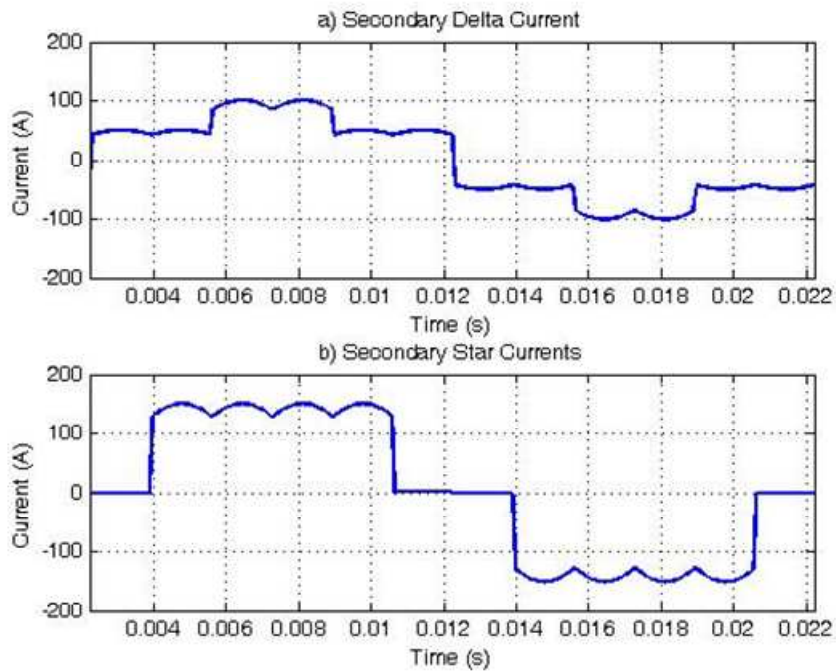
Figure XXXI. Courants dans les enroulements secondaires du transformateur ($\alpha = 40°$).

La dernière partie du chapitre permet de montrer que des grandeurs intégrales peuvent aisément être déduites de la solution analytique obtenue sur l'intervalle de 30°. C'est le cas des valeurs moyennes des grandeurs côté continu, comme le courant moyen dans l'inductance ou la tension moyenne aux bornes de la capacité. C'est aussi le cas des harmoniques côté alternatif qui s'obtiennent aisément, en dehors de la composante fondamentale pour laquelle la matrice à inverser dans le processus d'intégration s'avère singulière et pour lequel le calcul de la composante fondamentale est fait de façon légèrement différente.

Conclusion

La principale compagnie en charge de la production et du transport de l'électricité en Thaïlande est l'EGAT (*Electricity Generating Authority of Thailand*). L'EGAT est une société d'état dont la capacité de production est de l'ordre de 28 000 MW pour une production annuelle de 117 000 GWh. Malgré tout cette société ne fournit que 59 % de la production. Le reste vient de producteurs privés ou de pays étrangers.

EGAT est aussi en charge du transport de l'électricité. Un réseau d'une longueur de 28 000 km couvre le pays et délivre une tension de 500, 230 ou 115 kV. Ce réseau est interconnecté avec les pays voisins. Les principales connexions sont avec le Laos (en 115 et 230 kV) et la Malaisie (en 115 et 132 kV et 300 kV en CCHT). Une connexion CCHT en 500 kV est en projet avec la Chine.

La réalisation de la liaison CCHT entre la Thaïlande et la Malaisie a commencé en 1997. Cette liaison 300/600 kV permet un échange entre les réseaux des deux pays dans les deux sens. Il s'agit d'une liaison bipolaire dans son projet mais seul la configuration unipolaire est actuellement opérationnelle. Les convertisseurs de puissance sont des convertisseurs hexaphasés classiques mis en série afin de réaliser un convertisseur dodécaphasé. Chaque interrupteur comporte 48 thyristors en série, soit un total de 576 thyristors pour le convertisseur dodécaphasé. Malgré sa structure ce convertisseur produit des harmoniques sur le réseau alternatif.

Outre une description détaillée de cette liaison CCHT, cette thèse a rappelé les trois méthodes permettant de supprimer ces harmoniques. La première consiste à utiliser des déphasages introduits par des connexions d'enroulements de transformateurs. La deuxième utilise les chemins à faible impédance de filtres passifs dédiés à des harmoniques particuliers. La troisième à l'aide de filtre actif injecte des courants destinés à annuler, au niveau du réseau, les harmoniques produits par une source non linéaire.

Les filtres actifs sont créés à base de convertisseur statique et utilisent un élément de stockage d'énergie (une capacité dans le cas d'utilisation d'un onduleur de tension) pour générer les courants destinés à annuler les harmoniques de la charge. Un exemple de filtre développé au TFII a été présenté et a permis lors de sa connexion en parallèle sur un redresseur hexaphasé de réduire fortement le THD en courant.

Les fréquences nécessaires pour les commutations des interrupteurs du filtre actif devant être assez importantes, en très forte puissance on préfère utiliser, pour la suppression des harmoniques de rang bas, les déphasages introduits par des connexions d'enroulements secondaires de transformateur. C'est le cas par exemple pour la liaison CCHT Thaïlande - Malaisie où les convertisseurs sont de type dodécaphasé et introduisent un indice de pulsation 12 sur l'étage continu. Dans ce cas, on a besoin d'un déphasage de 30° des formes d'onde, déphasage obtenu en connectant en étoile le premier enroulement secondaire d'un transformateur et en triangle le second.

Afin d'étudier ce type de convertisseurs à indice de pulsation élevé, une méthode de modélisation originale a été développée. Celle-ci est basée sur une mise en équation analytique du problème sur un intervalle de largeur $2 \cdot \pi / p$ où p est l'indice de pulsation du convertisseur. Cette méthode permet de déterminer l'évolution en régime permanent des grandeurs tant côté continu qu'alternatif à l'échelle de la période de fonctionnement. Elle autorise aussi un calcul simple de diverses grandeurs intégrales, valeurs moyennes côté continu et harmoniques côté alternatif, et permet de souligner l'impact de la commutation des thyristors sur ces grandeurs moyennes ou spectres harmoniques.

Introduction

The problems related to the quality and stability of electrical power system have been taking importance due to the increasing numbers and power rating of the highly nonlinear load that are currently used in industries [1]. Power system distortion result in major losses and hazards in many different activities, for example, automated manufacturing process industries, communication systems, airports and hospitals. Beside the loads, the power system configuration can also cause harmonics in the system and High Voltage Direct Current (HVDC) interconnection is a clear example of that.

HVDC often has economic advantage for bulk transmission of electrical power between long distance compared with the conventional AC transmission [2], [3]. A recent example is the Thailand-Malaysia HVDC interconnection system which was begun in 1997. The system is 300/600 MW grid interconnected and is 110 km long. Since a power electronic converter is needed at each end of the transmission line, large amount of harmonics is generated on both side of the system. So that, some kind of harmonics mitigation for HVDC systems is needed.

The simplest harmonics mitigation is to use a passive filter. The passive filter provides a low impedance path for some certain harmonic frequency, so that, the harmonic is shorted-circuit at the HVDC station. Since one set of passive filter suppress harmonic only for a certain frequency, multiple set of filter is needed for eliminate a wide range of harmonics.

Another solution is to use an active filter. The active filter can be used both on DC and AC side [4]. The first active AC side filter for HVDC system was installed by Siemens in 1998 as a demonstration project at HVDC Converter Station in Denmark [3]. More than fourteen active filters have been installed at HVDC station worldwide. The installed filter ranges were from 0.6 to 22 MVA. The principle of the active filter is to generate an inverted harmonic waveform and to inject it into the system to cancel the existed harmonics. In order to have an arbitrary inverted harmonic waveform, the power electronics devices and PWM modulation is used. The control can be done by Digital Signal Processor (DSP) [5]. The configuration and control scheme of the active filter are still interested to many researchers. More details of its operation, control and prototypes can be found in this thesis.

Beside the mentioned method, the phase shifting transformer also can be used to suppress harmonics. The most common phase shifting transformer is Y/Δ which shifts the voltage output for π/6 degrees. This kind of transformer can be used to form the twelve-pulse operation which significantly reduces AC side harmonics [6].

This thesis is organized in four chapters, the first chapter deals with the presentation of the production, transmission and distribution system of electricity in Thailand.

The second chapter provides information on basic types of HVDC interconnection systems which are installed in the world today. Then, the 300/600 MW Thailand-Malaysia HVDC interconnection project will be discussed as an example.

The third chapter is concerned with the presentation of the power quality, especially harmonics problems, harmonics sources, harmonics effects and the solutions to improve its quality such as phase shifting and passive filter. The active harmonic filter is one of the most sophisticated solutions to harmonic problems, so that, the detailed information and realized example will be presented.

The fourth chapter presents an analytical based method for modelling multipulse converters such as 12-pulse converter which appears in HVDC interconnection. The model is based on an exact analytical solution of the state problem [7-8]. By using symmetrical properties, the whole period operation can be reduced into two sequences; nevertheless, the result model gives the full information both in time domain and frequency domain.

<div align="right">

Chapter 1

</div>

Production, Transmission and Distribution of Electricity in Thailand

1.1. Introduction

This first chapter deals with the presentation of the production, transmission and distribution system of electricity in Thailand. Then the efforts which are made to improve the quality of the delivered energy are detailed.

Thailand has followed the evolution of many countries. Producers and distributors are regrouped in the 60s in state companies, the only ones able to realize the huge investments necessary to modernize the network and the means of production. The originality of Thailand is, from the beginning, the separation of the tasks of production-transmission and distribution.

During the last ten years, these state companies are under programs or projects of privatization, particularly for the means of production.

As in many countries [9], the 90s have seen the development of an explicit power quality regulation regarding harmonics and flicker.

1.2. Electricity market in Thailand

1.2.1. Production, transmission and distribution system

The main company in charge of production and transmission of electricity in Thailand is EGAT (Electricity Generating Authority of Thailand, [10]). EGAT is a state company in charge of production and transmission of electricity within the country. Other producers sell electricity to EGAT and are independent producers (Independent Power Producers, IPP) or small producers (Small Power Producers, SPP). Most of the produced electricity is carried by

EGAT network before being delivered in the area of Bangkok by MEA (Metropolitan Electricity Authority) or in the Thai provinces by PEA (Provincial Electricity Authority).

The market organisation is directed by EPPO (Energy Policy and Planning Office) under the responsibility of the Ministry of Energy (Fig. 1.1).
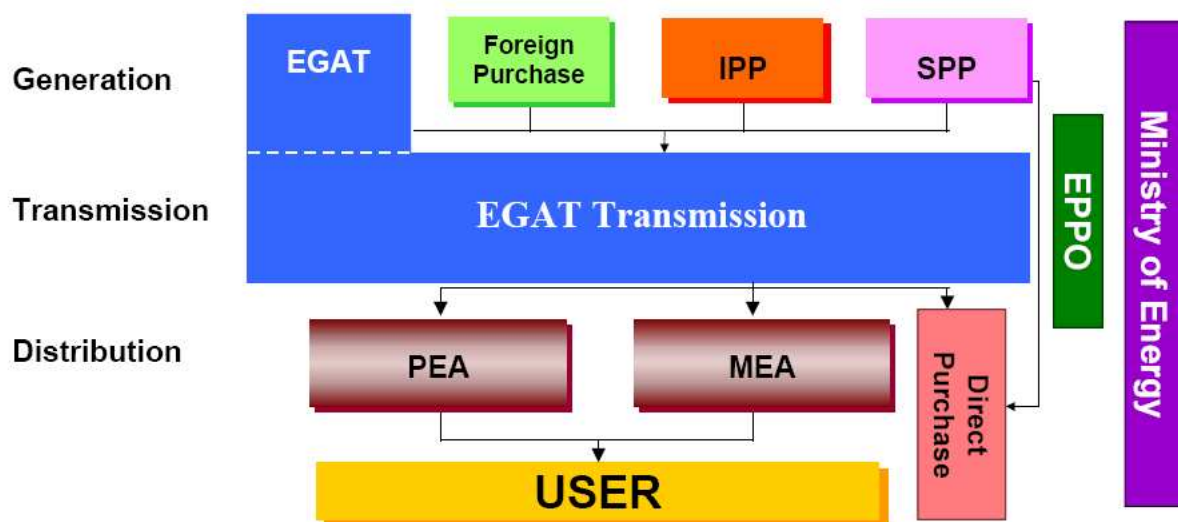
EGAT : Electricity Generating Authority of Thailand
PEA : Provincial Electricity Authority
MEA : Metropolitan Electricity Authority
IPP : Independent Power Producer
SPP : Small Power Producer
EPPO : Energy Policy and Planning Office

Fig. 1.1. Electricity market in Thailand [11].

Figure 1.1. Structure du marché de l'électricité en Thaïlande [11].

EGAT has been created the 1st may 1969 under the responsibility of the Ministry of Energy and has regrouped the activity of three state companies which previously share the production and distribution of electricity: YEA (Yanhee Electricity Authority), LA (Lignite Authority) and NEA (Northeast Electricity Authority).

Missions of EGAT were:
- To generate, acquire, transmit electric energy to the Metropolitan Electricity Authority (MEA) and the Provincial Electricity (PEA);
- To promote the production and use of electricity.

To these activities was added the necessity to promote the use of lignite. This obligation being justified by the existence of important lignite mines in north of Thailand (Mae Moh) which are mainly used to feed thermal power plants.

EGAT has the ambition to become the leading company for transmission and production of Electricity in the ASEAN[1] region.

1.2.2. Production of electricity

EGAT has a production capacity of about 28 000 MW for an annual production of 117 000 GWh[2]. 59 % of this capacity come from EGAT power plants. Others come from private producers or foreign countries (Fig. 1.2). A new operator RATCH appears on this picture. It has been created in 2000 by the privatisation of EGAT power plants (see Section 1.2.5.).

The actual capacity is sufficient and the maximum of the production (or of the consumption) is between March and May during the hot season. It is quite far from the maximal capacity of the country (Fig. 1.3). Nevertheless, an increase of 6 to 7% every year necessitates constant new investments (the capacity of production must be of 35 000 MW in 2010, [11]).

This encourages Thailand to develop different projects with the neighbouring countries. A Memorandum of Understanding has been signed with Laos in 1993 on the possibility to buy 1 500 MW in 2000 and 3 000 MW in 2006. Another one has been signed with China (1 500 MW in 2013, 3 000 MW en 2018). With Myanmar and Cambodia the possibility to buy them electricity will appear after 2010. Before, Thailand responds to the lack of electricity in these two countries by selling them electricity.

---

[1] ASEAN means the Association of Southeast Asian Nations. ASEAN was established on 8 August 1967 in Bangkok by the five original Member Countries, namely, Indonesia, Malaysia, Philippines, Singapore, and Thailand. Brunei Darussalam joined on 8 January 1984, Vietnam on 28 July 1995, Lao PDR and Myanmar on 23 July 1997, and Cambodia on 30 April 1999. The ASEAN region has a population of about 500 million, a total area of 4.5 million square kilometers, a combined gross domestic product of almost US$ 700 billion, and a total trade of about US$ 850 billion.

[2] Fiscal year 2003, October 2002 – September 2003.
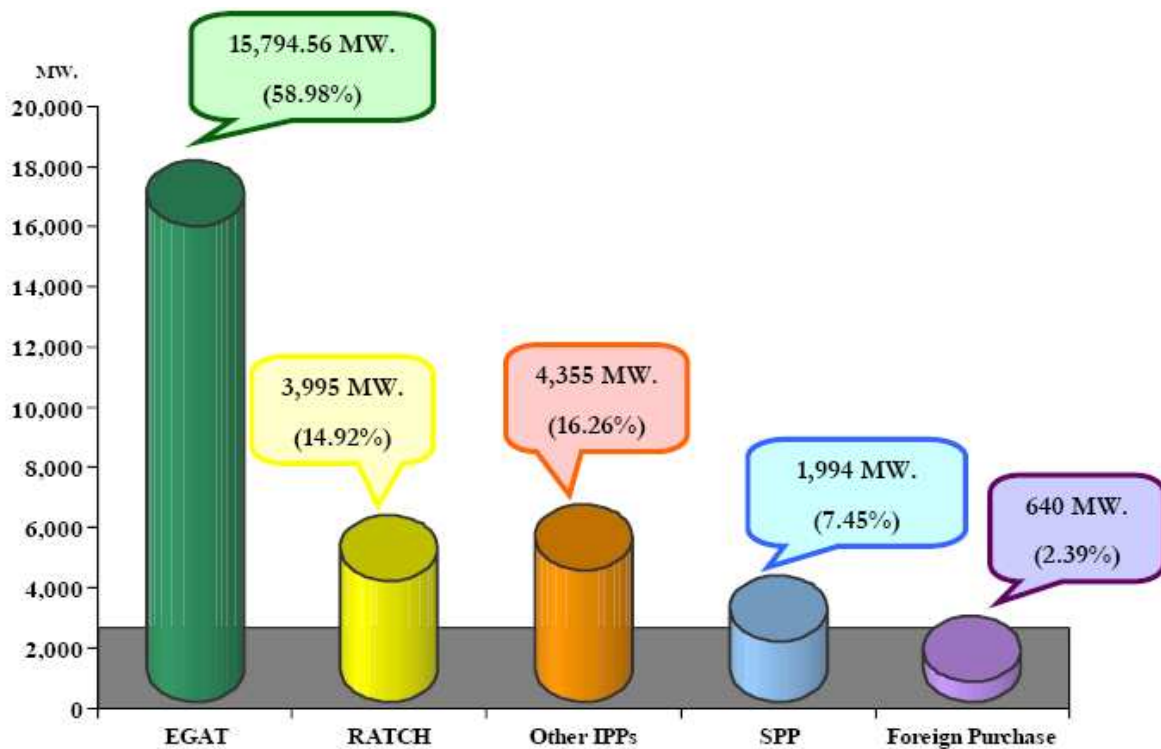
Fig. 1.2. Total installed capacity in April 2005 [11].

Figure 1.2. Capacité de production d'électricité en avril 2005 [11].

Generation is based on diversified fuels with an emphasis on the utilization of indigenous resources as natural gas, lignite and hydropower witch are at the origin of more than 85 % of the produced electricity (Fig. 1.4).

Generally, thermal power plants provide base load energy while hydro power plants perform peaking and backup functions.

The main thermal power plants are disseminated all other the country according to resources and consumption needs (Fig. 1.5 and 1.6).

The Bang Pakong power plant, located in south of Bangkok, is actually the most modern in Thailand. With a capacity of 4 000 MW it is the biggest power plant. Its development has followed the discovery of natural gas in the Gulf of Thailand. 70 % of the production of this plant is coming from classical thermal plant, the other 30 % coming from combined cycle plant. It uses natural gas or petrol. The generator cooling uses hydrogen produced in Bang Pakong. The hydrogen production is of 45 m^3 per hour and is used for the cooling of other plants of Bangkok area. A training centre provides services to EGAT staff but also to domestic industries and power utilities from neighbouring countries.
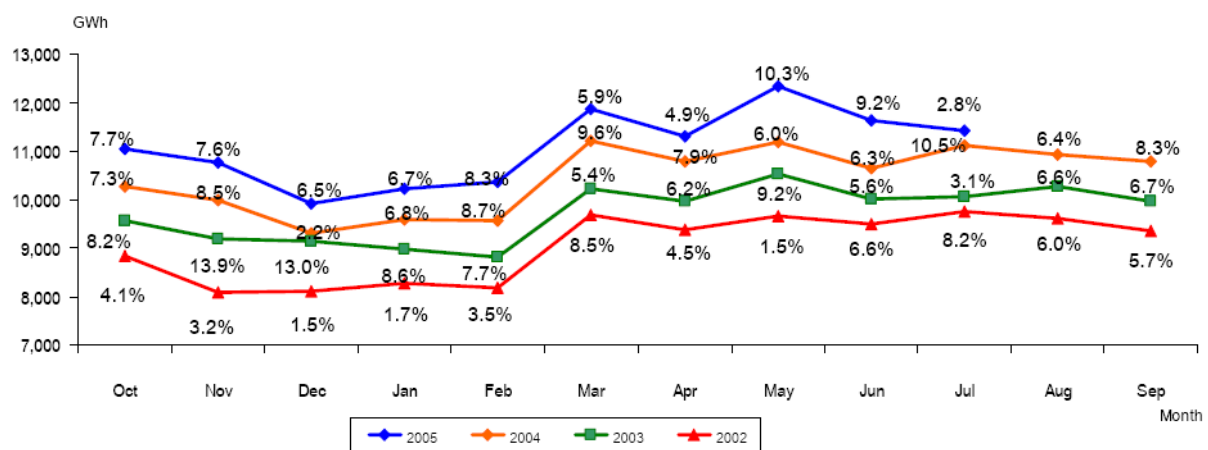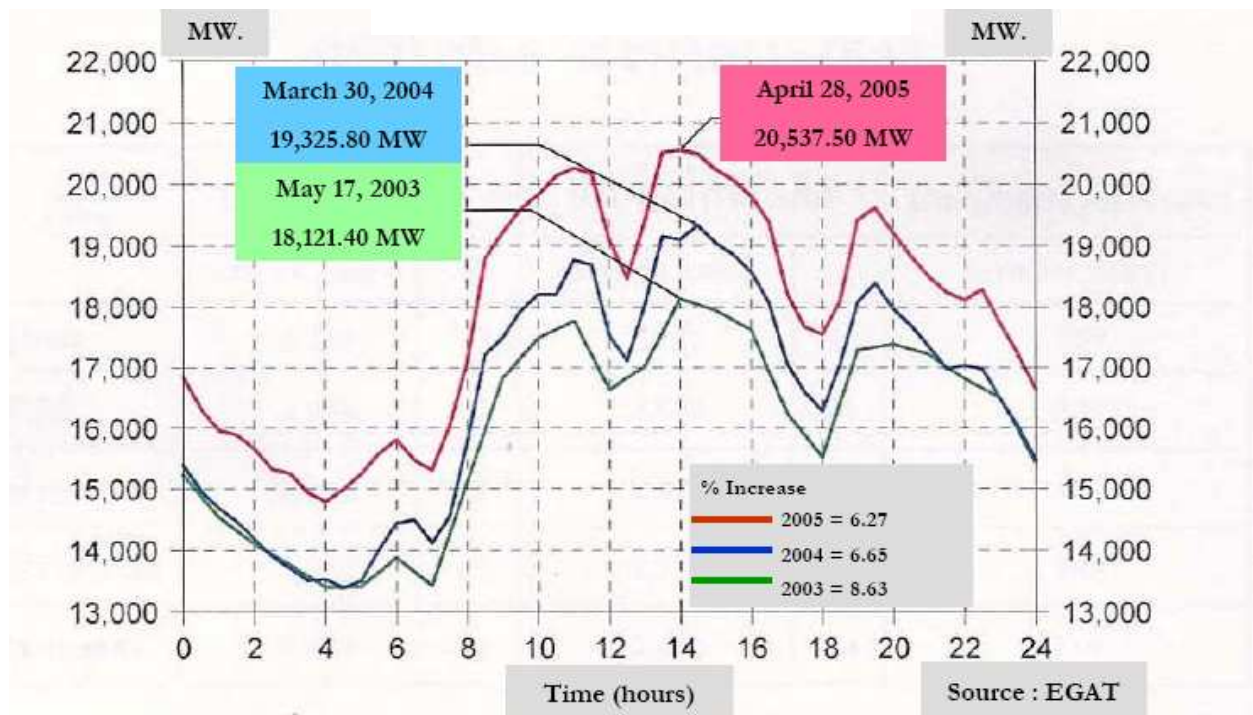
Fig. 1.3. Peak generation (top) and monthly generation (bottom[3]) [11].

Figure 1.3. Maximum de production (en haut) et production mensuelle (en bas)[4] [11].

The hydroelectricity capacity represents 6 % of the total installed capacity and concerns units located in west, north-west or north-east of Thailand. Theses power plants are small power ones (between 6 to 40 MW) except the 500 MW pumped storage power plant of Lam Takhong (Nakhom Ratchasima Province, north-east of Thailand) and the 136 MW "run-of-river[5] " dam of Pak Mun (d'Ubon Ratchathani Province, north-east of Thailand) built on the Mun river before its confluence with the Mekong River.

---

[3] Numbers on curves correspond to the increase according to the previous year.
[4] Les nombres sur les courbes correspondent à l'accroissement par rapport à l'année précédente.
[5] This plant utilizes the flow of water within the natural range of the river.
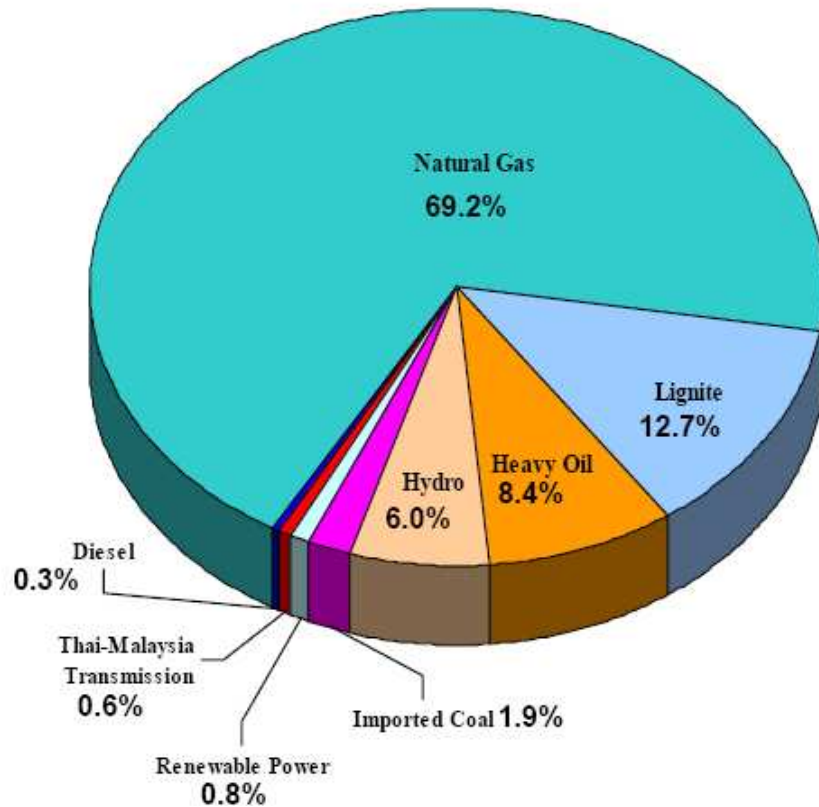
Fig. 1.4. Generation classified by fuel types [11].

Figure 1.4. Production par type d'énergie primaire [11].

Renewable energies are not well represented in the generation capacities. They appear mainly in testing projects of EGAT:

- Realisation of a 300 kW geothermal power plant which is in operation since 1989 ;
- Installation in 2000 on 62 different sites of 70 kW of solar cells;
- Installation of 150 kW wind turbine generator en Phuket Island in 1996 and EGAT plant to install large wind turbine generation with capacity of 2250 kW (3 x 750 kW) in 2008.

1.2.3. Transmission of electricity

EGAT is responsible for the transmission of electricity. A 28 000 km network covers the country with three voltage levels 500, 230 and 115 kV. The national control centre is based in Bangkok and controls the production (from EGAT and other producers) with the help of five regional centres which divided the country in five zones: metropolitan, central, northeastern, southern and northern regions.

1. Bang Pakong
2. Mae Moh
3. South Bangkok
4. Wang Noi
5. Nam Phong
6. Nong Chok
7. Sai Noi
8. North Bangkok
9. Surat Thani
10. Lan Krabue
11. Ratchaburi
12. Mae Hong Son
13. Krabi
14. Surat Thani
15. Thap Sakae

Fig. 1.5. Main thermal EGAT power plants [12].

Figure 1.5. Principales centrales d'EGAT [12].

EGAT network is interconnected with the neighbouring countries. The main connections are with Laos (115 and 230 kV, [13]) and Malaysia (115 and 132 kV, 300 kV in HVDC, [14-15]). A 500 HVDC connection is in project between Thailand and China [16].

a) 3680 MW, Bang Prakong Power Plant, Chachoengsao province

d) 710 MW, Nam Phong Power Plant, Khon Kaen province

b) 2625 MW, Mae Moh Power Plant, Lampang province

e) 2024 MW, Wang Noi Power plant, Ayutthaya province

c) 2288 MW, South Bangkok Power Plant, Samut Prakan province

f) 743.8 MW, Bhumibol Hydro Electric Dam, Tak province

Fig. 1.6. EGAT Thermal power plants and Hydro Electric Dam (from a to f, [12]).

Figure 1.6. Centrales thermiques et barrage d'EGAT [12].

1.2.4. Distribution of electricity

EGAT delivers the electricity produced to two state companies which are in charge of distribution. The first one MEA (Metropolitan Electricity Authority) is based in Bangkok area and uses about 35 % of the production. The second ones PEA (Provincial Electricity Authority) delivers the other 63 % to the different Thai provinces.

These companies depend on the Ministry of Interior and have been created in 1958 for MEA and 1960 for PEA.

At the beginning MEA produced a part of the electricity which was delivered in Bangkok area. In 1961, this activity was transferred to Yanhee Electricity Authority, one of the three companies regrouped to create EGAT. From that time, MEA is only in charged of distribution. Its network contains 13 main stations connected to EGAT network by HV lines and 122 sub-stations. The distribution is based on 12 or 24 kV lines on which are placed at intervals transformers on which are linked 220-380 consumers.

PEA takes care of the other 99 % of the country's area and tries from its creation to deliver electricity everywhere and had and has still nowadays an important role in the development of the country.

1.2.5. Privatisation of the electricity market

Following governmental decisions to privatize the electricity market and to increase private investments, two news companies were created in 1992 and 2000.

The first one EGCO (Electricity Generating Public Company) is born from the cession of EGAT power plant of Rayong (1 200 MW) and later of Khanom (750 MW). EGAT is the first shareholder of this society with at the origin a participation of 40.7 %, becoming today of 25.8 %.

The second one, RATCH (Ratchaburi Electricity Generating Holding Public Company) Limited regroups the power plants of Ratchaburi province (at least 4 000 MW) located in south of Bangkok. EGAT owns nowadays 45 % of this society. The proportion between Thai shareholders (EGAT, Banpu Public Company Limited, The Government Saving Bank, etc.) and foreign shareholders is 86.23 %/13.77 % [17].

In the medium term all the power plants will be privatized, EGAT becoming the network manager and the link between producers and consumers.

1.3. Quality of electricity

The development of industrial consumption and the apparition of polluting consumers lead EGAT and the distributors MEA and PEA to think to harmonics regulations concerning

"Electricity Business[6]" and Industry. A council has been created in 1995 and takes inspiration to works previously done in different industrial countries.

Today different documents have been produced. They correspond to advices for consumers and they were published in order to obtain their reactions. At a medium term, these advices will become regulations.

The first written documents concern harmonics [18] and voltage fluctuation [19]. Written in 1998, the given advices become regulations also in that written year.

1.3.1. Harmonic regulations

For harmonics, the regulations were made up following different scopes:
- The acceptable limit of current harmonics and of harmonic current distortion;
- The acceptable limit of harmonic voltage distortion;
- The use of non-linear load such as static converters.

Harmonics current limits for electricity user depend on the voltage level at the point of common coupling (Table 1.1).

It is the case also for the harmonic voltage distortion (Table 1.2) which is defined by:

$$THD\ (voltage) = \frac{\sqrt{V_2^2 + V_3^2 + ...}}{V_1}$$ (1.1)

Voltage (kV)	Harmonic order and current limit (A$_{rms}$)																	
	2	3	4	5	6	7	8	9	10	11	12	13	14	15	16	17	18	19
0 - 400	48	34	22	56	11	40	9	8	7	19	6	16	5	5	5	6	4	6
11 and 12	13	8	6	10	4	8	3	3	3	7	2	6	2	2	2	2	1	1
22, 24 and 33	11	7	5	9	4	6	3	2	2	6	2	5	2	1	1	2	1	1
69	8.8	5.9	4.3	7.3	3.3	4.9	2.3	1.6	1.6	4.9	1.6	4.3	1.6	1	1	1.6	1	1
115 and over	5	4	3	4	2	3	1	1	1	3	1	3	1	1	1	1	1	1

Table 1.1. Harmonic current limits at the point of common coupling.

Table 1.1. Limites des courants harmoniques au point de connexion au réseau.

---

[6] "Electricity Business" means the production, procurement, transmission, distribution of electricity, or control of power system.

Voltage (kV)	Total Harmonic Voltage Distortion (%)	Harmonic Voltage Distortion in each order (%)	
		Odd order	Even order
0 - 400	5	4	2
11, 12, 22 and 24	4	3	1.75
33	3	2	1
69	2.45	1.63	0.82
115 and over	1.5	1	0.5

Table 1.2. Harmonic voltage distortion limits at the point of common coupling.

Table 1.2. Limites de la distorsion en tension au point de connexion au réseau.

For equipments, the proposed regulations depend on their power and of the voltage level at the point of common coupling. For single-phase equipments, the rules defined in table 1.1. and table 1.2. are not applied to static converters whose power is under 5 kVA at 220 V and under 7.5 kVA at 415 V if they do not cause even harmonic currents. If they cause both even and odd harmonic currents, they will not be allowed on the mains. For three phase equipments, it will depend on the voltage level (Table 1.3).

Voltage (kV)	Three-phase converter			Three-phase AC regulator	
	3-pulse (kVA)	6-pulse (kVA)	12-pulse (kVA)	6-thyristors (kVA)	3 thyristors 3 diodes (kVA)
0 - 400	8	12	-	14	10
11 and 12	85	130	250	150	100

Table 1.3. Maximum power of converter and AC regulator according to the voltage level.

Table 1.3. Puissance maximale des convertisseurs en fonction du niveau de tension.

These limits correspond to all converters connected at the point of common coupling and not to each converter considered individually. In the case of the presence of several converters, coincidence factor can take into account the fact that the converters connected at the same point are not operated always at the same period of the day and that the currents are not always in phase (Table 1.4). The values given in this table is considered if no converter causes harmonic more than 60 % of the total harmonic current. If any converter causes

harmonic current more than 60 %, a multiplication factor is equal to 1. The multipliers in Table 1.4 will be used to consider the sum of harmonic current which come from the operation of many converters.

Group	Type and operation of converter	Multiplication factor
1	Non-controlled converter	0.9
2	Firing angle converter used many times each day	0.75
3	Firing angle converter used in some period or which causes harmonics at starting	0.6 when no more than 3 converters are used 0.5 when more of 4 converters are used

Table 1.4. Value of the multiplication factor for the calculation of harmonic current.

Table 1.4. Coefficient appliqué lors de la connexion au même point de plusieurs convertisseurs.

1.3.2. Voltage fluctuation regulations [19]

The goal is to avoid voltage fluctuation and voltage sag which can disturb other users. In evaluating the voltage fluctuations, there are three steps depending on the level of fluctuation at the point of common coupling:

- If the electric load causes voltage fluctuation less than 0.002 times of the rate kVA power, it will be available to be directly connected to the electrical network without a detail investigation of the fluctuation;

- If the electric load causes voltage fluctuation between 0.002 to 0.03 times of the rate kVA power, it will be available to be directly connected to the electrical network if the relative voltage fluctuation is under or not exceed a limited value given in Fig. 1.7. If the voltage fluctuations appear in a regular way the curve to be

considered on that figure corresponds to a Pst[7] of 1 (curve 2). In the other case, a Pst of 0.5 (curve 1) has to be considered;

- If the electric load causes fluctuation which does not fit in Fig. 1.7, or which is over 0.03 times of the rate kVA power, it is necessary to improve the system.

Different ways can be proposed to improve the system:

- Improving the load operation method to not having many machines working simultaneously or controlling the voltage change by ramp or limit the operating time of particular loads;

- Improving the load characteristics;

- Installing voltage fluctuation limitation equipments.

Annex 1 gives an example of calculating of the voltage change for a motor which starts 15 times per hour.

---

[7] Short-term severity values, Pst is the value to evaluate the severity of flicker in short periods (10 minutes)
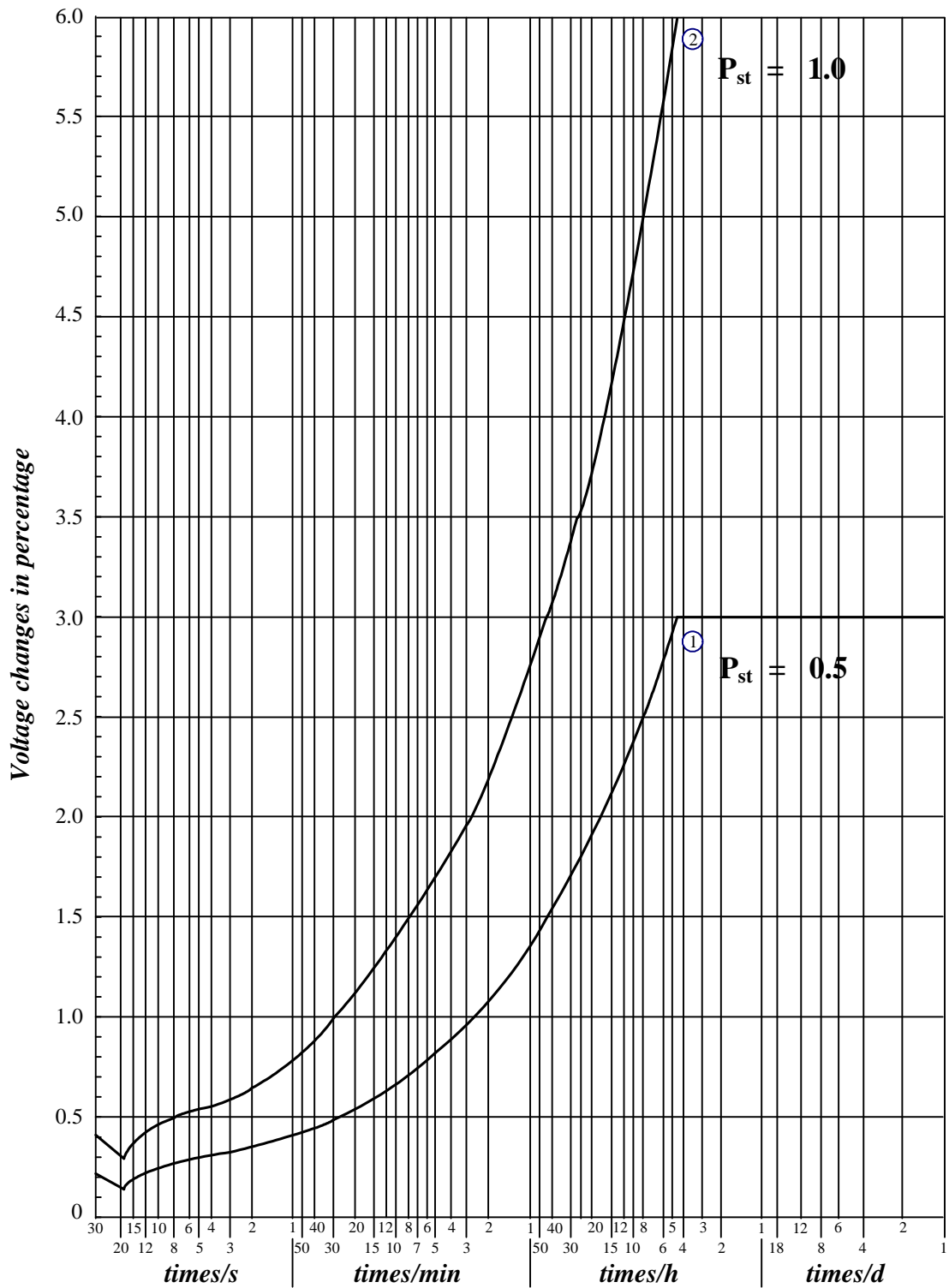
Fig. 1.7. Allowed relative voltage fluctuation according to the number of voltage changes.

Figure 1.7. Fluctuation relative acceptée en fonction du nombre de fluctuations de tension.

1.4. Conclusion

This chapter gives the opportunity to present the organisation of the production, transmission and distribution system of electricity in Thailand and its evolution. Then the efforts which are made to improve the quality of the delivered energy are detailed.

The end of this chapter presents the policy actually developed in Thailand in order to improve the quality of electricity, in terms of harmonic and voltage fluctuation regulations for Electricity Business and Industry. These regulations prepared officially in the 90s must be followed since 1998.

Chapter 2

Thailand-Malaysia HVDC Interconnection System

2.1. Introduction

The second chapter deals with the presentation of the basic types of High Voltage Direct Current (HVDC) interconnection systems which are installed in the world today. The basics of HVDC control is described with the combined steady state V_d-I_d characteristics of the converters. More over, this chapter will details the main components of HVDC system by using the 300/600 MW Thailand-Malaysia HVDC interconnection project as an example i.e. the power circuit arrangements, AC switchyard, AC filters, converter transformers, thyristor converter valves, smoothing reactor, DC filter, DC switchyard and DC control system respectively.

The Thailand-Malaysia HVDC interconnection system allows both countries bi-directional control for the energy exchange, improving reliability and operating in asynchronous mode. The construction of Thailand and Malaysia HVDC interconnection project begun in 1997 and the commercial operation was started in September 1, 2001 [15]. The 300/600 MW Thailand – Malaysia HVDC interconnection system is the grid interconnection between EGAT of Thailand and TNB[8] of Malaysia.

This interconnection, which represents the first cross-border DC link in the ASEAN region, was an important step to the realization of the ASEAN Power Grid which will enhance the energy security and economic integration of the region.

---

[8] Tenaga Nasional Berhad (TNB) is the largest electricity utility in Malaysia with more than RM67.0 billion (USD20.0 billion) in assets. The Company is listed on the main board of Bursa Malaysia and employs approximately 28,000 people. TNB's core businesses are in the generation, transmission and distribution of electricity. It has a total installed generation capacity of about 11,200 MW [26].

2.2 Different types of HVDC system [20]

Due to the ongoing technical development of DC equipment there is increasingly more flexibility in the selection of DC converter configurations. Basic DC power circuit arrangements are introduced and discussed in this section. The main types of DC system include back-to-back, monopolar and bipolar are briefly described.

The main types of HVDC interconnection converters are differentiated by their DC circuit arrangements. The current and the power flow are controlled by the difference between two controlled voltages. The current direction is fixed, meaning that the current can flow one direction only and the power direction is controlled by means of the voltage polarity of terminal voltages (V_{d1} and V_{d2}) of the controlled voltage sources. The block diagram (Fig. 2.1) and equivalent DC circuit (Fig. 2.2) are the simplified representation of HVDC system, where R_d is DC resistance of a DC transmission line system.
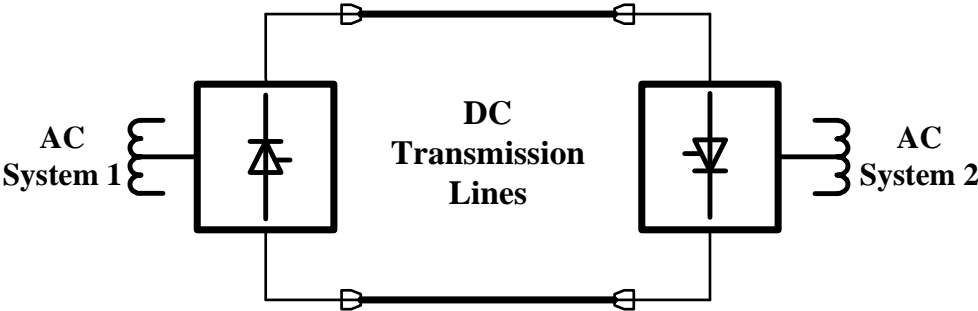
Fig. 2.1. Simplified block diagram of HVDC system.

Figure 2.1. Diagramme simplifié d'une liaison CCHT.
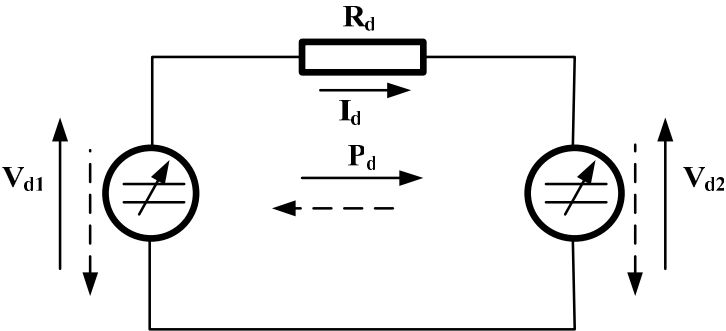
Fig. 2.2. Simplified equivalent DC circuits of HVDC system.

Figure 2.2. Schéma équivalent d'une liaison CCHT.

2.2.1. Back to back converters

The expression Back to Back (Fig. 2.3) indicates that the rectifier and inverter are located in the same station. Back to Back converters are mainly used for power transmission between adjacent AC grids which can not be synchronized. They can also be used within a meshed grid in order to achieve a defined power flow.
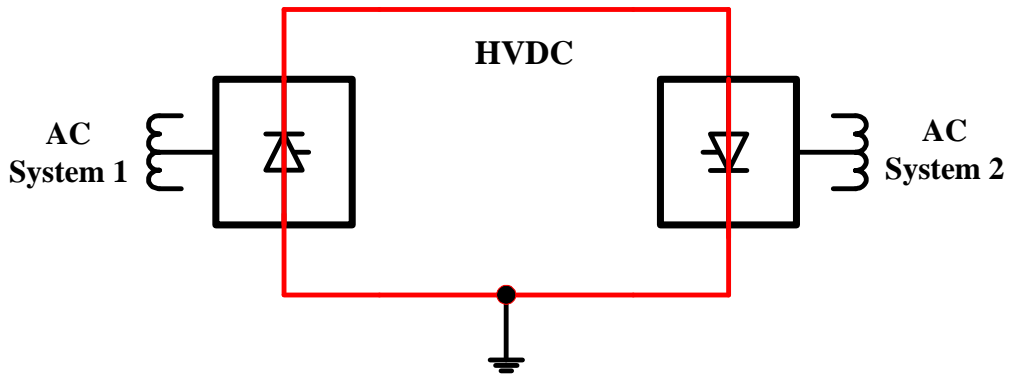
Fig. 2.3. Back to back converter link.

Figure 2.3. Liaison dos-à-dos.

2.2.2. Monopolar long distance transmission

In a common configuration, called monopole, normally used for very long distances and in particular for very long sea cable transmissions, a return path with ground- or sea-electrodes (Fig. 2.4) will be the most feasible solution. In many cases, existing infrastructure or environmental constrains prevent the use of electrodes. In such cases, metallic return path (Fig. 2.5) is used in spite of increased cost and losses.
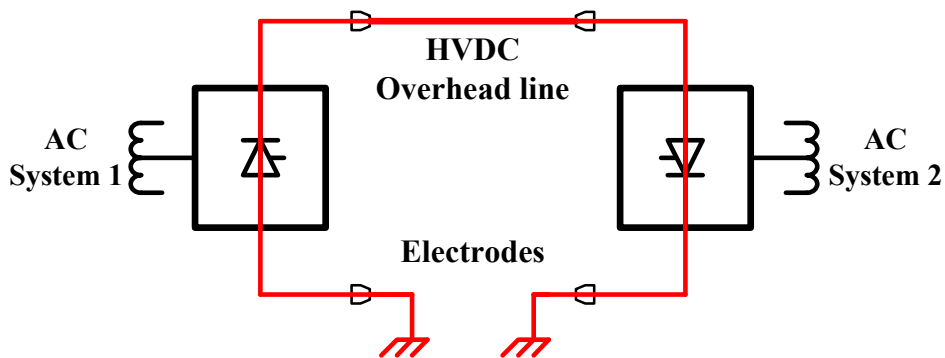
Fig. 2.4 Monopolar transmission with ground return path.

Figure 2.4. Liaison unipolaire avec retour par le sol.
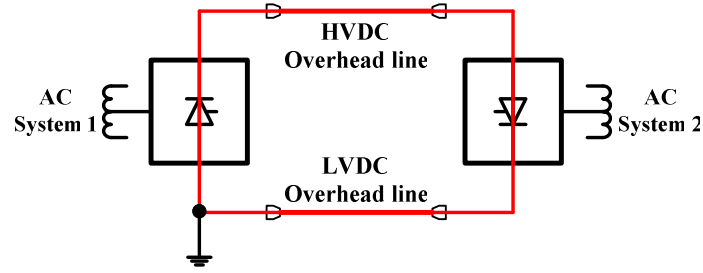
Fig. 2.5. Monopolar transmission with metallic return path.

Figure 2.5. Liaison unipolaire avec retour par conducteur métallique.

2.2.3. Bipolar long distance transmission

A normal bipole is a combination of two poles with a common low voltage return path. During a normal operation, the return path will only carry a small unbalance current.

This configuration is used if the required transmission energy exceeds that of a single pole. It is necessary to split the capacity on two poles.

During maintenance or outages of one pole, it is still possible to transmit part of the power. With the power at least 50% of the transmission capacity can be utilized, limited by the actual overload capacity of the remaining pole.

The advantages of a bipolar solution over a solution with two monopoles due to only one common return path are cost reduction and lower losses. The main disadvantage is that unavailability of the return path will affect both poles.

2.2.3.1 Bipolar transmission with ground return path

This is a commonly used configuration for a bipolar transmission system as in Fig. 2.6. The solution provides a high degree of flexibility with respect to operation with reduced capacity during contingencies or maintenance.
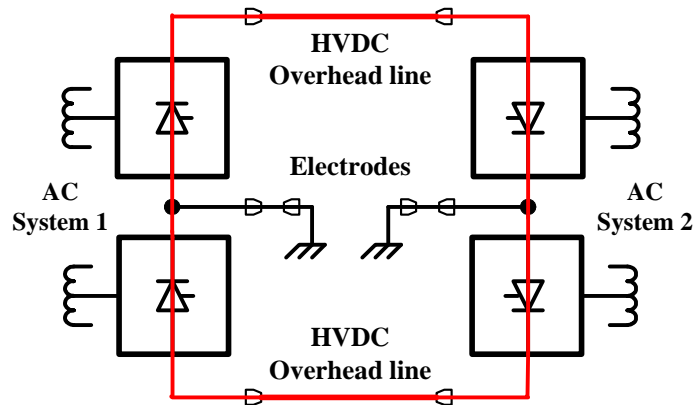
Fig. 2.6. Bipolar balanced operation.

Figure 2.6. Liaison bipolaire équilibrée.

On a single pole fault or the overhead line outage as shown in Fig. 2.7, the current of the faulty pole will be taken over by the ground return path and the faulty pole will be isolated.
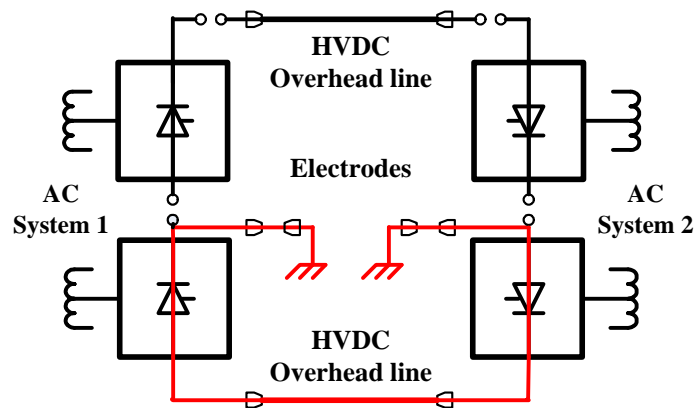
Fig. 2.7. Bipolar transmission with ground return operation (overhead line outage).

Figure 2.7. Liaison bipolaire avec retour par le sol lors de l'ouverture d'une des lignes aériennes.

Following a pole outage caused by the converter, the current can be commutated from the ground return path into a metallic return path (Fig. 2.8) provided by the HVDC conductor of the faulty pole.
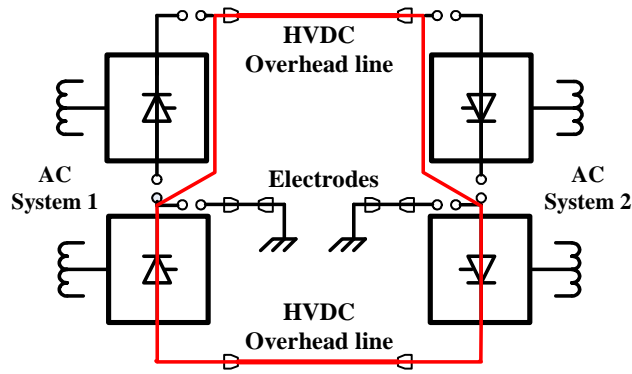
Fig. 2.8. Bipolar metallic return operation (converter pole outage)

Figure 2.8. Liaison bipolaire avec court-circuit lors de défaut d'un convertisseur.

2.2.3.2. Bipolar transmission with dedicated metallic return path for monopolar operation

If there are restrictions even to temporary use of electrodes or if the transmission distance is relatively short, a dedicated LVDC metallic return conductor as shown in Fig. 2.9 can be considered as an alternative to a ground return path with electrodes.
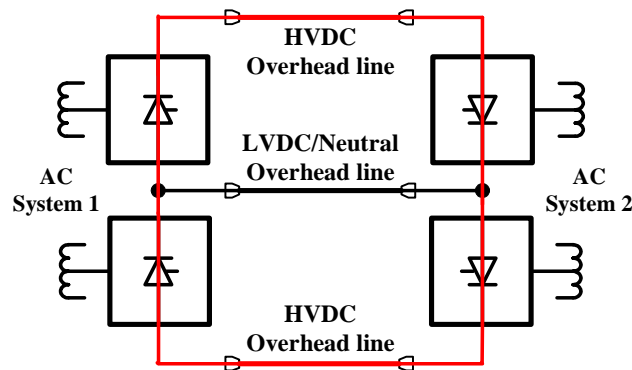
Fig. 2.9. Bipolar balanced operation with monopolar operation

Figure 2.9. Liaison bipolaire équilibrée avec retour unipolaire.

2.2.3.3. Bipolar transmission without dedicated return path for monopolar operation

In this case, we have a scheme without electrodes or a dedicated metallic return path. The currents flowing in the poles are essentially balanced for bipolar operation but for monopolar operation as shown in Fig. 2.10 will give the lowest initial cost.

Monopolar operation is possible by mean of bypass switches during a converter pole outage as shown in Fig. 2.8, but not during an HVDC conductor outage.
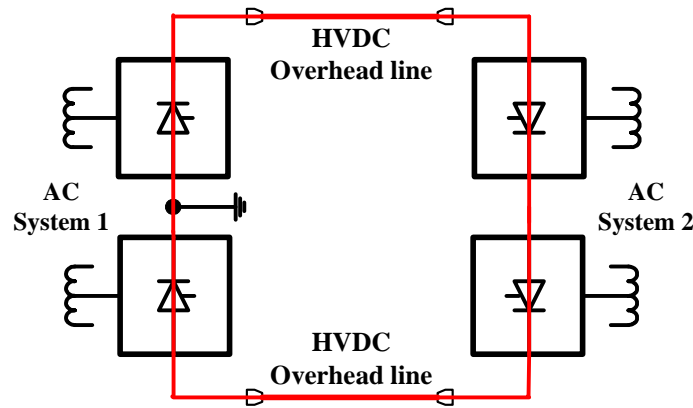
Fig. 2.10. Bipolar balanced operation without monopolar return path

Figure 2.10. Liaison bipolaire équilibrée sans retour unipolaire.

2.3. HVDC control [21]

Knowledge of the steady state DC voltage-current characteristics for the HVDC converter is important for understanding the principle of control of the HVDC system and the converter operations in rectifier- and inverter-operating modes. Therefore this section provides an explanation of the operating characteristics of the basic three-phase converter used in HVDC applications.

The object of the HVDC control is to provide the desired power transmission through the converters which DC current and DC voltage are controlled.

The main goals of the control are to:
- limit the DC current;
- maintain a maximum DC voltage to reduce losses;
- minimize reactive power consumption. This implies that the converters will operate at a low firing angle;
- prevent commutation failures at the inverter side.

2.3.1. Steady state V_d-I_d characteristics

To define the steady state characteristics let consider first the case of the conventional 6-pulse bridge converter. The theoretical analysis of a conventional 6-pulse bridge converter (Fig. 2.11) is examined based on the following assumptions: 1. The thyristors are ideal switches; 2. The DC current I_d is constant ($L_d = \infty$).
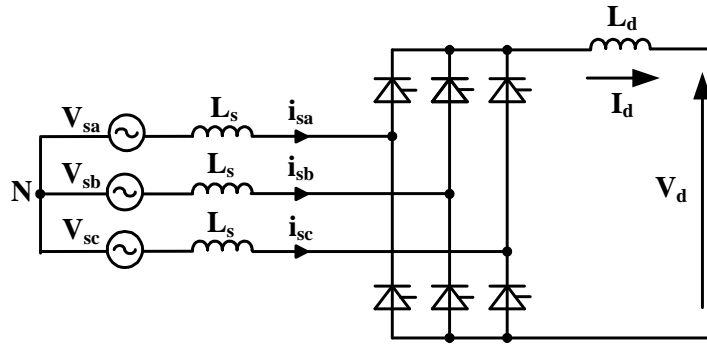
Fig. 2.11. 6-pulse bridge circuit.

Figure 2.11. Redresseur à indice de pulsation 6.

Because of the leakage inductance of the converter transformer (L_s), commutation of the current between the thyristors does not take place instantaneously and an overlap period appears.

The average DC output voltage of 6-pulse converter can be written as [21-23]:

$$V_d = V_{do} \cdot \cos\alpha \ - \ R_c \cdot I_d \qquad (2.1)$$

where:

V_d = converter direct voltage

V_{do} = no-load converter voltage obtained with $\alpha = 0^o$

α = delay or firing angle

R_c = equivalent commutation resistance, $R_c = \dfrac{3 \cdot \omega \cdot L_s}{\pi}$

I_d = DC current

One can also write the DC voltage as [21]:

$$V_d = V_{do} \cdot \cos(\alpha + \mu) \ + \ R_c \cdot I_d \qquad (2.2)$$

where μ is the commutation duration[9].

The HVDC system contains two converters, converter 1 operating in a rectifier mode and converter 2 in an inverter mode (Fig. 2.12) linked by the DC transmission line resistor R_d.

---

[9] See annex 2 for the detail of the calculation of the DC voltage.
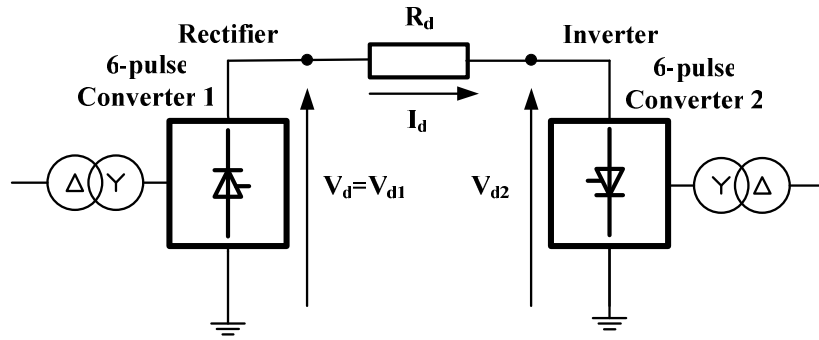
Fig. 2.12. Simplified circuit of HVDC system.

Figure 2.12. Schéma simplifié de la laison CCHT.

The voltage across that resistance is the difference between the voltages delivered by the two converters (in fact the opposite for converter 2). This defines the current exchanges by the converters:

$$R_d \cdot I_d = V_1 - V_2 \qquad (2.3)$$

For the rectifier, the control angle is the firing angle α and:

$$V_1 = V_{d1} = V_{do} \cdot \cos \alpha_1 - R_c \cdot I_d \qquad (2.4)$$

For the inverter, one chooses as control angle the extinction angle γ defines as:

$$\gamma_2 = \pi - \alpha_2 - \mu_2 \qquad (2.5)$$

As the control angles are different one can write:

$$V_1 = V_{d1} = V_{do} \cdot \cos \alpha - R_c \cdot I_d \qquad (2.6)$$

and:
$$V_2 = -V_{d2} = V_{do} \cdot \cos \gamma - R_c \cdot I_d \qquad (2.7)$$

2.3.2 12-pulse converters

The power converter unit consists of two three-phase 6-pulse converter bridges connected in series to form a 12-pulse converter unit. The bipolar configuration is shown in Fig. 2.13.

This does not change the basis of the control defined previously.
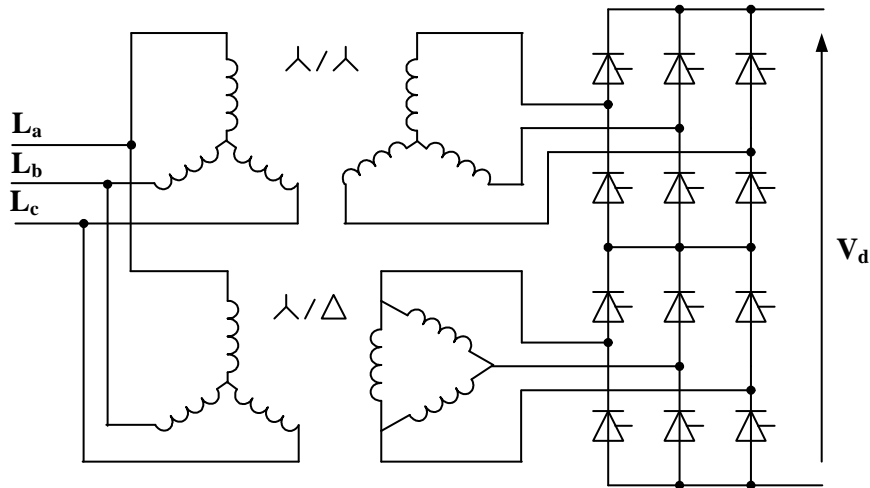
Fig. 2.13 Typical HVDC 12-pulse bridge power converter for monopolar operation with two units of three phase transformer.

Figure 2.13. Convertisseur dodécaphasé pour schéma unipolaire réalisé à l'aide de deux transformateurs triphasés.

2.3.3. Basic HVDC control [21-24]

To prevent commutation failures on the inverter side leads to control the inverter in a constant extinction angle mode (CEA mode). Then the rectifier will have to control the current (CCC, constant current control mode). As a consequence, the voltage is controlled by the inverter side.

For both converters, the control strategy shows two control modes (Fig. 2.14): alpha-min (line AB) and constant current (line BC) for the rectifier, gamma-min (line PQ) and constant current (line QR) for the inverter. The operating point for the DC link is the crossover point X of the two characteristics (the voltages are supposed to have the same values on both sides of the DC link).

The constant currents have not the same value for the rectifier and the inverter. This current margin (at least of about 0.1 pu) allows to have no interaction between the rectifier and inverter controls due to any current harmonics. This control strategy called the "Current Margin Method" is used in most HVDC systems. Another advantage is obvious if the voltage decreases suddenly at the rectifier side. The operating point moves automatically to point Y of Fig. 2.14 with the possibility to keep the main part of the power transmission.
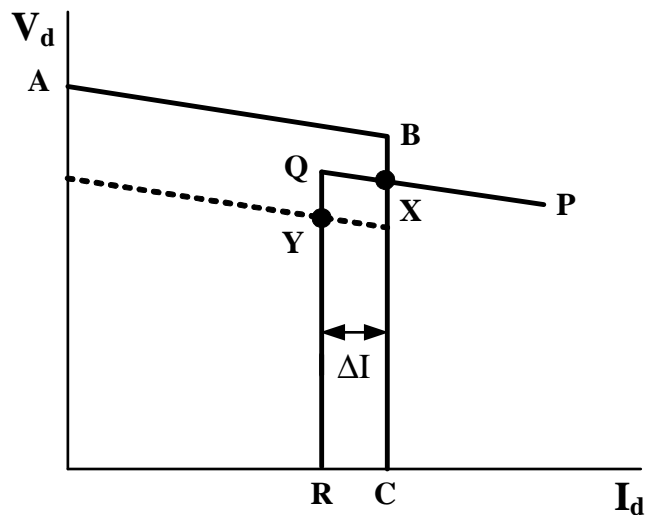
Fig. 2.14. Simplified Vd-Id characteristics.

Figure 2.14. Caractéristique simplifiée Vd-Id.

Practically, the characteristic defines other operating zones (Fig. 2.15):

- for the rectifier, the Voltage Dependent Current Limit (VDCL) which corresponds to the ability of the system to deliver a reduce power flow in case of a reduction of the AC voltage due to some perturbation. In this case, a current limit is introduced to avoid discontinuous operating mode;

- for the inverter an alpha-min limit to guaranty the operation in the inverter mode;

- in the current margin zone, the slope of the characteristic is generally modified to avoid multiple crossover with the rectifier characteristic.
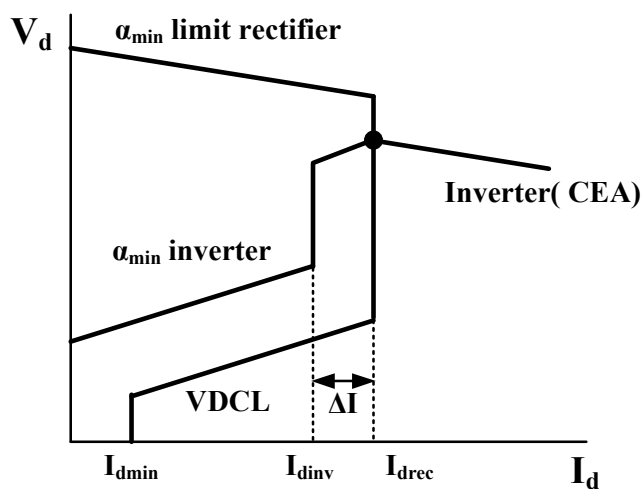
Fig. 2.15. Completed Vd-Id characteristics.

Figure 2.15. Caractèristique Vd-Id complète.

The principle of the different control loops used in the EGAT-TNB HVDC Interconnection will now be detailed.

2.3.3.1. Constant Current Control Loop (CCCL)

The rectifier is controlled to maintain the current I_d equal to its referenced valued I_{dref} (Fig. 2.16).
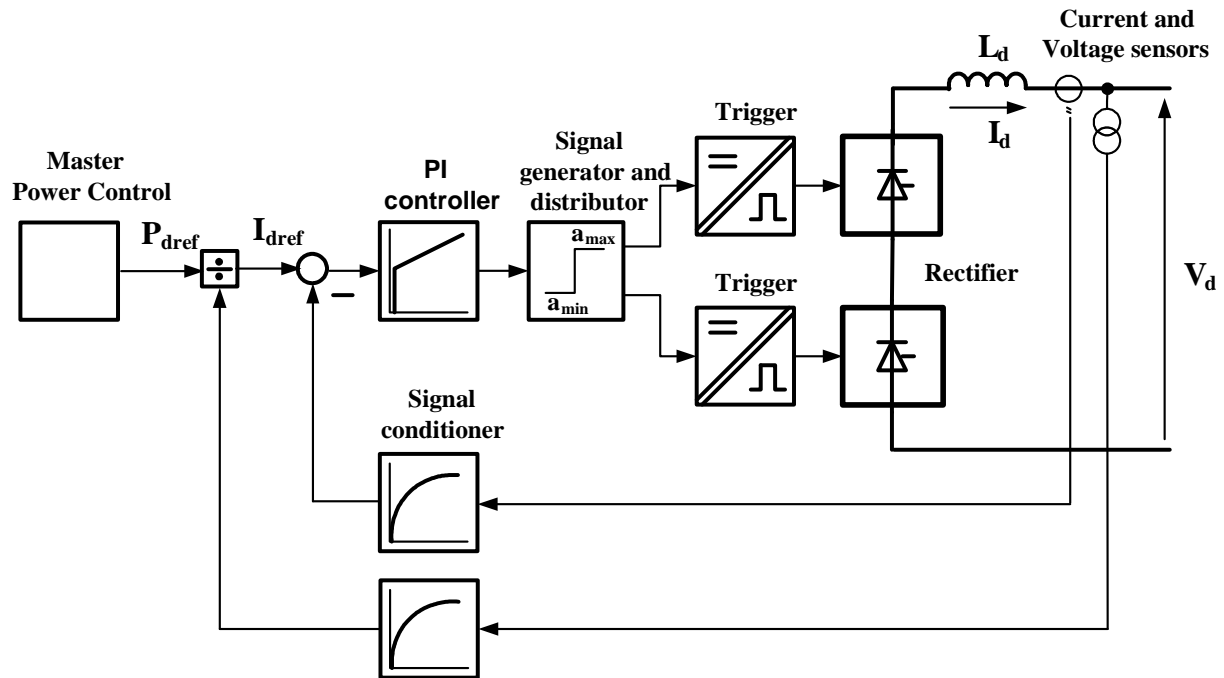
Fig. 2.16. Control structure of the rectifier current (CCC, constant current control).

Figure 2.16. Boucle de régulation du courant côté redresseur (contrôle à courant constant).

The actual current is measured by the current sensor, if the control error ($\Delta I_d = I_{dref} - I_d$) is positive (resp. negative), the rectifier firing angle α must decrease (resp. increase). Here a high gain current controller assures a perfect control of the power.

The firing angle will be as small as possible. Practically, a minimum value of 5° is imposed by the thyristors.

2.3.3.2. Gamma control loop

The Gamma control loop controls the firing angle of the inverter (Fig. 2.17). It contains in fact three loops:

- the first one, for the gamma angle (CEA, Constant Extinction angle Control);

- the second one for the current margin method;
- the third one for the voltage control (CVC, Constant Voltage Control).
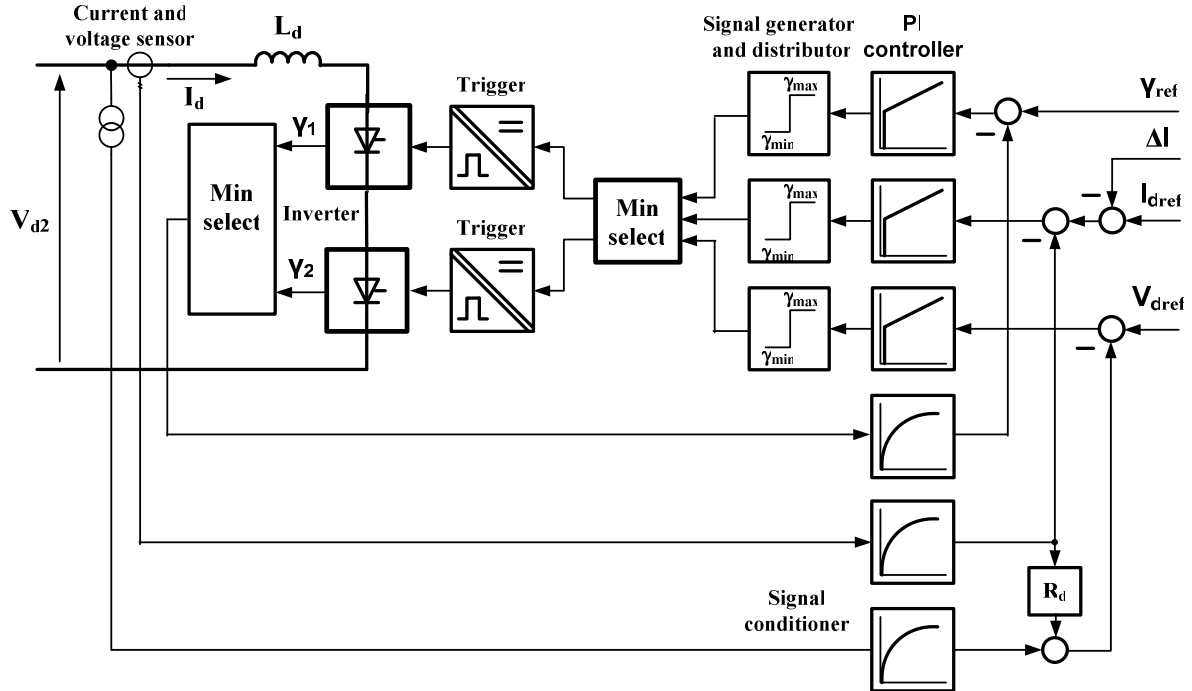
Fig. 2.17. Gamma control loop of the inverter.

Figure 2.17. Contrôle de l'angle gamma côté onduleur.

γ is obtained from the measurement of the thyristor current and voltage. Gamma value is a time interval which is initiated from the instant of anode current zero until the zero crossing of thyristor voltage is reached. From the gamma values of all 12 thyristors, the minimum value is selected and then used in the gamma control loop.

The current margin is subtracted from the current reference during normal operation, so that the inverter will operate at a firing angle determined by the inverter voltage V_{d2ref} or minimum extinction angle control. If there is a voltage decrease at the rectifier AC bus, the firing angle at the rectifier is no more available to maintain the current. In this case, the inverter will take over the current control, by decreasing the firing angle at the inverter to reduce the inverter voltage V_{d2} in order to keep the current reference $I_{dref(inv)}$.

- 31 -

With the chosen control concept, the inverter has to adjust the voltage. The rectifier voltage value required by the voltage controller at the inverter side must include the voltage drop due to the DC line resistance:

$$V_{d(cal)} = V_{d2} + I_d \cdot R_d \tag{2.8}$$

From the three control loops, the minimum value of γ is used to control the firing of the thyristors.

2.3.3.3 Voltage Dependent Current Limit (VDCL)

A voltage dependent current limit function is added to limit the referenced current I_{dref} at low voltage. The VDCL has a function to reduce the DC current during inverter end faults, DC line faults or AC system faults. This additional function assists the system on recovery after faults. Typically, the VDCL is applied instantaneously when the DC voltage falls below a defined level and is released with a ramp referenced signal with a given time constant to enable a rapid recovery after the fault clearance. The basis of the control with the VDCL function is represented in Fig. 2.18.
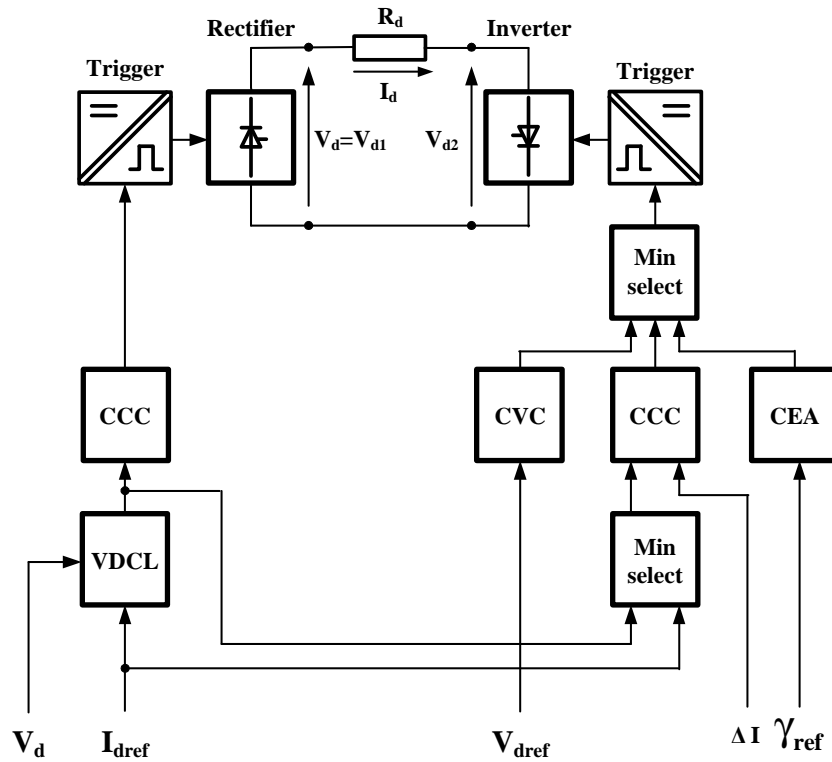
Fig. 2.18. Control system loops with VDCL function.

Figure 2.18. Boucle de régulation avec limitation du courant.

2.4. EGAT-TNB HVDC interconnection project

2.4.1. Purpose of the interconnection

The concept of interconnecting the electric power networks of Thailand and Malaysia was first conceived in the early seventies. The first interconnection resulted in the construction of a 80 MW 132/115 AC interconnection in 1982 [25] which allowed a section of the Thailand power network to be isolated from the rest of the network and to be connected to and supplied from the Malaysian power network. Further co-operation in this area between both countries has now resulted in the implementation of the 300/600 MW EGAT/TNB HVDC Interconnection Project.

The EGAT-TNB 300/600 MW HVDC interconnection project establishes an interconnection from Khlong Ngae in the southern part of Thailand to Gurun in the northern part of Malaysia as shown in Fig. 2.19. The DC connection allows both countries to be asynchronously operated while still obtaining the benefits of interconnection. The inter-connection consists of converter stations at Khlong Ngae and Gurun linked by a 110 km long (approximately 24 km on the Thai border and 86 km on the Malaysian border) 300 kV DC line with three conductors between the stations.

Initially, the converter station is configured as a monopolar converter with a power transfer capacity of 300 MW. Provision has also been made for adding a second 300 MW pole in the future to extend the system into a bipolar configuration with a total transfer capability of 600 MW.

The complete line transmission line suitable for the bipolar interconnection is installed at the initial phase. The addition of a reliable interconnection to the previously lightly connected AC systems will increase efficiency and the power transmission capacity between and within the countries. Surplus power produced by IPP's in Malaysia could be exported to Thailand and similarly surplus power from Thailand could be exported to Malaysia.

The one hour time difference between the two countries as well as a diversity of peak load of several hours means that the interconnection can be used effectively to support the peak loads in both countries by reversing the direction of power flow as required during peak periods. When utilized in this way, there will be little net exchange of energy. The

interconnection will also permit the power system in one country to provide support to the other country during emergency conditions.

Fig. 2.19. Location map of Khlong Ngae and Gurun.
Figure 2.19. Localisation de Khlong Ngae et Gurun.

The monopole has a short time (10 minutes) capability to transmit 450 MW. This overload capability together with the capability of fast power reversal will allow the link to be used to reduce the total amount of spinning reserve dispatched in the two countries.

An AC interconnection to Malaysia was considered but, during certain operating conditions, it was found difficult to maintain synchronism of the two AC systems and to control the flow of power. An HVDC system, however, is well suited for interconnection of the AC networks of the two countries. The EGAT-TNB HVDC Interconnection Project allows full bi-directional control of power interchange as well as improving reliability and dynamic performance of both AC systems.

The automatic reactive power controllers at the converter stations also allow independently controlling the reactive power exchange between the converter stations and the connected AC systems or voltage control at the converter buses.

The reinforcement of EGAT's existing AC transmission system involves the construction of the transmission activities as shown in Fig. 2.20. A 230 kV AC substation at Khlong Ngae

has to be built and it was necessary to reinforce the substation of the area (Hat Yai 2 and Ya La 2) and the lines between Khlong Ngae and the neighboring substations.
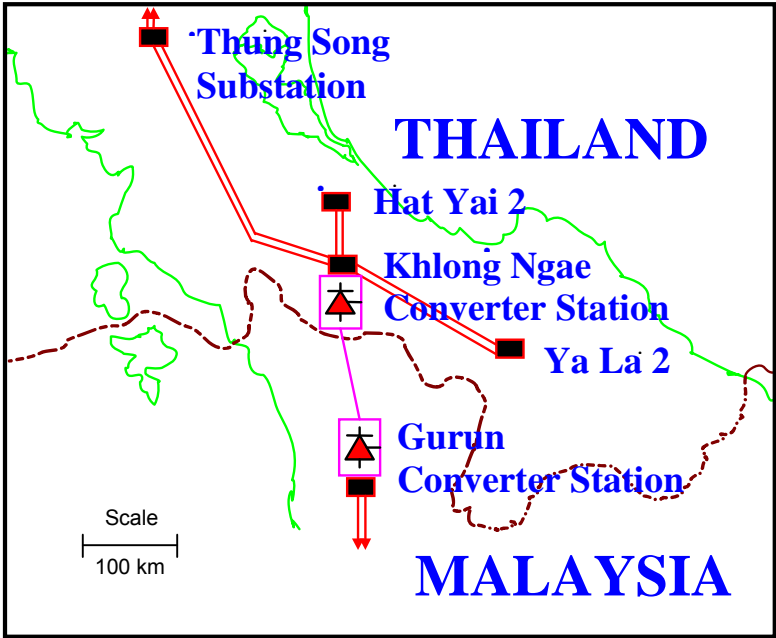
Fig. 2.20. Location map of converter stations at Khlong Ngae and Gurun.

Figure 2.20. Localisation des stations de conversion de Khlong Ngae et de Gurun.

2.4.2. HVDC power circuit configurations

The EGAT-TNB HVDC interconnection system was designed to be bipolar system in order to transfer power from 60-600 MW. However in the first stage it is a monopolar configuration with metallic return and it can be extended into a bipolar configuration later. The DC transmission lines was installed with three conductors namely two pole conductors and a neutral (metallic) return conductor between Klong Ngae and Gurun stations. Each converter station can be both rectifier and inverter station depending on the direction of transferring power.

With the monopolar operation, the EGAT-TNB HVDC system will have the possibility to operate in four different modes namely:

- Monopolar operation Mode 1 as shown in Fig. 2.21. HVDC overhead line 1 is the high voltage pole with the parallel connection of HVDC overhead line 2 and LVDC overhead line (neutral line) as the return paths;

- Monopolar operation Mode 2 as shown in Fig. 2.22. HVDC overhead line 1 is the high voltage pole with only neutral line return path;
- Monopolar operation Mode 3 as shown in Fig. 2.23. HVDC overhead line 1 is the high voltage pole with only HVDC overhead line 2 as the return path;
- Monopolar operation Mode 4 as shown in Fig. 2.24. HVDC overhead line 2 is the high voltage pole with neutral return path.
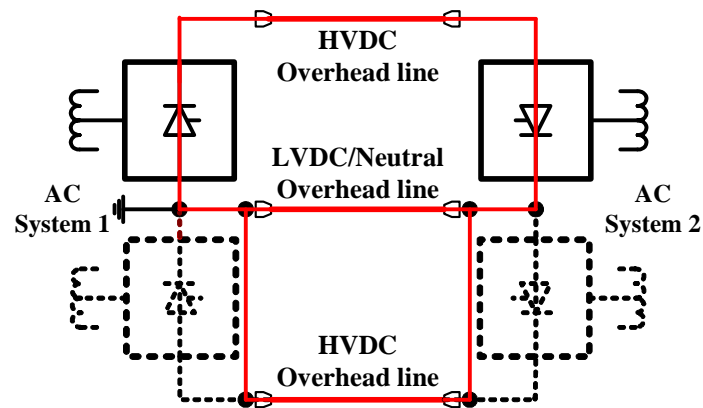
Fig. 2.21. Monopolar operation Mode 1.

Figure 2.21. Mode de fonctionnement unipolaire n° 1.
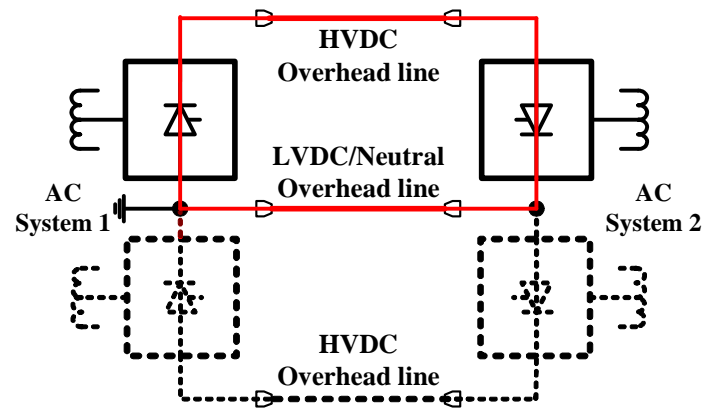
Fig. 2.22. Monopolar operation Mode 2.

Figure 2.22. Mode de fonctionnement unipolaire n° 2.
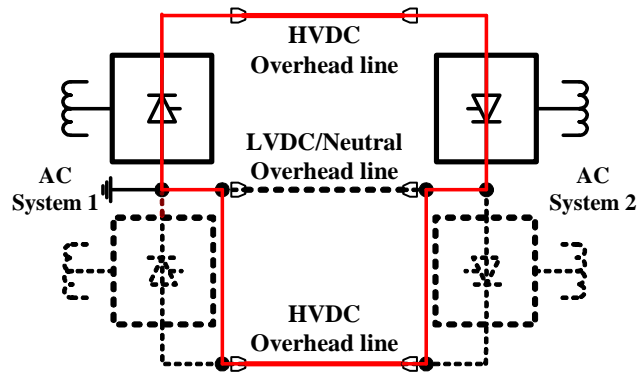
Fig. 2.23. Monopolar operation Mode 3.

Figure 2.23. Mode de fonctionnement unipolaire n° 3.
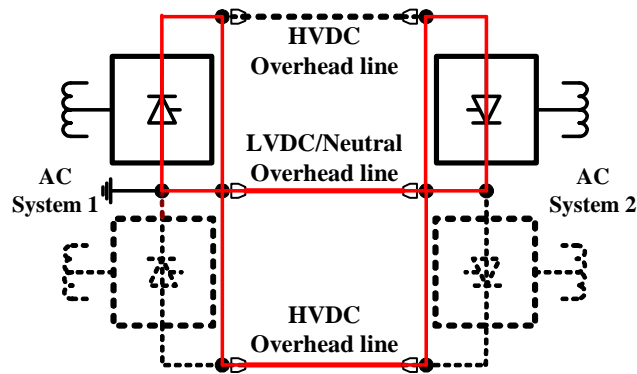
Fig. 2.24. Monopolar operation Mode 4.

Figure 2.24. Mode de fonctionnement unipolaire n° 4.

The first operation mode (Fig. 2.21) is normally used for EGAT-TNB HVDC, by connecting the high voltage pole to the first conductor (HVDC overhead line 1) and the low voltage pole is the parallel connection of the high voltage pole (HVDC overhead line 2), the neutral line being directly grounded at the Khlong Ngae station in order to reduce losses. The Khlomg Ngae and Gurun single line diagram for initial monopolar operation is shown in Fig. 2.25 [26].

The DC monopolar converter station is currently capable of transmitting a full rated power of 300 MW (300 kV, 1000 A) in either direction up to a maximum ambient temperature of 39° C. The DC transmission line also permits a 10-minutes–overload of 450 MW of power once per day. According to the agreement, both EGAT and TNB agreed to initially generate and deliver 30 MW power as an obligatory energy to enable the continuous operation of the HVDC interconnection. Commercial energy is the energy sold and purchased at any time request by either utility.

| 230 kV EGAT AC System | HVDC Station Khlong Ngae | HVDC/LVDC Overhead line | HVDC Station Gurun | 275 kV TNB AC System |

Triple-tuned AC filters
2x42 Mvar, 1x84 Mvar
Tuned to 12/24/36 harmonics

Triple-tuned AC filter
2x60 Mvar
Tuned to 11/13/21 harmonics

HVDC pole 1 overhead line

Smoothing reactor

Smoothing reactor

Thyristor valves

Thyristor valves

Active DC filter

Active DC filter

Converter transformer

Converter transformer

HVDC pole 2- and LVDC -overhead lines

Shunt capacitor 3x84 Mvar

Shunt capacitor 3x60 Mvar

Rated DC power	300 MW
Voltage	300 kV
Current	1000 A

Fig. 2.25. DC single line diagram for initial monopolar operation [26].

Figure 2.25. Schéma de principe de l'installation en mode de fonctionnement unipolaire [26].

2.5. Main system rating data of Khlong Ngae converter station

The Khlong Ngae (province of Songkla) Converter Station is the terminal in Thailand of the HVDC transmission scheme interconnecting the electrical systems of the countries of Thailand and Malaysia.

The HVDC converter station is initially designed and constructed for monopolar operation with the option of future expansion to bipolar operation. The system is capable of bi-directional power transfer at any level from 30 MW to 300 MW in the monopolar stage (60 MW – 600 MW bipolar). An overload capability is incorporated in the design, which allows for a short time (up to 10 minutes) power transfer of up to 450 MW on one pole.

The main DC rating data is summarized in Table 2.1 and the main AC data is summarized in Table 2.2.

DC Rating Data of the HVDC System		
Rated DC Power - Monopolar Operation	300	MW
Rated 10 Minute Overload	450	MW
Minimum DC Power	30	MW
Rated DC Current	1000	A
Rated 10 Minute Overload	1562	A
Minimum DC Current at 300 kV	100	A
Rated DC Voltage	300	kV
Maximum DC Voltage	308	kV
Minimum DC Voltage	292	kV
Reduced DC Voltage Operation	210	kV

Table 2.1. Main DC rating data of the HVDC system [23].

Table 2.1. Principales caractéristiques de la liaison CCHT [23].

Khlong Ngae AC System Data		
Nominal System Voltage	230	kV
Normal Maximum Voltage	240	kV
Normal Minimum Voltage	218	kV
Extreme Maximum Voltage	253	kV
Extreme Minimum Voltage	210	kV
Maximum Short Circuit Level (at X/R=15)	16000	MVA
Minimum Short Circuit Level (at X/R=4.3)	1220	MVA
Nominal Frequency	50.0	Hz
Maximum Frequency (for rating)	51.0	Hz
Minimum Frequency (for rating)	49.0	Hz

Table 2.2. AC system data [23].

Table 2.2. Caractéristique du réseau alternatif [23].

2.6. Description of main components of Khlong Ngae converter station

The Khlong Ngae Converter Station can be divided into different areas concerning the converter building, the AC side (AC switchyard, AC filters and shunt capacitors and converter transformer), the thyristors and the DC side (smoothing reactor, DC filter, DC switchyard and DC transmission line). These different parts of the station will be described hereafter.

2.6.1. Converter building

The converter building as shown in Fig. 2.26 consists of one valve hall, control equipment room, communication room, cooling equipment room and other facilities associated with the thyristor converters. The valve hall contains high power equipments, the thyristor converter valves, protection and auxiliary systems associated with thyristor converter values are also installed in this hall.

The converter transformers are located next to the converter building and the valve winding bushings project directly into the valve hall.

| a) Converter building | b) 300 kV, 300 MW DC Transmission line |

EGAT: Khlong Ngae, Songkla [25]

Fig. 2.26. HVDC converter station and 300 kV - 300 MW DC transmission line.

Figure 2.26. Station de conversion CCHT et liaison continue 300 kV - 300 MW.

2.6.2. AC switchyard

The 230 kV AC switchyard as shown in Fig. 2.27 is designed to ultimately have twelve breaker-and-a-half bays. Six breaker-and-a-half bays connected to two high voltage busbars were installed initially along with the first pole of the HVDC system. Of these six breaker bays, two do not contain the full complement of circuit breakers. These two bays will be completed when the second pole of the HVDC system will be installed. Three double-circuits, 230 kV overhead transmission lines terminating in the AC switchyard of the Khlong Ngae converter station were installed for the monopolar stage.

a) AC Switch Yards

d) Circuits breakers

b) Relay house

e) AC voltage and current measurements

c) 230 kV, AC transmission line

f) Disconnecting switches

EGAT: Khlong Ngae, Songkla [25]

Fig. 2.27. AC switch yards at Khlong Ngae station.

Figure 2.27. Disjoncteur côté alternatif à la station de Khlong Ngae.

2.6.2.1. High voltage AC circuit breakers and disconnection switches

The circuit breakers as shown in Fig. 2.27-d used in the AC switchyard are SF$_6$ type circuit breakers. On both side of each circuit breaker are motorized disconnected switches. The circuit breakers are adequately rated to handle the requirements for converter transformer and AC filter and shunt capacitor switching. Breakers used for switching converter transformers are equipped with pre-insertion resistors and breakers used for switching AC

filters and shunt capacitors are equipped with point on wave closing relays to minimize transients during breaker closing.

2.6.2.2 High voltage AC measuring devices

For the most part, capacitor voltage transformers are used for AC voltage measurement (Fig. 2.27-e). Inductive voltage transformers are however, used for certain functions where the accuracy and phase shift of the signal under transient conditions is of importance. Inductive transformers are used for the synchronizing signals and for the bus voltage signals for the reactive power controller.

Discharge potential transformers are used in combination with the 42 Mvar triple tuned filter sub-banks to rapidly discharge the filters and allow them to be reconnected within seconds after disconnection.

High voltage AC current measurements, for the most part, are made by post current transformers located throughout the switchyard converter transformer primary and secondary currents are made using current transformers built into the bushings of the transformer. As well, some smaller current transformers used in the AC filter and capacitor sub-banks are mounted on stand-off insulators.

2.6.2.3. AC side surge arresters

Gapless zinc-oxide surge arresters are installed close to the converter transformer line side bushing to limit overvoltages on both the primary and secondary sides of the transformer, taking into account the switching over voltages transferred from the AC side to the valve side of the converter transformers. Gapless zinc-oxide surge arresters are connected to the main busbars of the AC filter banks. These arresters protect the AC filters against lighting surges. Additionally, gapless zinc-oxide surge arresters are connected to the AC filter and shunt capacitor sub-banks to limit transient over voltages that may occur during recovery from AC faults. Arresters are also connected across the reactors within the AC filters to limit energization voltages across the reactors.

2.6.3. AC filters and shunt capacitors

The AC filters and shunt capacitors as shown in Fig. 2.28 are divided into two banks, each of which is connected to the main 230 kV high voltage busbars. Connected to one bank is one 42 Mvar triple-tuned filter sub-bank (12th, 24th and 36th harmonics) and two 84 Mvar shunt capacitor sub-banks. Connected to the other bank are one 42 Mvar triple-tuned filter sub-bank, one 84 Mvar triple-tuned filter sub-bank and one 84 Mvar shunt capacitor sub-bank. Provision has been made for the addition of one additional 84 Mvar triple-tuned filter sub-bank, which is required to meet the harmonic performance requirements of the complete bipolar HVDC scheme.
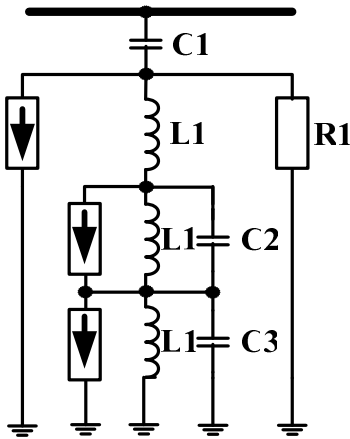
a) AC filters and shunt capacitors   b) Triple-tuned AC filter

EGAT: Khlong Ngae, Songkla [25]

Fig. 2.28. AC filters and shunt capacitors (a); Circuit diagram of Triple-Tuned AC Filter (b) [23].

Figure 2.28. Filtres alternatifs et capacités shunts (a) ; schéma des filtres alternatifs accordés sur trois fréquences (b) [23].

The AC filters are used to limit the level of harmonic voltage distortion on the AC bus due to the harmonic currents resulting from converter operation. The filters also limit the amount of harmonic current which will flow into the AC system by providing a low impedance shunt path for the harmonic current flow. The filters also provide reactive power generation capacity at fundamental frequency, which is used in overall var/voltage control. The following AC filter and reactive power sub-banks are provided as shown in Table. 2.3.

Type	Description	Quantity
A	42 Mvar triple-tuned filter	2
B	84 Mvar triple-tuned filter	1
C	84 Mvar shunt capacitor bank	3

Table 2.3. Provided AC filter and reactive power sub-banks [23].

Table 2.3. Différents filtres alternatifs et bancs capacitifs [23].

The Reactive Power Controller (RPC) which is part of the DC Station Control automatically switches the filter and shunt capacitor banks. The RPC switches the filters and shunt capacitors in a first on, first off manner according to a certain criteria. The switching criteria and hierarchy is as follows:

- AC busbar voltage within scheduled range;
- Correct combination of sub-banks connected to achieve harmonic filtering performance;
- Total station reactive power within scheduled range.

Under normal operating conditions, with all sub-banks available, the reactive power elements are switched in 42 Mvar steps. Switching of a Type B or a Type C element is always done in a binary manner with a Type A filter to maintain the 42 Mvar step size. When no type A elements are available and in conditions when switching of the type A element would result in the filter requirements not being met, switching of reactive power elements in 84 Mvar steps is permitted.

Potential transformers are provided for rapidly discharging the Type A filters, allowing them to be reconnected approximately 5 seconds after being disconnected. The Type B filter and the Type C capacitor bank do not have a facility for rapid discharge and require 5 minutes to discharge before they can be reconnected.

2.6.4. Converter transformer

The converter transformer connects the AC network to the converter valves and provides the voltage matching between the AC system and the converter valve group. Another important function of the converter transformers is to provide the necessary reactance for

limiting the thyristor current in the event of a fault. The converter transformers also provide the means of regulating the valve winding voltage, by way of an on-load tap changer.

The typical arrangements of transformer for 12 pulse converter are as following:
- 6-units of a 1-phase, 2-windings transformer;
- 2-units of 3-phase, 2-windings transformer;
- 3-units of a 1-phase, 3-windings transformer.

The three difference circuit configurations are shown in Fig. 2.29, Fig. 2.30 and Fig. 2.31. Three phase transformers are the most economical but have the largest weight for transportation and highest cost for a spare unit. Single phase three winding transformers (Fig. 2.31) were chosen for Khlong Ngae Converter Station as these are the most economical transformers whose shipping weight does not exceed allowed transportation limits.

Three of single phase three windings transformers are connected together to form a three phases transformer bank. The high voltage line windings of the transformers are connected in a star configuration with the star point solidly grounded. One set of secondary windings from the three transformers is also connected in a star configuration while the other set is connected in a delta configuration.
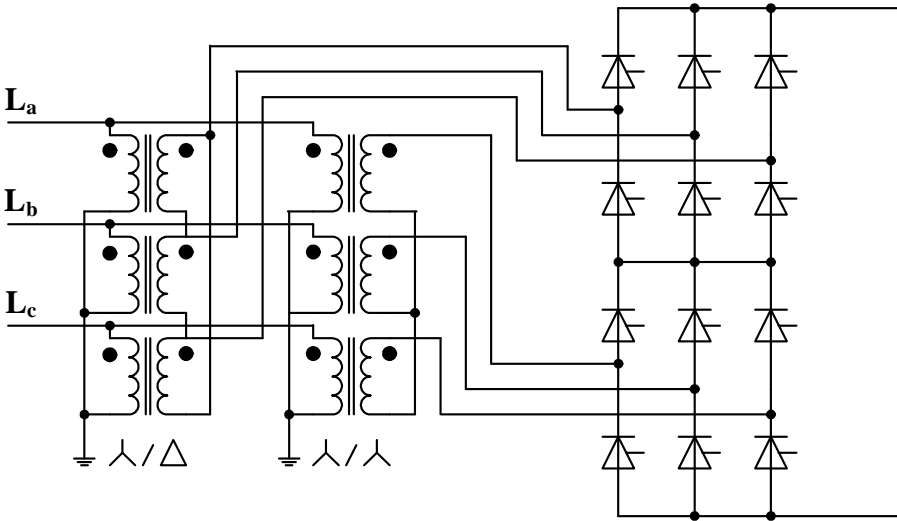
Fig. 2.29. Six units of a single phase, two windings transformer.

Figure 2.29. Six transformateurs monophasés à deux enroulements.
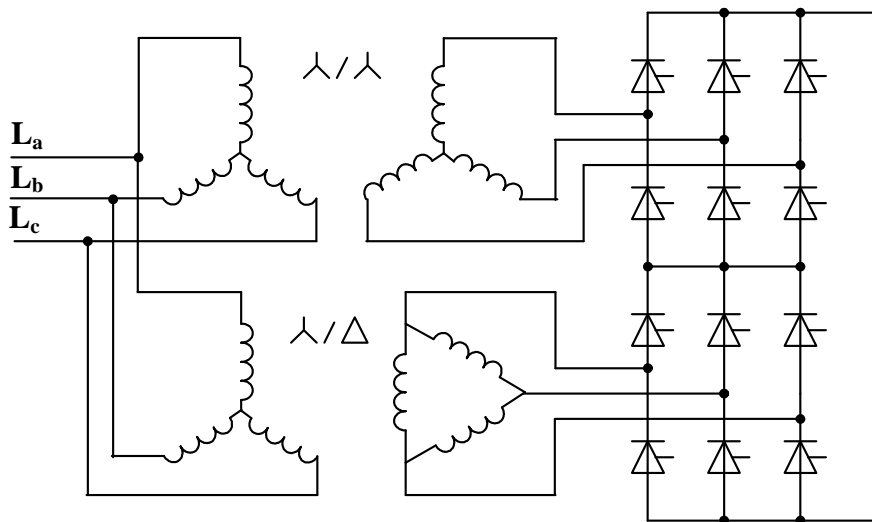
Fig. 2.30. Two units of three phases, two windings transformer.

Figure 2.30. Deux transformateur triphasés à deux enroulements.
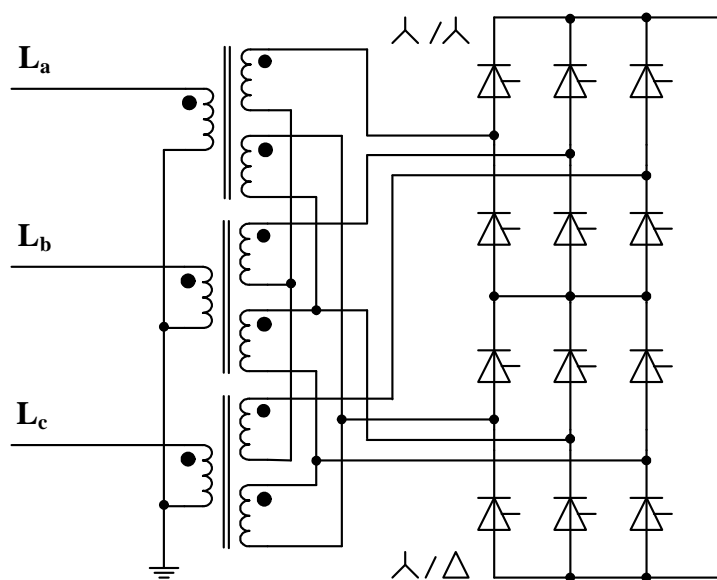
Fig. 2.31. Three units of a single phase, three windings transformer.

Figure 2.31. Trois transformateurs monophasés à trois enroulements.

The converter transformers are an integral part of the AC-DC conversion process. They provide the reactance necessary to limit the thyristor commutation current and provide a means to regulate the valve winding voltage, by way of an on-load tap changer, necessary to maintain efficient converter operating conditions.

The transformers are located adjacent to the converter building (Fig. 2.32). The valve winding bushings project into the valve hall with direct connections to the converter valves.

The converter transformers have on-load tap changers and are Oil Natural Air Force (ONAF[10]) design. The main data of EGAT converter transformer is summarized in Table 2.4.

a) Converter transformer station   b) Converter transformer inside valve hall station

EGAT: Khlong Ngae, Songkla [25]

Fig. 2.32. Converter transformers (a) and valve winding bushings inside valve hall (b).

Figure 2.32. Transformateurs alimentant le convertisseur (a) et connexions (b).

2.6.5. Thyristor converter valves

The thyristor converter valves for HVDC transmission systems as shown in Fig. 2.33 and Fig. 2.34 are complex structures made up of many series connected thyristors. The EGAT-TNB thyristor converters have 48 thyristors connected in series in each valve. The series connected thyristors are arranged in a hierarchically ascending fashion in the following groupings to make up the complete valve structure:

- Thyristor level;
- Valve section (12 thyristors levels);
- Modular unit (2 valve sections);
- Valve (2 modular units consist of 48 thyristors connected in series);
- Multiple Valve Unit (4 valves).

---

[10] ONAF/ONAN/OFAF, are the cooling combination system design for the converter transformer. ONAF is a non-forced oil, forced air design.

Main data of EGAT Converter Transformers				
a	**Continuous Rating (without redundant cooling)** **Rated power (line/star/delta)**	**MVA**	**116/58/58**	
b	**No Load Voltage Ratio** **line/star/delta** **Tolerance**	**kV** **%**	**230/√3/122.24/√3/122.24** **±0.5**	
c	**Superimposed Voltages to Ground** **Valve side (star), DC + AC** **Valve side (delta), DC + AC**	**kVpeak** **kVpeak**	**342** **177**	
d	**Winding Group**		**Ynyn0d1**	
e	**Tap changer range** **Step size** **Nominal tap no.** **Highest tap no.** **Lowest tap no.**	**%**	**1** **6 (230.0/122.24 kV)** **22 (240/(0.9x122.24 kV)** **1 (218.5/122.24 kV)**	
f	**Impedance (based on rated secondary MVA, nominal tap)** **Line side – valve side (star)** **Line side – valve side (delta)**	**%** **%**	**11** **11**	
g	**Cooling arrangement**		**ONAF**	

Table 2.4. Main data of EGAT converter transformer [23].

Table 2.4. Principales caractéristiques des transformateurs alimentant le convertisseur [23].

The complete thyristor converter is made up of three multiple valve units (MVU), one MVU for each phase. Each individual thyristor level consists of:

- The thyristor;
- The heat sinks for the thyristor;
- Parallel connected components for proper grading of voltage and control and protection of the individual thyristors;
- The Thyristor electronics (TE) which includes the gating and protection and monitoring systems.

Twelve thyristor levels are arranged into a valve section. Four reactor modules consist of saturable steel cores wound around the conductor and encapsulated are placed at one end of a valve section. Two valve sections compose one modular unit. When the valve sections are put together to form a modular unit, the four valve reactors of each valve section are placed at opposite ends of the completed modular unit.

a) Thyristor converter valves
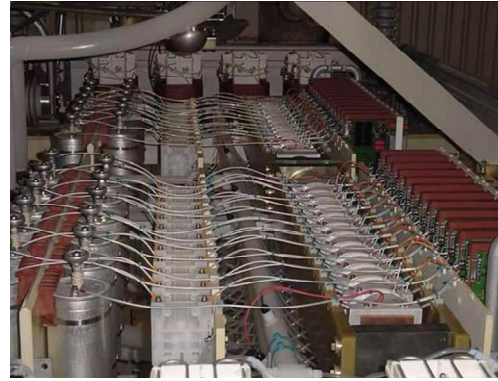
d) Valve sections
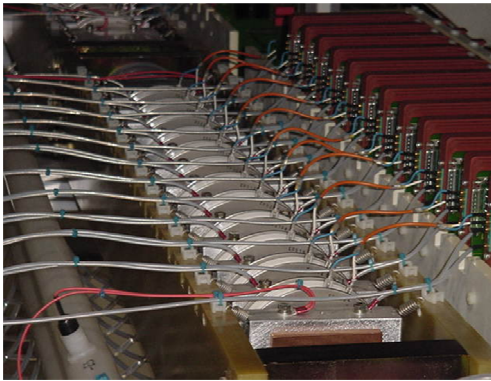
b) Thyristor levels
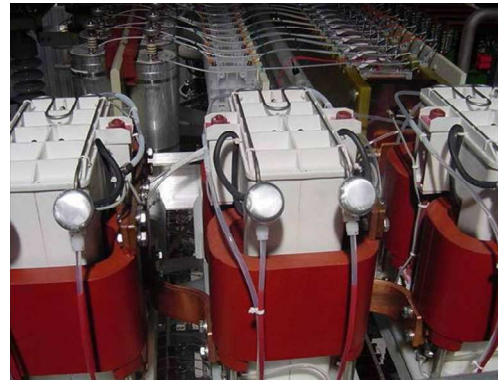
e) Saturable reactors
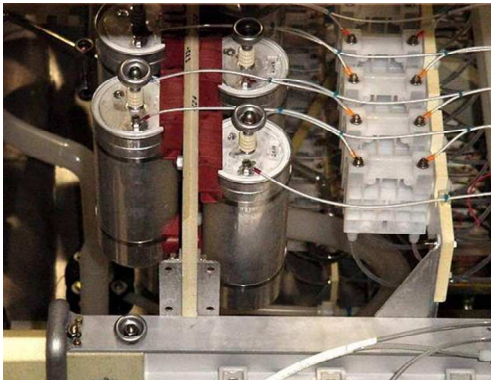
c) RC snubber circuits
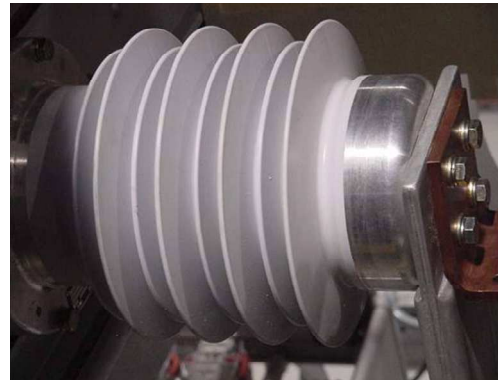
f) Grading capacitors

EGAT: Khlong Ngae, Songkla [25]

Fig. 2.33. Thyristor Levels and valve Sections with RC snubber circuits and saturable reactors.

Figure 2.33. Thyristors et valves (12 thyristors en série) avec circuits RC et inductances saturables.
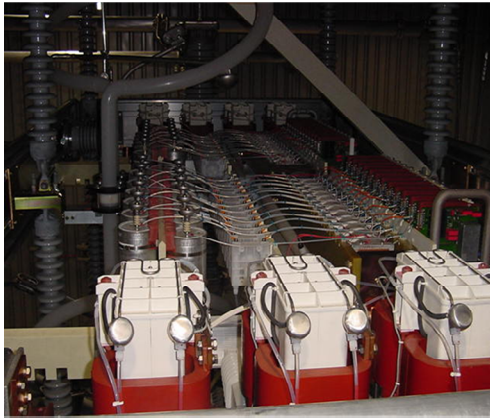
a) Valve sections

c) Surge arrester

b) Valve tower

d) Insulator structure

EGAT: Khlong Ngae, Songkla [25]

Fig. 2.34. Valve section, valve tower and valve surge arrester.

Figure 2.34. Valves, tour et limiteur de surtension.

The term valve is used to describe the series connection of sufficient modular units needed to make up one arm of one phase of a three phase 6-pulse Graetz bridge. A 3-phase Graetz bridge consists of six valves, two in each phase. Two 6-pulse Graetz bridges are required for twelve pulse operation. Therefore 12 valves are provided in each pole of an HVDC transmission system with one valve group per pole. The individual valves are arranged into

valve towers (Fig. 2.34-b) on a per phase basis. Four valves are needed in each phase and are arranged in a single unit known as a multiple valve unit (MVU). The complete thyristor converter is made up of three multiple valve units.

The main data of thyristor converter are summarized in Table 2.5.

Main Data of Thyristor Converter			
Steady State Operation	**Unit**	**100% Vdc**	**70% Vdc**
DC – power for 12- pulse group at rectifier	MW	300	210
DC – voltage for 12 pulse group at rectifier	kV	300	210
DC – current for 12-pulse group	A	1000	1000
Voltage between valve terminals	kV	122.24	0.9*122.24
Delay angle, rectifier	° el.	15.0	39.6
Commutation angle, rectifier	° el.	16.1	10.0
Extinction angle, inverter	° el.	19.6	43.4
Commutation angle, inverter	° el.	14.1	9.4
Number of thyristors in each complete valve	48		
Number of thyristors in the complete 12-pulse converter	576		
Snubber circuit	1.6 mF / 45 ohms		
Valve reactor (unsaturated/saturated)	16 * 0.5/0.02 mH = 8.0/0.32 mH		
Max. power loss of the 12-pulse group for the heat-exchanger unit		kW	1254
Max. power loss of the 12-pulse group dissipated into the air		kW	20

Table 2.5. Main data of the thyristor converter [23].

Table 2.5. Caractéristiques du convertisseur à thyristors [23].

2.6.5.1. Valve surge arresters

The valve surge arrester is an integral part of the valve design, having characteristics selected to meet the overall converter performance. The gapless zinc-oxide valve surge arresters are connected across each individual valve. The valve surge arresters protect the valves against overvoltages caused by switching surges coming from the AC system through the converter transformer as well as from ground faults between the converter transformer line and valve bushings.

The valve group surge arrester protects the 12-pulse converter group against overvoltages resulting from events on the AC and DC sides. This arrester is also a gapless zinc-oxide arrester. The valve and valve group surge arresters are mounted on the valve structure.

2.6.5.2. Valve cooling system

The components of the thyristor valves are water cooled using deionized water. Forced cooling of the thyristor valves is necessary because of the high current density of HVDC thyristor valves. This high current density results in large amounts of heat being generated in the components of the thyristor valves, which would result in a rapid failure if the heat were not removed.

The valve cooling system (Fig. 2.35) uses a pump to circulate the water through the thyristor valves and the cooling units. The cooling water enters and leaves the thyristor valves from the top of each valve structure. From the top of the structure, two main water supply pipes are run to each multiple value unit (MVU).
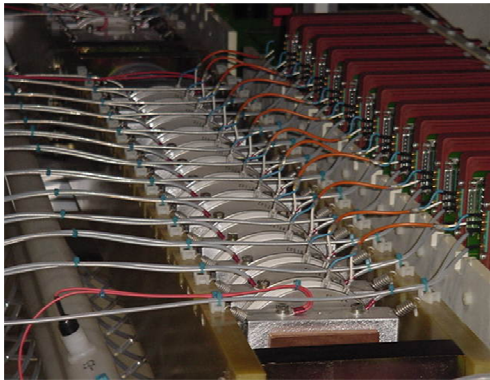
a) Thyristors electronics (TE) and thyristors

c) Valve cooling system b-Station
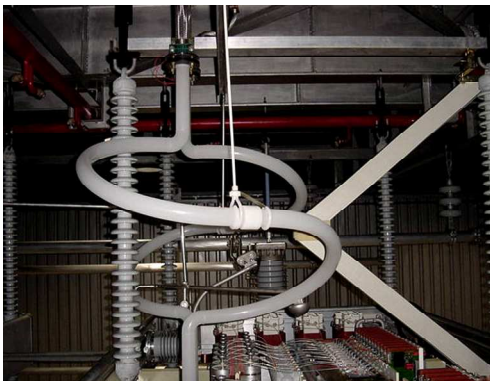
b) Valve cooling system a-Station
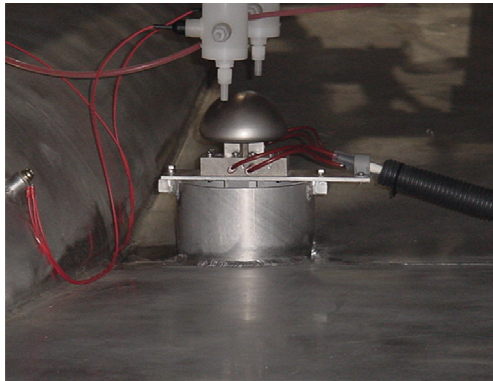
d) Valve cooling system c-Station

EGAT: Khlong Ngae, Songkla [25]

Fig. 2.35. Valve cooling or coolant distribution systems.

Figure 2.35. Système de refroidissement des valves.

The ion exchangers are used to keep the conductivity of the cooling water below 0.5 μS/cm. The ion exchangers are located in the valve cooling rooms inside the converter building.

The cooling circuit is operated with an open expansion tank and therefore it contains free oxygen. The metallic materials, which are in contact with the cooling medium, are alloys which develop a passivation layer under exposure to oxygen. This passivation layer protects the metals from further corrosion.

2.6.6. Smoothing reactor

The smoothing reactor (Fig. 2.36) is an air-cored reactor located immediately outside of the converter building and connected in series between the thyristor converter and the high voltage DC bus.

EGAT: Khlong Ngae, Songkla [25]

Fig. 2.36. Smoothing reactor (100 mH, 300 kV, 1000 A).

Figure 2.36. Inductance de lissage (100 mH, 300 kV, 1000 A).

The reactor is air cooled via natural convection. Smoothing reactors serve the following functions in an HVDC system namely:
- To reduce the incidence of commutation failure in inverters caused by dips in the AC voltage at the converter bus;
- To prevent consequent commutation failure in inverters by reducing the rate of rise of direct current in the bridge when the direct voltage of another series connected bridge collapses;

- To smooth the ripple in the direct current in order to prevent the current becoming discontinuous at light loads;
- To decrease the harmonic voltages and currents in the DC line;
- To limit the crest current in the rectifier due to a short circuit on the DC line;
- To limit the current in the thyristor valves during the converter bypass pair operation, due to the discharge of shunt capacitances in the DC line.

The main data of the smoothing reactor is summarized in Table 2.6.

Main Data of Smoothing Reactor		
Type		Air Core, Outdoor
Inductance (between no-load and maximum steady state dc current)	mH	100
Tolerance	%	±5
Nominal direct voltage	kV	300
Maximum direct voltage	kV	308
Nominal dc current at maximum ambient temperature	A	1000
Short-time current, 15 ms	Apeak	6000
Insulation class type		F

Table 2.6. Main data of the smoothing reactor [23].

Table 2.6. Caractéristiques de l'inductance de lissage [23].

2.6.7. DC filter

The HVDC conversion process creates voltage harmonics on the DC side. The DC side harmonic voltages superimposed on the DC voltage produce harmonic currents that enter into the DC line. The amplitude of these currents depends on the inductance of the smoothing reactor and the impedance of the DC filter. These harmonic currents may give rise to interference in the frequency range from 50 through 5000 Hz which may cause interference to voice frequency telephone circuits close to the DC line. DC filters are used to reduce the harmonic current flow on the HVDC transmission line by providing a low impedance path to the harmonic currents (Fig. 37):

- The DC filter is connected between the high voltage DC bus and the neutral bus just outside the DC smoothing reactor;
- The DC filter consists of two separate filters, a passive filter and an active filter;

- The passive DC filter is a double tuned filter, tuned to the 12th and 24th harmonics;
- An active DC filter is a device that injects harmonic currents into the DC line with the same magnitude but opposite polarity as the harmonic current generated by the HVDC converter. The net result is that very low harmonic currents enter the DC line and very low telephone interference is generated;
- The active filter operates in the frequency range from the 6th to the 48th harmonic.

Gapless zinc-oxide surge arresters are connected across the DC filter to protect the DC filter against overvoltages that may occur transiently during transferred switching surges with a subsequent DC bus fault to ground.

The main data of the components of the DC filter are summarized in Tables 2.7 and 2.8.
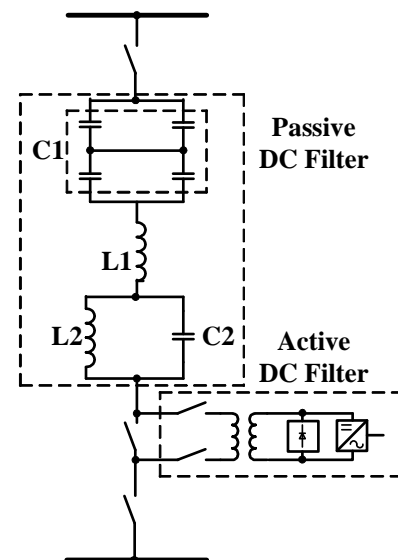
a) DC filter   b) Passive and active DC filters

EGAT: Khlong Ngae, Songkla [25]

Fig. 2.37. DC filter (a) and DC filter circuit diagram (b) [23].

Figure 2.37. Filtre continu (a) et schéma du filtre (b) [23].

EGAT-TNB Passive DC Filter Components			
Capacitors	unit	C1	C2
Nominal capacitance	mF	1.0	2.0
Tolerance of nominal capacitance	%	±0.5	±1.0
Maximum dc voltage	kV	308	-
Sum of harmonic voltages	kV rms	14.0	6.3
Total voltage	kV peak	328	8.9
RSS of harmonic currents	A	35.0	37.4
Arithmetic sum of harmonic currents	A	54.8	61.4

Table 2.7. Main data of passive DC capacitor components for DC filter [23].

Table 2.7. Caractéristiques des capacités du filtre côté continu [23].

EGAT-TNB Passive DC Filter Components			
Reactors	unit	L1	L2
Nominal inductance	mH	35.18	17.59
Tolerance of nominal capacitance	%	±0.5	±1.0
Quality factor	-	150	150
At the frequency	Hz	600	1200
Tolerance of nominal inductance	%	±1.0	0 ±1.0
Maximum dc voltage	kV	-	-
Sum of harmonic voltages	kV rms	10.2	6.3
Total voltage	kV peak	14.4	8.9
Sum of harmonic currents	A	35.0	66.9
Total current	A	35.0	66.9

Table 2.8. Main data of passive DC reactor components for DC filter [23].

Table 2.8. Caractéristiques des inductance du filtre côté continu [23].

2.6.8. DC switchyard

The DC switchyard as shown in Fig. 2.38 is used to connect the HVDC converter equipment to the overhead DC transmission line and to the DC filter. The switching devices in the DC switchyard are arranged so that the HVDC converter equipment can be connected to the DC transmission lines in the following configurations as shown in Table 2.9.
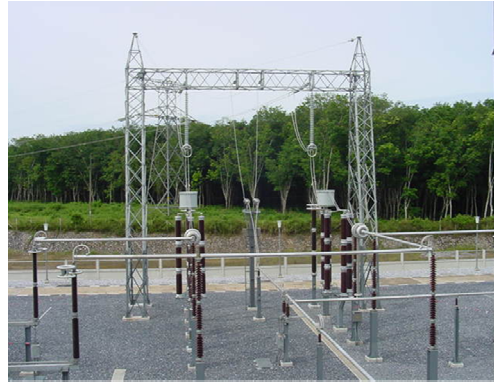
| a) Disconnecting switches | b) PLC (power Line Carrier) line trap and coupling |

EGAT: Khlong Ngae, Songkla [25]

Fig. 2.38. DC switchyard with disconnecting switches and PLC line trap and coupling.

Figure 3.38. Connecteurs côté continu et dispositif CPL (Courant Porteur en Ligne).

Monopolar stage		
Configuration/Mode	HVDC Line	LVDC Return line
1	Line 1	Line 2 and Neutral Line
2	Line 1	Neutral Line
3	Line 1	Line 2
4	Line 2	Neutral Line

Table 2.9. Connected configurations or mode of operations of the HVDC converter to the DC transmission lines in the monopolar system [23].

Table 2.9. Modes de fonctionnement et de connexion de la liaison CCHT en configuration unipolaire [23].

When the system is extended to a bipolar system, additional DC switching devices will be added as well as a second DC filter. Provision has been made for future expansion of the DC switchyard to accommodate this additional equipment. In the bipolar system, the following configurations as shown in Table 2.10 will be possible for connecting the HVDC converter equipment to the DC transmission lines:

Bipolar Stage		
Configuration/Mode	HVDC Line	LVDC Return line
1	Line 1 (monopolar operation)	Line 2 & Neutral Line
2	Line 1 (monopolar operation)	Neutral Line
3	Line 1 (monopolar operation)	Line 2
4	Line 2 (monopolar operation)	Neutral Line
5	Line 2 (monopolar operation)	Line 1
6	Line 2 (monopolar operation)	Line 1 & Neutral Line
7	Line 1 & Line 2 (bipolar operation)	Neutral Line

Table 2.10. Connected configurations of the HVDC converter to the DC transmission lines in the bipolar system [23].

Table 2.10. Modes de fonctionnement et de connexion de la liaison CCHT en configuration bipolaire [23].

2.6.9. DC transmission Line

Transmission line with measuring devices and switchyard are illustrated on Fig. 2.39.

2.6.9.1. DC disconnected switches

Motorized disconnected switches are used in the DC switchyard as shown in Fig. 2.39-b to connect and isolate the HVDC converter equipment to the overhead DC transmission line as well as for connecting and isolating the DC filters. The disconnected switches can be operated remotely from the DC initiation and monitoring system located in the control room. For maintenance and testing purposes, the disconnect switches can be operated locally at the device themselves.

2.6.9.2. Hybrid-optical DC current measuring system (Fig. 2.39-a)

The direct current measured value is an important quantity required to control and to protect HVDC systems. The hybrid-optical DC current measuring systems provided uses an ohmic shunt, which is series integrated into the DC circuit. The voltage drop across the shunt, which is proportional to the DC current, is measured and digitized by an electronic circuit which is located at high voltage potential. The measured signal is transmitted as a serial telegram via a fibre optic link to ground potential. Measuring systems are provided to measure the DC line and neutral line currents as well as the high and low voltage side pole current.

a) DC measuring devices

b) Monopolar system, 300 kV, 300 MW
DC transmission line

c) DC switchyard

EGAT: Khlong Ngae, Songkla [25]

Fig. 2.39. 300 kV, 300 MW DC transmission line with measuring devices and switchyard.

Figure 2.39. Ligne continue 300 kV, 300 MW avec instruments de mesure et de connexion.

2.6.9.3. High voltage DC bus surge arrester

A gapless zinc-oxide surge arrester is connected to the high voltage DC bus to protect the converter station against overvoltages coming from the DC side.

2.6.9.4. PLC equipment and DC side PLC filter

The Power line carrier (PLC) system on the DC line uses pole-to-pole coupling as the normal mode of transmission in a push-pull arrangement to achieve balanced signal injection and the lowest loss propagation of the signal along the line. A PLC filter is located between the converter transformer and the main AC busbars. These are two stage filters using series wavetraps with shunt connected PLC coupling capacitors and associated tuning units. In

addition to the PLC equipment, it is necessary to provide DC side PLC frequency filters to reduce the noise conducted into the DC line from the thyristor valves.

2.7. EGAT-TNB HVDC Control System

2.7.1. Hierarchical structure of control [24], [27]

The control systems for the HVDC system are organized into a hierarchic structure in order to enhance independent operation of pole 1 and the future pole 2 of the bipole. In the hierarchic structure, all of the DC system control and protection equipment is organized. There are four system level functions namely:

- The system control function;
- The station level function;
- The bipole-and the pole- level functions;
- The converter level function.

The system control functions coordinate the operation of the HVDC transmission system. Input for the system control level comes from both station controls and from operators at one control location. Generated orders are sent to both station controls.

The station level functions generate outputs for switching sequences to change the main DC circuit connections to the transmission line and neutral conductors and for switching AC filters and shunt capacitors as required for reactive power control.

For EGAT and TNB system, the bipole level functions are integrated in the pole level function. This function is used to measure DC voltage and DC current, and information from the system control functions concerning ordered system quantities. The bipole and pole level functions transmit orders to the converter controls in order to achieve a desired voltage and current or power level in the DC system.

The converter level control functions are implemented using measured values of the commutating voltages, the DC current, the DC voltage together with status of the valves. The firing pulses to the valves are the primary output of the converter unit control functions.

2.7.2. Basic operating modes

The HVDC system is designed to accommodate the basics operating modes of dc control used on the EGAT-TNB system are as follow [24]:

- Power control (P-mode);
- Current control (I-mode);
- Minimum extinction angle control (CEA) or commutation margin angle control;
- DC voltage control;
- Voltage dependent current limit (VDCL);
- Converter unit firing control;
- Tap changer control;
- Maximum and minimum current limits;
- Reduced pole voltage operation;
- Direction of pole power transfer;
- Power reversal;
- Open line test mode.

The fast closed loop controls are used for HVDC transmission systems together with slower supplementary controls. The control system for the EGAT-TNB system normally works with:

- Fast closed loop pole DC current control to control firing of rectifier valves;
- Fast closed loop pole DC voltage (rectifier end) control to control firing of inverter valves;
- Slower converter transformer tap changer control at rectifier end to maintain firing angle within pre-determined limits;
- Slower converter transformer tap changer control at inverter end to maintain extinction angle within pre-determined limits;
- Bipole power controller to adjust current referenced setting to the rectifier pole current controls to a calculated value so as to obtain the requested power transfer.

The designed converter V_d-I_d characteristics for the EGAT-TNB system are given in Fig. 2.40. The EGAT-TNB system normally operates with the rectifier controlling current and the inverter controlling rectifier side DC voltage. The current reference in the local station must be coordinated with the current reference sent to the remote station via telecommunications.

At the normal operating point (I_d=1 p.u.), the inverter is operated as the voltage controller to control the rectifier DC voltage ($V_d = V_{d2} + I_d \cdot R_d$) so that the terminal voltage at the rectifier is always maintained. Current margin (ΔI=0.1 p.u.) compensation controls are provided to decrease the inverter current reference to let the inverter takes over current control in order to minimize the power reduction, if there is a voltage decrease at the rectifier AC bus. The VDCL is used with the I_{dmin}-limit at 0.2 p.u. and at steady state operation, the delay angle and extinction angle are shown in Table 2.11.
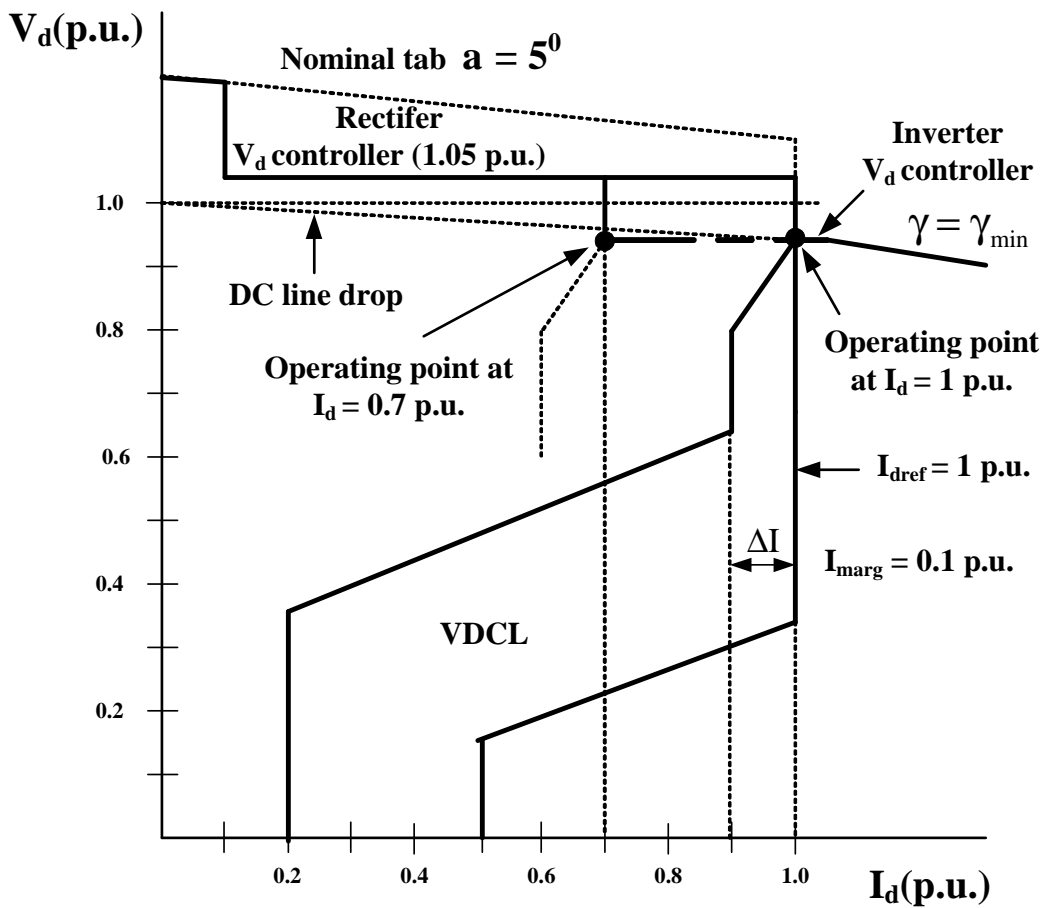
Fig. 2.40. EGAT-TNB operating V_d-I_d characteristics with inverter and rectifier V_d control [23].

Figure 2.40. Caractérisque V_d-I_d avec contrôle de la tension V_d au niveau onduleur et redresseur [23].

Delay or Firing angle and Extinction angle at Steady State Operation			
Steady State Operation	Unit	100% Vdc	70% Vdc
Rectifier			
Delay or firing angle, α_{min} (minimum)	° el.	**5.0**	**5.0**
Delay or firing angle, α_{nom} (nominal)	° el.	**15.0**	**39.6**
Commutation angle, u_{rec}	° el.	**16.1**	**10.0**
Inverter			
Extinction angle, γ_{min} (minimum)	° el.	**15.0 to 18.0**	**15.0 to 18.0**
Extinction angle, γ_{nom} (nominal)	° el.	**19.6**	**43.4**
Commutation angle, u_{inv}	° el.	**14.1**	**9.4**

Table 2.11. Delay and extinction angles at steady state operation [23].

Table 2.11. Angles d'amorçage et d'extinction en régime permanent [23].

2.7.3. Current and voltage step response tests

Tests were conducted to determine the dynamic response of the rectifier current controls at each station, by applying step or pulse current references with 0.08 p.u. (920 A to 1000 A) and a width of 300 ms. The result of the current step response test is shown in Fig. 2.41. The response time to the 0.08 p.u. step current reference was 15 ms which was lower than the 30 ms specified maximum and the response was well damped.
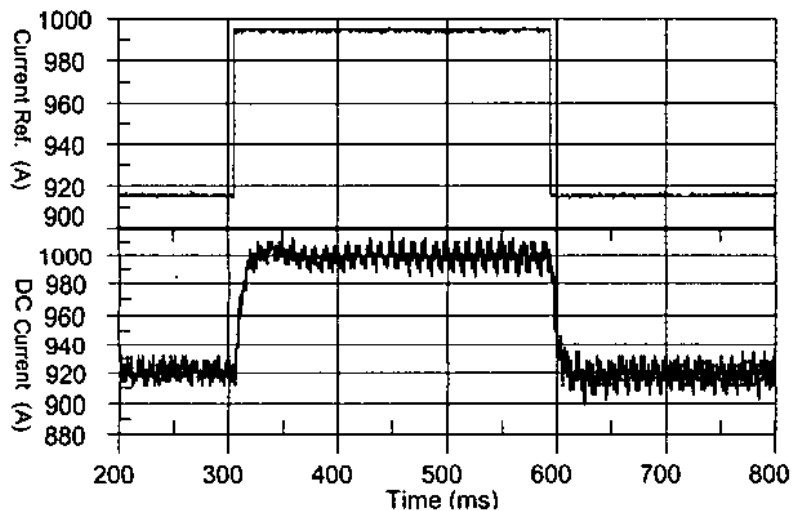
Fig. 2.41. Dynamic response of the current after reference step from 920 to 1000 A [14].

Figure 2.41. Réponse à des échelons de référence du courant entre 920 et 1000 A [14].

The voltage step response tests were conducted to demonstrate that the voltage control at the inverter achieved a good response to voltage changes. The response time criterion for the voltage test was not specified. The test was conducted by applying step voltage reference with 0.2 p.u. (300 kV to 240 kV and vice versa). The response of the inverter control to the step changes was very smoothly in both directions without overshoot as shown in Fig. 2.42. The controls are designed to respond very fast during the negative step. The voltage decreasing at the inverter causes immediate increased in current until the current controls at the rectifier can respond. In the positive direction the response was nearly linear with a ramp rate 0.4 kV per ms. This slower response is necessary to avoid a chance of firing angle overshoot which would result in a commutation failure as the gamma of the inverter is increased to bring up the DC voltage.
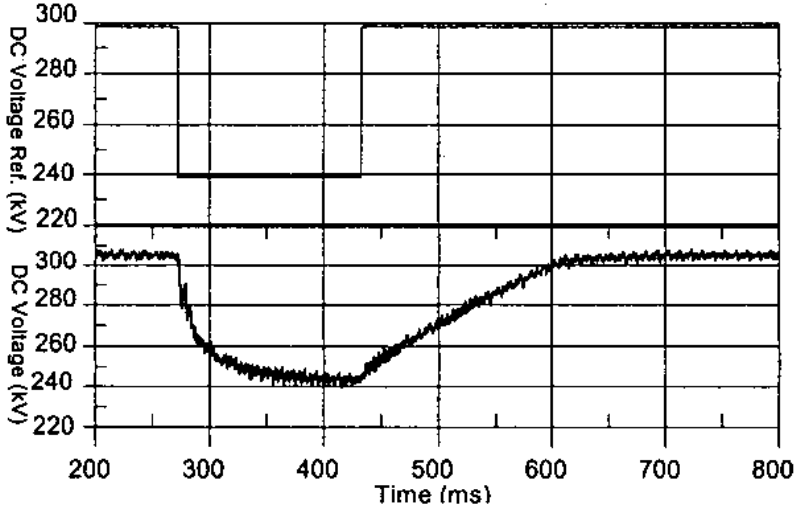
Fig. 2.42. Dynamic response of the voltage reference from 240 to 300 kV [14].

Figure 2.42. Réponse à des échelons de référence de tension entre 240 et 300 kV [14].

2.7.4. Starting procedure [24]

The HVDC system assumed to be in the block status. During the block status, there is no DC current and DC voltage in the system. For the results, firing angles are set at 160 degree of both stations. Once the converters are stated at 0.1 second, each of PI controllers would set the firing angles at 90 degree of both sides in order to start at low voltage level. In normal operation, the system is started at minimum power 30 MW. The first step, the current reference of the rectifier is equal to 100 A, while the voltage reference of the inverter station is equal to 300 kV.

The PI current controller adjusts the converter firing angle until the current controlled error is equal zero. At the inverter station, the DC voltage controller normally controls the rectifier DC voltage to the rated value, 300 kV.

The result from the real recoding signal is shown in Fig. 2.43. The transient response as shown in Fig. 2.44 was simulated by ATP[11]. After receiving the starting command, the DC referenced current I_{dref} is increased to 300 A for 100 ms in order to improve building up of DC current and DC voltage. Then the DC line current is controlled by adjusting the DC voltage of the rectifier terminal to maintain at 100 A (α = 28.91 degree). At the inverter station, the DC voltage of inverter terminal is also controlled to maintain at 300 kV (α = 152.6 degree) and 100 A at DC current line. However the current and voltage fluctuation problems did not happen in the real system because the filters of Khlong Nage and Gurun stations were installed to minimize the effect of switching transients during starting process.
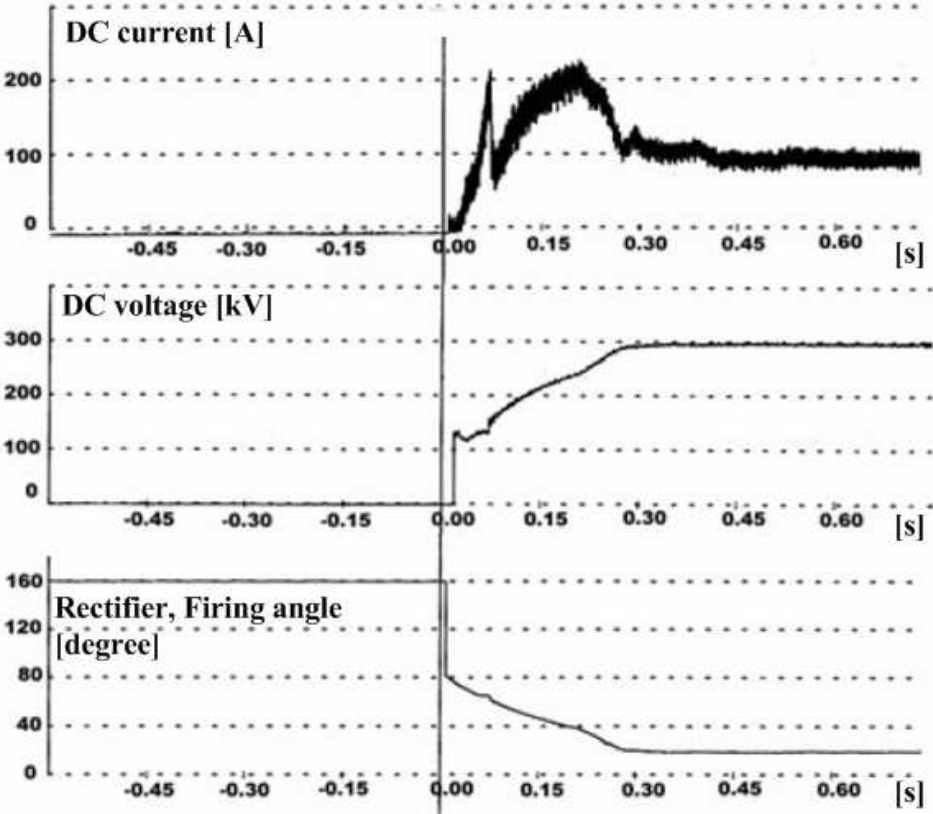
Fig. 2.43. Starting of the system, recording signal from field testing.

Figure 2.43. Démarrage du système, résultats expérimentaux.

[11] Alternative Transients Program (ATP) is a program system for digital simulation of transient phenomena of electromagnetic as well as electromechanical nature. With this digital program, complex networks and control systems of arbitrary structure can be simulated, for example the simulation of a 12-pulse HVDC converter station used by EGAT.
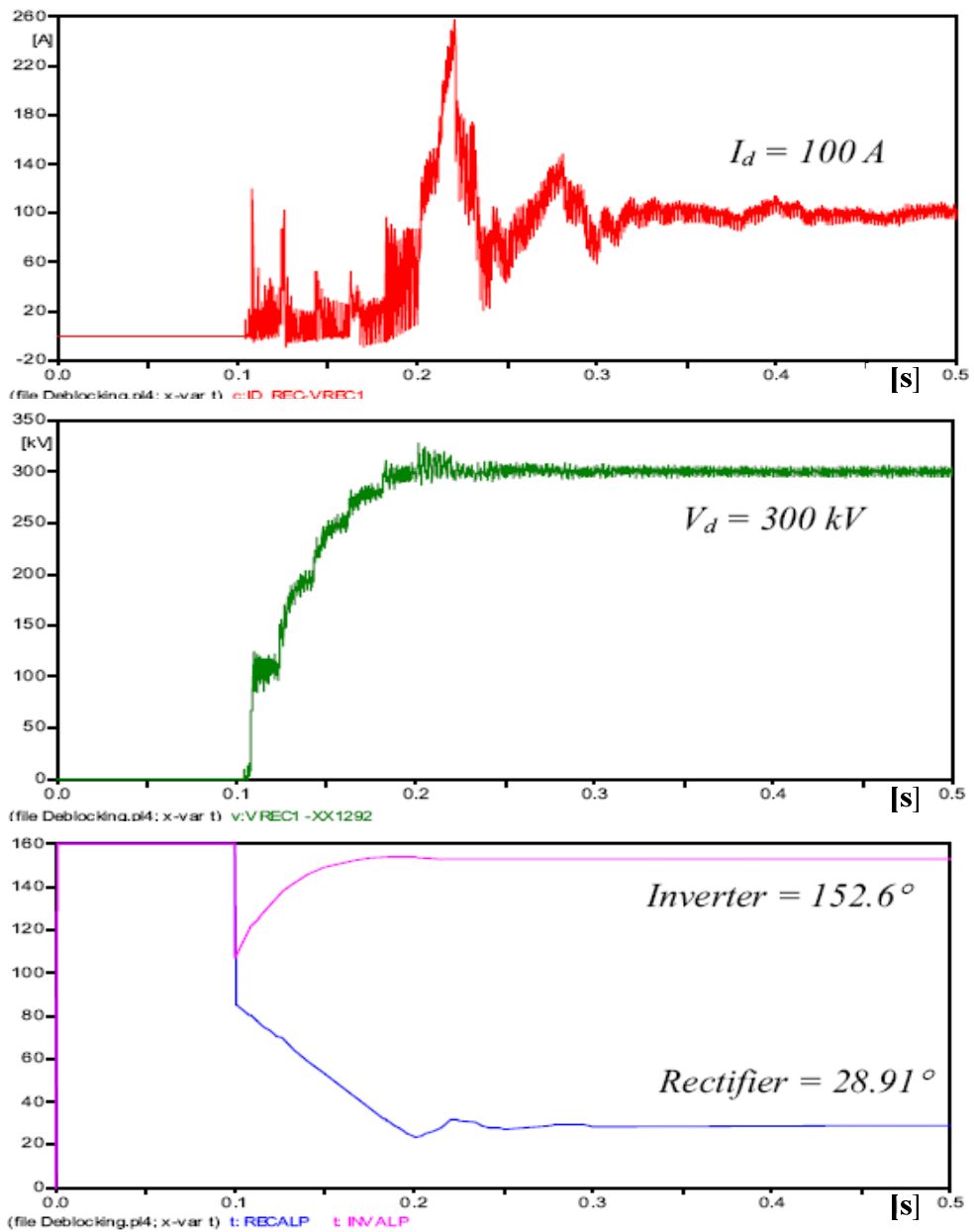
Fig. 2.44. Starting of the system, results from ATP simulation program.

Figure 2.44. Démarrage du système, résultats de simulation du logiciel ATP.

2.8. Conclusion

The HVDC interconnection system marks another successful cooperation effort between Thailand and Malaysia in future building up mutual energy security. The project will not only benefit the two nations, but also all ASEAN countries as a whole. As the first cross-border DC link in the region, the Thailand – Malaysia HVDC interconnection system has been included in the ASEAN Interconnection Master Plan Study as part of the ASEAN Power Grid. The success of the Thailand – Malaysia interconnection will greatly help accelerate the integration of the ASEAN power networks (Fig. 2.45) which will significantly enhance the region's sustainability and security of energy supply for the benefit of the people of all countries in the region.
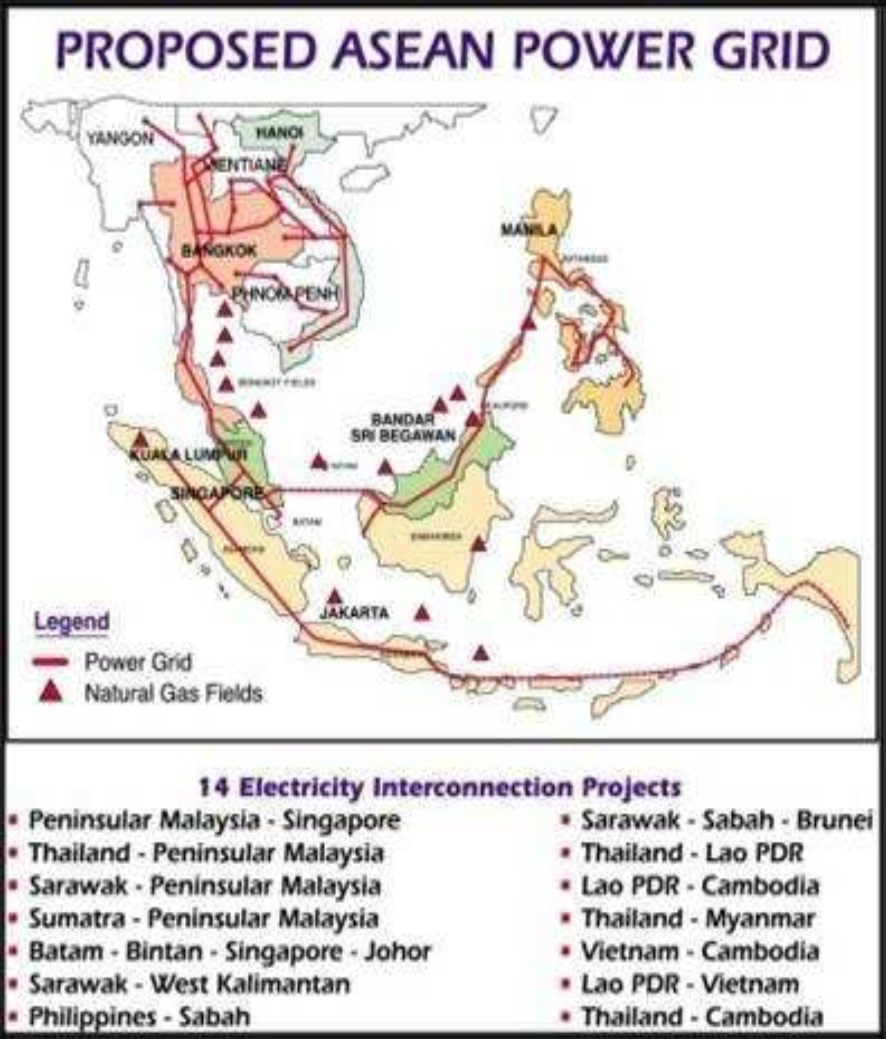
Fig. 2.45. Asean Power Interconnection Projects.

Figure 2.45. Projets d'interconnexion au niveau des pays de l'ASEAN.

Chapter 3

Power Quality and Harmonics

3.1. Introduction

The third chapter is concerned with the presentation of the power quality especially harmonics problems, harmonics sources, harmonics effects and the solutions to improve this quality such as phase shifting- and passive filter. The active harmonic filter is one of the most sophisticated solutions to harmonic problems. So that, in this chapter will also be detailed a realized example[12] of an active harmonic filter i.e. power circuit and control circuit and the experimental results.

3.2. Power quality

Power quality is a problem that involves the producing and supplying electric utilities, including end users equipments and manufacturing machines. The power quality problem is become a growing problem which is facing the utilities now and the future due to the rapid development of the power electronics technology. The power switching semiconductor devices are increasingly used in modern industrial applications that have increased the occurrence of unbalanced currents, unacceptable harmonic levels and low power factor in power distribution and transmission systems.

The term power quality relates to the amplitude, frequency and distortion of the electrical supply. While the utility provides a supply, which has the amplitude and frequency within the controlled limits, it is the consumers and their equipments that distort both the voltage and current waveforms.

Power quality can be roughly broken into categories as follows [28-29]:

---

[12] The first 3-phase active harmonic filter employing DSP that has been developed in Thailand since 2003.

- Steady-state voltage magnitude and frequency;
- Voltage sags;
- Grounding;
- Harmonics;
- Voltage fluctuations and flicker;
- Transients;
- Monitoring and measurement.

3.3. Harmonics

In most cases, power electronics equipments are considered to be the cause of harmonics. While power electronic loads such as AC-DC and DC-DC converters produce harmonics because of the nonlinear relationship between the voltage and current across the power electronic devices, harmonics are also produced by a large variety of conventional equipments such as electrical machines and transformers. Harmonics are currents, usually in multiples of the fundamental frequency of supply. For example, on a 50 Hz supply, the 5th harmonic is 250 Hz, 7th harmonic is 350 Hz, etc. These are called integer harmonics that is exact multiples of the supply frequency.

Any alternating current flow through any circuit at any frequency will produce a voltage drop at the same frequency. Harmonic currents, which are produced by power electronic loads, will produce voltage drops in the power supply impedance at those same harmonic frequencies. Because of this interrelationship between current flow and voltage drop, harmonic currents generated at any location will distort in the supply circuit.

3.3.1. Harmonics sources

The main sources of voltage and current harmonics within the power system are classified into two categories as follows [28]:
- Classical harmonics sources, and
- Static converter or Power electronics harmonics sources.

3.3.1.1. Classical harmonics sources

Prior to the development of static converter plant, power system harmonic distortion was primarily associated with the design and operation of electric machines and transformers.

Indeed the principal harmonic source present in the system in earlier day was the magnetizing current of the power transformers. Electric power generators provided the main secondary source since their practical economic design required that some departure from the ideal sinusoidal wave shape must be accepted.

Modern transformers and rotating machines under normal steady state operating conditions do not of themselves cause significant distortion in the network. However, during transient disturbance and when operating outside their normal state range, they can considerably increase their harmonic contribution. The classical harmonics sources are presented as follows:

- Transformer magnetization nonlinearities (magnetizing current harmonics, symmetrical over excitation, inrush current harmonics, DC magnetization);
- Rotating machine harmonics (MMF distribution of three phase winding, slot harmonics, voltage harmonics produced by synchronous machine, voltage harmonics produced by induction motor);
- Distortion caused by arc-furnaces;
- Fluorescent lighting harmonics.

All these devices will cause harmonic currents to flow, and some devices directly produce voltage harmonics.

3.3.1.2. Static converter harmonics sources

The derivation of the harmonic currents produced by static power converters requires accurate information of the AC voltage waveforms at the converter terminals, converter configuration, type of control, AC system impedance and DC circuit parameters. However, the introduction of so many factors at the outset would obscure the basic principles involved. It is probably more appropriate to start by assessing the effect of the control philosophy and converter configuration under idealized AC and DC system conditions and then to introduce the other factor one by one. Static converter harmonic sources are presented as follows:

- Line commutated converter (AC-DC converter);
- Pulse width modulated converter (DC-DC and DC-AC converters) i.e. switched-mode power supplies, uninterruptible power supplies or adjustable speed drives;
- Cycloconverter;
- Static Var compensator.

3.3.2 Harmonics effects

Harmonics are specifically identified as a potential power quality problem within the power system and interference with communications [30].

3.3.2.1 Harmonic effects within the power system

Once the harmonic sources and their magnitudes are clearly defined, they must be interpreted in terms of their effect on system and equipment operation. Individual elements of the power system must be examined for their sensitivity to harmonics as a basic for recommendations on the allowable levels.

The main effects of voltage and current harmonics within the power system are:

- Amplification of harmonics levels resulting from series and parallel resonance;
- Reduction of efficiency of power generation, transmission, and utilization;
- Aging of the insulation of electrical plant components and thus shortening of their useful life;
- Plant mal-operation;
- Effects of resonance on system behaviour (overloading, overheating and failure of power factor correction capacitors caused by resonance due to interaction of capacitors with harmonics);
- Effects of harmonics on rotating machines (overheating from harmonics losses, harmonics torque or pulsation torque);
- Effect of harmonics on static power plant (overloading and overheating of distribution transformers and neutral conductors);
- Harmonic interference with ripple control system;
- Harmonics interference with power system protection (spurious operation of fuse, circuit breakers and other protective equipment);
- Effect of harmonics on consumer equipments (malfunction and failure of electronic equipments namely: radio, television receivers, fluorescent and mercury arc lighting, computers, converter equipments);
- Effect of harmonic on power measurements (excessive measurement errors in metering equipment);
- Effect of harmonic distortion on power factor;

- Damage and disruption to standby generators and associated AVR (Automatic Voltage Regulator);
- Voltage glitches in computers workstation systems resulting in lost data. Excessive flicker on visual display units (VDUs).

3.3.2.2. Harmonic interference with communications

Noise in the form of Electromagnetic interference on communication circuits and telephone systems degrades the transmission quality and can interfere with signaling. At low levels noise causes annoyance; at higher levels the transmission quality is degraded and results in loss of information; in extreme cases noise can render a communication circuit unusable.

The signal to noise ratio, commonly used in communication circuits as a measure of the quality of transmission, must be used with caution when considering power system interference because of the relative power levels of power (MW) and communication circuits (mW). Due to the large difference in power levels, small unbalanced audio frequency components within the power network may easily produce considerable noise voltage levels when coupled into a metallic communication circuit.

3.3.3. Power quality indices

The problems with harmonics have lead to the development of a number of indices to define acceptable levels of a harmonic distortion. In AC applications, different measures of harmonics level are given. In most cases, there are the total harmonic distortion (THD), crest factor (F_c), power factor P_F and $\cos\varphi$, derating factor (K) and telephone harmonic form factor $(THFF)$. These indices are defined as follows [30-31].

3.3.3.1. Total harmonic distortion

The total harmonic distorsion (THD) is a value used to quantify harmonics at a given measurement point and defined by following equations (3.1 and 3.2):

$$THD_f = \frac{\sum_{n=2}^{\infty} h_n^2}{h_1} \cdot 100\% \tag{3.1}$$

where THD_f is the total harmonic distortion with respect to the fundamental and $h_1, h_2, ... h_n$ are the RMS value of each harmonic order

THD_r is the total harmonic distortion with respect to the RMS value of the signal defined as:

$$\text{THD}_r = \frac{\sqrt{\sum_{n=2}^{\infty} h_n^2}}{\sqrt{\sum_{n=1}^{\infty} h_n^2}} \cdot 100\% \qquad (3.2)$$

THD_f is used in Europe, which means that in the electrical system with high levels of harmonic disturbances, the total harmonic distortion may be greater than the fundamental i.e. $\text{THD}_f > 100\%$. THD must be normally as low as possible, practically a current THD less than 10% to 15% is an acceptable level [30]. Two THD values must be taken into account, THD_v for the voltage and THD_i for the current. THD_i is caused by the load, whereas THD_v occurs at the source and is a consequence of a high level of current harmonics.

3.3.3.2. Crest factor

The ratio between the peak voltage and the RMS voltage is the crest factor (F_c). This indicates the distortion of the signal and it is defined as follows:

$$F_c = \frac{V_{peak}}{V_{rms}} \qquad (3.3)$$

For a sinusoidal signal, the crest factor F_c is $\sqrt{2}$. In distorted signal, the crest factor can be as high as 4 [30].

3.3.3.3. Power factor and cos φ

The power factor and $\cos\varphi$ are often thought to be the same. Their values are identical only when the current and voltage waveforms are sinusoidal.

The power factor P_F is defined as follows:

$$P_F = \frac{P}{S} \qquad (3.4)$$

where P is the active power in W and S the apparent power in VA.

and:

$$\cos\varphi = \frac{P_{h1}}{S_{h1}} \qquad (3.5)$$

where P_{h1} is the fundamental of active power in W and S_{h1} the fundamental of apparent power in VA.

3.3.3.4. Derating factor

The low voltage transformers are particularly sensitive to harmonic currents which are the major sources of additional temperature rise and breakdown. When a transformer operates at rated load, the rated power and heat losses are calculated by assuming that a transformer will supply linear loads without harmonic current. The derating factor K relates to transformer derating and is used to calculate the maximum power available at the transformer output when there are harmonics as shown in equation 3.6:

$$K = \frac{I_{peak}}{I_{rms}} \cdot \frac{1}{\sqrt{2}} \qquad (3.6)$$

For example, if the current measurements at the secondary winding of a 1000 kVA transformer produced a derating factor of 1.2, therefore, the maximum power that the transformer can supply is 833.33 kVA.

CENELEC[13] provides the definition for the derating factor in the document HD428.4 S1:

$$K = \sqrt{1 + \frac{e}{1+e} \cdot \left(\frac{I_{h1}}{I_{rms}}\right)^2 \cdot \sum_{n=2}^{n=N} n^q \cdot \left(\frac{I_n}{I_{h1}}\right)^2} \qquad (3.7)$$

where:

> n = the harmonic order
>
> I_{rms} = the total RMS current, including distortion
>
> I_n = the RMS value of order *n* harmonic current
>
> I_{h1} = the RMS value of the fundamental current (50 Hz)

---

[13] CENELEC, the **European Committee for Electrotechnical Standardization**, was created in 1973 as a result of the merger of two previous European organizations: CENELCOM and CENEL. Nowadays, CENELEC is a non-profit technical organization set up under Belgian law and composed of the National Electrotechnical Committees of 30 European countries. In addition, 8 National Committees from neighbouring countries are participating in CENELEC work with an Affiliate status.

N = the maximum harmonic order taken in to account

q = constant that depends on the type of transformer winding and the frequency of distribution system, q is generally equal to 1.7 [30].

e = the ratio between losses due to the fundamental and those caused by a DC current, e is generally equal to 0.3 [30].

3.3.3.5. Telephone harmonic form factor

The telephone harmonic form factor (THFF) is defined as follows:

$$THFF = \frac{1}{V_{h1}} \cdot \sqrt{\sum_{n=1}^{n=50} (K_n \cdot P_n \cdot V_n)^2} \tag{3.8}$$

where: n = the harmonic order

V_{h1} = the RMS value of the fundamental voltage

V_n = the RMS value of order n harmonic voltage

P_n = (Psophometric weighting[14] of order n harmonic)/1000

and: $K_n = \dfrac{n \cdot 50}{800}$

3.4. Harmonics mitigation methods

3.4.1. Phase shifting

A phase shift transformer is the most common used to create the phase shift of two power supplies. For example 30 degree is obtained by connecting two 6-pulse converter bridges in series to create a 12-pulse converter, for example with 2 units of 3-phase transformers (Y/Y, Y/Δ) as shown in Fig. 3.1. With this solution for instance 24-pulse operation is achieved by means of 4 units of 3-phase transformers with 15 degree phase shifts and 48-pulse operation required 8 units of 3-phase transformers with 7.5 degree phase shifts.

The 12-pulse converter configuration consist of two 6-pulse converters in series connection fed from 2 units of 3-phase transformers with the equal fundamental voltage and

---

[14] Psophometric weighting: A <u>noise weighting</u> established by the International Consultative Committee for Telephony (<u>CCIF</u>, which became <u>CCITT</u> and, more recently, <u>ITU-T</u>), A statistical approach is used to evaluate the limits for harmonic currents in AC power lines, the goal being to prevent excessive telephone noise interference voltages in subscriber cables in rural areas. The analysis is based on a Monte Carlo simulation which takes into account the effect of the experimental probability distributions of the relevant parameters.

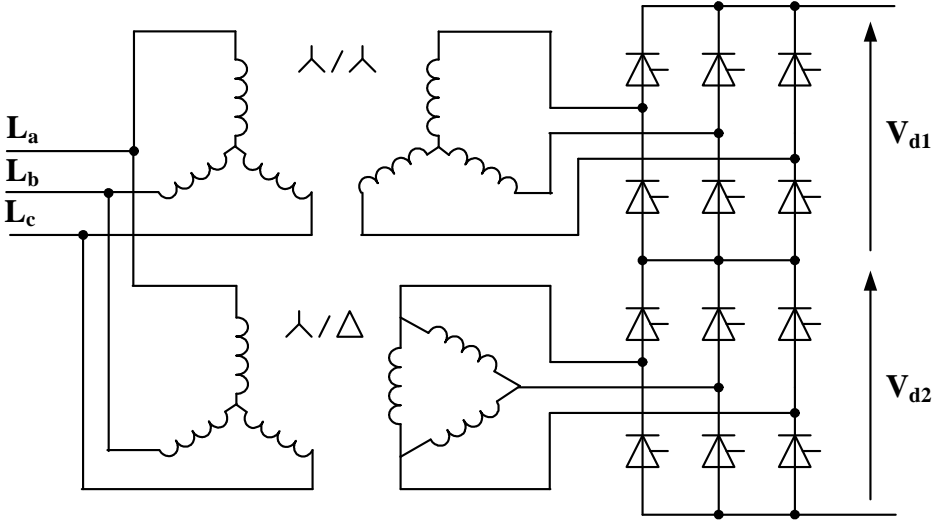phase shifted by 30 degree. The transformer connection has effectively eliminated the 6-pulse harmonics.

Fig. 3.1. Twelve-pulse bridge circuit with 2 units of 3-phase transformers.

Figure 3.1. Redresseur dodécaphasé réalisé à partir de deux transformateurs triphasés.

3.4.2. Passive filters

The purpose of a harmonic filter is to reduce the amplitude of one or more fixed frequency current or voltage. In general harmonics filters are shunt filters because there are connected in parallel with the power system by providing shunt paths of low impedance to ground for current at one or more harmonic frequencies. For the power applications, shunt filters are always more economical than series filters in term of the power rating, sizes and costs of the components.

Shunt filters are designed in three basic categories as follows [28-29]:
- Single-tuned filters;
- Multiple- or double-tuned filters;
- Damped filters.

The single tuned filter as shown in Fig. 3.2-a. is series circuit of RLC tuned to the frequency of one harmonic, normally for a lower characteristic harmonic i.e. 5th harmonic. The multiple or double-tuned filter is a transformation of two single-tuned filters as shown in Fig. 3.2-b into double-tuned filter in Fig. 3.2-c tuned to frequency of two harmonics i.e. 5th and 7th harmonics.

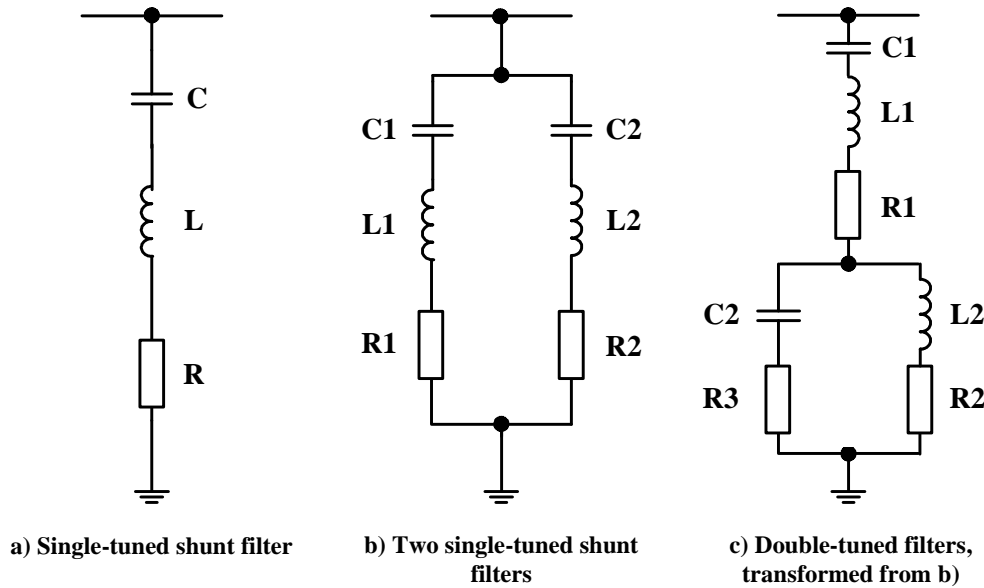| a) Single-tuned shunt filter | b) Two single-tuned shunt filters | c) Double-tuned filters, transformed from b) |

Fig. 3.2. Single-tuned and double-tuned harmonic filters.

Figure 3.2. Filtres harmoniques centrés sur une ou deux fréquences.

The damped filter provides low impedance for a wide range of frequencies. There are fundamentally 4-types of damped filters as show in Fig. 3.3:

- The first order filter (Fig. 3.3-a) requires a large capacitor and has excessive loss at the fundamental frequency;

- The second order filter (Fig. 3.3-b) provides the best filtering performance but has high loss at the fundamental frequency;

- The third order filter (Fig. 3.3-c) has lower loss at the fundamental frequency as compared with the second order filters. The rating of C_2 is very small compared with C_1 because of the increased impedance at that frequency caused by capacitor C_2;

- The C-type filter (Fig. 3.3-d) lies in between the second order and third order. The reduction in fundamental frequency loss is an advantage of the C-type filter because C_2 and L are series tuned at that frequency.

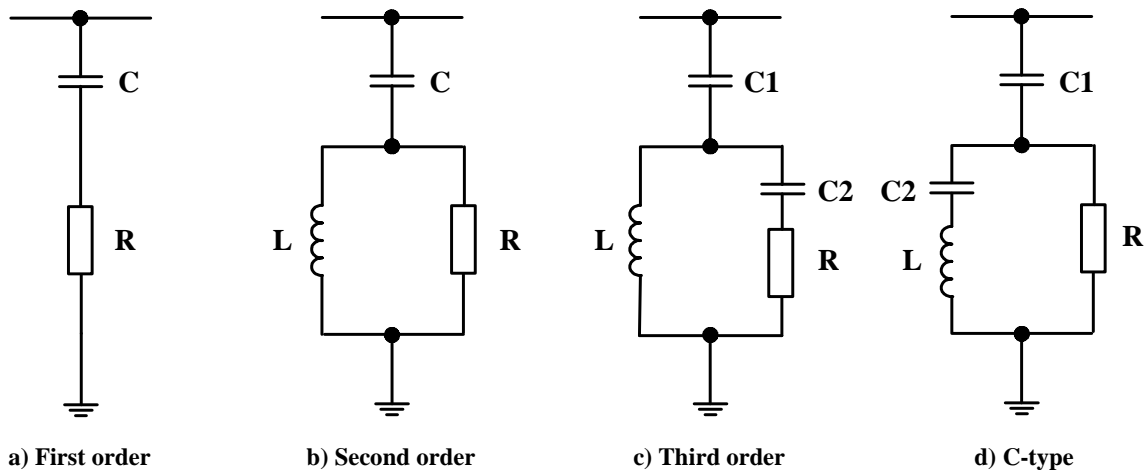a) First order   b) Second order   c) Third order   d) C-type

Fig. 3.3. High-pass damped filters.

Figure 3.3. Filtres amortis.

3.4.3. Active filters

The active filters are dynamic and adjustable solutions to power quality problems. The active filters are able to compensate current and voltage harmonics, reactive power, suppress flicker, to improve voltage balance in 3-phase network and to regulate terminal voltage.

The advantage of active filtering is that it automatically adapts to changes in the network and load fluctuations. They can compensate for several harmonic orders and are not affected by major changes in network characteristics, eliminating the risk of resonance between the filter and network impedance.

The active filters are developed with PWM-current source or -voltage source inverters. The active filter topology is mostly the PWM voltage source inverter which is lighter, cheaper and expandable to multilevel structure, to improve its performance for high power rating compensation with lower switching frequencies. The PWM-voltage source inverter has to be connected to the AC mains through coupling reactors and an electrolytic capacitor keep a DC voltage constant and ripple free.

The active filters can be classified based on the type of a converter, topology, control structure and compensation characteristics. The classification is based on the topology such as shunt active filter (Fig. 3.4), series active filter (Fig. 3.5) and hybrid active filter (Fig. 3.6), [32-34].
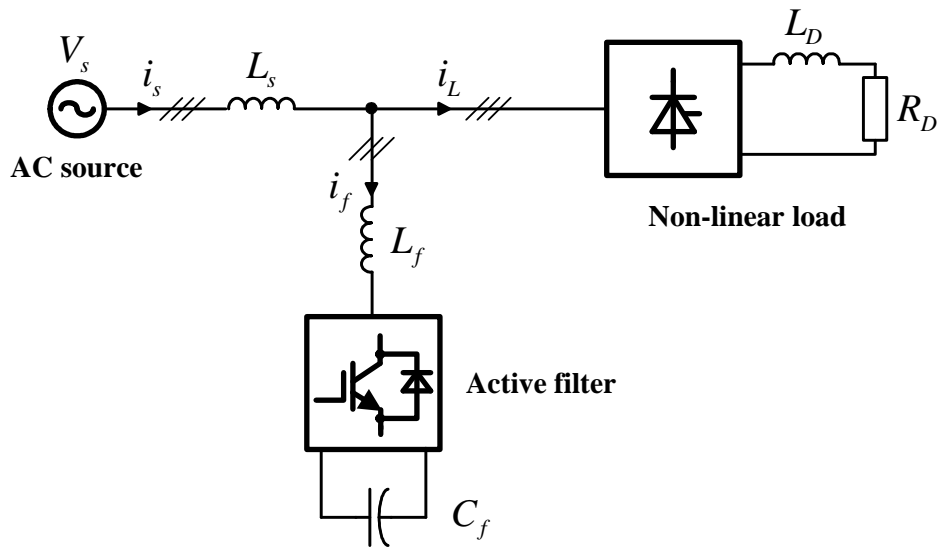
Fig. 3.4. Shunt active filter with PWM-voltage source inverter.

Figure 3.4. Onduleur de tension à MLI pour filtre actif parallèle.
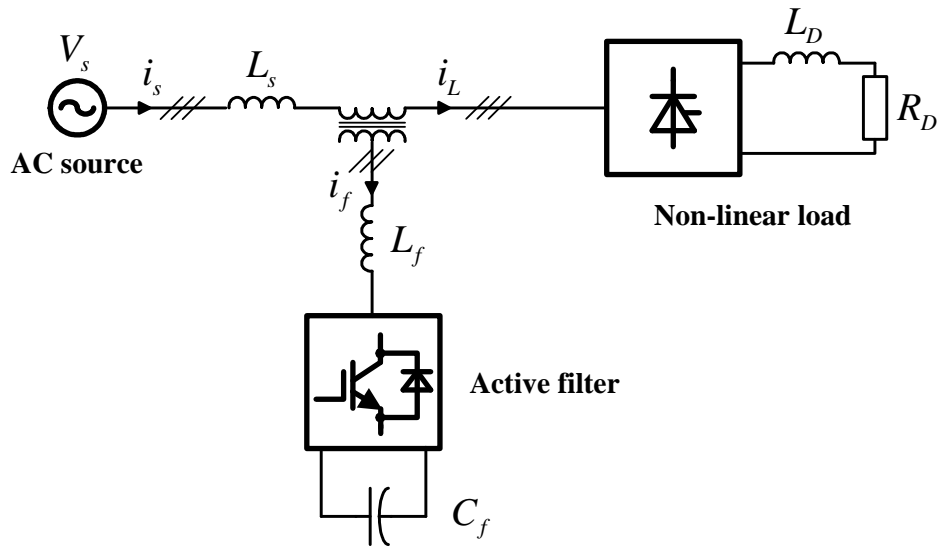

Fig. 3.5. Series active filter with PWM-voltage source inverter.

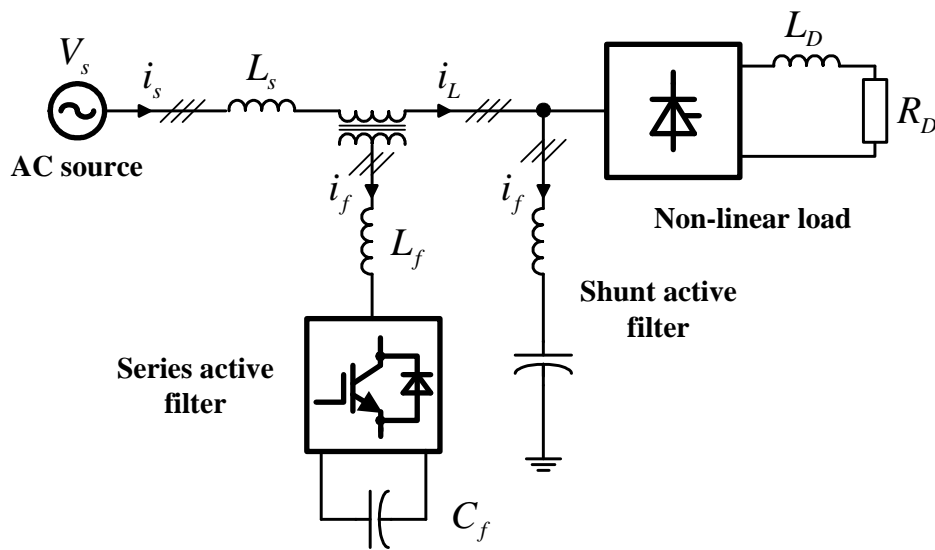Figure 3.5. Onduleur de tension à MLI pour filtre actif série.

Fig. 3.6. Hybrid active filter with PWM-voltage source inverter.

Figure 3.6. Onduleur de tension à MLI pour filtre actif hybride.

The shunt active filters are widely used to compensate current harmonics, reactive power and unbalanced load current. The series active filter is connected in series with the AC mains through a coupling transformer to eliminate voltage harmonics and to balance and control the terminal voltage of the load. The hybrid active filter is a combination of series active filter and passive shunt filter. This filter can be used for the compensation of high power system because the rated power of the filter is reduced. The passive LC filter is used to compensate lower order current harmonics and reactive power.

The active filters can compensate specific power quality problems therefore the selection of shunt, series and hybrid active filters to improve power quality depends on the source of the problem.

3.5. Shunt active filter as test system

The shunt active filter is a six-switch voltage source inverter (VSI) connected in parallel at the point of common coupling of the system as shown in Fig. 3.7 [35-36]. The DC capacitor C_f acts as an energy source which provides the reactive powers for the non linear load. This filter is applicable to any type of nonlinear load. Moreover, with appropriate control structure, the active filter can also compensate the power factor of the load.
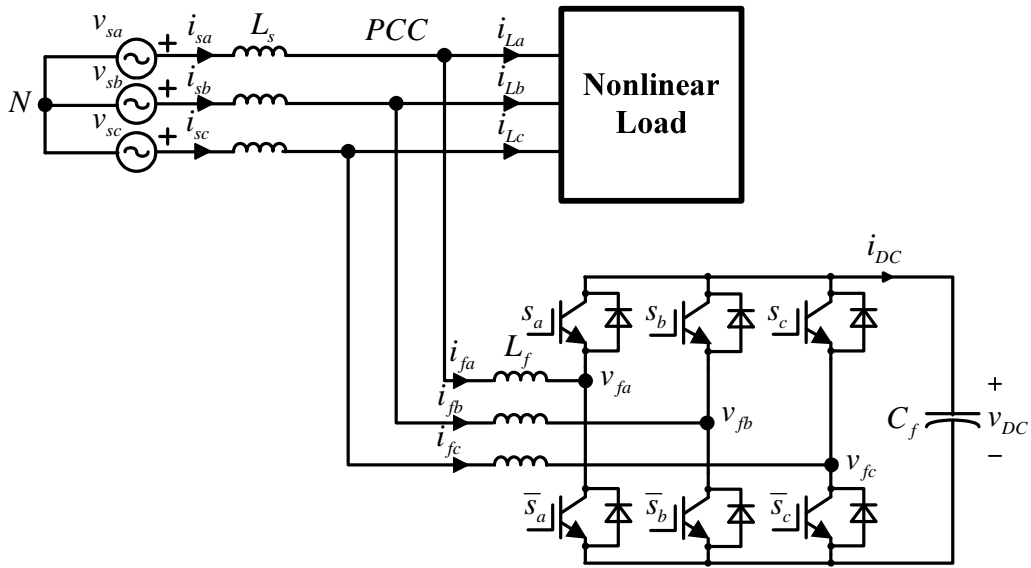
Fig. 3.7. Power circuit of the shunt active filter with six-switch VSI.

Figure 3.7. Onduleur de tension utilisé comme filtre actif parallèle.

The shunt active filter operates as a current source by injecting the compensating currents I_f with the same amount of harmonic components I_h generated by the load but 180 degree phase shifts. Therefore the harmonic currents contained in the load current are cancelled and the line current I_s remains sinusoidal. The line current I_s as shown in Fig. 3.8 is:

$$i_s = i_L + i_f \tag{3.9}$$

Fig. 3.8. Single line diagram of the shunt active filter.

Figure 3.8. Schéma monophasé du filtre actif parallèle.

The current from a nonlinear load is:

$$i_L = i_l + i_h \tag{3.10}$$

where:

i_s = line currents from AC power supply

i_L = nonlinear load currents

i_1 = fundamental component of a nonlinear load current

i_h = harmonic components generated by a nonlinear load

i_f = compensating currents generated by the active filter

The compensating current from the active filter is:

$$i_f = -i_h \tag{3.11}$$

therefore:

$$i_s = i_1 \tag{3.12}$$

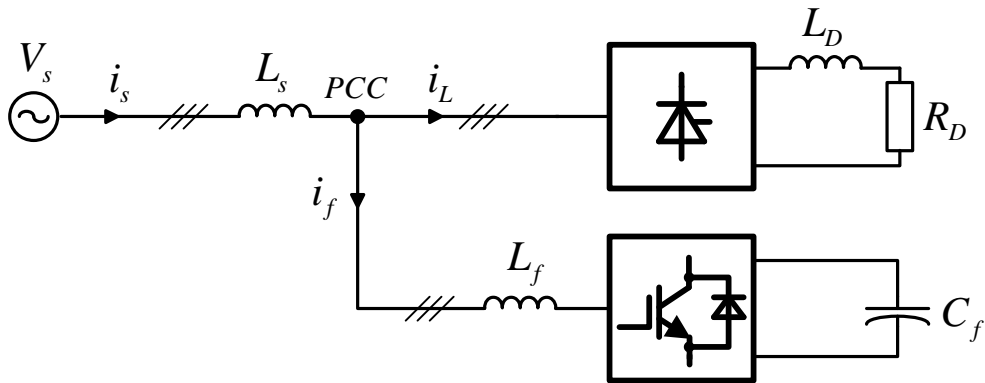### 3.5.1. Mathematical model of the shunt active filter

In Fig. 3.6, it is assumed that there is no line inductances ($L_s = 0$) and the 3-phase system is balanced. The instantaneous voltages of the 3-phase system are expressed as:

$$v_{sa}(t) = \sqrt{2} \cdot V_s \cos \omega t \tag{3.13}$$

$$v_{sb}(t) = \sqrt{2} \cdot V_s \cos(\omega t - \frac{2\pi}{3}) \tag{3.14}$$

$$v_{sc}(t) = \sqrt{2} \cdot V_s \cos(\omega t + \frac{2\pi}{3}) \tag{3.15}$$

where V_s is the effective value of the line voltage.

The voltage differential equations of the shunt active filter are as follows [37-38]:

$$L_f \cdot \frac{di_{fa}}{dt} = v_{sa} - f_a \cdot v_{DC} \tag{3.16}$$

$$L_f \cdot \frac{di_{fb}}{dt} = v_{sb} - f_b \cdot v_{DC} \tag{3.17}$$

$$L_f \cdot \frac{di_{fc}}{dt} = v_{sc} - f_c \cdot v_{DC} \tag{3.18}$$

and:

$$C_f \cdot \frac{dv_{DC}}{dt} = f_a \cdot i_{fa} + f_b \cdot i_{fb} + f_c \cdot i_{fc} \tag{3.19}$$

where:

C_f = DC capacitance of the active filter

i_{fa}, i_{fb}, i_{fc} = input currents of the active filter in phase a, b, and c

f_a, f_b, f_c = switching functions which have the values: $\in \left\{ 0, \ \pm\dfrac{1}{3}, \ \pm\dfrac{2}{3} \right\}$

s_a, s_b, s_c = switching status of the positive DC bus switches in each branch,

$\in \left\{ 0, \ 1 \right\}$

In this case, the switching functions can be obtained from following equations that used with the 2-level voltage source inverter [39-40]:

$$f_a = \frac{1}{3}(2 \cdot s_a - s_b - s_c) \tag{3.20}$$

$$f_b = \frac{1}{3}(-s_a + 2 \cdot s_b - s_c) \tag{3.21}$$

$$f_c = \frac{1}{3}(-s_a - s_b + 2 \cdot s_c) \tag{3.22}$$

The set of equations 3.16 to 3.19 in fixed reference frame (a,b,c-axis / α,β-axis) are transformed into the rotating reference frame (d,q-axis) by using coordinate transformation (Clarke's and Park's transformation) and the transformation matrix is equal to [41]:

$$\begin{bmatrix} x_d \\ x_q \end{bmatrix} = \frac{2}{3} \begin{bmatrix} \cos\omega t & \cos(\omega t - \dfrac{2\pi}{3}) & \cos(\omega t + \dfrac{2\pi}{3}) \\ -\sin\omega t & -\sin(\omega t - \dfrac{2\pi}{3}) & -\sin(\omega t + \dfrac{2\pi}{3}) \end{bmatrix} \begin{bmatrix} x_a \\ x_b \\ x_c \end{bmatrix} \tag{3.23}$$

where x_d and x_q are the vectors in d- and q-axis and represent the voltage, the current or the switching function. In this case, the equations on the rotating reference frame are:

$$L_f \cdot \frac{di_{fd}}{dt} = v_{sd} + \omega \cdot L_f \cdot i_{fq} - f_d \cdot v_{DC} \tag{3.24}$$

$$L_f \cdot \frac{di_{fq}}{dt} = v_{sq} - \omega \cdot L_f \cdot i_{fd} - f_q \cdot v_{DC} \tag{3.25}$$

$$C_f \cdot \frac{dv_{DC}}{dt} = \frac{3}{2} \cdot (f_d \cdot i_{fd} + f_q \cdot i_{fq}) \tag{3.26}$$

where:

v_{sd}, v_{sq} = voltage of the 3-phase system in d- and q-axis

$$i_{fd}, i_{fq} = \text{active filter current in d- and q-axis}$$

$$f_d, f_q = \text{switching function in d- and q-axis}$$

$$\omega = \text{angular velocity of the 3-phase system}$$

In case of the balanced 3-phase system, the voltage equations 3.13 to 3.15 on the rotating reference frame are as follows:

$$v_{sd} = \sqrt{2} \cdot V_s \tag{3.27}$$

and:
$$v_{sq} = 0 \tag{3.28}$$

Therefore, equations 3.16 and 3.17 can be written as:

$$L_f \cdot \frac{di_{fd}}{dt} = \sqrt{2} \cdot V_s + \omega \cdot L_f \cdot i_{fq} - f_d \cdot v_{DC} \tag{3.29}$$

$$L_f \cdot \frac{di_{fq}}{dt} = -\omega \cdot L_f \cdot i_{fd} - f_q \cdot v_{DC} \tag{3.30}$$

The system variables i.e. i_{fd}, i_{fq} and v_{DC} are directly controlled by the patterns of switching function of the six-switch inverter as shown in the mathematic model, Fig. 3.9.
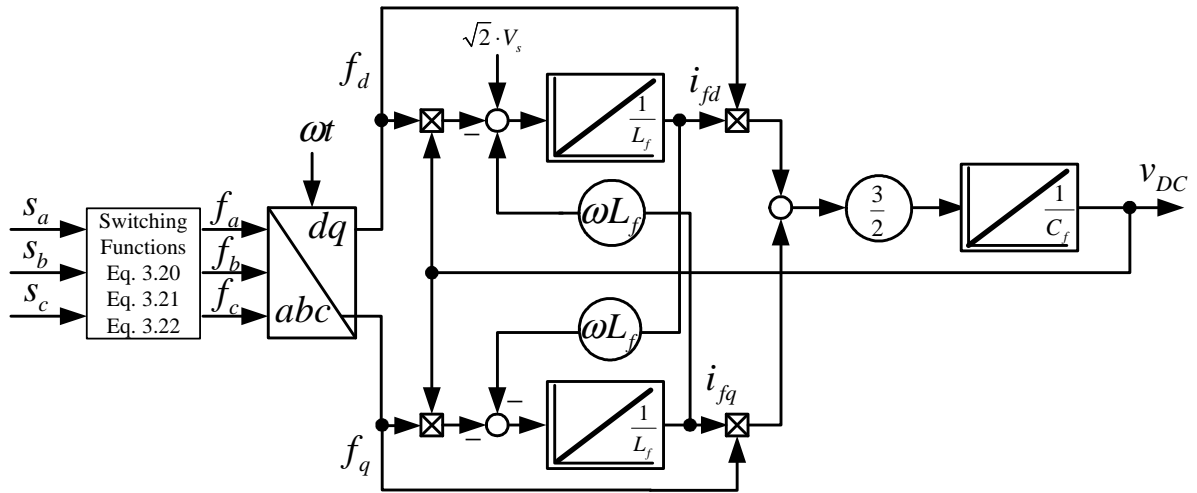

Fig. 3.9. Mathematical model of the shunt active filter.

Figure 3.9. Modèle mathématique du filtre actif parallèle.

3.5.2. Harmonic currents and power compensation

In the balanced 3-phase system, the corresponding Fourier series for the nonlinear load currents in phase a, b and c in the frequency domain are:

$$i_{La}(t) = \sqrt{2} \cdot I_1 \cdot \cos(\omega t - \varphi_1) + \sum_{n=1}^{n=\infty} I_{(6n\pm1)} \cdot \cos((6n \pm 1)\omega t - \varphi_{(6n\pm1)}) \tag{3.31}$$

$$i_{Lb}(t) = \sqrt{2} \cdot I_1 \cdot \cos(\omega t - \frac{2\pi}{3} - \varphi_1) + \sum_{n=1}^{n=\infty} \sqrt{2} \cdot I_{(6n\pm1)} \cdot \cos((6n \pm 1)(\omega t - \frac{2\pi}{3}) - \varphi_{(6n\pm1)}) \tag{3.32}$$

$$i_{Lc}(t) = \sqrt{2} \cdot I_1 \cdot \cos(\omega t + \frac{2\pi}{3} - \varphi_1) + \sum_{n=1}^{n=\infty} \sqrt{2} \cdot I_{(6n\pm1)} \cdot \cos((6n \pm 1)(\omega t + \frac{2\pi}{3}) - \varphi_{(6n\pm1)}) \tag{3.33}$$

The orders of the characteristic harmonic currents from equations 3.31 to 3.33 are $6n \pm 1$. For the integer values of n (1, 2, 3...), the harmonics of order $6 \cdot n + 1$ (7, 13, 19...) are the positive sequences and the harmonics of order $6 \cdot n - 1$ (5, 11, 17...) are the negative sequences. In this case, all non-characteristics harmonics i.e. zero sequence- and triple- harmonics are not considered. The load currents are also transformed into the rotating reference frame by using transformation matrix from equation 3.23:

$$\begin{bmatrix} i_{Ld} \\ i_{Lq} \end{bmatrix} = \frac{2}{3} \begin{bmatrix} \cos \omega t & \cos(\omega t - \frac{2\pi}{3}) & \cos(\omega t + \frac{2\pi}{3}) \\ -\sin \omega t & -\sin(\omega t - \frac{2\pi}{3}) & -\sin(\omega t + \frac{2\pi}{3}) \end{bmatrix} \begin{bmatrix} i_{La} \\ i_{Lb} \\ i_{Lc} \end{bmatrix} \tag{3.34}$$

Therefore, equations 3.31 to 3.33 can be written as:

$$i_{Ld}(t) = \sqrt{2} \cdot I_1 \cos \varphi_1 + \sum_{n=1}^{n=\infty} \left\{ \sqrt{2} \cdot I_{(6n-1)} \cos(6n\omega t - \varphi_{(6n-1)}) + \sqrt{2} \cdot I_{(6n+1)} \cos(6n\omega t - \varphi_{(6n+1)}) \right\} \tag{3.35}$$

$$i_{Lq}(t) = -\sqrt{2} \cdot I_1 \sin \varphi_1 + \sum_{n=1}^{n=\infty} \left\{ \sqrt{2} \cdot I_{(6n+1)} \sin(6n\omega t - \varphi_{(6n+1)}) - \sqrt{2} \cdot I_{(6n-1)} \sin(6n\omega t - \varphi_{(6n-1)}) \right\} \tag{3.36}$$

The load currents of d- and q-axis contain the fundamental component of the current and harmonic currents i.e.:

$$i_{Ld} = i_{Ld1} + i_{Ldh} \tag{3.37}$$

and: $\quad\quad\quad\quad i_{Lq} = i_{Lq1} + i_{Lqh} \tag{3.38}$

where:

$$i_{Ld1} = \sqrt{2} \cdot I_1 \cdot \cos \varphi_1 \tag{3.39}$$

$$i_{Lq1} = -\sqrt{2} \cdot I_1 \cdot \sin \varphi_1 \tag{3.40}$$

$$i_{Ldh} = \sum_{n=1}^{n=\infty} \left\{ \sqrt{2} \cdot I_{(6n-1)} \cdot \cos(6n\omega t - \varphi_{(6n-1)}) + \sqrt{2} \cdot I_{(6n+1)} \cdot \cos(6n\omega t - \varphi_{(6n+1)}) \right\} \tag{3.41}$$

and: $\quad i_{Lqh} = \sum\limits_{n=1}^{n=\infty} \left\{ \sqrt{2} \cdot I_{(6n+1)} \cdot \sin(6n\omega t - \varphi_{(6n+1)}) - \sqrt{2} \cdot I_{(6n-1)} \cdot \sin(6n\omega t - \varphi_{(6n-1)}) \right\}$ (3.42)

All the harmonics components generated by the load are compensated by the active filter which has current references for the current control loop as follows:

$$i_{fdref} = -i_{Ldh}$$ (3.43)

$$i_{fqref} = -i_{Lqh}$$ (3.44)

The instantaneous reactive power theory [42] is applied for the power factor compensation on the rotating reference frame as follows:

$$p(t) = \frac{3}{2} \cdot (v_d \cdot i_d + v_q \cdot i_q)$$ (3.45)

and: $\qquad q(t) = \frac{3}{2} \cdot (v_d \times i_q + v_q \times i_d)$ (3.46)

According to the vector product as shown in Fig. 3.10, the instantaneous reactive power can also express as:

$$q(t) = \frac{3}{2} \cdot (v_d \cdot i_q + v_q \cdot i_d)$$ (3.47)

Putting equations 3.27, 3.28, 3.37, and 3.38 in equations 3.45 and 3.47:

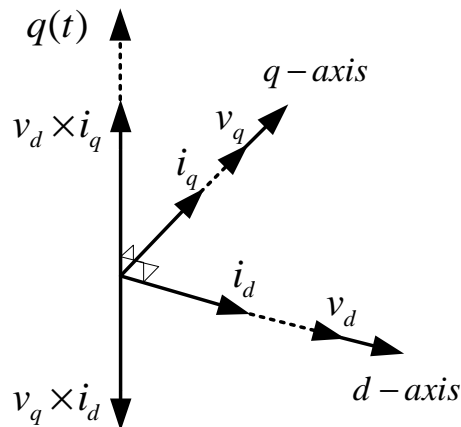$$p_L(t) = \frac{3}{2} \cdot \sqrt{2} \cdot V_s \cdot i_{Ld}$$ (3.48)

Fig. 3.10. Vector diagram of instantaneous reactive power.

Figure 3.10. Diagramme vectoriel de la puissance réactive instantanée.

$$q_L(t) = \frac{3}{2} \cdot \sqrt{2} \cdot V_s \cdot i_{Lq} \tag{3.49}$$

Therefore, the powers consumed by the nonlinear load can be written as:

$$p_L(t) = P + \tilde{p}_L(t) \tag{3.50}$$

$$q_L(t) = Q + \tilde{q}_L(t) \tag{3.51}$$

where:

P = effective power generated by the fundamental component i_{Ld1}

Q = reactive power generated by the fundamental component i_{Lq1}

$\tilde{p}_L(t)$ = instantaneous effective power generated by harmonic components

$\tilde{q}_L(t)$ = instantaneous reactive power generated by harmonic components

The instantaneous effective- and reactive power are compensated by the active filter which supply the instantaneous power $\tilde{p}_L(t)$ and $\tilde{q}_L(t)$ with the same amount of the harmonic power generated by the nonlinear load and 180 degree phase shifts:

$$p_f(t) = -\tilde{p}_L(t) \tag{3.52}$$

$$q_f(t) = -\tilde{q}_L(t) \tag{3.53}$$

Therefore, the effective power at the 3-phase system is:

$$p_s(t) = p_L(t) + p_f(t) = P + \tilde{p}_L(t) - \tilde{p}_L(t) = P \tag{3.54}$$

From equation 3.48, the effective power from the fundamental component is:

$$p_s(t) = \frac{3}{2} \cdot \sqrt{2} \cdot V_s \cdot i_{Ld1} \tag{3.55}$$

From equation 3.39, one obtains:

$$p_s(t) = \frac{3}{2} \cdot \sqrt{2} \cdot V_s \cdot \sqrt{2} \cdot I_1 \cdot \cos \varphi_1 = 3 \cdot V_s \cdot I_1 \cdot \cos \varphi_1 \tag{3.56}$$

and the reactive power at the 3-phase system is:

$$q_s(t) = q_L(t) + q_f(t) = q_L(t) - q_L(t) = 0 \tag{3.57}$$

From equation 3.56 is shown that only the effective power generated by the fundamental component is supplied by the 3-phase power system at the point of common coupling. In this case, the current references from equations 3.43 and 3.44 can be written as:

$$i_{fdref} = -i_{Ldh} = i_{Ld1} - i_{Ld} \tag{3.58}$$

$$i_{fqref} = -i_{Lqh} = -i_{Lq} \tag{3.59}$$

Where i_{Ld1} is obtained by using a low-pass filter and with the inverse transformation matrix applied to equations 3.58 and 3.59. The current references on the fixed reference frame are shown in Fig. 3.11. The inverse transformation matrix is:

$$\begin{bmatrix} i_{faref} \\ i_{fbref} \\ i_{fcref} \end{bmatrix} = \begin{bmatrix} \cos\omega t & -\sin\omega t \\ \cos(\omega t - \dfrac{2\pi}{3}) & -\sin(\omega t - \dfrac{2\pi}{3}) \\ \cos(\omega t + \dfrac{2\pi}{3}) & -\sin(\omega t + \dfrac{2\pi}{3}) \end{bmatrix} \cdot \begin{bmatrix} i_{fdref} \\ i_{fqref} \end{bmatrix} \tag{3.60}$$

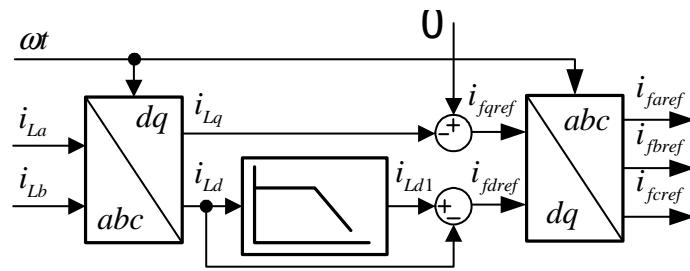Fig. 3.11. Block diagram of estimated current references on the fixed reference frame.

Figure 3.11. Diagramme de calcul des courants de référence dans le référentiel fixe.

3.5.3. Control system of the active filters

The control system of the active filter as shown in Fig. 3.12 consists of two main parts:

-   Harmonic current compensation control;
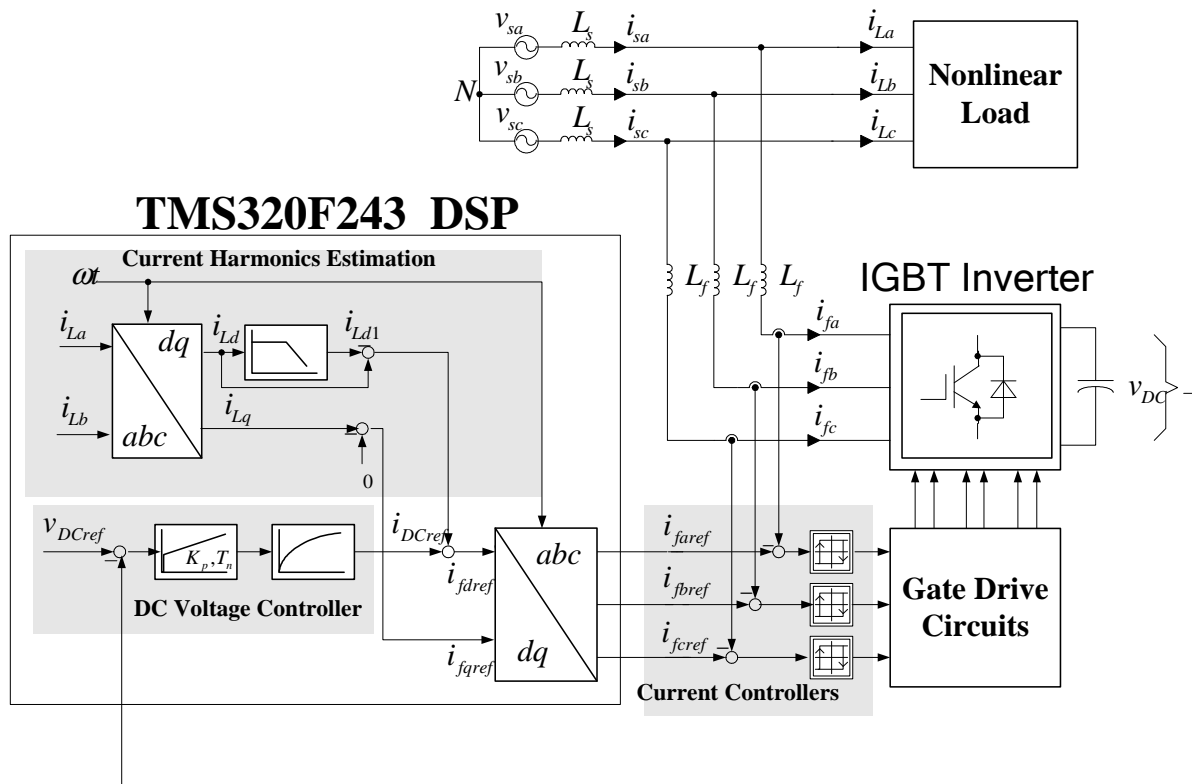-   DC voltage control at the DC bus of the active filter.

Fig. 3.12. Structure of voltage-current cascade control system of the active harmonic filter.

Figure 3.12. Contrôle en cascade de la tension et du courant du filtre actif à structure parallèle.

3.5.3.1. Harmonic current compensation control

The current control loop is a minor loop of the DC voltage control system. The hysteresis controllers [43] were applied to control the compensating harmonic currents. The current control loops are independently controlled from each other. The current controlled deviation (for example $D_{fa} = i_{faref} - i_{fa}$) is compared with optimized hysteresis band of the controller in order to get an appropriated switch position and avoid simultaneous operation of branch switches. The current controlled deviation normally should not exceed two time of the hysteresis band. The current control structure is shown in Fig. 3.13.
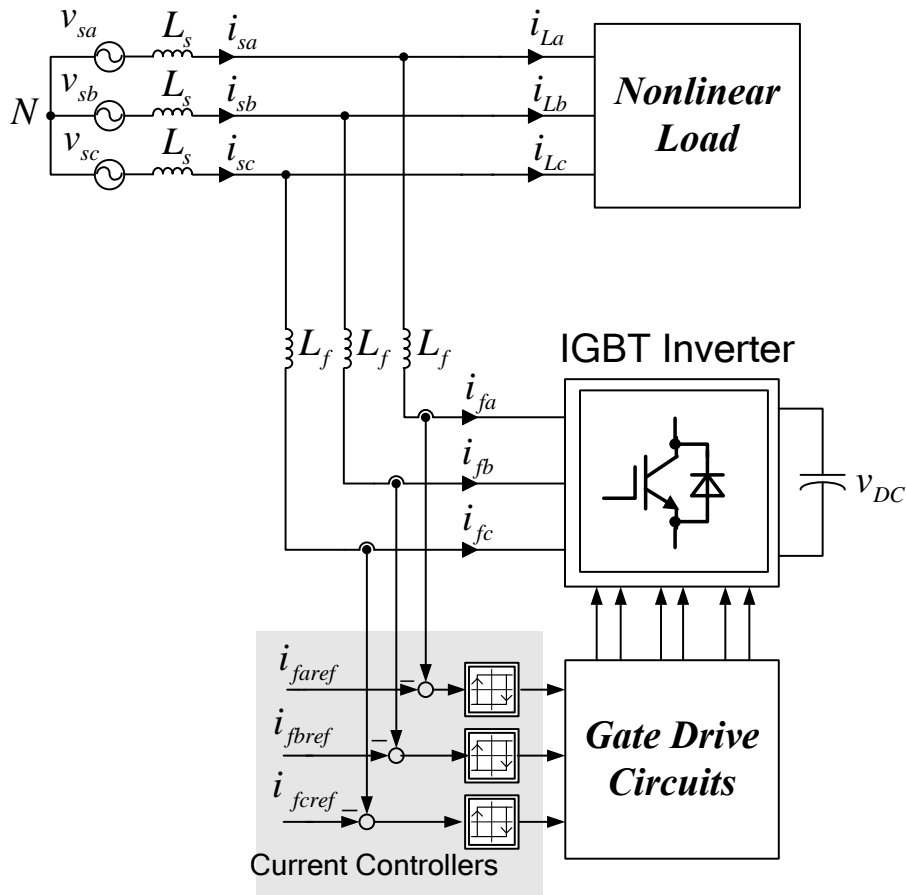
Fig. 3.13. Structure of harmonic currents control system with hysteresis controllers.

Figure 3.13. Contrôle par hystérésis des harmoniques de courants.

3.5.3.2. DC voltage control

The voltage control is a major loop of the control system. In order to avoid a steady state error but with constant controlled voltage at the DC capacitor, this can be achieved by conventional PI-controller. The effect of DC voltage ripple at DC capacitor is reduced by the referenced low-pass filter for i_{DCref} before the summation of the referenced current i_{DCref} and the fundamental component. Therefore, the capacitor charging current is in phase with the AC input voltage of active filter (unity power factor). The mathematic model of this controlled system can be derived under these assumptions i.e. $i_{DC}(t) = i_{DCref}$ and $v_{DC}(t) = V_{DCref}$.

The charging current and power of DC capacitor are:

$$i_c(t) = C_f \cdot \frac{dv_{DC}(t)}{dt} \tag{3.61}$$

and:

$$p_c(t) = v_c(t) \cdot C_f \frac{dv_{DC}(t)}{dt} = V_{DCref} \cdot C_f \frac{dv_{DC}(t)}{dt} \tag{3.62}$$

The instantaneous power (from equation 3.45) at the input of the active filter can be expressed as [36]:

$$p_f(t) = \frac{3}{2} \cdot (v_d \cdot i_{fd} + v_q \cdot i_{fq}) \tag{3.63}$$

since $v_q = 0, v_d = \sqrt{2} \cdot V_s$ and $i_{fd} = i_{DC}(t)$:

$$p_f(t) = \frac{3}{2} \cdot \sqrt{2} \cdot V_s \cdot i_{DC}(t) \tag{3.64}$$

For ideal inverter, power losses are neglected, thus:

$$p_f(t) = p_c(t)$$
$$\frac{dv_{DC}(t)}{dt} = \frac{3}{2} \cdot \frac{\sqrt{2} \cdot V_s}{C_f \cdot V_{DCref}} \cdot i_{DC}(t) \tag{3.65}$$

From equation 3.65 one defines the transfer function as:

$$F(S) = \frac{V_{DC}(S)}{I_{DC}(S)} = \frac{1}{T_{DC} \cdot S} \tag{3.66}$$

where T_{DC} is the time constant of the controlled system, defined by:

$$T_{DC} = \frac{2}{3} \cdot \frac{C_f \cdot V_{DCref}}{\sqrt{2} \cdot V_s} \tag{3.67}$$

3.5.3.3. PI-controller design for the DC voltage control loop

The DC voltage control loop as shown in Fig. 3.14 is designed by using the symmetrical optimum (SO) or pole placing method to obtain the optimum parameters of PI-controller i.e. optimum gain K_p and integrating time/reset time T_i / T_n.
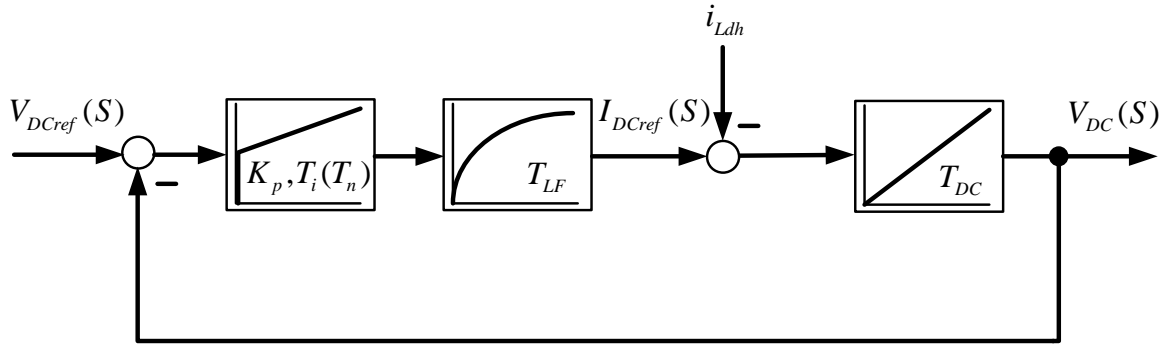
Fig. 3.14. Voltage control loop with PI-controller.

Figure 3.14. Régulation de la tension avec un controlleur PI.

From Fig. 3.14, the open loop transfer function of the control system with PI-controller is:

$$F_o(S) = K_P \cdot \frac{T_n \cdot S + 1}{T_n \cdot S} \cdot \frac{1}{T_{LF} \cdot S + 1} \cdot \frac{1}{T_{DC} \cdot S} \tag{3.68}$$

where:

K_P = proportional gain of PI-controller

T_i = integrating time of PI-controller

T_n = reset time of PI-controller, where:

$$T_n = K_P \cdot T_i \tag{3.69}$$

T_{LF} = time constant of the low-pass filter

T_{DC} = time constant of DC voltage controlled system

The transfer function with double integrator becomes:

$$F_o(S) = \frac{K_P}{T_n \cdot T_{DC} \cdot S^2} \cdot \frac{T_n \cdot S + 1}{T_{LF} \cdot S + 1} = |F_o(S)| \cdot e^{j\varphi_0} \tag{3.70}$$

This system can only be stabilized with $T_n > T_{LF}$, otherwise $\varphi_0 < -\pi$ for all frequencies. At the crossover frequency:

$$\omega = \omega_d = \frac{1}{\sqrt{T_n \cdot T_{LF}}} \tag{3.71}$$

then the phase margin has the maximum value:

$$\phi_d = \tan^{-1} a - \tan^{-1} \frac{1}{a} \tag{3.72}$$

For a specified phase margin ϕ_d, the normalization parameter a can be obtained from:

$$a = \sqrt{\frac{T_n}{T_{LF}}} = \frac{1 + \sin\phi_d}{\cos\phi_d} \tag{3.73}$$

From equation 3.70, the cross over frequency becomes:

$$\omega_d = \frac{1}{a(\phi_d) \cdot T_{LF}} \tag{3.74}$$

Therefore, the reset time of the PI-controller is determined by the assumed phase margin:

$$T_n = a^2(\phi_d) \cdot T_{LF} \tag{3.75}$$

The stability condition at the cross-over frequency is:

$$\left| F_0(j\omega_d) \right| = 1 \tag{3.76}$$

Therefore, the PI-controller gain K_P is evaluated from:

$$K_P = \frac{1}{a} \cdot \frac{T_{DC}}{T_{LF}} \tag{3.77}$$

The transfer function of the closed loop control system is:

$$F_{CL}(q) = \frac{F_0(q)}{1 + F_0(q)} = \frac{aq+1}{q^3 + aq^2 + aq + 1}$$
$$= \frac{aq+1}{(q+1)(q^2 + (a-1)q + 1)} \tag{3.78}$$

where the normalization of the complex frequency is:

$$q = \frac{S}{w_d} = a \cdot T_{LF} \cdot S \tag{3.79}$$

The poles of the DC voltage control loop from equation 3.78 can be calculated as follows:

$$q_1 = -1$$
$$q_{2,3} = -\frac{a-1}{2} \pm \sqrt{\left(\frac{a-1}{2}\right)^2 - 1} \tag{3.80}$$

or:
$$q_1 = -1$$
$$q_{2,3} = -\frac{a-1}{2} \pm j\sqrt{1 - \left(\frac{a-1}{2}\right)^2} = e^{\pm j(\pi-\vartheta)} \tag{3.81}$$

with:

$$\vartheta = \cos^{-1} D = \cos^{-1}\left(\frac{a-1}{2}\right)$$ (3.82)

and:

$$a = 2 \cdot \cos \vartheta + 1 = 2 \cdot D + 1$$ (3.83)

where D is the damping ratio of the closed loop control system and ϑ is an angle of the complex conjugate pair of poles $q_{2,3}$ refer to the real axis as shown in Fig. 3.15.
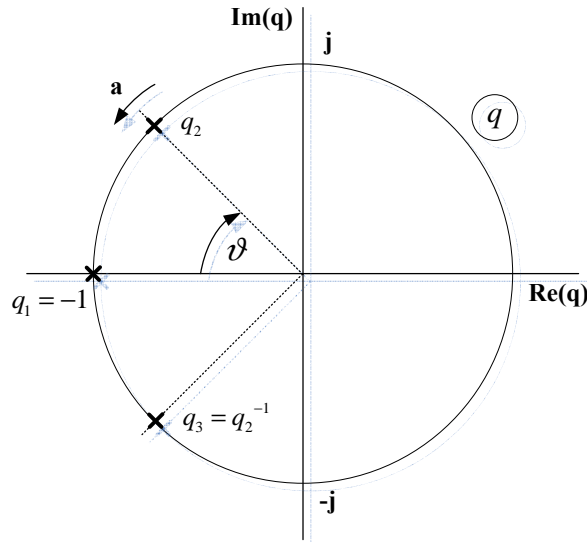
Fig. 3.15. Poles $q_{2,3}$ as a function of the normalization parameter a.

Figure 3.15. Pôles $q_{2,3}$ en fonction du paramètre normalisé a.

For the periodic response, if $\vartheta = 45^0$ is specified, therefore:

$$a = 2 \cdot \frac{\sqrt{2}}{2} + 1 = 2.414$$ (3.84)

From equations 3.74 and 3.76, the reset time and proportional gain of PI-controller can be obtained from:

$$T_n = (2.414)^2 \cdot T_{LF}$$ (3.85)

and:

$$K_P = \frac{1}{2.414} \cdot \frac{T_{DC}}{T_{LF}}$$ (3.86)

3.5.4. Active filter power circuit study and design

The study of operation of the active filter was an essential element to design the power- and control circuits of the active filter. Conditions and constraints at different operating points of nonlinear loads were considered in order to obtain optimal designed values of power circuit components such as boost inductances L_f, DC capacitance C_f as well as the optimal cutoff or break frequency of the low-pass filter. The designed study was done by using Matlab/Simulink to simulate the designed active filter with different operating conditions which are briefly described as follows.

3.5.4.1. Analysis of balanced and unbalanced nonlinear load

The 6-pulse bridge controlled converter as shown in Fig. 3.16 is a typical balanced nonlinear load which is widely used in industrial applications. The AC input currents or load currents at firing angle $\alpha = 0$ degree are illustrated in Fig. 3.17 and Fig. 3.18.
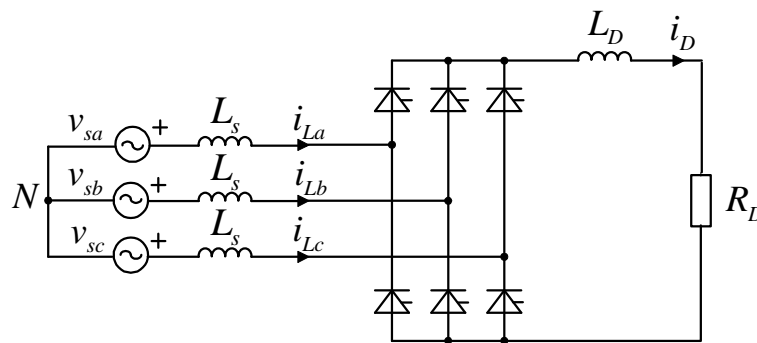
Fig. 3.16. Typical 6-pulse bridge controlled converter.

Figure 3.16. Redresseur controlé d'indice de pulsation 6 (ou hexaphasé).
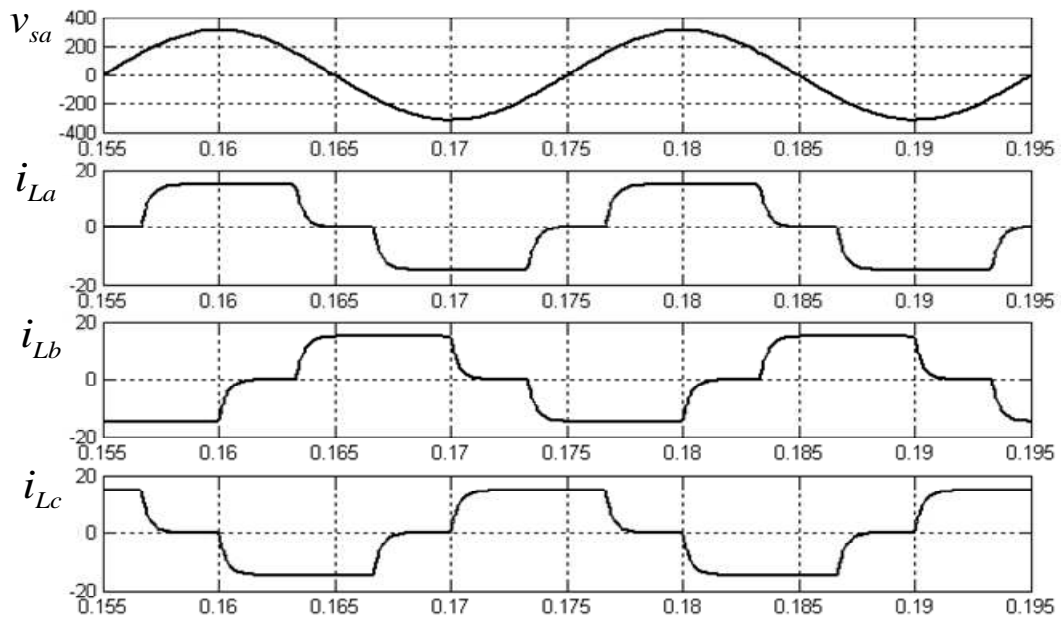
Fig. 3.17. Load currents at firing angle $\alpha = 0$ degree.

Figure 3.17. Courant de charge pour un angle de retard à l'amorçage $\alpha = 0$.

Fig. 3.18. Load currents on the rotating reference frame at firing angle $\alpha = 0$ degree.

Figure 3.18. Courants de charge dans le référentiel tournant, pour un angle de retard à l'amorçage $\alpha = 0$.

The corresponding Fourier series for the AC current in phase a, b, and c in the frequency domain are given by equations 3.31, 3.32, and 3.33 as well as by equations 3.35 and 3.36 on the rotating reference frame.

The 6-pulse bridge converter with its 1-phase rectifier for electronic control circuit as shown in Fig.3.19 is an example for unbalanced nonlinear load.
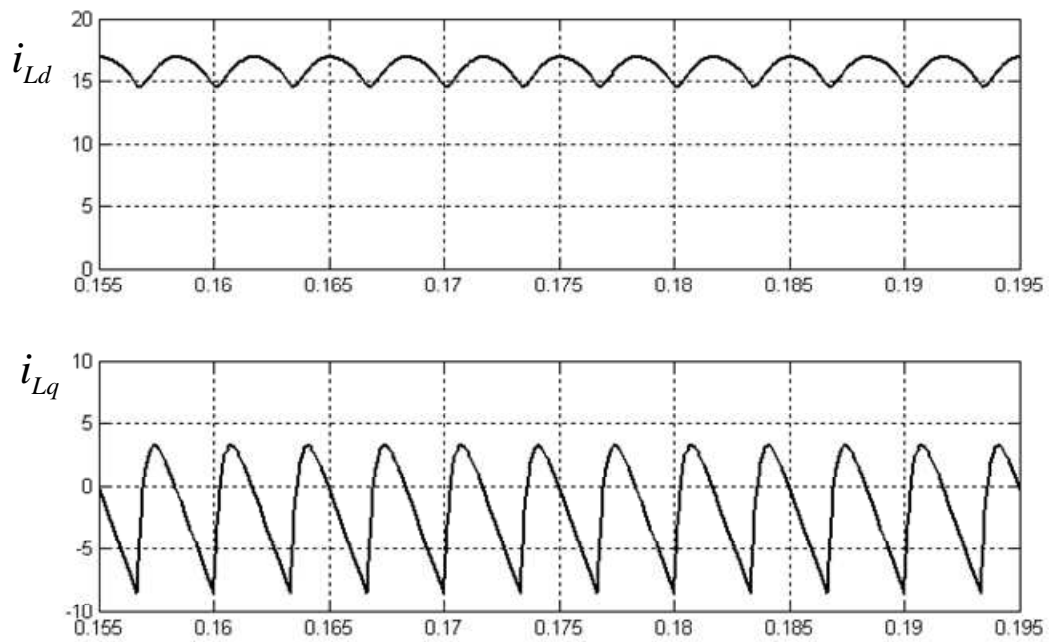
In this case, the corresponding Fourier series for additional unbalanced load current i'$_{La}$, i'$_{Lb}$ and i'$_{Lc}$ are expressed as the equations 3.87, 3.88, and 3.89 as well as equations 3.90 and 3.91 on the rotating reference frame [37].

The currents equations on fixed or stationary reference frame are [37]:

$$i'_{La} = \sqrt{2} \cdot I'_1 \cdot \cos(\omega t + \frac{\pi}{6} + \phi'_1) + \sum_{n=1}^{\infty} \sqrt{2} \cdot I'_{(2n+1)} \cdot \cos\left\{(2n+1)\cdot(\omega t + \frac{\pi}{6}) + \phi'_{(2n+1)}\right\} \quad (3.87)$$

$$i'_{Lb} = -i'_{La} \quad (3.88)$$

and:
$$i'_{Lc} = 0 \quad (3.89)$$
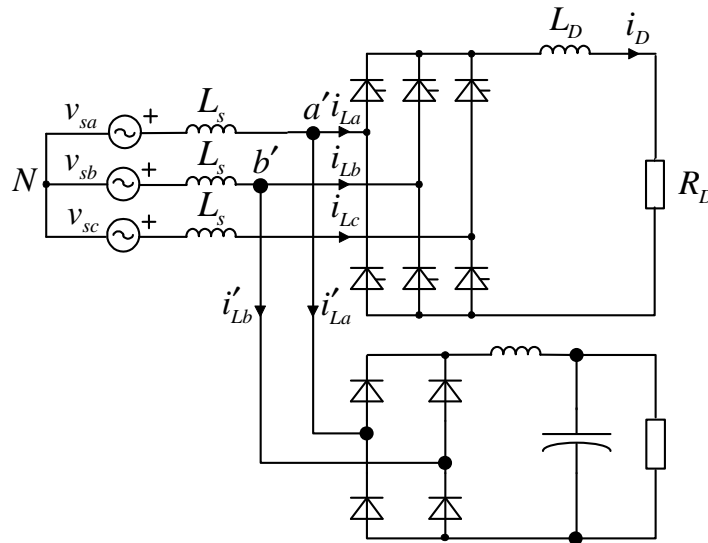
Fig. 3.19. 6-pulse bridge controlled converter with 1-phase diode bridge rectifier.

Figure 3.19. Redresseur hexaphasé et redresseur monophasé.

The additional unbalanced load currents on the stationary- and rotating reference frame are shown in Fig. 3.20 and 3.21 respectively.
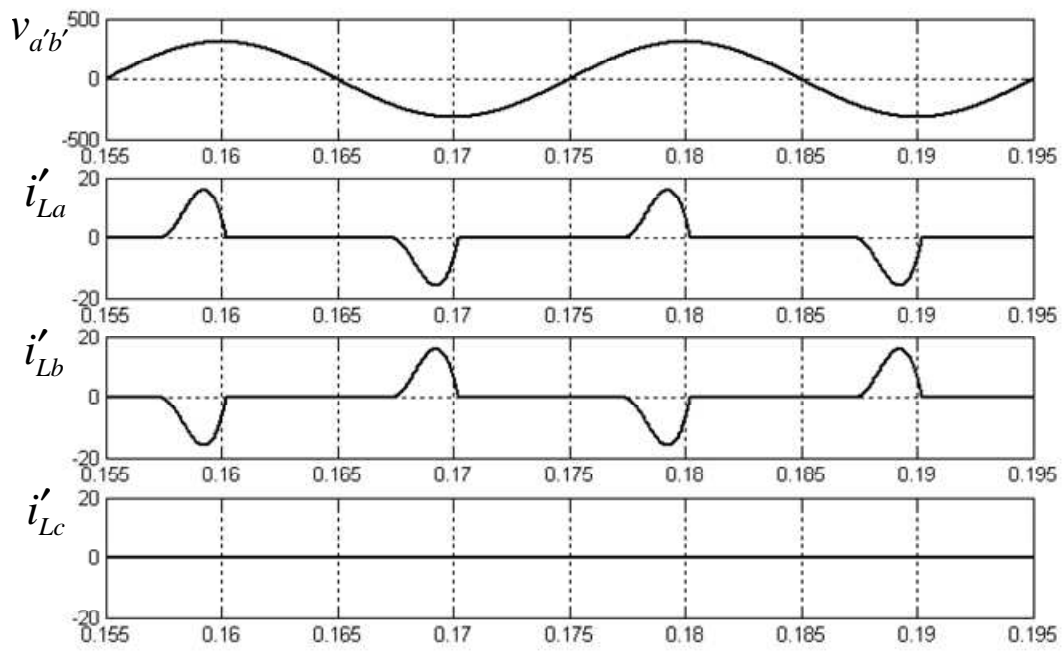
Fig. 3.20. Additional unbalanced load current on the stationary reference frame.

Figure 3.20. Courants réels de la charge déséquilibrée.

Fig. 3.21. Additional unbalanced load current on the rotating reference frame.

Figure 3.21. Courants dans le référentiel tournant de la charge déséquilibrée.

On the rotating reference frame, the additional unbalanced load currents are:

$$i'_{Ld} = \frac{\sqrt{2} \cdot I'_1}{\sqrt{3}} \cdot \cos\varphi'_1 + \frac{\sqrt{2} \cdot I'_1}{\sqrt{3}} \cdot \cos(2\omega t + \frac{\pi}{6} + \varphi'_1)$$
$$+ \sum_{n=1}^{\infty} \frac{\sqrt{2} \cdot I'_{(2n+1)}}{\sqrt{3}} \cdot \left\{ \cos\{2n \cdot (\omega t + \frac{p}{6}) + \varphi'_{(2n+1)}\} \right\} \qquad (3.90)$$
$$+ \sum_{n=1}^{\infty} \frac{\sqrt{2} \cdot I'_{(2n+1)}}{\sqrt{3}} \cdot \cos\left\{ (2n+2) \cdot (\omega t + \frac{\pi}{6}) + \varphi'_{(2n+1)} \right\}$$

and:

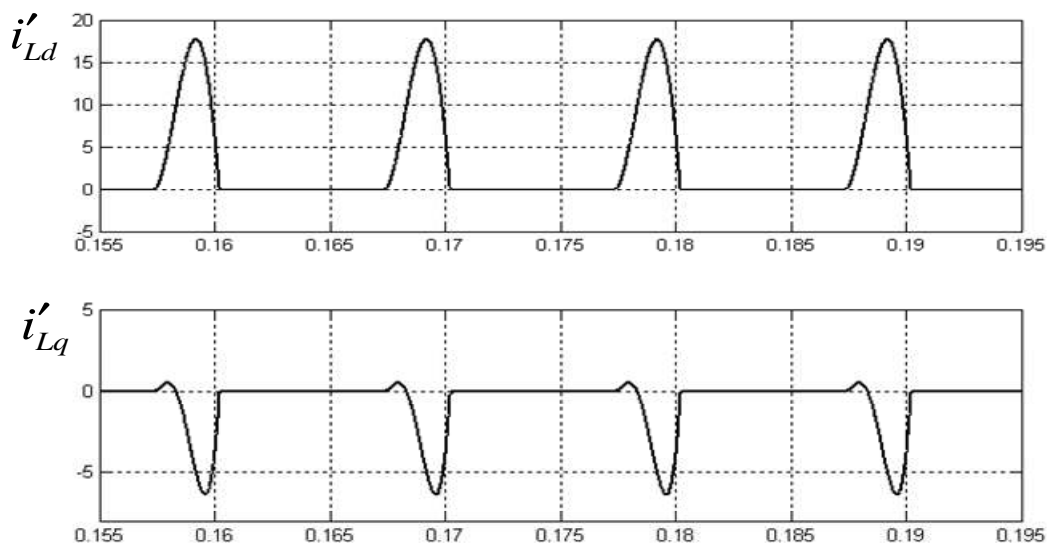$$i'_{Lq} = -\frac{\sqrt{2} \cdot I'_1}{\sqrt{3}} \times \sin\varphi'_1 - \frac{\sqrt{2} \cdot I'_1}{\sqrt{3}} \sin(2\omega t + \frac{\pi}{6} + \varphi'_1)$$
$$+ \sum_{n=1}^{\infty} \frac{\sqrt{2} \cdot I'_{(2n+1)}}{\sqrt{3}} \cdot \left\{ \sin\{2n \cdot (\omega t + \frac{\pi}{6}) + \varphi'_{(2n+1)}\} \right\} \qquad (3.91)$$
$$- \sum_{n=1}^{\infty} \frac{\sqrt{2} \cdot I'_{(2n+1)}}{\sqrt{3}} \cdot \sin\left\{ (2n+2) \cdot (\omega t + \frac{\pi}{6}) + \varphi'_{(2n+1)} \right\}$$

3.5.4.2. Low-pass filter on the rotating reference frame

The harmonic contents of balanced load currents on rotating reference frame from equations 3.35 and 3.36 show that the minimum harmonic frequency is $300\,\text{Hz}\,(6 \cdot f_s)$ and $100\,\text{Hz}\,(2 \cdot f_s)$ in case of unbalanced load currents from equations 3.90 and 3.91. Therefore, the fundamental component of load current i_{Ld1} is obtained by using a 4th order Butterworth filter. The frequency response of Butterworth filter is monotonic characteristic which has consistently decreased of the magnitude to the change of frequency. The results of this study are illustrated as shown in Fig. 3.22, Fig. 3.23, and Fig. 3.24.

In case of the balanced nonlinear load as shown in Fig. 3.22 and 3.23, the dynamic response of low –pass filter at the cutoff frequency of 100 Hz was well performed as well as in the steady state operation. For the unbalanced nonlinear load, the 100 Hz cutoff frequency was insufficient to filter all harmonic frequencies. The reducing of cutoff frequency can solve this harmonic problem but the result is a decrease of the dynamic response of the filter system as shown in Fig. 3.24.

Fig. 3.22. Load currents i_{Ld} and i_{L1} of 6-pulse bridge controlled converter with different cutoff frequencies ($f_p = 100$ Hz, 150 Hz, and 200 Hz at $\alpha = 0$ degree).

Figure 3.22. Courants i_{Ld} et i_{L1} du redresseur hexaphasé pour différentes fréquences de coupure ($f_p = 100$ Hz, 150 Hz et 200 Hz, $\alpha = 0°$).
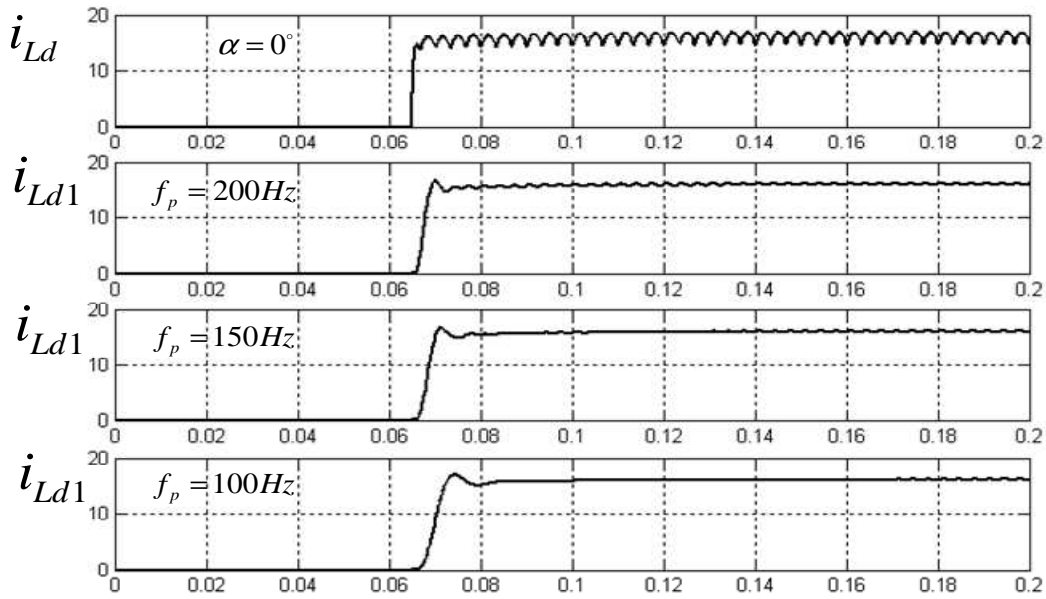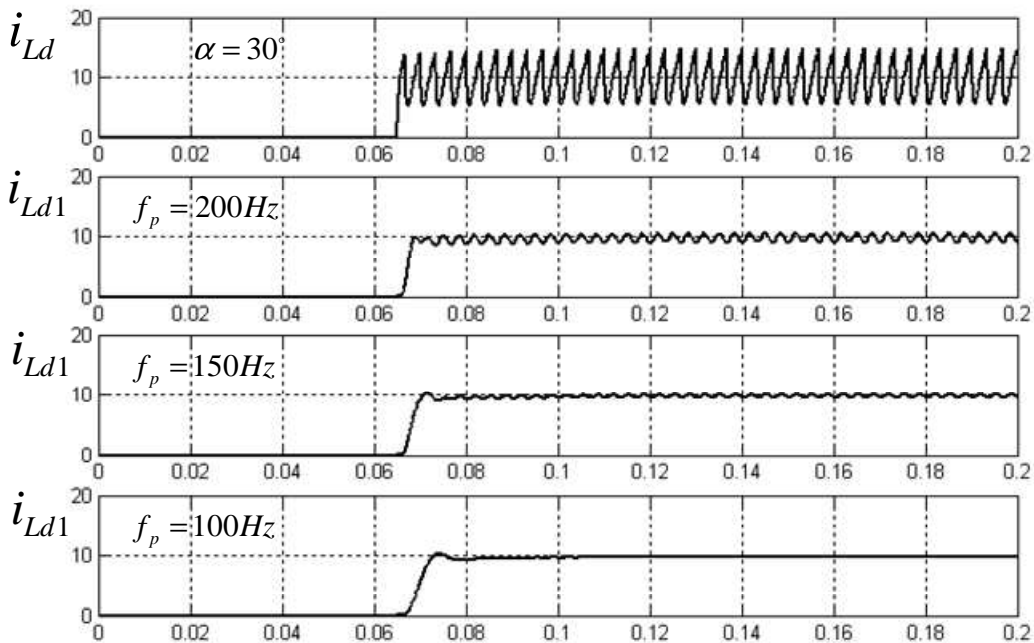

Fig. 3.23. Load currents i_{Ld} and i_{L1} of 6-pulse bridge controlled converter with different cutoff frequencies ($f_p = 100$ Hz, 150 Hz, and 200 Hz at $\alpha = 30$ degree).

Figure 3.23. Courants i_{Ld} et i_{L1} du redresseur hexaphasé pour différentes fréquences de coupure ($f_p = 100$ Hz, 150 Hz et 200 Hz, $\alpha = 30°$).
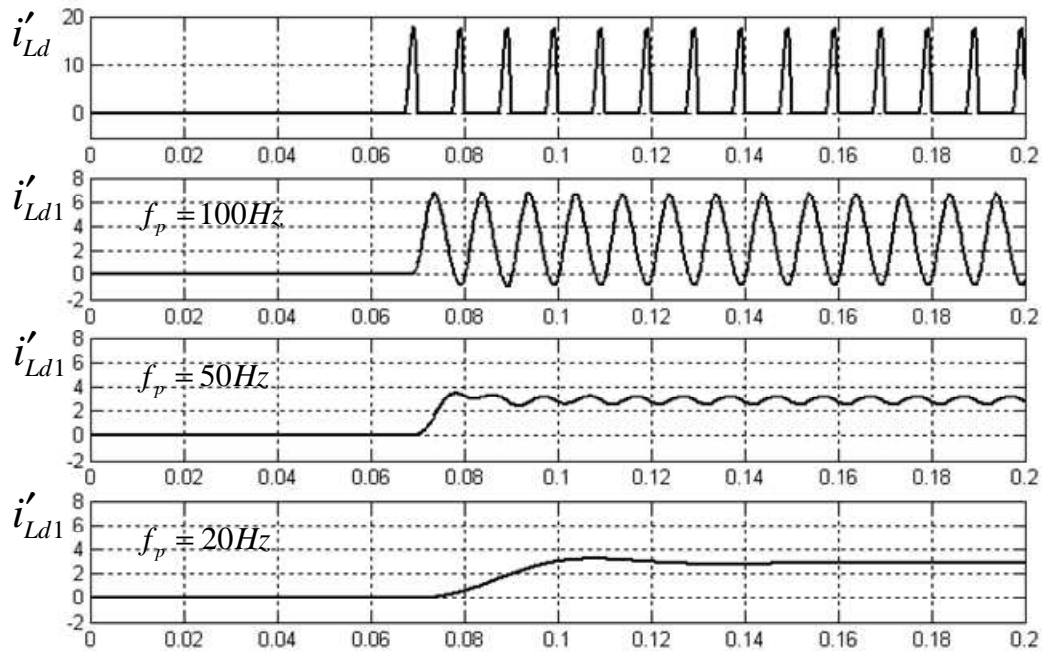
Fig. 3.24. Load currents i'$_{Ld}$ of 1-phase bridge rectifier with different cutoff frequencies

(f$_p$ = 20 Hz, 50 Hz, and 100 Hz).

Figure 3.24. Courants i'$_{Ld}$ du redresseur monophasé pour différentes fréquences de coupure

(f$_p$ = 20 Hz, 50 Hz et 100 Hz).

3.5.4.3. Boost inductance and capacitor voltage

The inductance L$_f$ in the active filter circuit is a boost inductance to provide a capacitor voltage that is greater than the peak of the line voltage. Therefore, the inductance is related to the rate of rise of its current and the switching frequency f$_s$ of IGBT. For the maximum rate of rise of the current, θ_{max} has to be considered for the design and from equations 3.16, 3.17 and 3.18, the approximation of the maximum inductance is given by [44]:

$$L_{fmax} \cdot \frac{di_{fmax}}{dt} = v_s - f_{a,b,cmax} \cdot v_{DC} \tag{3.92}$$

$$L_{fmax} = \frac{\frac{2}{3} \cdot V_{DCref} - \sqrt{2} \cdot V_s \sin\theta_{max}}{\frac{di_{fref_{max}}}{dt}} \tag{3.93}$$

where:

$$\frac{di_{fref_{max}}}{dt} = \text{the maximum rate of change of the referenced current}$$

$\dfrac{2}{3} \cdot V_{DCref}$ = the maximum voltage at the maximum switching function

$$f_{a,b,c} = \pm \dfrac{2}{3}$$

At $\omega t = 0$ ($V_s = 0$) with the maximum switching frequency f_{SWmax}, in this case equation (3.92) becomes:

$$L_f \cdot \dfrac{di}{dt} = \pm \dfrac{2}{3} \cdot V_{DCref} \qquad (3.94)$$

where:

Δi = hysteresis band of the current controller

Therefore:

$$f_{SWmax} = \dfrac{1}{2 \cdot \Delta t} = \dfrac{1}{3} \cdot \dfrac{V_{DCref}}{L_f \cdot \Delta i} \qquad (3.95)$$

$$L_f = \dfrac{1}{3} \cdot \dfrac{V_{DCref}}{f_{SWmax} \cdot \Delta i} \qquad (3.96)$$

As can be seen, the inductance is inversely proportional to the hysteresis band and the switching frequency but less effected by the capacitor voltage. The capacitor voltage is not allowed to exceed the blocking voltage of the switching transistors and not less than the peak voltage of the line voltage i.e.:

$$V_{DCref} {}^3 \sqrt{2} \cdot V_{sab} \qquad (3.97)$$

The maximum switching frequency f_{SWmax} as a function of boost inductance L_f from equation 3.95 is shown in Fig. 3.25. The following designed parameters are given i.e. $\dfrac{di_{fref_{max}}}{dt} = 32.5$ kA/s at $\omega t = 90^o$, $f_{SWmax} = 100$ kHz and $\Delta i = 1.25$ A.
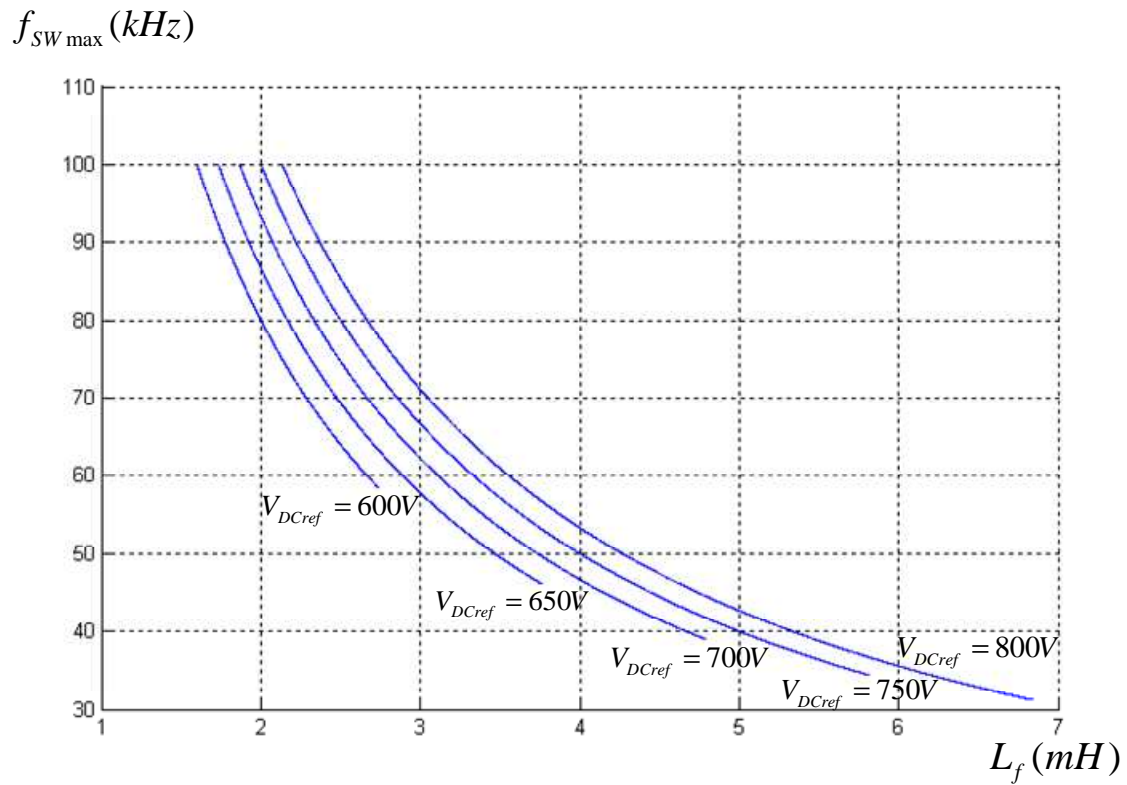
Fig. 3.25. Maximum switching frequency as a function of boost inductance at different referenced capacitor voltages.

Figure 3.25. Fréquence de découpage maximale en fonction de l'inductance du filtre pour différentes valeurs de référence de la tension capacité.

From equation 3.54, the instantaneous power of the active filter system can be written as [45-46]:

$$p_s(t) - p_L(t) = p_f(t) + \frac{1}{2} \cdot L_f \cdot \frac{d}{dt}(i_{fa}^2 + i_{fb}^2 + i_{fc}^2) \tag{3.98}$$

where:

$$\frac{1}{2} \cdot L_f \cdot \frac{d}{dt}(i_{fa}^2 + i_{fb}^2 + i_{fc}^2) = \text{the instantaneous power at boost inductances in phase } a, b, c$$

$$p_f(t) = P_s - P - \tilde{p}_L(t) - \frac{1}{2} \cdot L_f \cdot \frac{d}{dt}(i_{fa}^2 + i_{fb}^2 + i_{fc}^2) \tag{3.99}$$

In steady state operation, the effective power in the 3-phase system P_s is equal to P. Therefore:

$$p_f(t) = -\tilde{p}_L(t) - \frac{1}{2} \cdot L_f \cdot \frac{d}{dt} \cdot (i_{fa}^2 + i_{fb}^2 + i_{fc}^2) \tag{3.100}$$

The capacitor voltage and current can be defined from:

$$v_{DC}(t) = V_{DC} + \tilde{v}_{DC}(t)$$
(3.101)

$$i_{DC}(t) = I_{DC} + \tilde{i}_{DC}(t)$$
(3.102)

and the capacitor power is:

$$p_C(t) = v_{DC}(t) \cdot i_{DC}(t)$$
(3.103)

where:

V_{DC} = the average value of the capacitor voltage

$\tilde{v}_{DC}$ = the capacitor voltage ripple

I_{DC} = the capacitor charging current

$\tilde{i}_{DC}$ = the capacitor current ripple

In steady state operation, I_{DC} is equal to zero and $\tilde{v}_{DC}$ is neglected when it compares to V_{DC}. From equations 3.101 and 3.102, the capacitor power can be written as:

$$p_C(t) = V_{DC} \cdot \tilde{i}_{DC}(t) = p_f(t)$$
(3.104)

Therefore:

$$V_{DC} \cdot \tilde{i}_{DC} = -\tilde{p}_L(t) - \frac{1}{2} L_f \cdot \frac{d}{dt}(i_{fa}^2 + i_{fb}^2 + i_{fc}^2)$$
(3.105)

$$\tilde{i}_{DC} = -\frac{\tilde{p}_L(t)}{V_{DC}} - \frac{1}{2} \cdot \frac{L_f}{V_{DC}} \cdot \frac{d}{dt}(i_{fa}^2 + i_{fb}^2 + i_{fc}^2)$$
(3.106)

The capacitor voltage ripple can be derived from:

$$\tilde{v}_{DC}(t) = \frac{1}{C_f} \cdot \int \tilde{i}_{DC}(t)\,dt$$
(3.107)

Putting equation 3.106 in equation 3.107:

$$\tilde{v}_{DC} = -\frac{1}{C_f \cdot V_{DC}} \cdot \int \tilde{p}_L(t)\,dt - \frac{1}{2} \cdot \frac{L_f}{C_f \cdot V_{DC}} \cdot (i_{fa}^2 + i_{fb}^2 + i_{fc}^2)$$
(3.108)

From equation 3.48, the capacitor voltage ripple on the rotating reference frame (d-axis) is:

$$\tilde{v}_{DC} = -\frac{3}{2} \cdot \frac{\sqrt{2} \cdot V_s}{C_f \cdot V_{DC}} \cdot \int i_{Ld}(t)\,dt - \frac{1}{2} \cdot \frac{L_f}{C_f \cdot V_{DC}} \cdot (i_{fa}^2 + i_{fb}^2 + i_{fc}^2)$$
(3.109)

When the energy storage in the inductance L_f is not considered, the capacitor voltage ripple is approximately:

$$\tilde{v}_{DC} = -\frac{3}{2} \cdot \frac{\sqrt{2} \cdot V_s}{C_f \cdot V_{DC}} \cdot \int i_{Ld}(t)\, dt \qquad (3.110)$$

From equation 3.110, the capacitor voltage ripple is directly proportional to the load current i_{Ld} of d- axis (equation 3.35) and inversely proportional to the capacitance C_f and the average value of the capacitor voltage V_{DC}.

3.5.4.4. Simulation of the active filter

The simulation of balanced nonlinear load has been done with the designed system parameters shown in Table 3.1 and are given on Fig. 3.26 and Fig. 3.27.

Active filter parameters						
	v_{DC}	L_f	Δi	C_f	f_p	i_{Lmax}
$\alpha = 0,\ 60$ degrees	650 V	2.2 mH	1.25 A	470 μF	100 Hz	12.5 A

Table 3.1. Designed parameters of the active filter.

Table 3.1. Paramètres de dimensionnement du filtre actif.
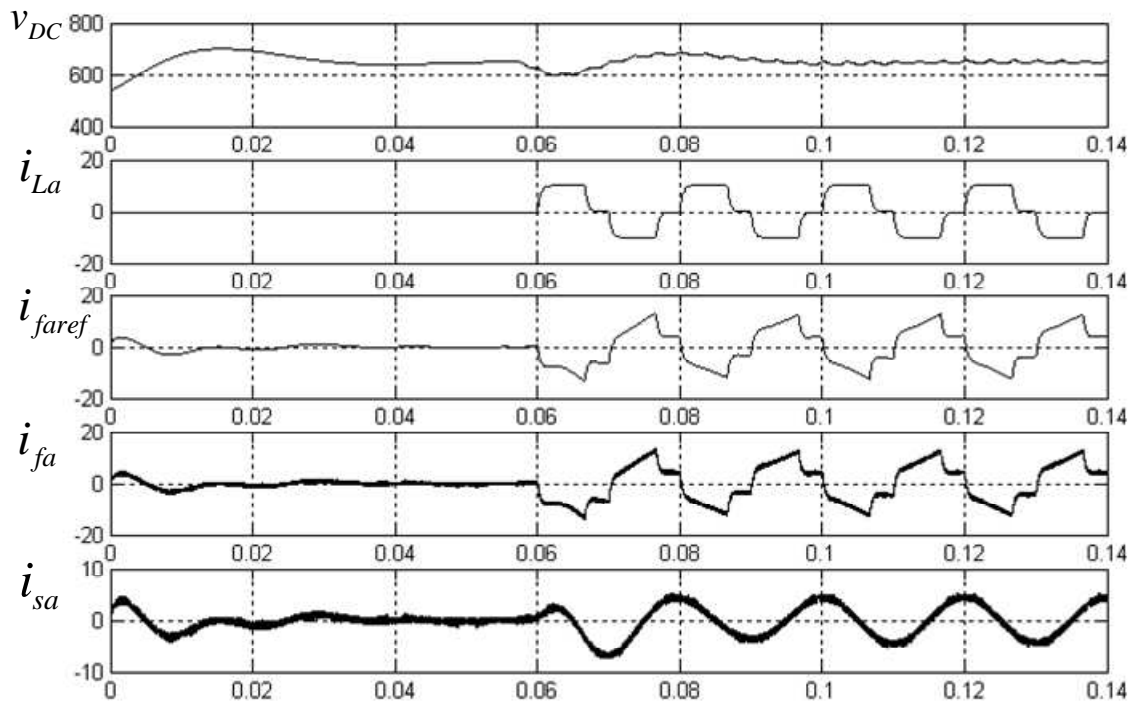
Fig. 3.26. Response of the active filter to a step load i.e. $i_{La} = i_{Lmax} = 12.5\,A$ ($\alpha = 0$ degree).

Figure 3.26. Réponse du filtre à un échelon de charge $i_{La} = i_{Lmax} = 12,5\,A$ ($\alpha = 0$).
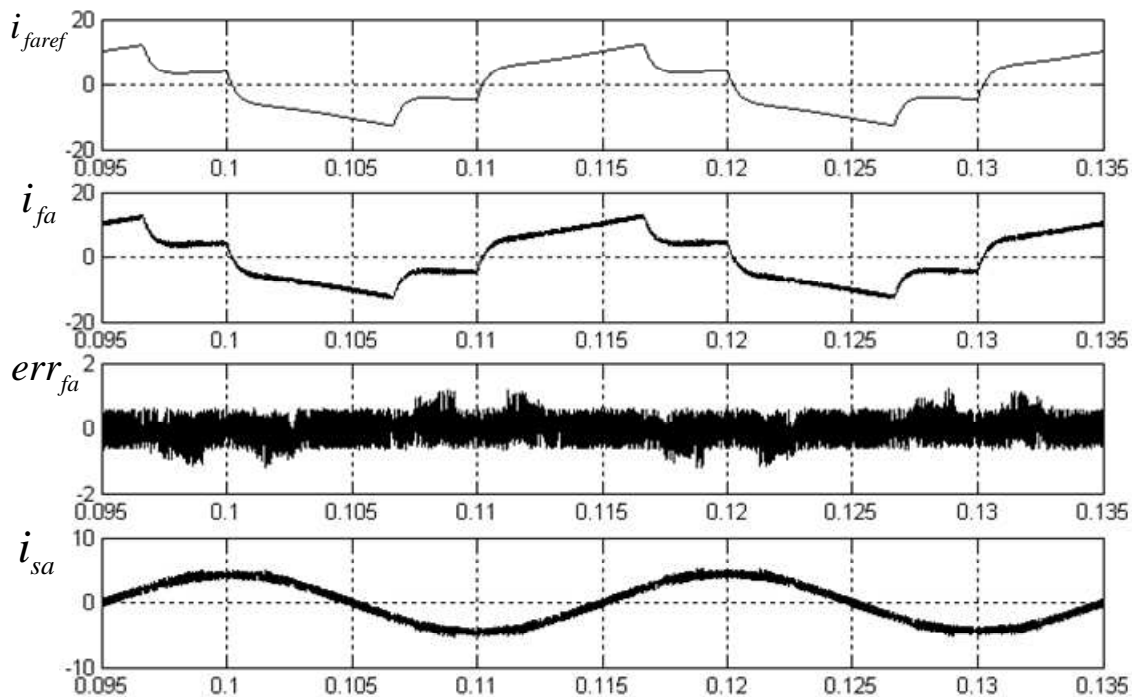
Fig. 3.27. Compensating current i_{fa} and line current i_{sa} ($\alpha = 60$ degree).

Figure 3.27. Courant de compensation i_{fa} et courant de ligne i_{sa} ($\alpha = 60°$).

For the unbalance nonlinear load with the same designed parameters from Table 3.1 the system is simulated in order to verify the design of the low-pass filter at 100 Hz- and 50 Hz cutoff frequencies. The results of these simulations are illustrated in Fig. 3.28 and 3.29.
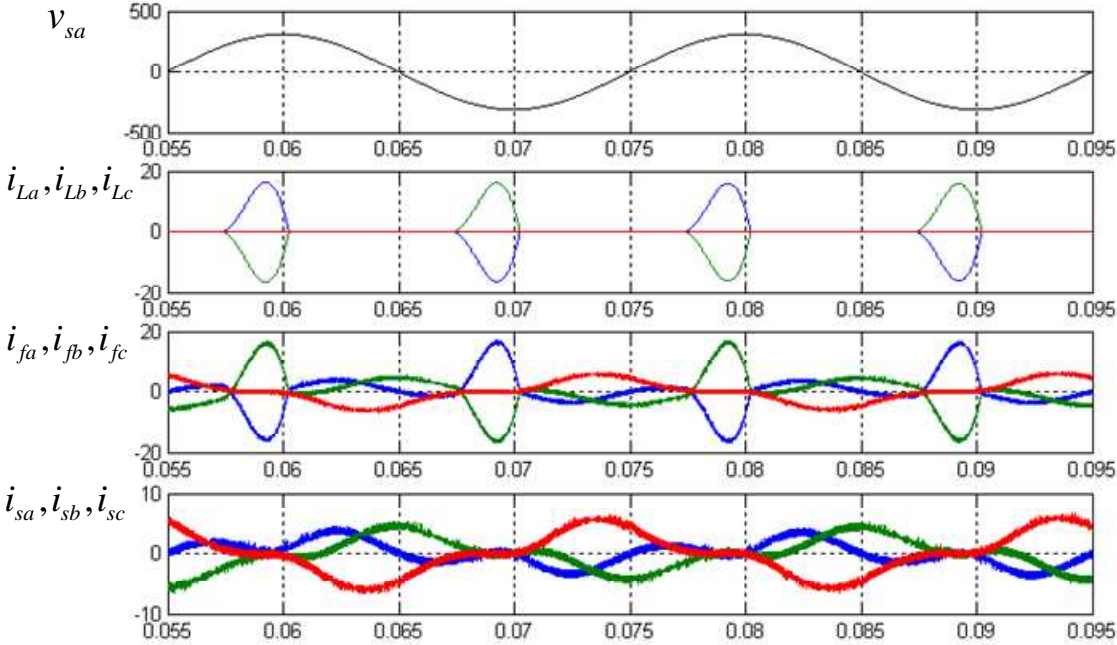
Fig. 3.28. Response of the active filter for an unbalanced load (cutoff frequency = 100 Hz).

Figure 3.28. Réponse du filter actif pour une charge déséquilibrée ($f_{coupure}$ = 100 Hz).

The simulated results in Fig. 3.28 and 3.29 are the currents drawn by the rectifier load, the active filter currents and the currents supplied by the source. At the 50 Hz cutoff frequency, the line currents are in phase with the line voltage at the point of common coupling. Therefore, the load presents at PCC a unity power factor.
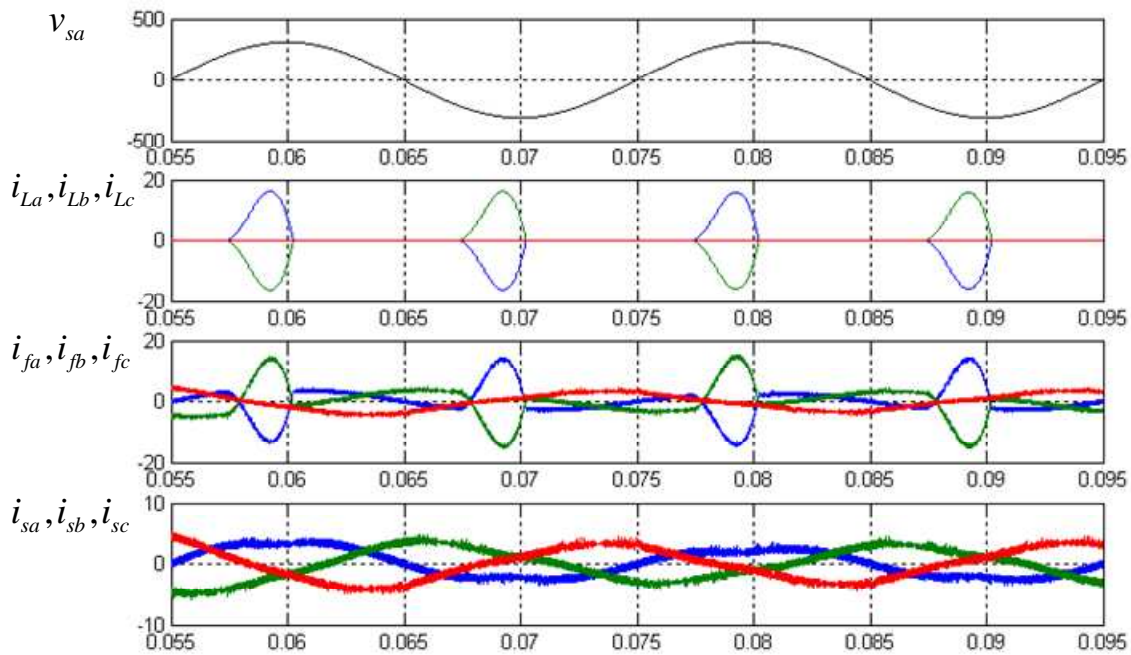
Fig. 3.29. Response of the active filter for an unbalanced load (cutoff frequency = 50 Hz).

Figure 3.29. Réponse du filtre actif pour une charge déséquilibrée ($f_{coupure}$ = 50 Hz).

3.5.5 Test results [47]

3.5.5.1 Test system

The hardware of the constructed active filter consists of two main circuits the power circuit and the control circuits built of:

- Digital signal processor;
- Zero-crossing detector;
- Digital to Analog converter;
- Hysteresis current controller;
- Voltage and current sensors.

The power circuit consists of 6-switch topology (VSI), AC inductors (2.2 mH) and DC capacitor (1000 µF, 800 V). The IGBT modules with the rate of 1000 V, 50 A were used as switches and operate at the average switching frequency of 25 kHz. The power circuit of the tested active filter is shown in Fig. 3.30.

The TMS320F243 [48-49] was used for the control circuit of the 3-phase shunt active filter to compute and generate the compensated harmonics currents, and also to generate the

reference current signal for the hysteresis current controller. An estimation method of the line inductances and the maximum switching frequency has been used to build the power circuit of the active filter. The control circuits are shown in Fig. 3.31.
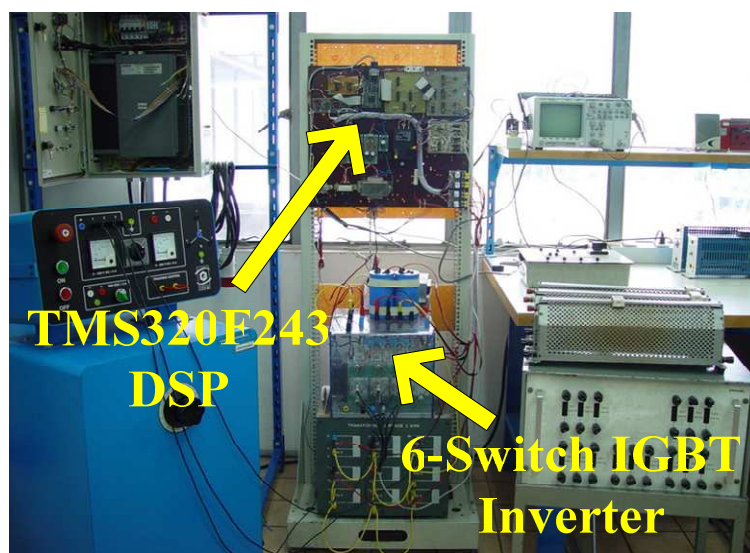
Fig. 3.30. Power and control circuits of the active filter.

Figure 3.30. Circuits de puissance et de contrôle du filtre actif.
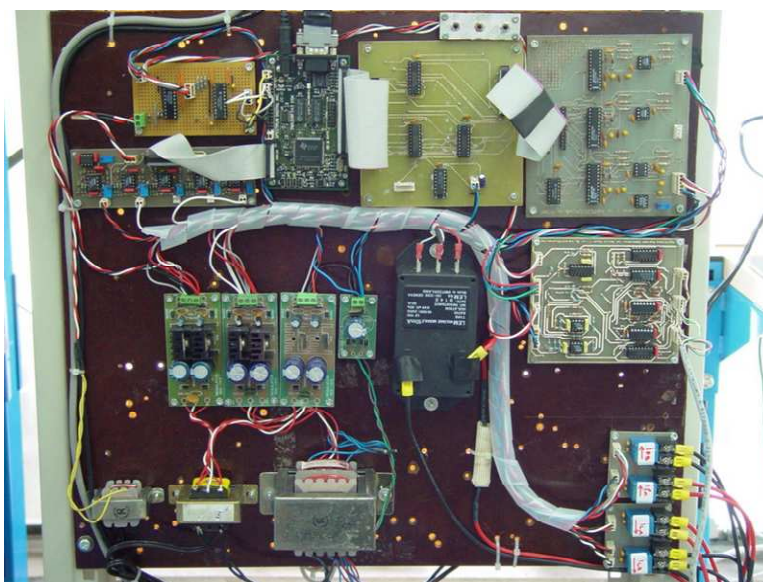
Fig. 3.31. TMS320F243 DSP with digital to analog converter, zero detection circuit, current controller and sensors.

Figure 3.31. DSP TMS320F243 avec ses circuits auxiliaires (convertisseur digital-analogique, détection de passage par zéro, controlleur de courant et capteurs).

3.5.5.2 Steady state and transient performance of the active filter

The first results correspond to a 3-phase diode bridge rectifier with resistive load as a test load presented on Fig. 3.32.
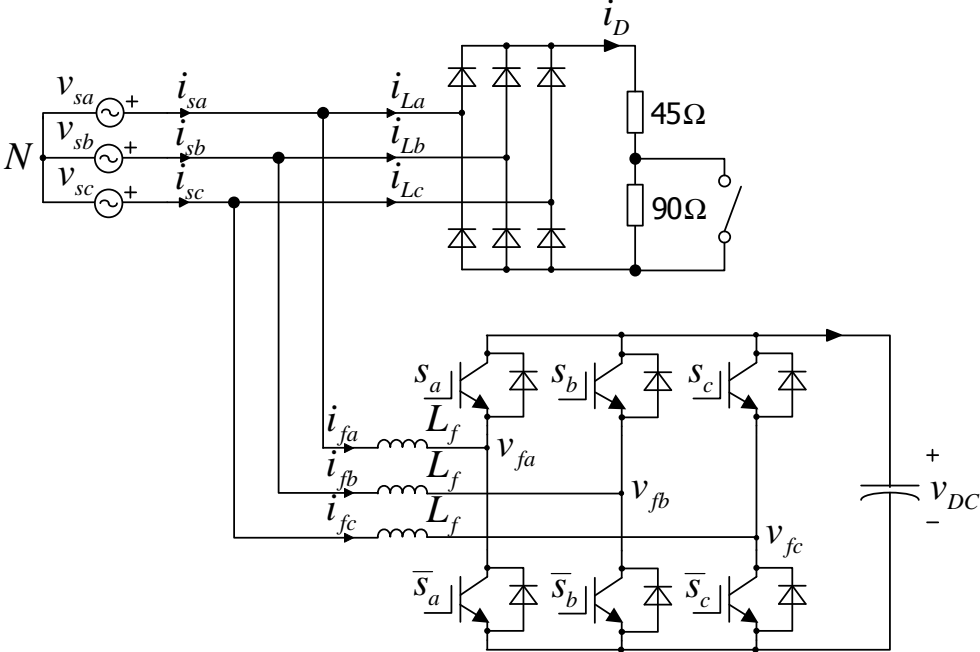
Fig. 3.32. 3-phase diode bridge rectifier with pure resistive load.

Figure 3.32. Pont de diodes triphasé débitant sur une charge résistive.

Fig. 3.33, Fig. 3.34 and Fig. 3.35 illustrate different current waveforms of the whole system. The current of nonlinear load i_{La} is shown in Fig. 3.33 which is distorted by the harmonic components $i_h = -i_f$ where i_f is the compensating currents generated by the active filter (Fig. 3.34). Therefore, the line current from AC power supply i_s is only the fundamental current of nonlinear load current i_l which is in phase with the phase voltage (Fig. 3.35).

V$_{sa}$: 200 V/Div   **i$_{La}$:10 A/Div**
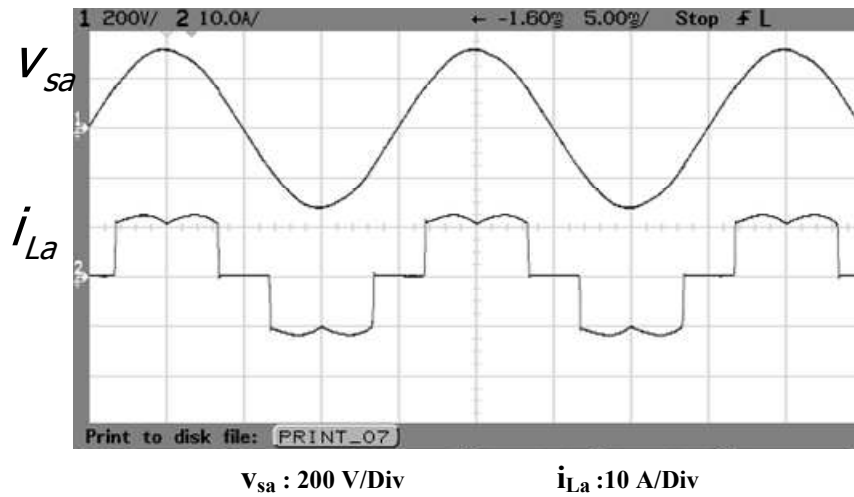
Fig. 3.33. Input voltage and current waveforms of 3-phase diode bridge converter.

Figure 3.33. Tension d'alimentation et courant absorbé par le redresseur à diodes.

i$_{fa}$: 10 A/Div   **i$_{sa}$: 10 A/Div**
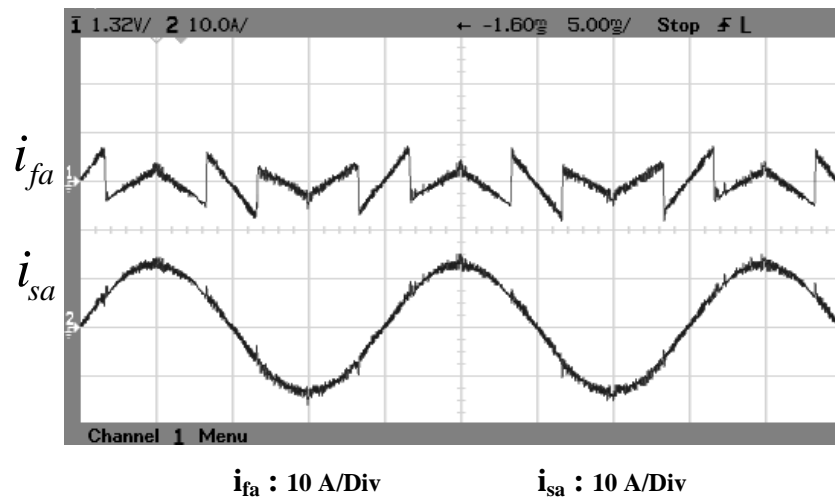
Fig. 3.34. Active filter current i$_{fa}$ and line current i$_{sa}$ supplied by the source.

Figure 3.34. Courant i$_{fa}$ du filtre actif et courant de ligne i$_{sa}$ délivré par la source.

V_sa : 200 V/Div　　　　　**i_sa : 10 A/Div**
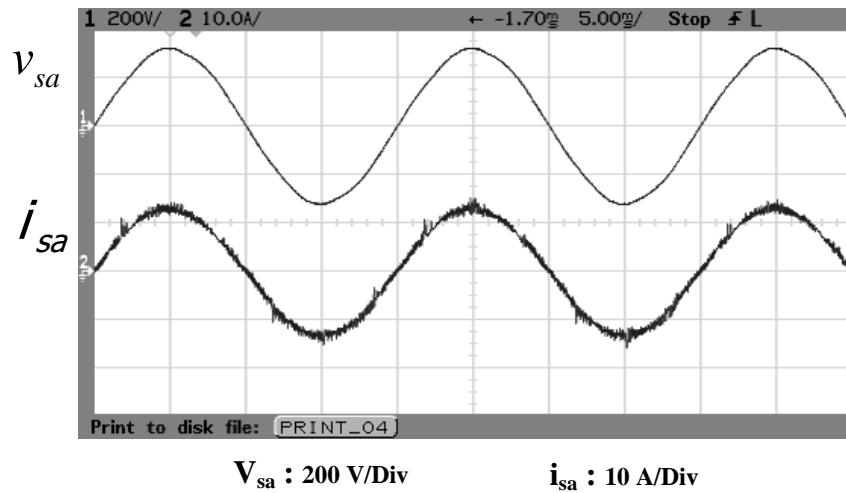
Fig. 3.35. Line current i_{sa} in phase with its line voltage v_{sa}.

Figure 3.35. Courant de ligne i_{sa} et tension simple v_{sa}.

The harmonic components are cancelled by the compensating currents generated by the active filter. This is is shown in Fig. 3.36 where are presented the harmonic spectrums of i_{La}, i_{fa} and i_{sa}.

The transient response of the capacitor voltage v_{DC} (Fig. 3.37) is optimized by using the pole placing method but the overshoot is high even though the response is well damped.
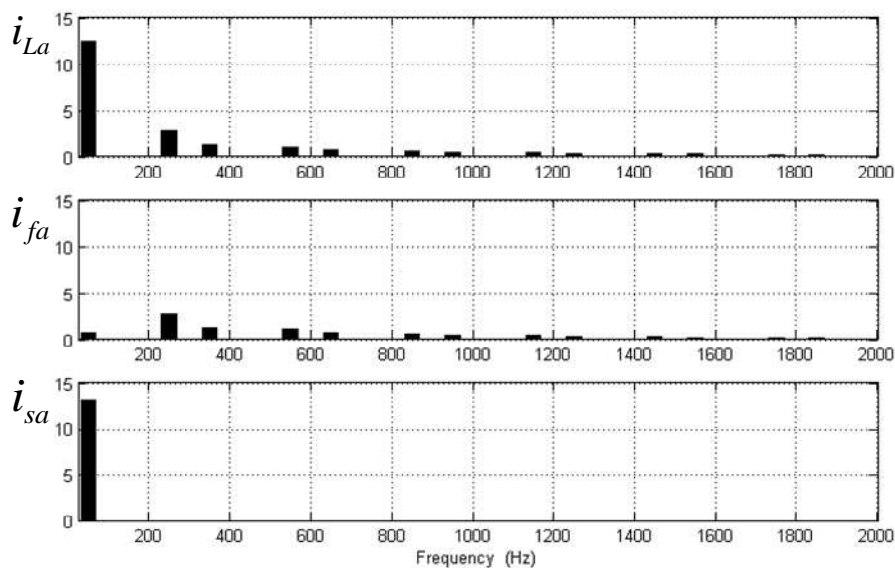
Fig. 3.36. Harmonic spectrums of load current i_{La}, active filter current i_{fa} and line current i_{sa}.

Figure 3.36. Spectres harmoniques des courants de charge i_{La}, du filtre i_{fa} et de ligne i_{sa}.

To eliminate the overshoot which is caused by the lead term of the PI-controller, corresponding lag term should be inserted into the reference of the voltage controller. The transient response of nonlinear load current i_{La}, line current i_{sa}, load currents i_{Ld} and i_{Ld1} by the step change of resistive load are shown in Fig. 3.38 and Fig. 3.39 respectively.

v_{DC} : 200 V/Div i_{fa} : 5 A/Div   t : 100 ms/Div
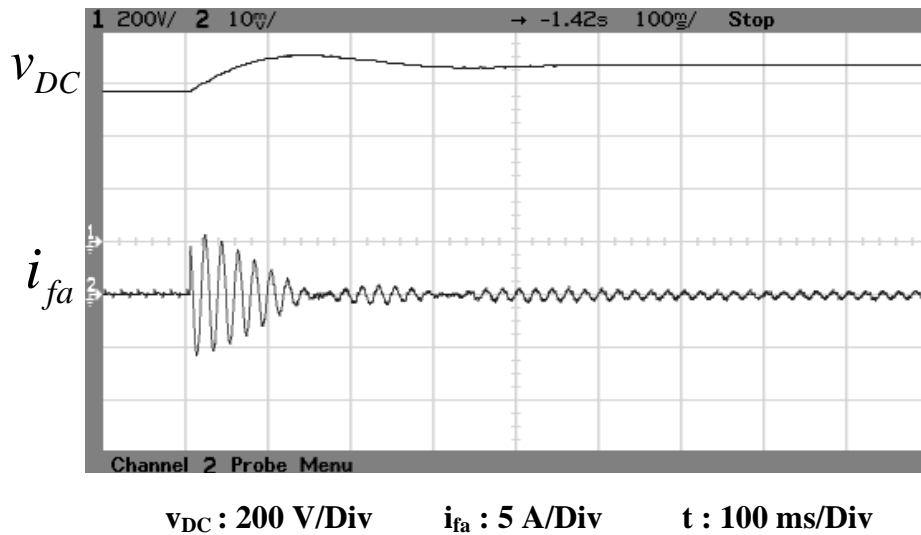
Fig. 3.37. Transient response of the capacitor voltage v_{DC} and compensating current i_{fa} for the starting of operation at the initial voltage of 560 V.

Figure 3.37. Réponse de la tension capacité v_{DC} et courant délivré par le filtre i_{fa} au démarrage pour une tension initiale de 560 V.

i_{La} : 10 A/Div i_{Sa} : 10 A/Div   t : 20 mS/Div
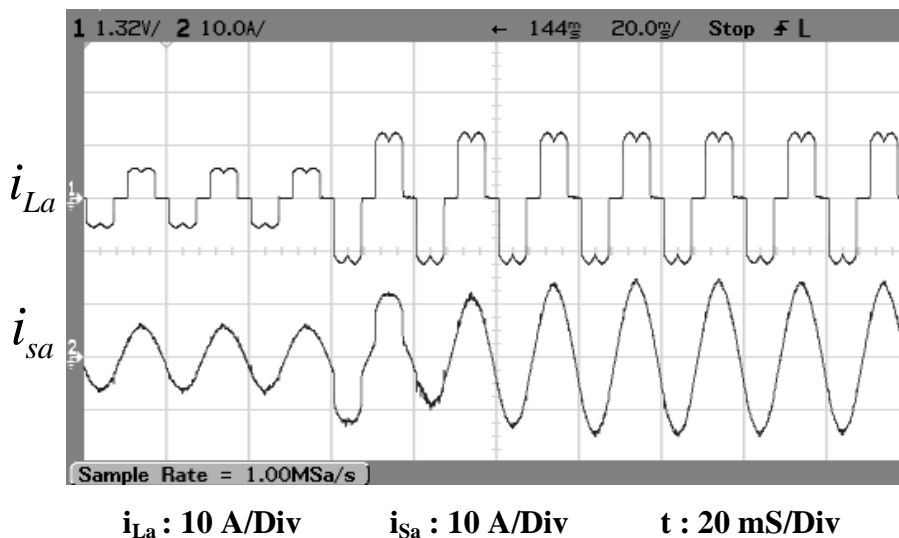
Fig. 3.38. Transient response of the nonlinear load current i_{La} and line current i_{sa} by the step change of the resistive load from 135 Ω to 45 Ω .

Figure 3.38. Courant de charge i_{La} lors d'un échelon de charge résistive (de 135 Ω à 45 Ω).

i_Ld : 3 A/Div   **t : 5 mS/Div**
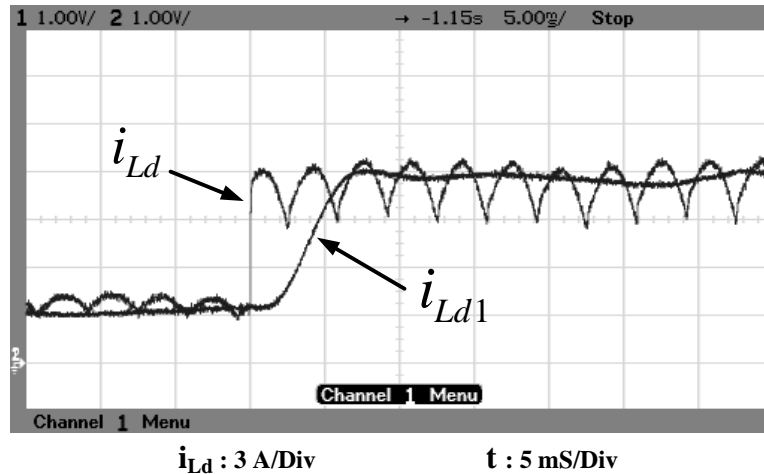
Fig. 3.39. Transient response of the load current by the step change of the resistive load

from 135 Ω to 45 Ω before and after the low-pass filter with 100 Hz cutoff frequency.

Figure 3.39. Réponse lors d'un échelon de charge résistive (de 135 Ω à 45 Ω), avant et

après le filtre pour une fréquence de coupure de 100 Hz.

The experimental results in terms of power, power factor and THD_i for the line currents were measured and evaluated. The power factor and THD_i for the line currents were improved by the active filter as shown in Table 3.2.

Experimental results with resistive load as a test load						
Test conditions	Apparent Power (kVA)	Active Power (kW)	P.F.	THD i_{sa} (%)	THD i_{sb} (%)	THD i_{sc} (%)
Without the active filter	6.334	6.072	0.957	29.48	29.66	29.54
With the active filter	6.313	6.250	0.99	3.10	3.19	3.20

Table 3.2. Comparison of the test results when the test load is connected without- and with-

the active filters.

Table 3.2. Comparaison des résultats obtenus sans filtre actif et avec filtre actif.

The second results correspond to a 3-phase diode bridge with LC filter and resistive load as a test load presented on Fig. 3.40.
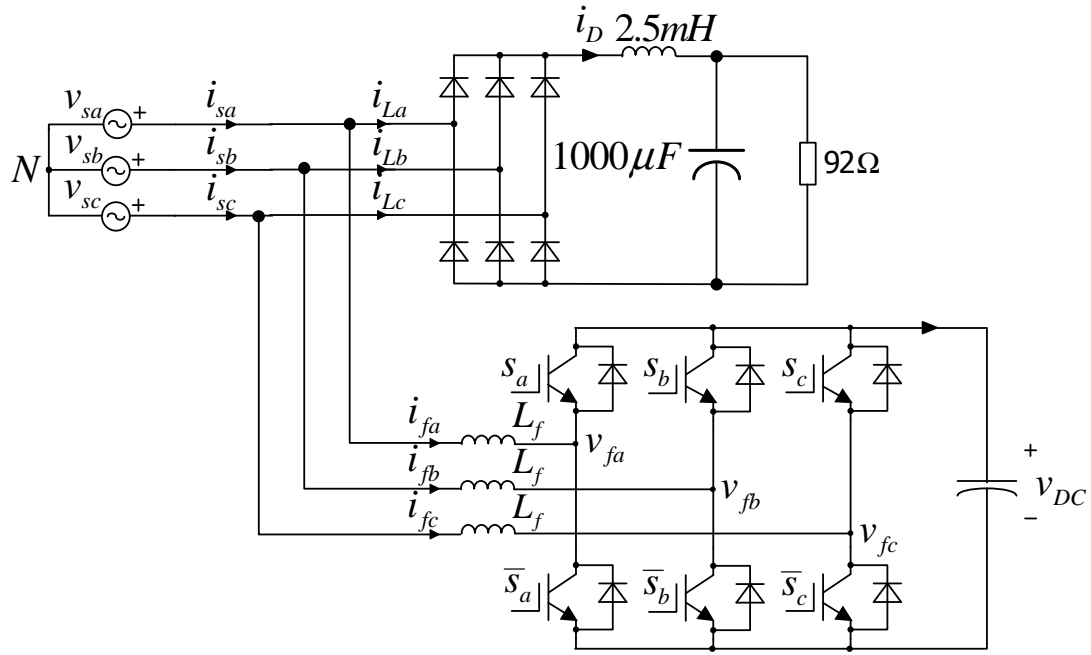
Fig. 3.40. 3-phase diode bridge with LC-filter loads as test load for the active filter.

Figure 3.40. Pont de diodes triphasé débitant sur une charge L-C-R.

Fig. 3.41 shows the distorted current waveforms of 3-phase nonlinear load i_{La}, i_{Lb} and i_{Lc} which is caused by 3-phase diode bridge with LC filter and resistive load. The harmonic components are cancelled by the compensating currents generated by the active filter which is shown in Fig. 3.42, Fig. 3.43 and 3.44 for the currents in phase a, b, and c. The harmonic spectrums of the currents i_L, i_f and i_s are shown in Fig. 3.45, 3.46 and 3.47 respectively.
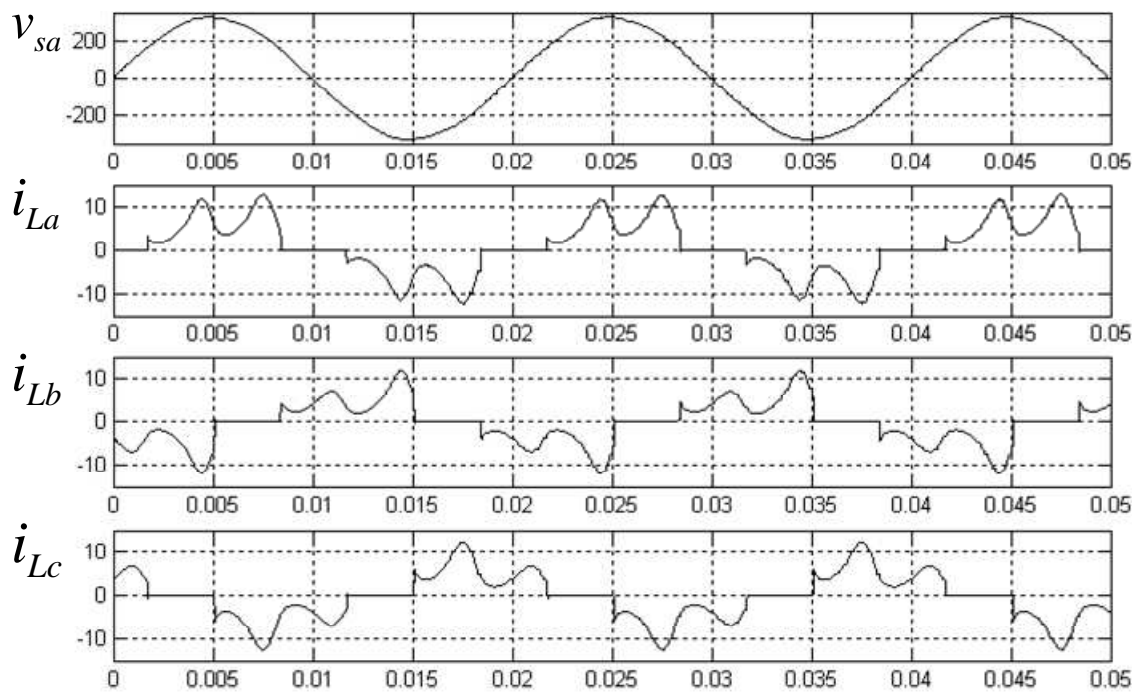
Fig. 3.41. Load current waveforms of the 3-phase diode bridge with LC-filter load.

Figure 3.41. Courants de phase du pont de diodes triphasé débitant sur une charge L-C-R.
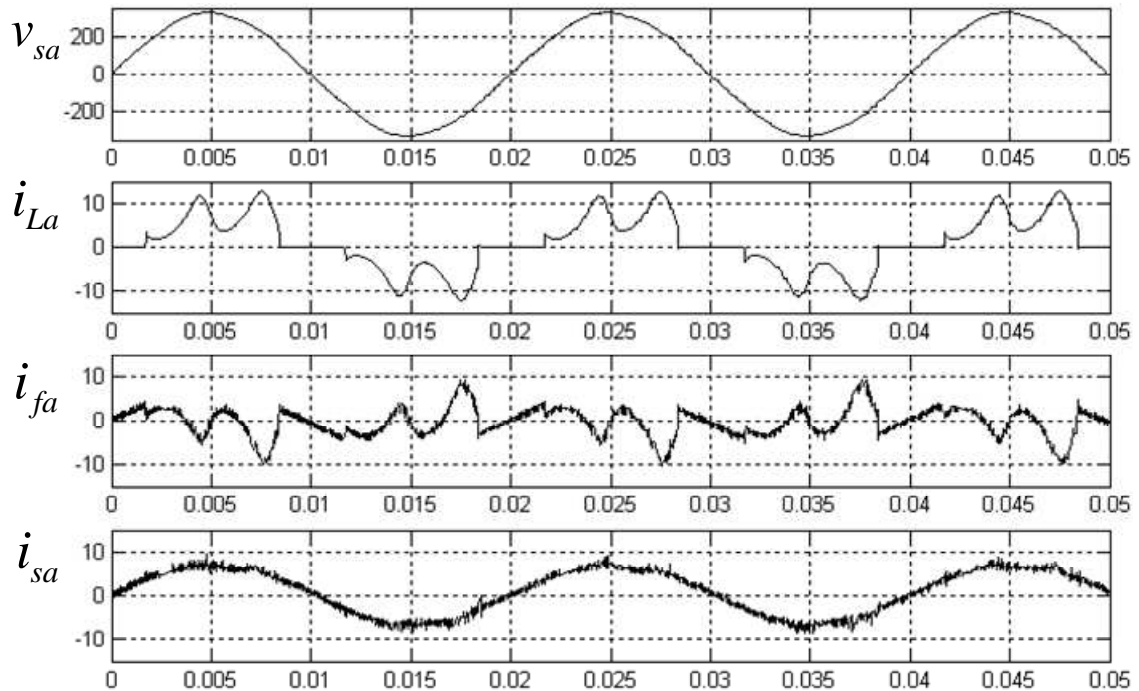
Fig. 3.42. Load current i_{La}, active filter current i_{fa} and line current i_{sa} of phase a.

Figure 3.42. Courants de charge i_{La}, du filtre actif i_{fa} et de ligne i_{sa} pour la phase a.
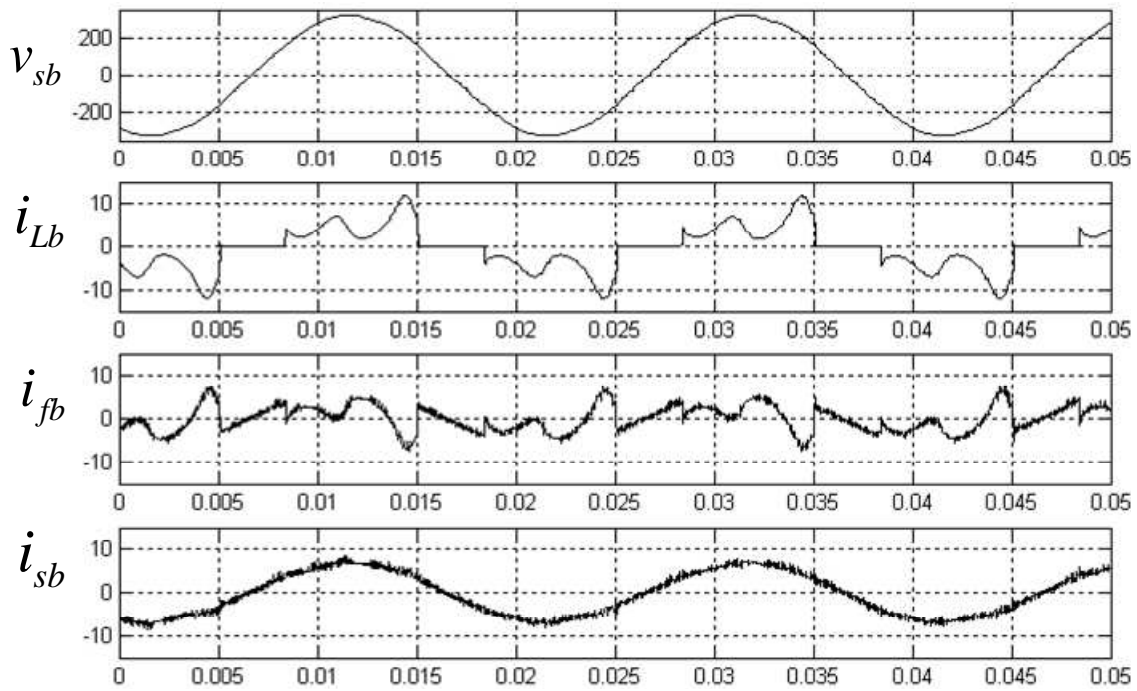
Fig. 3.43. Load current i$_{Lb}$, active filter current i$_{fb}$ and line current i$_{sb}$ of phase b.

Figure 3.43. Courants de charge i$_{Lb}$, du filtre actif i$_{fb}$ et de ligne i$_{sb}$ pour la phase b.
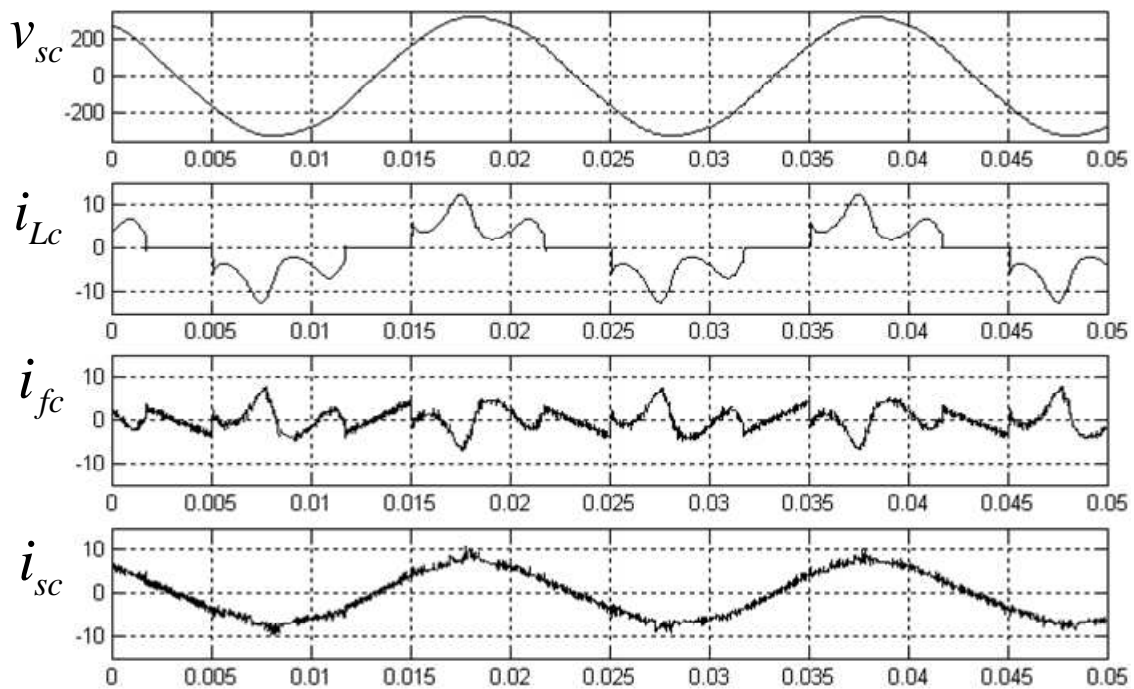
Fig. 3.44. Load current i$_{Lc}$, active filter current i$_{fc}$ and line current i$_{sc}$ of phase c.

Figure 3.44. Courants de charge i$_{Lc}$, du filtre actif i$_{fc}$ et de ligne i$_{sc}$ pour la phase c.
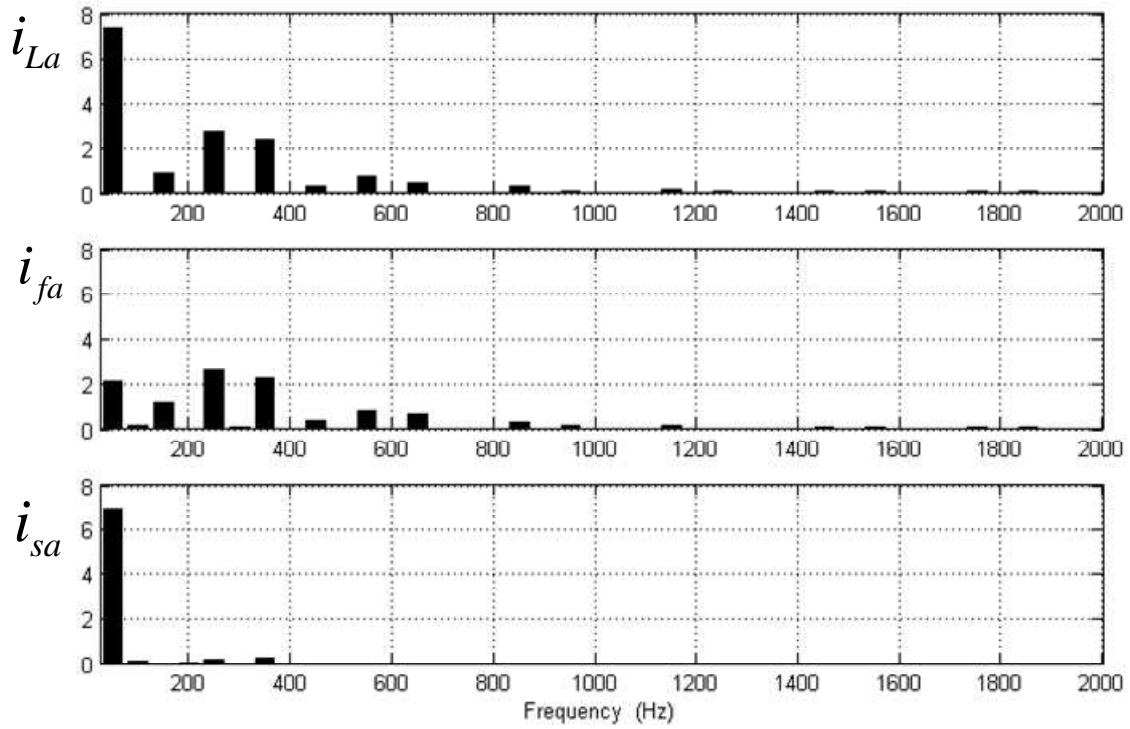
Fig. 3.45. Harmonic spectrums of load current i$_{La}$, active filter current i$_{fa}$ and line current i$_{sa}$.

Figure 3.45. Spectres harmoniques des courants de charge i$_{La}$, du filtre actif i$_{fa}$ et de ligne i$_{sa}$.
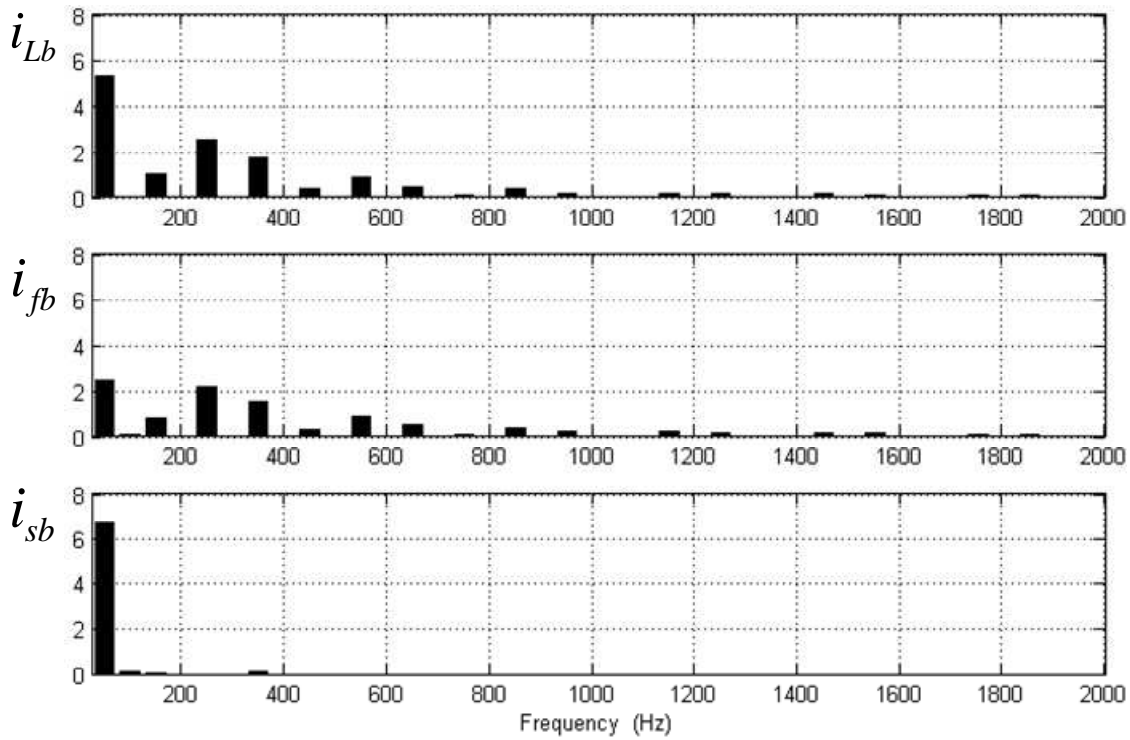
Fig. 3.46 Harmonic spectrums of load current i$_{Lb}$, active filter current i$_{fb}$ and line current i$_{sb}$.

Figure 3.46. Spectres harmoniques des courants de charge i$_{Lb}$, du filtre actif i$_{fb}$ et de ligne i$_{sb}$.
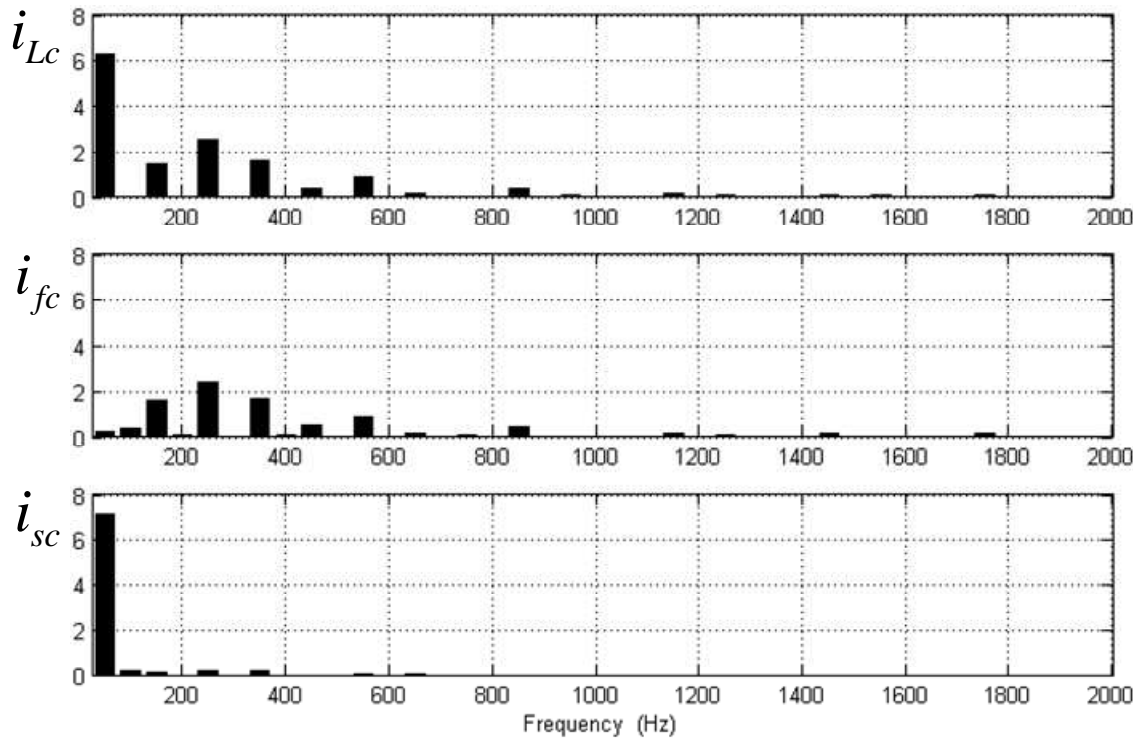
Fig. 3.47 Harmonic spectrums of load current i_{Lc}, active filter current i_{fc} and line current i_{sc}.

Figure 3.47. Spectres harmoniques des courants de charge i_{Lc}, du filtre actif i_{fc} et de ligne i_{sc}.

Fig. 3.48 shows 3-phase line currents supplied by AC source which contain only the fundamental current of nonlinear load current. These currents are in phase with their own phase voltage.

The experimental results in terms of power, power factor and THD_i for the line currents were measured and evaluated. The power factor and THD_i for the line currents were improved by the active filter as shown in Table 3.3.

The possibility to improve both the power factor and the THD is practically possible for low power system as presented here. For a real high power system only the THD will be improved if we want to keep the size of the active filter reasonable.
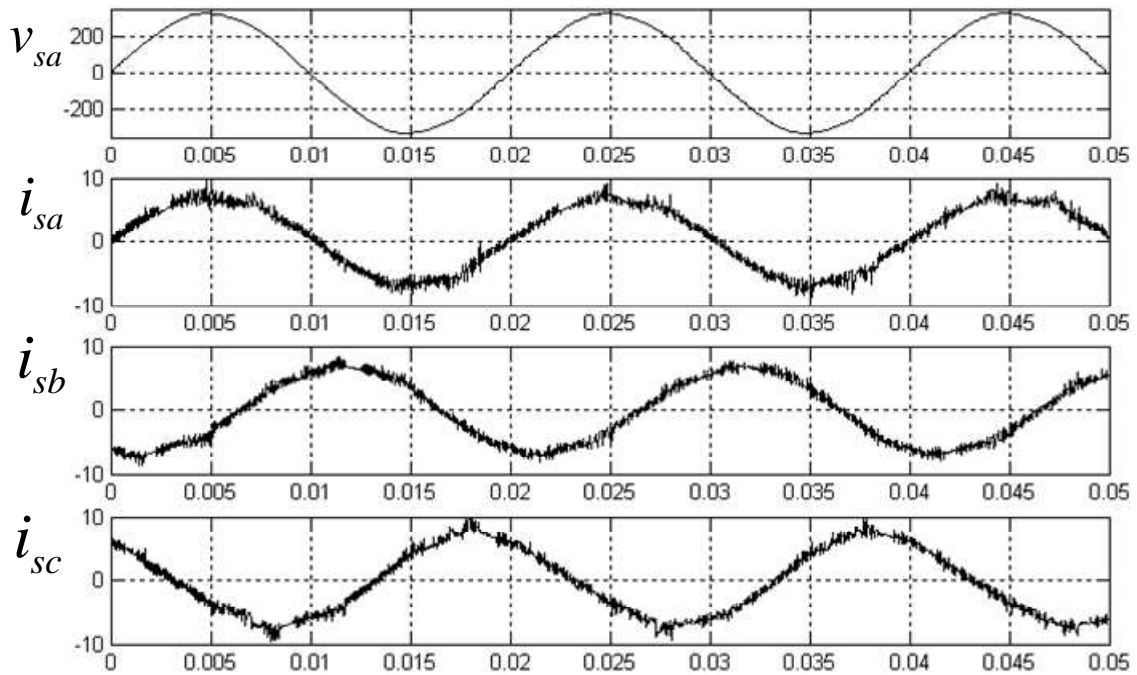
Fig. 3.48. 3-phase line currents supplied by the AC source.

Figure 3.48. Courants dans les trois phases du réseau d'alimentation.

Experimental results with LC-filter and resistive load as a test load						
Test conditions	Apparent Power (kVA)	Active Power (kW)	P.F.	THD i_{sa} (%)	THD i_{sb} (%)	THD i_{sc} (%)
Without the active filter	3.732	3.172	0.849	53.33	67.07	56.75
With the active filter	3.370	3.293	0.981	6.81	5.35	6.97

Table 3.3. Comparison of the test results when the test load is connected without- and with-

the active filters.

Table 3.3. Comparaison des résultats obtenus sans filtre actif et avec filtre actif.

3.6. Conclusion

This chapter gave us the opportunity to present the active filter we have developed these last years. The analysis and design of 3-phase shunt active filter employing digital signal processor TMS320F243 for computing and generating compensated harmonics currents and also to generate reference current signals for hysteresis current control has been conducted. An estimation method of line inductance and maximum switching frequency has been introduced for building the power circuit. The IGBT modules with the rate of 1000 V, 50 A were used as switches and operate at the average switching frequency of 25 kHz

The study and design of an active filter has been done first by simulation. The prototype is connected directly to a 3-phase diode bridge rectifier with 2 different types of load i.e. resistive load and LC-filter load. The experimental results show that the constructed active filter is capable to compensate harmonics current very well. In steady state operation, the average value of total harmonics distortion of line (THD_I) current is decreased from 29.56 % to 3.16 % for rectifier with a resistive load (Table 3.2). In the case of resistive load with LC filter, the average value of THD_I is decreased from 59.05 % to 6.38 % respectively.

Chapter 4

Modelling Method of Multipulse Converters

4.1. Introduction

The fourth chapter is concerned with the presentation of an exact analytical study of multipulses converter at steady state operation. Multipulse converters are a solution to harmonic problems which have the advantages in high power rating, low cost and robustness compared with solution using passive filters or active filters [1], [6], [50-52].

To study multipulse converters, a simulation tool such as Matlab/Simulink or SPICE can be used to simulate the steady state operation, and then FFT function will be used to find the harmonics generated by the converter. However, this process is time-consuming and sometimes the simulation might fail by numerical instabilities [53]. The averaging technique which is widely used to boost the speed of simulation [54] is not proper in this area since the harmonics characteristic does not appear in the averaged model.

An exact analytical solution is proposed and gives the possibility to calculate different quantities either on the DC side or on the AC side of the system. This method considers the smallest interval of time, on which one can define the elementary operating sequences of the converter. This method has been presented for an inverter in [55] and for a rectifier in [56]. It is developed here for multipulse converters [7-8].

For a p-pulse rectifier, the study interval can be reduced to $(2.\pi/p)$. Then, the information from the analysis interval is used to calculate the operation on the whole period. On this analysis interval if the converter operates in continuous conducting mode one has to consider only two operating sequences of the converter: the commutation sequence and the normal conduction sequence. A few unknown quantities have to be calculated, the state variables at

the beginning of the considered interval and the instant where the system changes of sequence.

To simplify the representation of the p-pulse converter we will also use a complex representation of 3-phase quantities. With this complex representation, it will be easy to show that even on the AC side the study interval can be reduced to $2.\pi/p$.

4.2. Complex transformation

The complex transformation is used to analyze 3-phase system. With the Complex transformation, a set of instantaneous 3-phase variables can be transformed into a unique point on the complex plane $(a, b\text{-axis})$ if the variables do not contain any homopolar components. When the instantaneous 3-phase variables change, the point on the complex plane will move to another position and provide a graphical perception of 3-phase operation on the complex plane.

4.2.1. Transformation of 3-phase system

The transformation of the variables from $a, b, c - \text{axis}$ into $\alpha, \beta - \text{axis}$ is calculated by the transformation matrix $K_{\alpha\beta/abc}$:

$$\begin{bmatrix} x_\alpha \\ x_\beta \end{bmatrix} = K_{\alpha\beta/abc} \cdot \begin{bmatrix} x_a \\ x_b \\ x_c \end{bmatrix} \tag{4.1}$$

where:

$$K_{\alpha\beta/abc} = \sqrt{\frac{2}{3}} \cdot \begin{bmatrix} 1 & -\dfrac{1}{2} & -\dfrac{1}{2} \\ 0 & \dfrac{\sqrt{3}}{2} & -\dfrac{\sqrt{3}}{2} \end{bmatrix} \tag{4.2}$$

The definition of the complex variable is:

$$\overline{x} = \frac{1}{\sqrt{2}} \cdot (x_\alpha + j \cdot x_\beta) \tag{4.3}$$

and the complex variable can be also written as:

$$\overline{x} = \frac{1}{\sqrt{3}} \cdot \begin{bmatrix} 1 & a & a^2 \end{bmatrix} \cdot \begin{bmatrix} x_a \\ x_b \\ x_c \end{bmatrix} \tag{4.4}$$

where the unit vectors of each axis of 3-phase system are:

$$e^{j0} = 1$$
$$e^{j\frac{2\pi}{3}} = -\frac{1}{2} + j\frac{\sqrt{3}}{2} = a \tag{4.5}$$
$$e^{j\frac{4\pi}{3}} = -\frac{1}{2} - j\frac{\sqrt{3}}{2} = a^2$$

Adding the conjugate part in equation 4.3 gives:

$$\overline{X} = \begin{bmatrix} \overline{x} \\ \overline{x}^* \end{bmatrix} = \frac{1}{\sqrt{3}} \cdot \begin{bmatrix} 1 & a & a^2 \\ 1 & a^2 & a \end{bmatrix} \cdot \begin{bmatrix} x_a \\ x_b \\ x_c \end{bmatrix} = K_s \cdot X \tag{4.6}$$

where K_s is the transformation matrix.

Therefore, the inverse transformation is:

$$X = \frac{1}{\sqrt{3}} \cdot \begin{bmatrix} 1 & 1 \\ a^2 & a \\ a & a^2 \end{bmatrix} \cdot \overline{X} = K_s' \cdot \overline{X} \tag{4.7}$$

where the transformation matrix K_s' is:

$$K_s' = K_s^{*T} \tag{4.8}$$

4.2.2. Study interval

On the DC side, it is obvious that if p is the pulse number of the rectifier, the period of the different variables is equal to $\frac{2\pi}{p}$ if the load does not introduce its own harmonics. It is possible also with a few hypothesis to show that a study interval of $\frac{2\pi}{p}$ is enough for the AC variables.

Let consider three balanced harmonics:

$$x_1 = \sqrt{2} \cdot X_{rms} \cdot \sin\left(k \cdot \omega \cdot t - \alpha\right)$$

$$x_2 = \sqrt{2} \cdot X_{rms} \cdot \sin\left(k \cdot \omega \cdot t - \alpha - k \cdot \frac{2 \cdot \pi}{3}\right) \qquad (4.9)$$

$$x_3 = \sqrt{2} \cdot X_{rms} \cdot \sin\left(k \cdot \omega \cdot t - \alpha - k \cdot \frac{4 \cdot \pi}{3}\right)$$

The corresponding complex quantity is:

$$\overline{x_k} = -j \cdot \frac{1}{\sqrt{6}} \cdot X_{rms} \cdot$$

$$\left[e^{j \cdot (k \cdot \omega \cdot t - \alpha)} \cdot \left(1 + e^{j \cdot (1-k) \cdot \frac{2 \cdot \pi}{3}} + e^{j \cdot (1-k) \cdot \frac{4 \cdot \pi}{3}}\right) - e^{-j \cdot (k \cdot \omega \cdot t - \alpha)} \cdot \left(1 + e^{j \cdot (1+k) \cdot \frac{2 \cdot \pi}{3}} + e^{j \cdot (1+k) \cdot \frac{4 \cdot \pi}{3}}\right) \right] \qquad (4.10)$$

For a well design rectifier, with perfect ratio for the different transformers, one has the different results:

- the pulse number p is a multiple of 3;
- the harmonics pulsations on the DC side are multiple of $p.\omega$;
- the harmonics ranks on the AC side are in $k \cdot p \pm 1$.

Then, if one considers the previous complex quantity for three particular values of k, one obtains:

$$\overline{x_1} = -j \cdot \sqrt{\frac{3}{2}} \cdot X_{rms} \cdot e^{j \cdot (\omega \cdot t - \alpha)} \qquad (4.11)$$

$$\overline{x_{kp-1}} = j \cdot \sqrt{\frac{3}{2}} \cdot X_{rms} \cdot e^{-j \cdot ((k \cdot p - 1) \cdot \omega \cdot t - \alpha)} \qquad (4.12)$$

$$\overline{x_{kp+1}} = -j \cdot \sqrt{\frac{3}{2}} \cdot X_{rms} \cdot e^{j \cdot ((k \cdot p + 1) \cdot \omega \cdot t - \alpha)} \qquad (4.13)$$

The AC waveforms will only contain a fundamental component under the form of equation 4.11 and harmonics under the form of 4.12 or 4.13. These different terms verify the following relationship:

$$\overline{x_1}\left(\omega \cdot t + \frac{2 \cdot \pi}{p}\right) = -j \cdot \sqrt{\frac{3}{2}} \cdot X_{rms} \cdot e^{j \cdot \left(\omega \cdot t - \alpha + \frac{2 \cdot \pi}{p}\right)} = \overline{x_1}(\omega \cdot t) \cdot e^{j \frac{2 \cdot \pi}{p}}$$

$$\overline{x_{kp-1}}\left(\omega \cdot t + \frac{2 \cdot \pi}{p}\right) = j \cdot \sqrt{\frac{3}{2}} \cdot X_{rms} \cdot e^{-j \cdot \left((k \cdot p - 1) \cdot \omega \cdot t - \alpha + (k \cdot p - 1) \cdot \frac{2 \cdot \pi}{p}\right)} = \overline{x_{kp-1}}(\omega \cdot t) \cdot e^{j \frac{2 \cdot \pi}{p}} \quad (4.14)$$

$$\overline{x_{kp+1}}\left(\omega \cdot t + \frac{2 \cdot \pi}{p}\right) = -j \cdot \sqrt{\frac{3}{2}} \cdot X_{rms} \cdot e^{j \cdot \left((k \cdot p + 1) \cdot \omega \cdot t - \alpha + (k \cdot p + 1) \cdot \frac{2 \cdot \pi}{p}\right)} = \overline{x_{kp+1}}(\omega \cdot t) \cdot e^{j \frac{2 \cdot \pi}{p}}$$

Then any AC variable which contains a fundamental and such harmonics can be obtained in the complex plane on an interval of length $\frac{2\pi}{p}$ by a rotation of $\frac{2\pi}{p}$ from its value on the previous interval.

4.2.3. Star or delta connection

Relationship between star and delta variable can be deduced from Fig. 4.1.
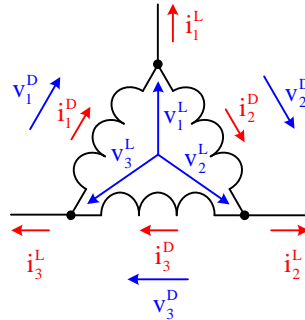
Fig. 4.1. Delta connection of the windings.

Figure 4.1. Connexion en triangle des enroulements.

If we consider that the sum of any three-phase quantities, with no homopolar component, is equal to zero, one has for the currents:

$$I^L = \begin{vmatrix} i_1^L \\ i_2^L \\ i_3^L \end{vmatrix} = \begin{vmatrix} 1 & -1 & 0 \\ 0 & 1 & -1 \\ -1 & 0 & 1 \end{vmatrix} \cdot \begin{vmatrix} i_1^D \\ i_2^D \\ i_3^D \end{vmatrix} = C \cdot I^D \quad (4.15)$$

and:

$$I^D = \frac{1}{3} \cdot \begin{vmatrix} 1 & 0 & -1 \\ -1 & 1 & 0 \\ 0 & -1 & 1 \end{vmatrix} \cdot I^L = \frac{1}{3} \cdot C^T \cdot I^L \quad (4.16)$$

For the voltages:

$$\mathbf{V^D} = \begin{vmatrix} v_1^D \\ v_2^D \\ v_3^D \end{vmatrix} = \begin{vmatrix} 1 & 0 & -1 \\ -1 & 1 & 0 \\ 0 & -1 & 1 \end{vmatrix} \cdot \begin{vmatrix} v_1^L \\ v_2^L \\ v_3^L \end{vmatrix} = \mathbf{C^T} \cdot \mathbf{V^L} \tag{4.17}$$

and:

$$\mathbf{V^L} = \frac{1}{3} \cdot \begin{vmatrix} 1 & -1 & 0 \\ 0 & 1 & -1 \\ -1 & 0 & 1 \end{vmatrix} \cdot \mathbf{V^D} = \frac{1}{3} \cdot \mathbf{C} \cdot \mathbf{V^D} \tag{4.18}$$

Applying the complex transformation to the current:

$$\overline{\mathbf{I^L}} = \mathbf{K_S} \cdot \mathbf{I^L} = \mathbf{K_S} \cdot \mathbf{C} \cdot \mathbf{I^D} = \mathbf{K_S} \cdot \mathbf{C} \cdot \mathbf{K_S}^{*T} \cdot \overline{\mathbf{I^D}} = \mathbf{S} \cdot \overline{\mathbf{I^D}} \tag{4.19}$$

with:

$$\mathbf{S} = \begin{vmatrix} 1-a^2 & 0 \\ 0 & 1-a \end{vmatrix} \tag{4.20}$$

This means:

$$\overline{i^L} = \left(1-a^2\right) \cdot \overline{i^D} = \sqrt{3} \cdot e^{j\frac{\pi}{6}} \cdot \overline{i^D} \tag{4.21}$$

and:

$$\overline{\mathbf{I^D}} = \mathbf{S}^{-1} \cdot \overline{\mathbf{I^L}} = \frac{1}{3} \cdot \mathbf{S}^* \cdot \overline{\mathbf{I^L}} \tag{4.22}$$

For the voltage:

$$\overline{\mathbf{V^L}} = \mathbf{K_S} \cdot \mathbf{V^L} = \mathbf{K_S} \cdot \frac{1}{3} \cdot \mathbf{C} \cdot \mathbf{V^D} = \frac{1}{3} \cdot \mathbf{K_S} \cdot \mathbf{C} \cdot \mathbf{K_S}^{*T} \cdot \overline{\mathbf{V^D}} = \frac{1}{3} \cdot \mathbf{S} \cdot \overline{\mathbf{V^D}} \tag{4.23}$$

so:

$$\overline{v^L} = \frac{1}{3} \cdot \left(1-a^2\right) \cdot \overline{v^D} = \frac{1}{\sqrt{3}} \cdot e^{j\frac{\pi}{6}} \cdot \overline{v^D} \tag{4.24}$$

and:

$$\overline{\mathbf{V^D}} = 3 \cdot \mathbf{S}^{-1} \cdot \overline{\mathbf{V^L}} = \mathbf{S}^* \cdot \overline{\mathbf{V^L}} \tag{4.25}$$

4.3. 12-pulse converter using Y/YΔ transformer

As seen in chapter 2, the 12-pulse converter is widely used in high power applications to reduce harmonics on networks. The principle of the 12-pulse converter is to suppress the

harmonic currents of one 6-pulse bridge converter by the harmonic currents of another converter. This is achieved by providing two power supplies with 30 degree phase shift. A phase shifting transformer i.e. Y/YΔ transformer is the most common used to create the 30 degree phase shift. This section will present the complex variables based analysis and model development of the 12-pulse converter using Y/YΔ transformer.

4.3.1. Overview of 12-pulse converter using Y/YΔ transformer

Fig. 4.2 shows the phase shifting transformer, where the primary winding is connected in star and the secondary windings are connected in star and delta respectively. Each secondary winding is connected to a 6-pulse bridge converter and the 12-pulse converter configuration is created by a series connection of these two converters. On the DC side, one considers the losses in the smoothing inductance and an R-C element representing the load.
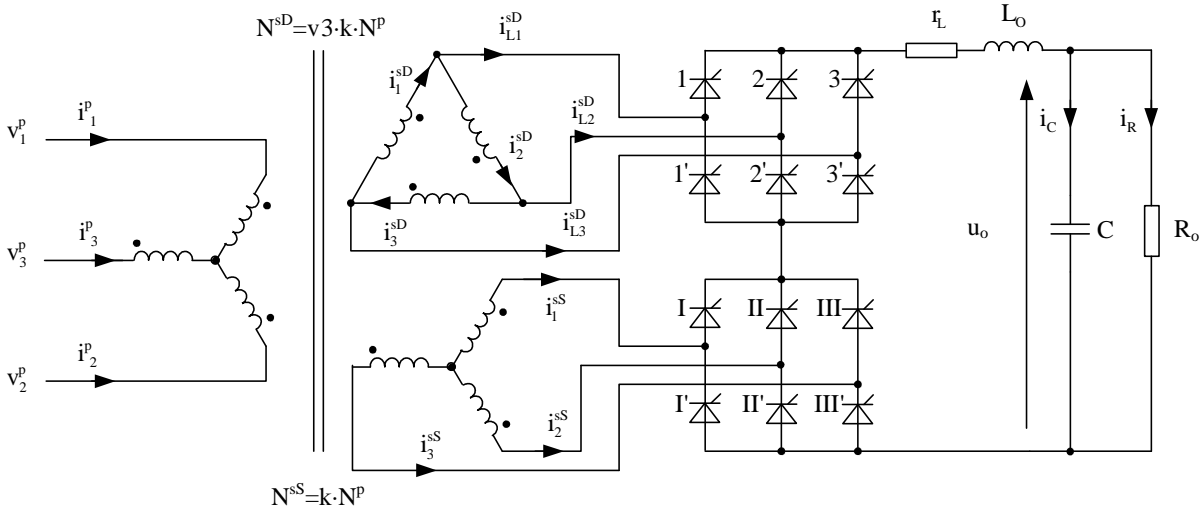
Fig. 4.2. Circuit configuration of 12-pulse converter.

Figure 4.2. Schéma du redresseur dodécaphasé.

4.3.2. Transformer model

The equivalent circuit of Y/YΔ transformer in Fig. 4.3 illustrates the windings, their parameters and variables according to winding group and phase.

The voltage equations of Y/YΔ transformer in the $\alpha\beta$ -coordinate are as follow:

$$v_\alpha^p = R_p \cdot i_\alpha^p + L_p \cdot \frac{d}{dt} i_\alpha^p - M_{psD} \cdot \frac{d}{dt} i_\alpha^{sD} - M_{psS} \cdot \frac{d}{dt} i_\alpha^{sS}$$

$$v_\alpha^{sD} = -R_{sD} \cdot i_\alpha^{sD} - L_{sD} \cdot \frac{d}{dt} i_\alpha^{sD} + M_{psD} \cdot \frac{d}{dt} i_\alpha^p - M_{ss} \cdot \frac{d}{dt} i_\alpha^{sS} \qquad (4.26)$$

$$v_\alpha^{sS} = -R_{sS} \cdot i_\alpha^{sS} - L_{sS} \cdot \frac{d}{dt} i_\alpha^{sS} + M_{psS} \cdot \frac{d}{dt} i_\alpha^p - M_{ss} \cdot \frac{d}{dt} i_\alpha^{sD}$$

and:

$$v_\beta^p = R_p \cdot i_\beta^p + L_p \cdot \frac{d}{dt} i_\beta^p - M_{psD} \cdot \frac{d}{dt} i_\beta^{sD} - M_{psS} \cdot \frac{d}{dt} i_\beta^{sS}$$

$$v_\beta^{sD} = -R_{sD} \cdot i_\beta^{sD} - L_{sD} \cdot \frac{d}{dt} i_\beta^{sD} + M_{psD} \cdot \frac{d}{dt} i_\beta^p - M_{ss} \cdot \frac{d}{dt} i_\beta^{sS} \qquad (4.27)$$

$$v_\beta^{sS} = -R_{sS} \cdot i_\beta^{sS} - L_{sS} \cdot \frac{d}{dt} i_\beta^{sS} + M_{psS} \cdot \frac{d}{dt} i_\beta^p - M_{ss} \cdot \frac{d}{dt} i_\beta^{sD}$$

Fig. 4.3. Y/YΔ transformer windings.

Figure 4.3. Enroulements Y/YΔ du transformateur.

By using the complex transformation, the transformer equations are:

$$\overline{V^p} = R^p \cdot \overline{I^p} + L^p \cdot \frac{d}{dt} \overline{I^p} - M^{psD} \cdot \frac{d}{dt} \overline{I^{sD}} - M^{psS} \cdot \frac{d}{dt} \overline{I^{sS}} \qquad (4.28)$$

$$\overline{V^{sD}} = -R^{sD} \cdot \overline{I^{sD}} - L^{sD} \cdot \frac{d}{dt} \overline{I^{sD}} + M^{psD} \cdot \frac{d}{dt} \overline{I^p} - M^{ss} \cdot \frac{d}{dt} \overline{I^{sS}} \qquad (4.29)$$

$$\overline{V}^{sS} = -R^{sS} \cdot \overline{I}^{sS} - L^{sS} \cdot \frac{d}{dt} \overline{I}^{sS} + M^{psS} \cdot \frac{d}{dt} \overline{I}^{P} - M^{ss} \cdot \frac{d}{dt} \overline{I}^{sD} \tag{4.30}$$

For the complex equations, all transformer parameters appear in the diagonal of 2x2 matrices. For example, the resistance of the primary winding R_p appears in complex equation as R^P:

$$R^P = \begin{bmatrix} R_p & 0 \\ 0 & R_p \end{bmatrix} \tag{4.31}$$

4.3.3. Ideal operation of the 12-pulse converter using Y/YΔ transformer

The study of the ideal operating of multi-pulse converter is one of the best application examples of complex modeling of 3-phased variables.

Let consider the primary line voltage under the form of:

$$v_{L,n} = V \cdot \sqrt{2} \cdot \sin\left[\omega \cdot t - (n-1) \cdot \frac{2 \cdot \pi}{3}\right] \tag{4.32}$$

then, for a star connection of the primary winding, we have:

$$\overline{v}^P = -j \cdot V \cdot \sqrt{\frac{3}{2}} \cdot e^{j \cdot \omega \cdot t} \tag{4.33}$$

At no load, we have:

$$\begin{aligned} \overline{\varphi}^P &= L_p \cdot \overline{i}^P \\ \overline{\varphi}^{sD} &= M_{psD} \cdot \overline{i}^P \\ \overline{\varphi}^{sS} &= M_{psS} \cdot \overline{i}^P \end{aligned} \tag{4.34}$$

Then:

$$\overline{\varphi}^{sD} = \frac{M_{psD}}{L_p} \cdot \overline{\varphi}^P = \frac{M_{psD}}{M_{psS}} \cdot \overline{\varphi}^{sS} \tag{4.35}$$

If we neglect the primary resistances, these relationships within the flux exist also for the voltages:

$$\overline{v}^{sD} = \frac{M_{psD}}{L_p} \cdot \overline{v}^P = \frac{M_{psD}}{M_{psS}} \cdot \overline{v}^{sS} \tag{4.36}$$

Then for a star connection of the primary winding, one obtains:

$$\overline{v^{sS}} = \frac{M_{psS}}{L_p} \cdot \overline{v^p} \tag{4.37}$$

For, the secondary delta winding, the corresponding line voltage is according to equation 4.23:

$$V_L^{sD} = \frac{1}{3} \cdot S \cdot V^{sD} \tag{4.38}$$

then:

$$\overline{v_L^{sD}} = \frac{1-a^2}{3} \cdot \overline{v^{sD}} = \frac{1}{\sqrt{3}} \cdot e^{j\frac{\pi}{6}} \cdot \overline{v^{sD}} = \frac{1}{\sqrt{3}} \cdot e^{j\frac{\pi}{6}} \cdot \frac{M_{psD}}{L_p} \cdot \overline{v^p} \tag{4.39}$$

Equations 4.37 and 4.36 show that the line voltages of the star winding are then lagging the delta ones with a 30° phase shift. Furthermore, to obtain the same amplitude for the two voltages, one needs:

$$M_{psS} = \frac{M_{psD}}{\sqrt{3}} \tag{4.40}$$

so the delta secondary winding must have $\sqrt{3}$ more turns than the star ones.

The phase shift between the voltages lead to the conducting scheme of the thyristor bridges represented on Fig. 4.4. On each 30° interval, one has two elementary sequences, a commutation sequence and a normal conducting sequence.
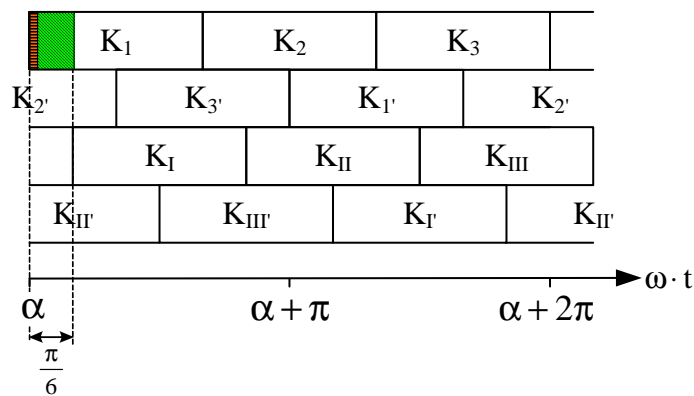
Fig. 4.4. Conduction scheme of the two rectifiers.

Figure 4.4. Diagramme de conduction des deux redresseurs.

- 132 -

As a result of the previous section, the study interval of this 12-pulse rectifier will be of 30° and will correspond for an ideal operating of the converter (instantaneous commutation and DC current equal to a constant I) where switches K_1, $K_{2'}$, K_{III} and $K_{II'}$ are on.

On the considered interval, which follows the turn-on of switch K_1, one has:

$$
\begin{aligned}
i_1^{sS} &= 0 & i_{L1}^{sD} &= I \\
i_2^{sS} &= -I & i_{L2}^{sD} &= -I \\
i_3^{sS} &= I & i_{L3}^{sD} &= 0
\end{aligned}
\tag{4.41}
$$

The columns of the transformer are carrying currents, the sum of which being equal to zero, so:

$$
n_p \cdot I^P = n_{sS} \cdot I^{sS} + n_{sD} \cdot I^{sD}
\tag{4.42}
$$

where I^P, I^{sS} and I^{sD} represent the different currents on a column of the transformer.

Then:

$$
I^P = \frac{n_{sS}}{n_p} \cdot I^{sS} + \frac{n_{sD}}{n_p} \cdot I^{sD}
\tag{4.43}
$$

If k is the transformation ratio between the primary winding and the secondary star winding, this leads to:

$$
I^P = k \cdot \left(I^{sS} + \sqrt{3} \cdot I^{sD} \right)
\tag{4.44}
$$

This relationship is also verified with complex variables. One has on interval $\left[0, \dfrac{\pi}{6} \right]$ following the switch on of K_1:

$$
\begin{aligned}
\overline{i^{sS}} &= \frac{I}{\sqrt{3}} \cdot \left(-a + a^2 \right) = -j \cdot I \\
\overline{i_L^{sD}} &= \frac{I}{\sqrt{3}} \cdot (1 - a) = -a^2 \cdot \overline{i^{sS}} \\
\overline{i^{sD}} &= \frac{\overline{i_L^{sD}}}{1 - a^2} = -\frac{I}{\sqrt{3}} \cdot a = -\frac{a^2}{1 - a^2} \cdot \overline{i^{sS}} = \frac{1}{\sqrt{3}} \cdot e^{j\frac{\pi}{6}} \cdot \overline{i^{sS}}
\end{aligned}
\tag{4.45}
$$

so for the primary current:

$$
\begin{aligned}
\overline{i^P} &= k \cdot \frac{I}{\sqrt{3}} \cdot \left[-a + a^2 - \sqrt{3} \cdot a \right] = -k \cdot I \cdot (a + j) \\
&= k \cdot \left(1 + e^{j\frac{\pi}{6}} \right) \cdot \overline{i^{sS}} = k \cdot \sqrt{2 + \sqrt{3}} \cdot e^{j\frac{\pi}{12}} \cdot \overline{i^{sS}}
\end{aligned}
\tag{4.46}
$$

Then from the value of $\overline{i^{sS}}$ one obtains the values of the different other currents (Fig. 4.5).

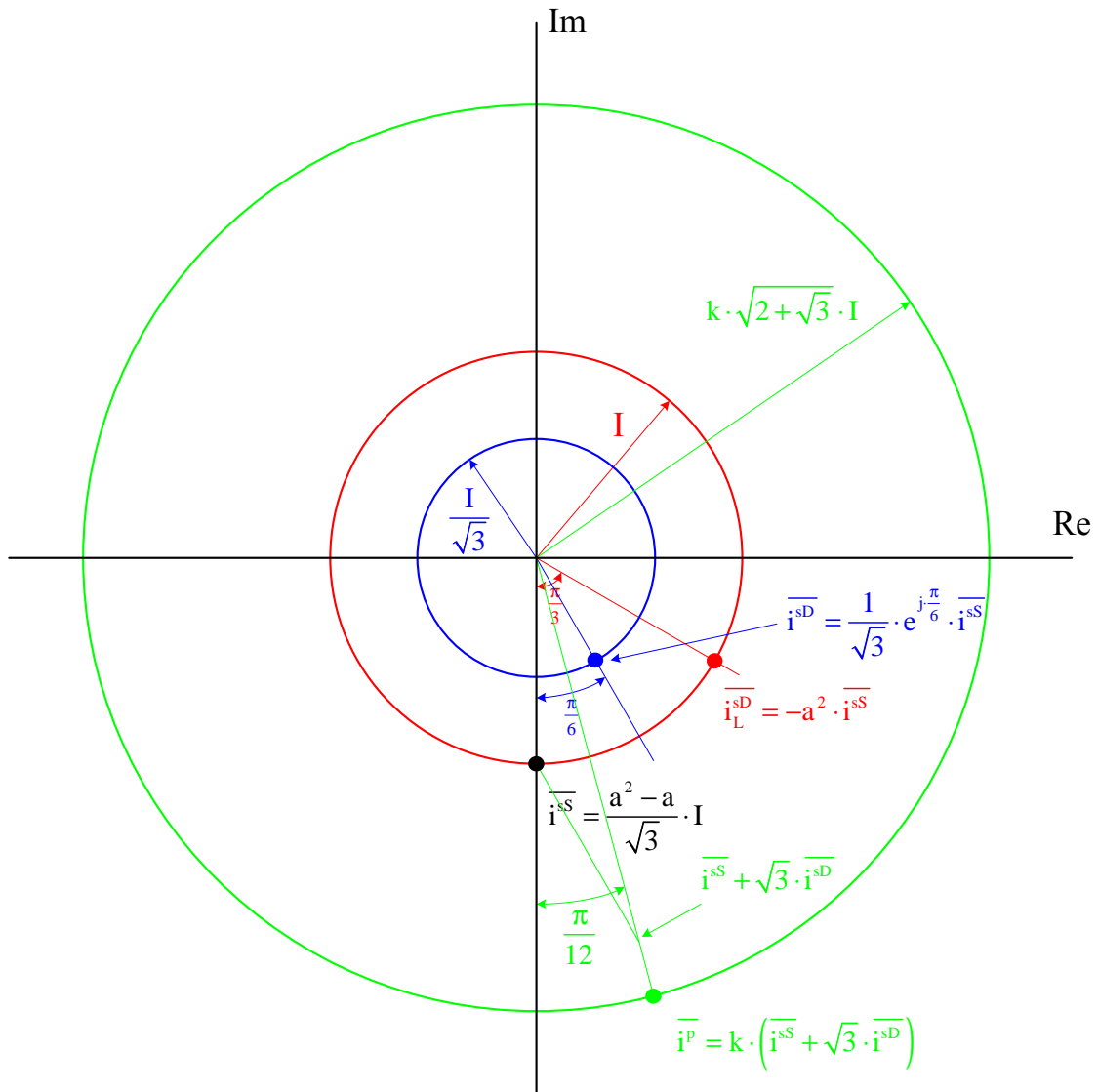Fig. 4.5. Complex currents on interval $\left[0, \dfrac{\pi}{6}\right]$.

Figure 4.5. Courants complexes sur l'intervalle $\left[0, \dfrac{\pi}{6}\right]$.

From the complex currents, one can obtain the three primary line currents:

$$i_1^p = \frac{2}{\sqrt{3}} \cdot \text{Re}\left(\overline{i^p}\right) = k \cdot I \cdot \frac{1}{\sqrt{3}}$$

$$i_2^p = \frac{2}{\sqrt{3}} \cdot \text{Re}\left(a^2 \cdot \overline{i^p}\right) = -k \cdot I \cdot \left(1 + \frac{2}{\sqrt{3}}\right) \tag{4.47}$$

$$i_2^p = \frac{2}{\sqrt{3}} \cdot \text{Re}\left(a \cdot \overline{i^p}\right) = k \cdot I \cdot \left(1 + \frac{1}{\sqrt{3}}\right)$$

One can consider that the study is finished. It is true on the primary as rotation of 30° will lead to the value of the primary current on the different operating interval. For the secondary converters, as they are 6-pulse converters, one needs to consider the next interval.

On $\left[\dfrac{\pi}{6}, \dfrac{\pi}{3}\right]$, one can use the same method than before and considering the different currents in the different secondary windings which appear on this interval, or calculate directly the primary current given in equation 4.46 with a rotation of $2.\pi/12$:

$$\overline{i^p} = -k \cdot I \cdot (a + j) \cdot e^{j\frac{\pi}{6}} = -k \cdot I \cdot \left(a - j \cdot a^2\right) \tag{4.48}$$

On the secondary side, as currents, in the delta connected rectifier, do not change, on this interval, $\overline{i_L^{sD}}$ and $\overline{i^{sD}}$ have the same values given in 4.45. Then $\overline{i^{sS}}$ is obtained from equation 4.44:

$$\overline{i^{sS}} = \frac{\overline{i^p}}{k} - \sqrt{3} \cdot \overline{i^{sD}} = -I \cdot \left(a - j \cdot a^2\right) + I \cdot a = I \cdot j \cdot a^2 \tag{4.49}$$

The different currents are represented on this interval on figure Fig. 4.6 and on a period on Fig. 4.7.

The three primary lines current are obtained as before:

$$i_1^p = \frac{2}{\sqrt{3}} \cdot \text{Re}\left(\overline{i^p}\right) = k \cdot I \cdot \left(2 + \sqrt{3}\right)$$

$$i_2^p = \frac{2}{\sqrt{3}} \cdot \text{Re}\left(a^2 \cdot \overline{i^p}\right) = -k \cdot I \cdot \left(1 + \sqrt{3}\right) \tag{4.50}$$

$$i_3^p = \frac{2}{\sqrt{3}} \cdot \text{Re}\left(a \cdot \overline{i^p}\right) = -k \cdot I$$
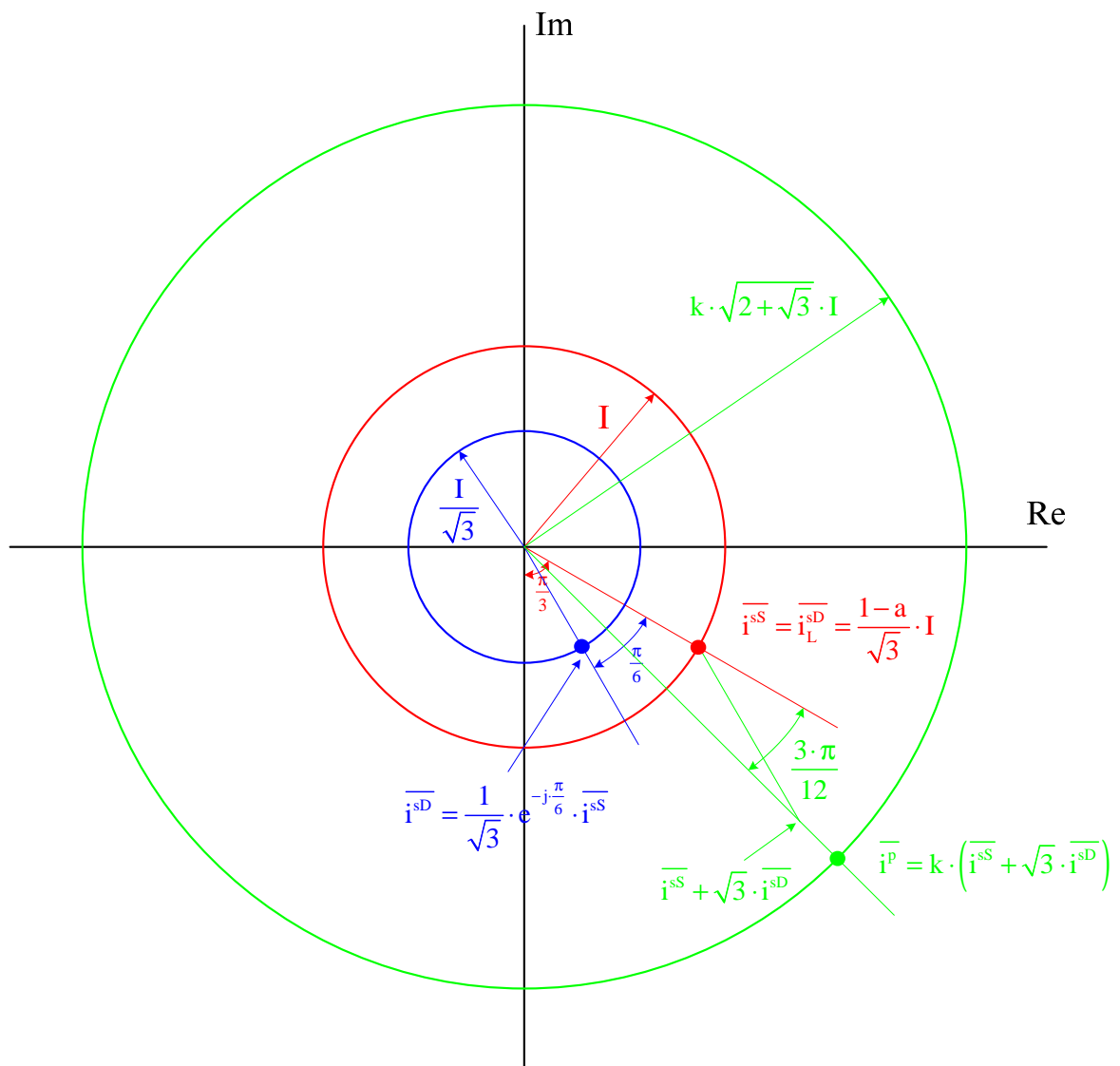
Fig. 4.6. Complex currents on interval $\left[\dfrac{\pi}{6}, \dfrac{\pi}{3} \right]$.

Figure 4.6. Courants complexes sur l'intervalle $\left[\dfrac{\pi}{6}, \dfrac{\pi}{3} \right]$.
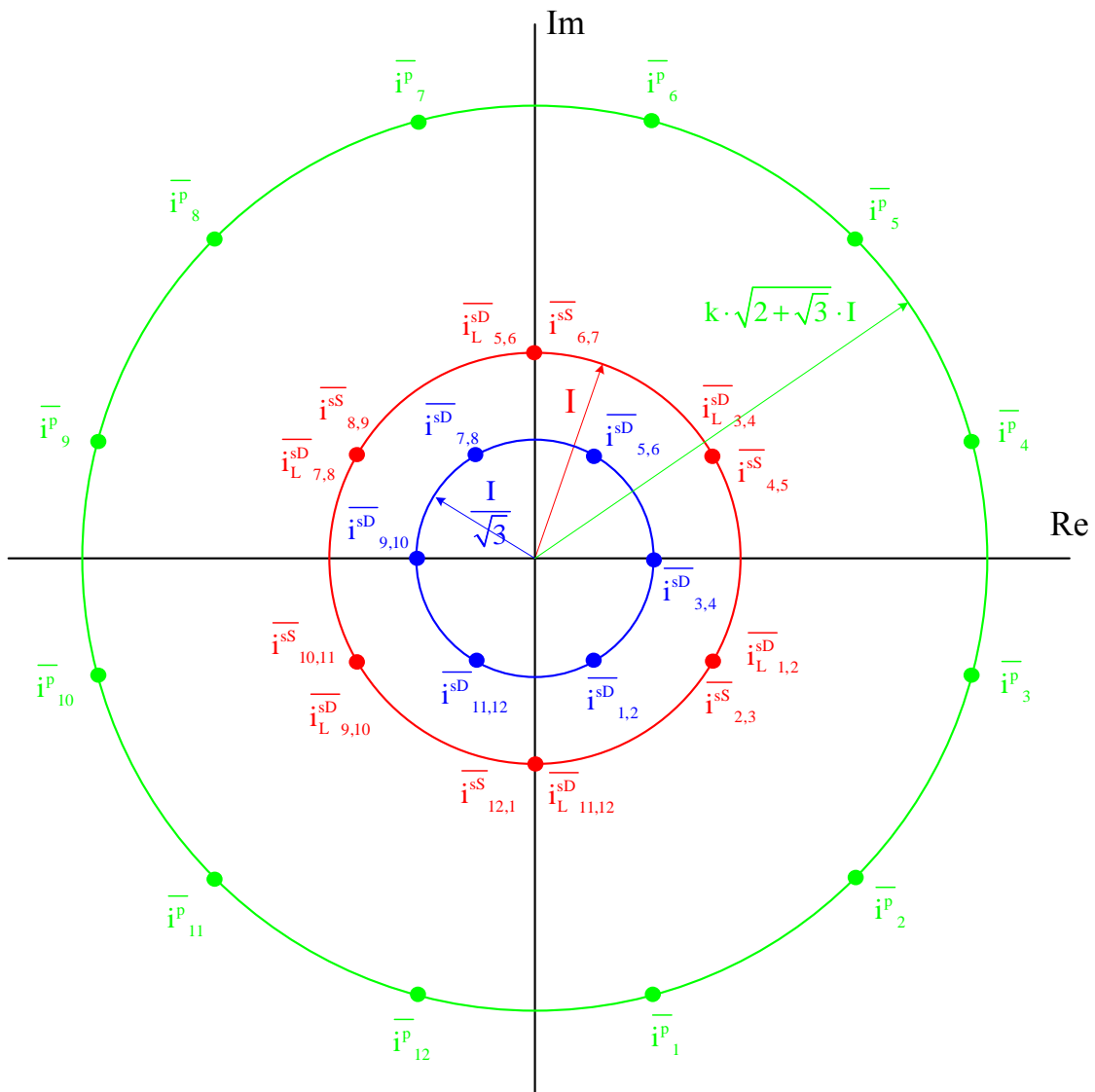
Fig. 4.7. Complex currents on a period.

Figure 4.7. Courants complexes sur une période.

The knowledge of the three real line currents on $1/6^{th}$ of the period gives the current on the whole period (Fig. 4.8) as in three phase system where there are not even harmonics [55]:

$$i_n^p\left(\omega \cdot t + \frac{\pi}{3}\right) = -i_{n+1}^p(\omega \cdot t) \tag{4.51}$$
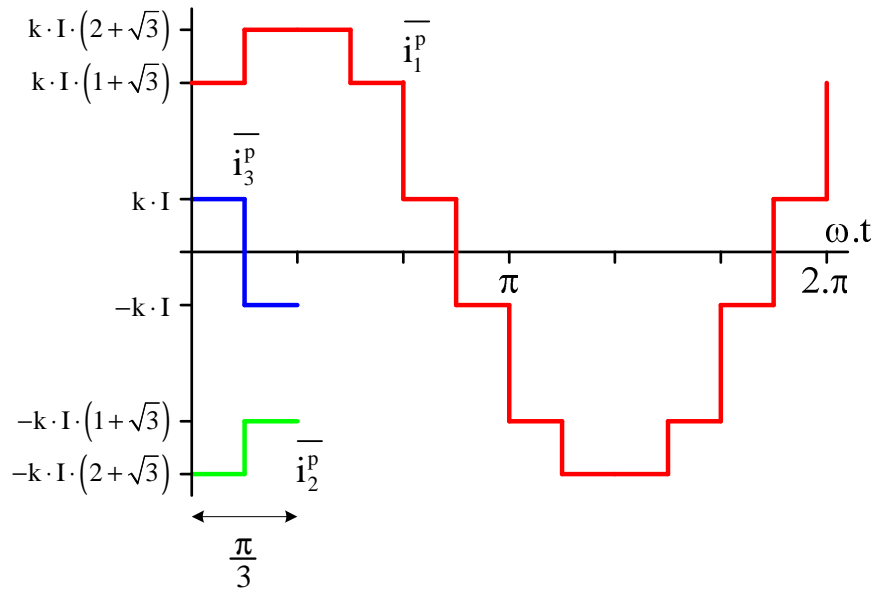
Fig. 4.8. Current wave form in phase 1 of the primary (origin in time correspond to the switch on of thyristor K_1).

Figure 4.8. Courant dans la phase 1 du primaire (l'origine du temps correspond à l'amorçage du thyristor K_1).

4.3.4. Exact modeling of the 12-pulse converter using Y/YΔ transformer

Since the AC source is not ideal, the transition of current during the commutation process does not occur instantly, but need a small certain period as shown in Fig. 4.9.

In the 30° study interval we will have two operating sequence corresponding to the commutation sequence between switches K_3 and K_1, where switches K_3, K_1, $K_{2'}$, K_{III} and $K_{II'}$ are on and a normal operating sequence where K_3 has been turn-off.
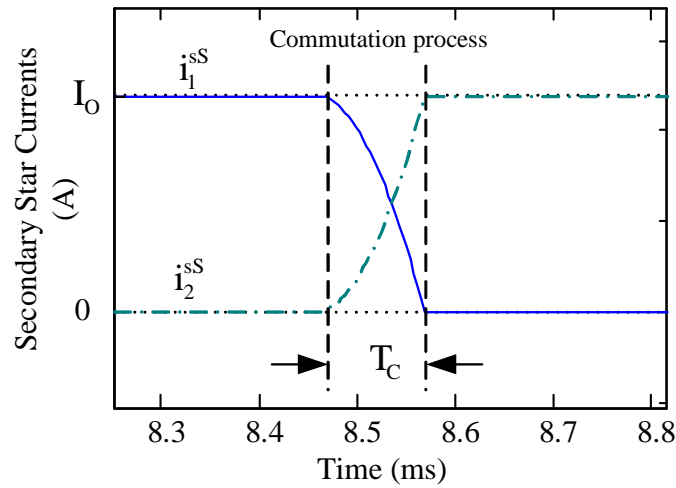
Fig. 4.9. Transition of thyristor currents during a commutation process.

Figure 4.9. Evolution du courant pendant la commutation.

4.3.4.1. State model

The general form of the state equations of linear system is:

$$\frac{d}{dt}X(t) = A \cdot X(t) + B \cdot U(t) \tag{4.52}$$

And the solution equation is under the form:

$$X(t) = e^{A(t-t_0)} \cdot X(t_0) + \int_{t_0}^{t} e^{A(t-\tau)} \cdot B \cdot U(\tau)d\tau \tag{4.53}$$

If the source vector $U(t)$ contains only constant or sinusoidal source, one can introduce the sources in the state vector to obtain the following reduced equation:

$$\frac{d}{dt}X(t) = A \cdot X(t) \tag{4.54}$$

The solution of the reduced form is simple as follow:

$$X(t) = e^{A(t-t_0)} \cdot X(t_0) \tag{4.55}$$

This simple analytical solution will be used to represent the operating of the 12-pulse converter on the two considered sequences.

4.3.4.2. Converter model during commutation

This model describes the operation of 12-pulse converter while the commutation process occurs. In this period, the current commutates from thyristors K_3 to K_1 and result in a connection between two terminals of the secondary delta winding, as shown in Fig. 4.10, thus:

$$v_1^{sD} = 0 \tag{4.56}$$

In complex form as:

$$K_1 \cdot \overline{V^{sD}} = 0 \tag{4.57}$$

where:

$$K_1 = \frac{1}{\sqrt{3}} \cdot \begin{bmatrix} 1 & 1 \end{bmatrix} \tag{4.58}$$

Substituting 4.57 in 4.29 leads to:

$$0 = -R_{sD} \cdot K_1 \cdot \overline{I^{sD}} - L_{sD} \cdot K_1 \cdot \frac{d}{dt}\overline{I^{sD}} + M_{psD} \cdot K_1 \cdot \frac{d}{dt}\overline{I^p} - M_{ss} \cdot K_1 \frac{d}{dt}\overline{I^{sS}} \tag{4.59}$$

As:

$$i_1^{sD} = K_1 \cdot \overline{I^{sD}} \tag{4.60}$$
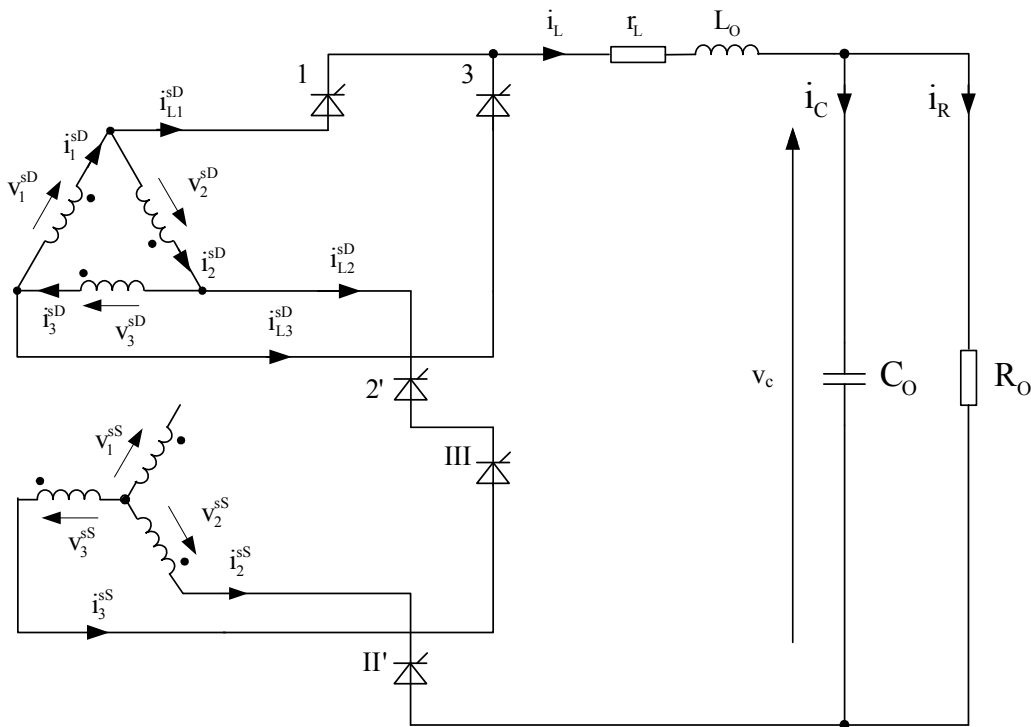
Fig. 4.10. Equivalent circuit on secondary side during commutation.

Figure 4.10. Schéma au secondaire lors de la commutation.

and as shown in Fig. 4.10, the 1st phase of the secondary star winding has no current, so that the term $K_1 \cdot \overline{I^{sS}}$ is null. Then equation 4.59 reduces to:

$$0 = -R_{sD} \cdot i_1^{sD} - L_{sD} \frac{d}{dt} i_1^{sD} + M_{psD} \cdot K_1 \cdot \frac{d}{dt} \overline{I^p} \tag{4.61}$$

Equation 4.61 becomes the first differential equation for forming the state equation model.

Now let consider the secondary delta line current shown in Fig. 4.10. All of current i_L flows through line 2 of the secondary delta winding. Hence:

$$i_{L2}^{sD} = -i_L \tag{4.62}$$

which can be expressed in complex form as:

$$\frac{1}{\sqrt{3}} \cdot \begin{bmatrix} a^2 & a \end{bmatrix} \cdot \begin{bmatrix} \overline{i_L^{sD}} \\ \overline{i_L^{sD}}^* \end{bmatrix} = -i_L \tag{4.63}$$

With the following relation of line and phase current in complex:

$$\overline{i_L^{sD}} = (1 - a^2) \cdot \overline{i^{sD}} \tag{4.64}$$

Equation 4.62 is in the form:

$$a^2 (1 - a^2) \overline{i^{sD}} + a (1 - a) \overline{i^{sD}}^* = -\sqrt{3} \cdot i_L \tag{4.65}$$

or:

$$\overline{i^{sD}} - \overline{i^{sD}}^* = -j \cdot i_L \tag{4.66}$$

With equation 4.60 and 4.66, it is possible to write $\overline{I^{sD}}$ as a function of i_1^{sD} and i_L :

$$\overline{I^{sD}} = \begin{bmatrix} \overline{i^{sD}} \\ \overline{i^{sD}}^* \end{bmatrix} = \begin{bmatrix} \dfrac{\sqrt{3}}{2} i_1^{sD} - j \cdot \dfrac{1}{2} i_L \\ \dfrac{\sqrt{3}}{2} i_1^{sD} + j \cdot \dfrac{1}{2} i_L \end{bmatrix} = \frac{1}{2} \cdot \begin{bmatrix} 3 \cdot K_1^T \cdot i_1^{sD} + K_2^T \cdot i_L \end{bmatrix} \tag{4.67}$$

where:

$$K_2 = \begin{bmatrix} -j & j \end{bmatrix} \tag{4.68}$$

With the same manner, let consider the current in the secondary star winding where currents exist only in phases 2 and 3. The complex secondary star current is:

$$\overline{i^{sS}} = \frac{1}{\sqrt{3}} \cdot \begin{bmatrix} 1 & a & a^2 \end{bmatrix} \cdot \begin{bmatrix} 0 \\ -i_L \\ i_L \end{bmatrix} = -j \cdot i_L \qquad (4.69)$$

Then:

$$\overline{I^{sS}} = \begin{bmatrix} -j \\ j \end{bmatrix} \cdot i_L = K_2^{\ T} \cdot i_L \qquad (4.70)$$

With the expressions of $\overline{I^{sD}}$ and $\overline{I^{sS}}$ in equations 4.67 and 4.70, equation 4.28 becomes:

$$\overline{V^P} = R^P \cdot \overline{I^P} + L^P \frac{d}{dt} \overline{I^P} - \frac{3}{2} M_{psD} \cdot K_1^{\ T} \frac{d}{dt} i_1^{sD} - \left(\frac{1}{2} M_{psD} + M_{psS} \right) \cdot K_2^{\ T} \frac{d}{dt} i_L \qquad (4.71)$$

This equation is the second differential equation of the state equation model where:

$$v_n^P = V_{rms} \sqrt{2} \sin \left(\omega t - (n-1) \frac{2\pi}{3} \right) \qquad (4.72)$$

and:

$$\overline{V^P} = K_S \begin{bmatrix} v_1^P \\ v_2^P \\ v_3^P \end{bmatrix} = \begin{bmatrix} -j \cdot V_{rms} \sqrt{\dfrac{3}{2}} \cdot e^{j \cdot \omega \cdot t} \\ j \cdot V_{rms} \sqrt{\dfrac{3}{2}} \cdot e^{-j \cdot \omega \cdot t} \end{bmatrix} \qquad (4.73)$$

This expression of the primary voltages means that the commutation sequence starts at time t = 0 if the firing angle is null.

The third differential equation comes from the voltage loop of the DC side as:

$$v_C + r \cdot i_L + L_O \frac{d}{dt} i_L + v_2^{sD} + \left(v_2^{sS} - v_3^{sS} \right) = 0 \qquad (4.74)$$

from:

$$v_2^{sD} = \frac{1}{\sqrt{3}} \cdot \begin{bmatrix} a^2 & a \end{bmatrix} \cdot \overline{V^{sD}} = K_3 \cdot \overline{V^{sD}} \qquad (4.75)$$

where:

$$K_3 = \frac{1}{\sqrt{3}} \cdot \begin{bmatrix} a^2 & a \end{bmatrix} \qquad (4.76)$$

and:

$$v_2^{sS} - v_3^{sS} = \frac{1}{\sqrt{3}} \cdot \left(\begin{bmatrix} a^2 & a \end{bmatrix} - \begin{bmatrix} a & a^2 \end{bmatrix} \right) \cdot \overline{V^{sS}} = K_2 \cdot \overline{V^{sS}} \qquad (4.77)$$

Substituting 4.75 and 4.77 in 4.74 to obtain:

$$v_C + r_L \cdot i_L + L_O \frac{d}{dt} i_L + K_3 \cdot \overline{V^{sD}} + K_2 \cdot \overline{V^{sS}} = 0 \qquad (4.78)$$

$K_3 \cdot \overline{V^{sD}}$ and $K_2 \cdot \overline{V^{sS}}$ can be expressed by their expressions in 4.29 and 4.30 with the use of currents given by 4.67 and 4.70:

$$K_3 \cdot \overline{V^{sD}} = \frac{1}{2} \cdot R_{sD} \cdot \left(i_1^{sD} + i_L \right) + \frac{1}{2} \cdot L_{sD} \cdot \frac{d}{dt} \left(i_1^{sD} + i_L \right) + M_{ss} \cdot \frac{d}{dt} i_L + M_{psD} \cdot K_3 \cdot \frac{d}{dt} \overline{I^p}$$

$$K_2 \cdot \overline{V^{sS}} = 2 \cdot R_{sS} \cdot i_L + 2 \cdot \left(L_{sS} + M_{sS} \right) \cdot \frac{d}{dt} i_L + M_{psS} \cdot K_2 \cdot \frac{d}{dt} \overline{I^p} \qquad (4.79)$$

This gives the third differential equation as:

$$\frac{1}{2} R_{sD} \cdot i_1^{sD} + \frac{1}{2} L_{sD} \frac{d}{dt} i_1^{sD} + \left(r_L + \frac{1}{2} R_{sD} + 2 \cdot R_{sS} \right) \cdot i_L + v_C$$

$$+ \left(L_O + \frac{1}{2} L_{sD} + 2 \cdot L_{sS} + 3 \cdot M_{ss} \right) \frac{d}{dt} i_L + \left(M_{psD} K_3 + M_{psS} \cdot K_2 \right) \frac{d}{dt} \overline{I^p} = 0 \qquad (4.80)$$

The last differential equation is simply the equation that describes the output currents:

$$i_L - \frac{v_C}{R_O} - C_O \cdot \frac{d}{dt} v_C = 0 \qquad (4.81)$$

Equations 4.61, 4.71, 4.80 and 4.81 can be written in the form:

$$a_1' \cdot x_1 + b_1' \frac{d}{dt} x_1 = d_1 \cdot \begin{bmatrix} e^{j \cdot \omega \cdot t} \\ e^{-j \cdot \omega \cdot t} \end{bmatrix} \qquad (4.82)$$

where:

$$x_1 = \begin{bmatrix} i_1^{sD} \\ \overline{I^p} \\ i_L \\ v_C \end{bmatrix} \qquad (4.83)$$

$$a_1' = \begin{bmatrix} -R_{sD} & [0 \quad 0] & 0 & 0 \\ \begin{bmatrix} 0 \\ 0 \end{bmatrix} & R^p & \begin{bmatrix} 0 \\ 0 \end{bmatrix} & \begin{bmatrix} 0 \\ 0 \end{bmatrix} \\ \frac{1}{2} R_{sD} & [0 \quad 0] & \left(r_L + \frac{1}{2} R_{sD} + 2 \cdot R_{sS} \right) & 1 \\ 0 & [0 \quad 0] & 1 & -\frac{1}{R_O} \end{bmatrix} \qquad (4.84)$$

$$b_1' = \begin{bmatrix} -L_{sD} & M_{psD} \cdot K_1 & 0 & 0 \\ -\dfrac{3}{2} \cdot M_{psD} \cdot K_1^{\ T} & L^P & -\left(\dfrac{1}{2} \cdot M_{psD} + M_{psS}\right) \cdot K_2^{\ T} & \begin{bmatrix} 0 \\ 0 \end{bmatrix} \\ \dfrac{1}{2} \cdot L_{sD} & M_{psD} \cdot K_3 + M_{psS} \cdot K_2 & L_O + \dfrac{1}{2} \cdot L_{sD} + 2 \cdot L_{sS} + 3 \cdot M_{ss} & 0 \\ 0 & [0 \quad 0] & 0 & -C_O \end{bmatrix} \quad (4.85)$$

$$d_1 = \begin{bmatrix} 0 & 0 \\ -j \cdot V_{rms}\sqrt{\dfrac{3}{2}} & 0 \\ 0 & j \cdot V_{rms}\sqrt{\dfrac{3}{2}} \\ 0 & 0 \\ 0 & 0 \end{bmatrix} \quad (4.86)$$

Equation 4.80 can be modified into the general form of state equation as:

$$\frac{d}{dt} x_1 = a_1 \cdot x_1 + b_1 \cdot \begin{bmatrix} e^{j \cdot \omega \cdot t} \\ e^{-j \cdot \omega \cdot t} \end{bmatrix} \quad (4.87)$$

where:

$$a_1 = -\left(b_1'\right)^{-1} \cdot a_1' \quad (4.88)$$

and:

$$b_1 = \left(b_1'\right)^{-1} \cdot d_1 \quad (4.89)$$

Finally, one obtains:

$$\frac{d}{dt} X_1 = A_1 \cdot X_1 \quad (4.90)$$

where:
$$X_1 = \begin{bmatrix} i_1^{sD} \\ \overline{I^P} \\ i_L \\ v_C \\ e^{j \cdot \omega \cdot t} \\ e^{-j \cdot \omega \cdot t} \end{bmatrix} \quad (4.91)$$

where:
$$A_1 = \begin{bmatrix} a_1 & b_1 \\ \hline [0]_{2x5} & \begin{matrix} j \cdot \omega & 0 \\ 0 & -j \cdot \omega \end{matrix} \end{bmatrix} \quad (4.92)$$

The purpose of this manipulation is to archive the simple analytical solutions form as:

$$X_1(t) = e^{A_1 \cdot (t - t_0)} \cdot X_1(t_0)$$ (4.93)

where t_0 is the time when switch K_1 starts to conduct.

4.3.4.3. Converter model during normal operation

This model expresses the operation of the 12-pulse converter after commutation finished. After thyristor K_3 turn-off, the converter returns to the normal operation and all current i_L flows through thyristor K_1. As a result, i_1^{sD} is not any more a state variable and they are only 3 differential equations to describe behaviors of variables $\overline{I^p}$, i_L and v_C. The schematic diagram for this operation is shown in Fig. 4.11.
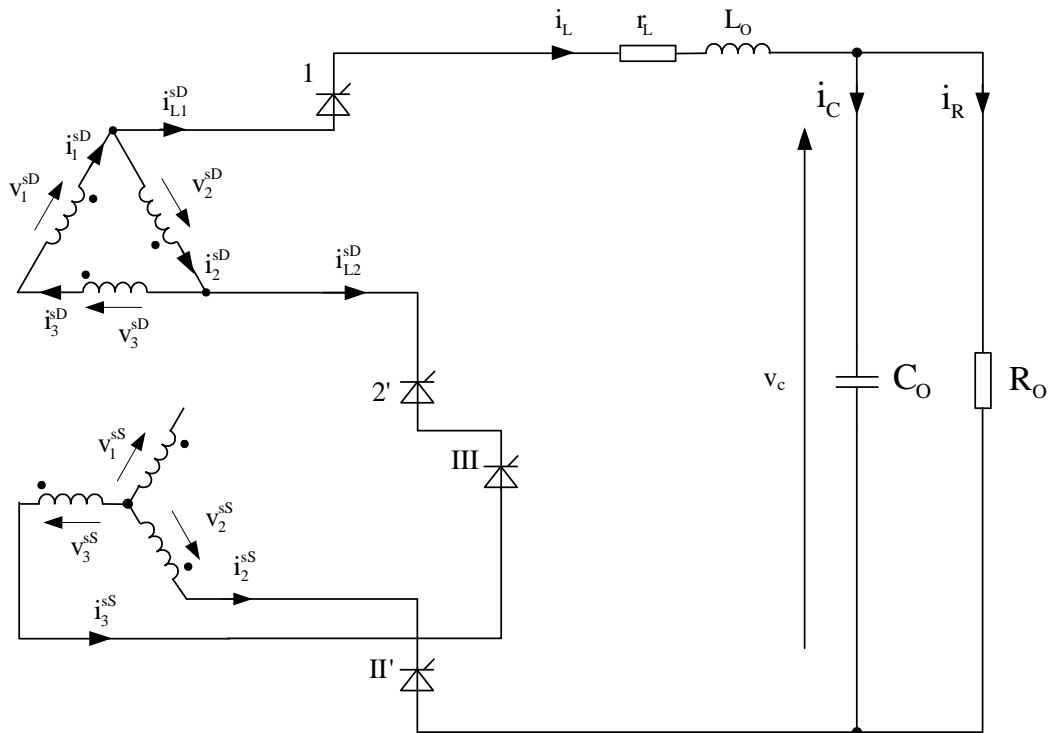

Fig. 4.11. Equivalent schematic on secondary side during normal operation.

Figure 4.11. Schéma au secondaire en dehors des commutations.

From figure 4.11, current i_L flows through line 1 and 2 of secondary delta winding, so that:

$$\overline{i_L^{sD}} = \frac{1}{\sqrt{3}}(1-a) \cdot i_L$$ (4.94)

From the relation of line and phase current, this equation becomes:

$$\overline{i^{sD}} = \frac{1}{\left(1-a^2\right)} \cdot \overline{i_L^{sD}} = \frac{1}{\sqrt{3}} \cdot \frac{\left(1-a\right)}{\left(1-a^2\right)} \cdot i_L = -\frac{1}{\sqrt{3}} \cdot a \cdot i_L \tag{4.95}$$

so:

$$\overline{I^{sD}} = -\frac{1}{\sqrt{3}} \cdot \begin{bmatrix} a \\ a^2 \end{bmatrix} \cdot i_L = -K_4{}^T \cdot i_L \tag{4.96}$$

where:

$$K_4 = \frac{1}{\sqrt{3}} \cdot \begin{bmatrix} a & a^2 \end{bmatrix} \tag{4.97}$$

With equations 4.69 and 4.94, equation 4.28 becomes:

$$\overline{V^p} = R^p \cdot \overline{I^p} + L^p \cdot \frac{d}{dt}\overline{I^p} + \left(M_{psD} \cdot K_4{}^T - M_{psS} \cdot K_2{}^T\right) \cdot \frac{d}{dt} i_L \tag{4.98}$$

Equation 4.78 which links the voltage across the capacitor with the secondary voltages is unchanged and still contains terms $K_3 \cdot \overline{V^{sD}}$ and $K_2 \cdot \overline{V^{sS}}$. These terms can be expressed by their expressions in 4.29 and 4.30 with the use of currents given by 4.70 and 4.96:

$$
\begin{aligned}
K_3 \cdot \overline{V^{sD}} &= \frac{2}{3} \cdot R_{sD} \cdot i_L + \left(\frac{2}{3} \cdot L_{sD} + M_{ss}\right) \cdot \frac{d}{dt} i_L + M_{psD} \cdot K_3 \cdot \frac{d}{dt}\overline{I^p} \\
K_2 \cdot \overline{V^{sS}} &= 2 \cdot R_{sS} \cdot i_L + \left(2 \cdot L_{sS} + M_{ss}\right) \cdot \frac{d}{dt} i_L + M_{psS} \cdot K_2 \cdot \frac{d}{dt}\overline{I^p}
\end{aligned}
\tag{4.99}
$$

and so:

$$
\left(r_L + \frac{2}{3} R_{sD} + 2 \cdot R_{sS}\right) i_L + v_C + \left(M_{psS} \cdot K_2 + M_{psD} \cdot K_3\right) \frac{d}{dt}\overline{I^p} \\
+ \left(L_O + \frac{2}{3} L_{sD} + 2 \cdot L_{sS} + 2 \cdot M_{ss}\right) \frac{d}{dt} i_L = 0
\tag{4.100}
$$

Equations 4.81, 4.98 and 4.100 can be written under the following form:

$$a_2' \cdot x_2 + b_2' \cdot \frac{d}{dt} x_2 = d_2 \cdot \begin{bmatrix} e^{j \cdot \omega \cdot t} \\ e^{-j \cdot \omega \cdot t} \end{bmatrix} \tag{4.101}$$

where:

$$x_2 = \begin{bmatrix} \overline{I_p} \\ i_L \\ v_C \end{bmatrix} \tag{4.102}$$

$$a_2' = \begin{bmatrix} R^p & \begin{bmatrix} 0 \\ 0 \end{bmatrix} & \begin{bmatrix} 0 \\ 0 \end{bmatrix} \\ \begin{bmatrix} 0 & 0 \end{bmatrix} & r_L + \dfrac{2}{3}R_{sD} + 2 \cdot R_{sS} & 1 \\ \begin{bmatrix} 0 & 0 \end{bmatrix} & 1 & -\dfrac{1}{R_O} \end{bmatrix} \tag{4.103}$$

$$b_2' = \begin{bmatrix} L^p & M^{psD} \cdot K_4{}^T - M^{psS} \cdot K_2{}^T & \begin{bmatrix} 0 \\ 0 \end{bmatrix} \\ M^{psS} \cdot K_2 + M^{psD} \cdot K_3 & L_O + \dfrac{2}{3}L_{sD} + 2 \cdot L_{sS} + 2 \cdot M_{ss} & 0 \\ \begin{bmatrix} 0 & 0 \end{bmatrix} & 0 & -C_O \end{bmatrix} \tag{4.104}$$

$$d_2 = \begin{bmatrix} -j \cdot V_{rms}\sqrt{\dfrac{3}{2}} & 0 \\ 0 & j \cdot V_{rms}\sqrt{\dfrac{3}{2}} \\ 0 & 0 \\ 0 & 0 \end{bmatrix} \tag{4.105}$$

Equation 4.101 can be written as:

$$\frac{d}{dt}x_2 = a_2 \cdot x_2 + b_2 \cdot \begin{bmatrix} e^{j \cdot \omega \cdot t} \\ e^{-j \cdot \omega \cdot t} \end{bmatrix} \tag{4.106}$$

where:

$$a_2 = -\left(b_2'\right)^{-1} \cdot a_2' \tag{4.107}$$

and:

$$b_2 = \left(b_2'\right)^{-1} \cdot d_2 \tag{4.108}$$

The reduced form of the equation 4.106 is:

$$\frac{d}{dt}X_2 = A_2 X_2 \tag{4.109}$$

where:

$$X_2 = \begin{bmatrix} \overline{I^p} \\ i_L \\ v_C \\ e^{j \cdot \omega \cdot t} \\ e^{-j \cdot \omega \cdot t} \end{bmatrix} \tag{4.110}$$

and:

$$A_2 = \begin{bmatrix} a_2 & \vdots & b_2 \\ \hline [0]_{2x4} & \vdots & \begin{matrix} j \cdot \omega & 0 \\ 0 & -j \cdot \omega \end{matrix} \end{bmatrix} \tag{4.111}$$

An analytical solution for this model is:

$$X_2(t) = e^{A_2 \cdot (t-t_1)} X_2(t_1) \tag{4.112}$$

Where t_1 is the time when thyristor K_3 completely turn-off. The initial vector $X_2(t_1)$ can be obtained from the final state vector of the previous sequence where element i_1^{sD} has been suppressed:

$$X_2(t_1) = N_1 \cdot X_1(t_1) = N_1 \cdot e^{A(t_1-t_0)} X_1(t_0) \tag{4.113}$$

where:

$$N_1 = \begin{bmatrix} 0 & 1 & 0 & 0 & 0 & 0 & 0 \\ 0 & 0 & 1 & 0 & 0 & 0 & 0 \\ 0 & 0 & 0 & 1 & 0 & 0 & 0 \\ 0 & 0 & 0 & 0 & 1 & 0 & 0 \\ 0 & 0 & 0 & 0 & 0 & 1 & 0 \\ 0 & 0 & 0 & 0 & 0 & 0 & 1 \end{bmatrix} \tag{4.114}$$

4.3.5. Determination of unknown quantities

Equations 4.93 and 4.112 are the time solution of the state model for each operating sequence. However, the initial state vector of the steady state operation is required for evaluating the steady state operation. The initial state vector consists of four unknown quantities: $\overline{i^p}$, $\overline{i^p}^*$, i_L and v_C. Another unknown quantity is T_c, the duration of the commutation sequence. These five terms can be found numerically using the Newton-Raphson method [57].

The Newton-Raphson method is a technique for finding the roots of a multivariable functions. To understand its principle, let consider the Taylor series:

$$F(x + \Delta x) = F(x) + J \cdot \Delta x + O(\Delta x) \quad (4.115)$$

where F is a vector of functions defined as:

$$F = \begin{bmatrix} f_1(x_1 \ldots x_n) \\ f_2(x_1 \ldots x_n) \\ \vdots \end{bmatrix} \quad (4.116)$$

and J is the Jacobian matrix defined as:

$$J = \begin{bmatrix} J_{1,1} & J_{1,2} & \ldots & J_{1,n} \\ J_{2,1} & J_{2,2} & \ldots & J_{2,n} \\ \vdots & \vdots & \ddots & \vdots \\ J_{n,1} & J_{n,2} & \ldots & J_{n,n} \end{bmatrix} \quad (4.117)$$

where:

$$J_{i,j} = \frac{\partial f_i}{\partial x_j} \quad (4.118)$$

and term $O(\Delta x^k)$ is the sum of higher order differential part.

If one neglects the higher order term and solves for $F(x + \Delta x) = 0$, one can find Δx which lead $F(x + \Delta x)$ to zero, i.e. the root of the function. Since the term $O(\Delta x)$ was neglected, the term $(x + \Delta x)$ may have a truncated error. Then the iterate calculation is used to reduce the error and drive the vector x approaching the root of the function as follow:

$$x^{k+1} = x^k + \Delta x^k \quad (4.119)$$

where:

$$\Delta x^k = -J^{-1} \cdot F(x^k) \quad (4.120)$$

Since the Newton-Raphson method is the procedure for finding the root of the function F(x), one need to form n functions which result in zero when the steady state values of the circuit are applied to the functions.

As vector $\overline{i^p}$ is an AC variable in a 12-pulse converter, the final value of this vector is obtained, from the initial one, by a rotation of $\dfrac{\pi}{6}$:

$$f_1 = \overline{i^p}(t_0) \cdot e^{j\frac{\pi}{6}} - G_1 \cdot e^{A_2 \left(\frac{1}{12 \cdot f} - T_C\right)} \cdot N_1 \cdot e^{A_1 \cdot T_C} \cdot X_1(t_0) \tag{4.121}$$

and for its conjugate:

$$f_2 = \overline{i^p}(t_0)^* \cdot e^{-j\frac{\pi}{6}} - G_2 \cdot e^{A_2 \left(\frac{1}{12 \cdot f} - T_C\right)} \cdot N_1 \cdot e^{A_1 \cdot T_C} \cdot X_1(t_0) \tag{4.122}$$

where:

$$\begin{aligned} G_1 &= \begin{bmatrix} 1 & 0 & 0 & 0 & 0 & 0 \end{bmatrix} \\ G_2 &= \begin{bmatrix} 0 & 1 & 0 & 0 & 0 & 0 \end{bmatrix} \end{aligned} \tag{4.123}$$

As i_L and v_C are the variables on the DC side, their values at the beginning and the end of the study interval in steady state operation are the same. So that:

$$f_3 = i_L(t_0) - G_3 \cdot e^{A_2 \left(\frac{1}{12 \cdot f} - T_C\right)} \cdot N_1 \cdot e^{A_1 \cdot T_C} \cdot X_1(t_0) \tag{4.124}$$

and:

$$f_4 = v_C(t_0) - G_4 \cdot e^{A_2 \left(\frac{1}{12 \cdot f} - T_C\right)} \cdot N_1 \cdot e^{A_1 \cdot T_C} \cdot X_1(t_0) \tag{4.125}$$

where:

$$\begin{aligned} G_3 &= \begin{bmatrix} 0 & 0 & 1 & 0 & 0 & 0 \end{bmatrix} \\ G_4 &= \begin{bmatrix} 0 & 0 & 0 & 1 & 0 & 0 \end{bmatrix} \end{aligned} \tag{4.126}$$

The last function involves with the commutation duration T_C. The commutation process ends when the current i_{L1}^{sD} is equal to i_L. Relation 4.95 characterizes the end of the commutation process and gives the relationship between two state variables:

$$i_1^{sD} = \frac{2}{\sqrt{3}} \cdot \text{Re}\left(\overline{i^{sD}}\right) = \frac{2}{\sqrt{3}} \cdot \text{Re}\left(-\frac{1}{\sqrt{3}} \cdot a \cdot i_L\right) = \frac{1}{3} \cdot i_L \tag{4.127}$$

Then the last function is:

$$f_5 = M_1 e^{A_1 \cdot T_C} \cdot X_1(t_0) \tag{4.128}$$

where:

$$M_1 = \begin{bmatrix} 1 & 0 & 0 & -\dfrac{1}{3} & 0 & 0 & 0 \end{bmatrix} \tag{4.129}$$

With the five functions described above, the Newton-Raphson method can be used to determine all unknown quantities.

4.3.6. Simulation examples

Let consider two simulation examples for two different firing angles which are $\alpha = 0°$ and $\alpha = 40°$. The data of the converter are given in Annex 3 (Tables A3.1 and A3.2). Using the equations given in 4.93 and 4.112 and the Newton-Raphson method described in the previous section, one can find the steady state operation of the converter on the study interval.

Fig. 4.12, Fig. 4.13 and Fig. 4.14 depict the result for a firing angle of 0 degree and Fig. 4.15, Fig. 4.16 and Fig. 4.17 for a firing angle of 40 degree.

⊖— Primary current
△— Secondary delta current
∗— Secondary star current

Fig. 4.12. Trajectory of current in complex plane for the studied interval of $\pi/6$ at $\alpha = 0°$.

Figure 4.12. Trajectoire du courant dans le plan complexe sur l'intervalle d'étude de $\pi/6$ et $\alpha = 0°$.

Fig. 4.13. Primary voltage and current waveforms of the transformer ($\alpha = 0°$).

Figure 4.13. Tension et courant au primaire du transformateur ($\alpha = 0°$).

Fig. 4.14. Secondary delta and star currents on the secondary side of transformer ($\alpha = 0°$).

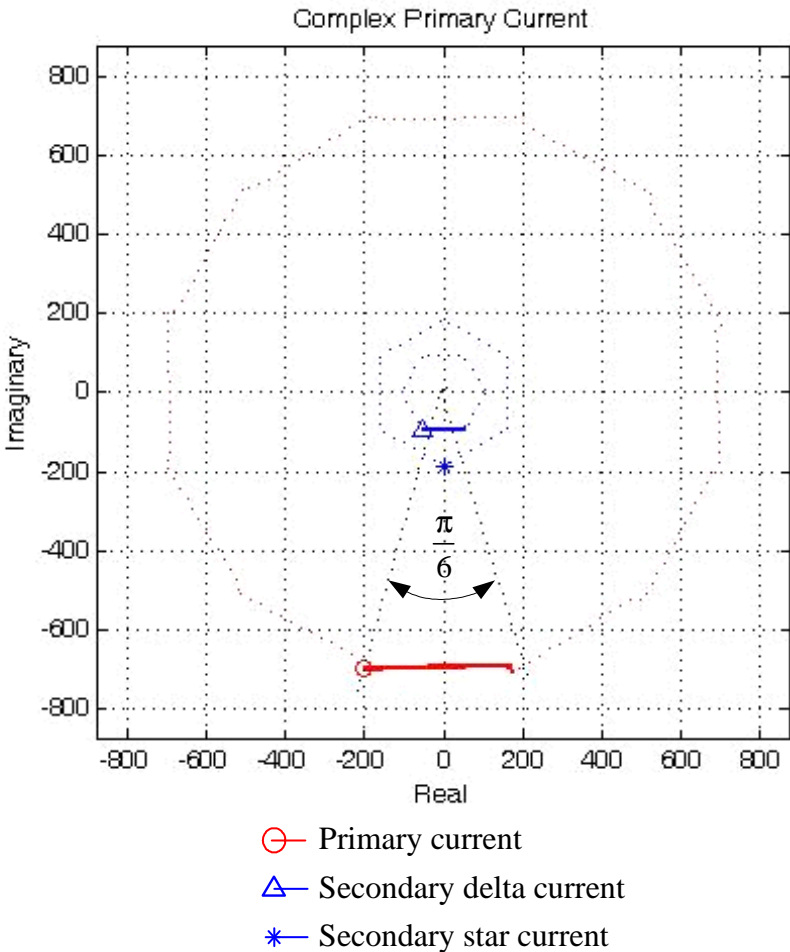Figure 4.14. Courants dans les enroulements secondaires du transformateur ($\alpha = 0°$).

Fig. 4.15. Trajectory of current in complex plane for the studied interval of $\pi/6$ at $\alpha = 40°$.

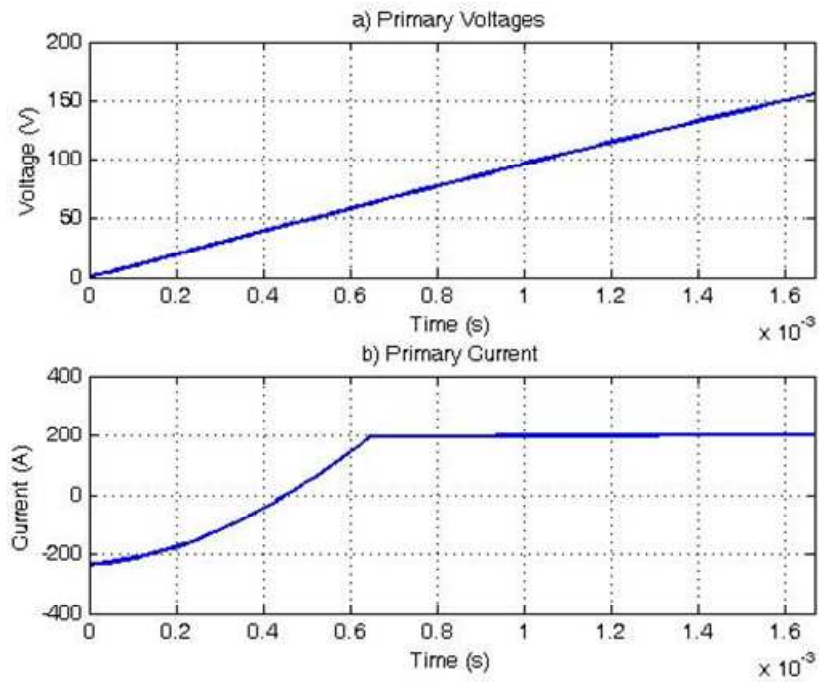Figure 4.15. Trajectoire du courant dans le plan complexe sur l'intervalle d'étude de $\pi/6$ et $\alpha = 40°$
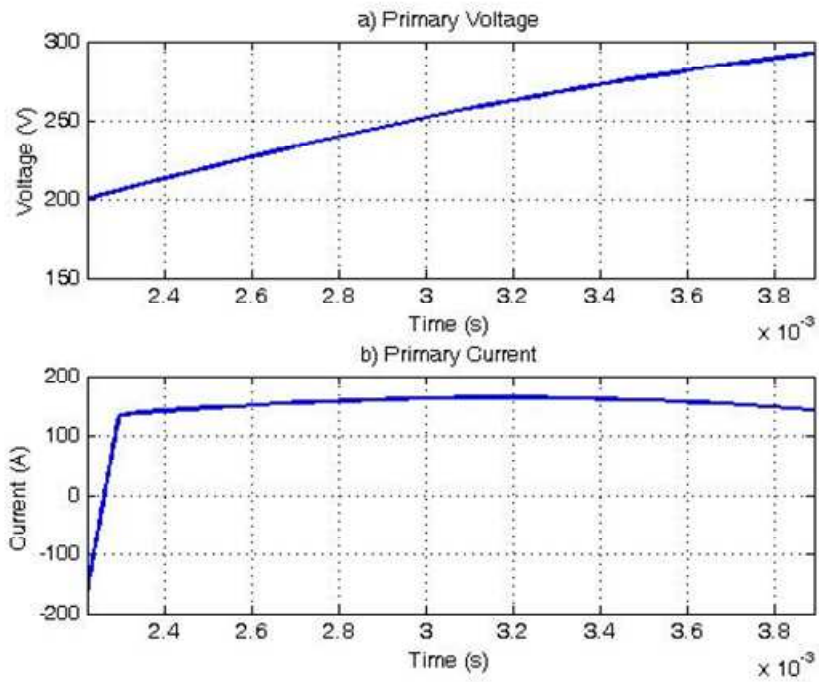
Fig. 4.16. Primary voltage and current waveforms of the transformer ($\alpha = 40°$).

Figure 4.16. Tension et courant au primaire du transformateur ($\alpha = 40°$).
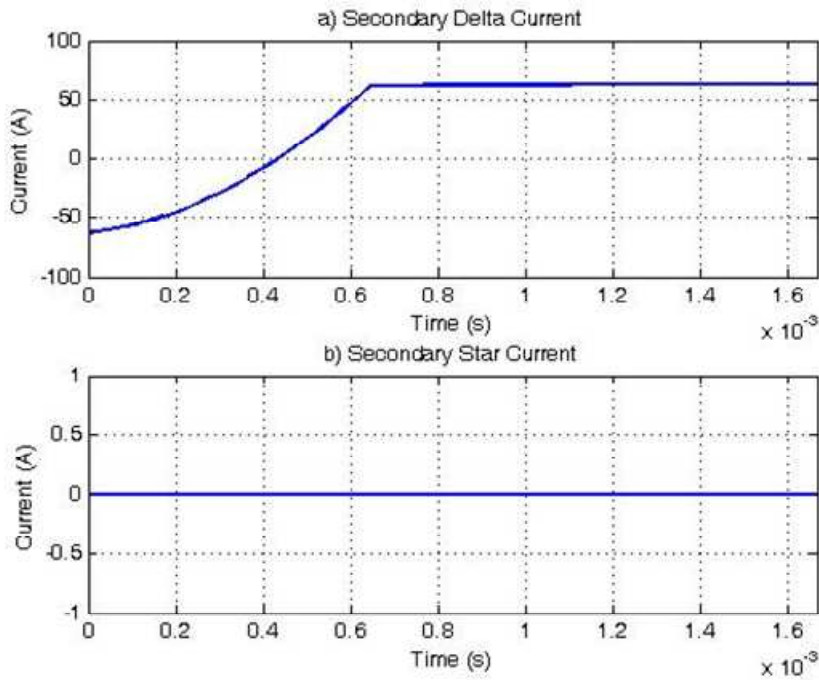

Fig. 4.17. Secondary delta and star currents on the secondary side of transformer ($\alpha = 40°$).

Figure 4.17. Courants dans les enroulements secondaires du transformateur ($\alpha = 40°$).

Then by a rotation process, one obtains the AC quantities on the whole period at the firing angle of 0 degree as shown in Fig. 4.18, Fig. 4.19 and Fig. 4.20.

Fig. 4.21, Fig. 4.22 and Fig. 4.23 show the AC quantities on the whole period at the firing angle of 40 degree.
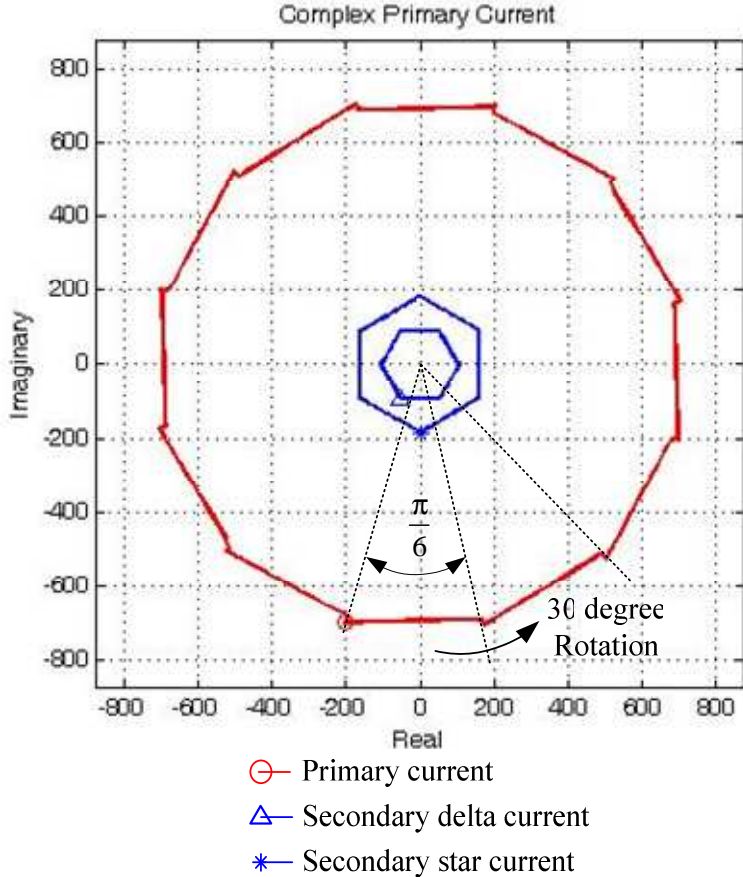
Fig. 4.18. Trajectory of current in complex plane for a period at $\alpha = 0°$.

Figure 4.18. Trajectoire du courant dans le plan complexe sur une période pour $\alpha = 0°$.
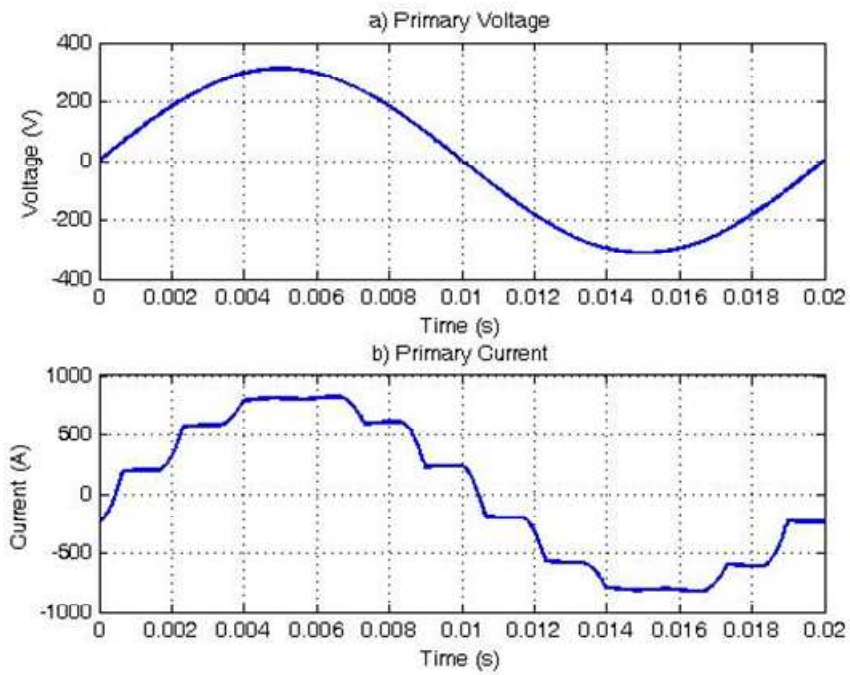
Fig. 4.19. Primary voltage and current waveforms of the transformer ($\alpha = 0°$).

Figure 4.19. Tension et courant au primaire du transformateur ($\alpha = 0°$).
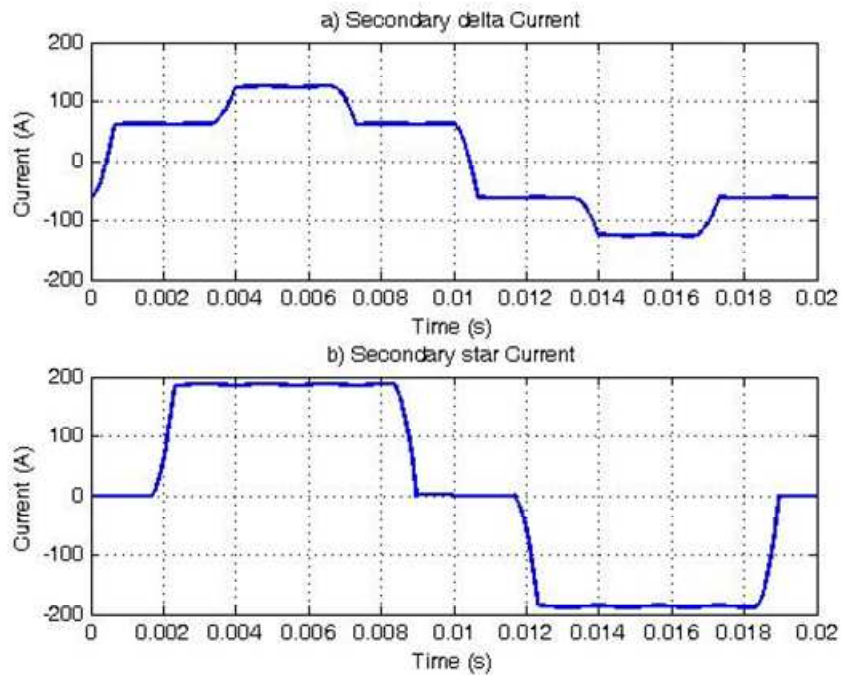
Fig. 4.20. Secondary delta and star currents on the secondary side of transformer ($\alpha = 0°$).

Figure 4.20. Courants dans les enroulements secondaires du transformateur ($\alpha = 0°$).
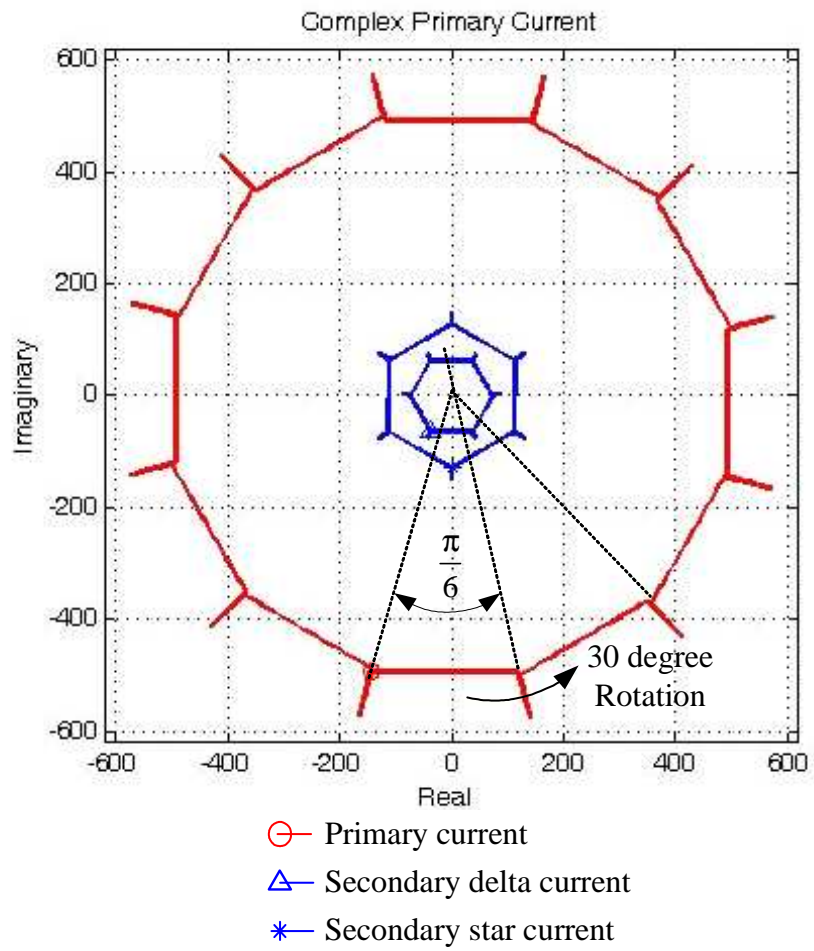
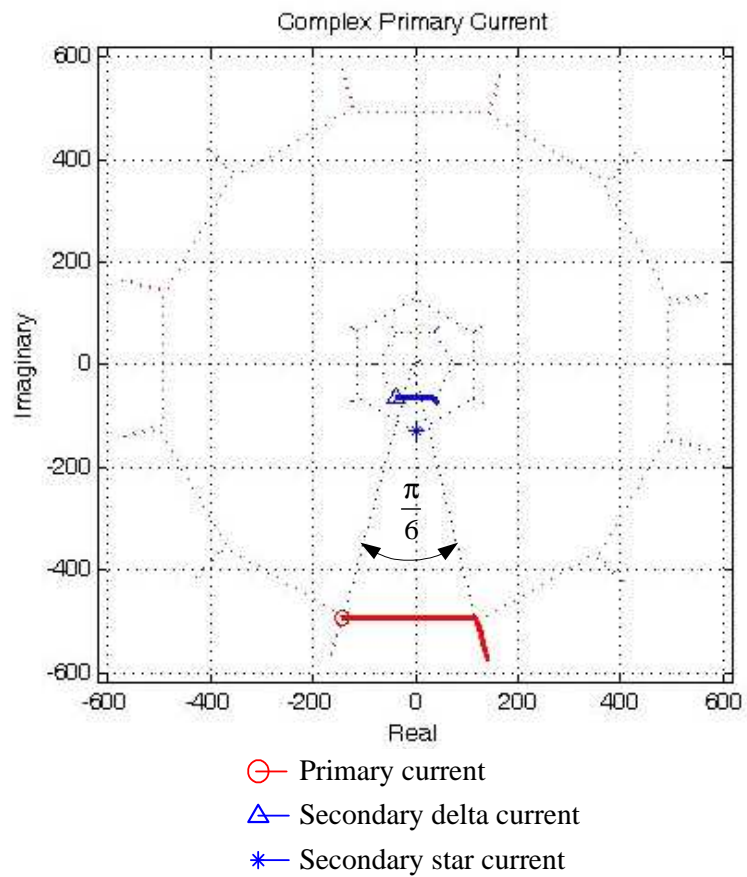Fig. 4.21. Trajectory of current in complex plane for a period at $\alpha = 40°$.

Figure 4.21. Trajectoire du courant dans le plan complexe pour $\alpha = 40°$.
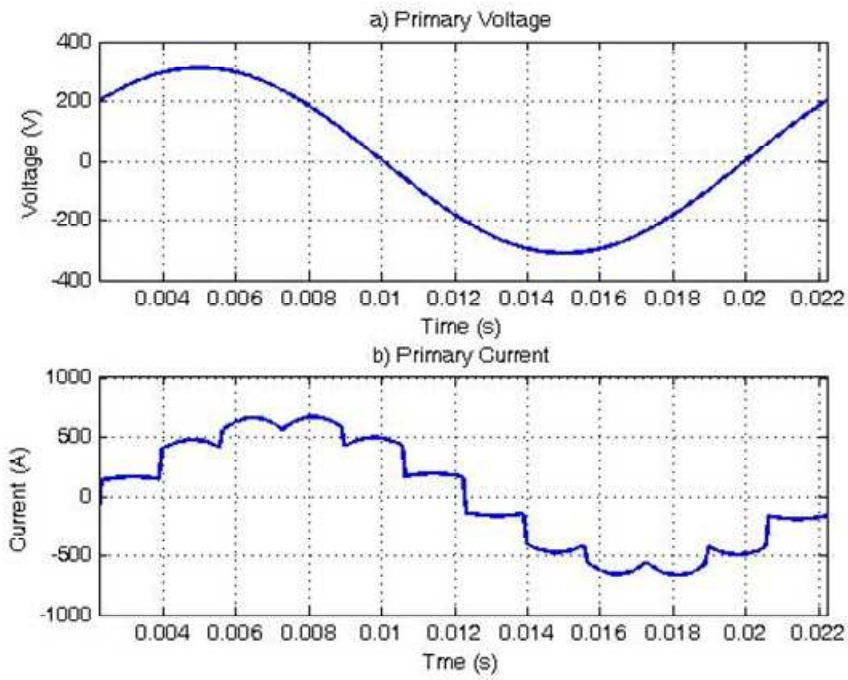
Fig. 4.22. Primary voltage and current waveforms of the transformer ($\alpha = 40°$).

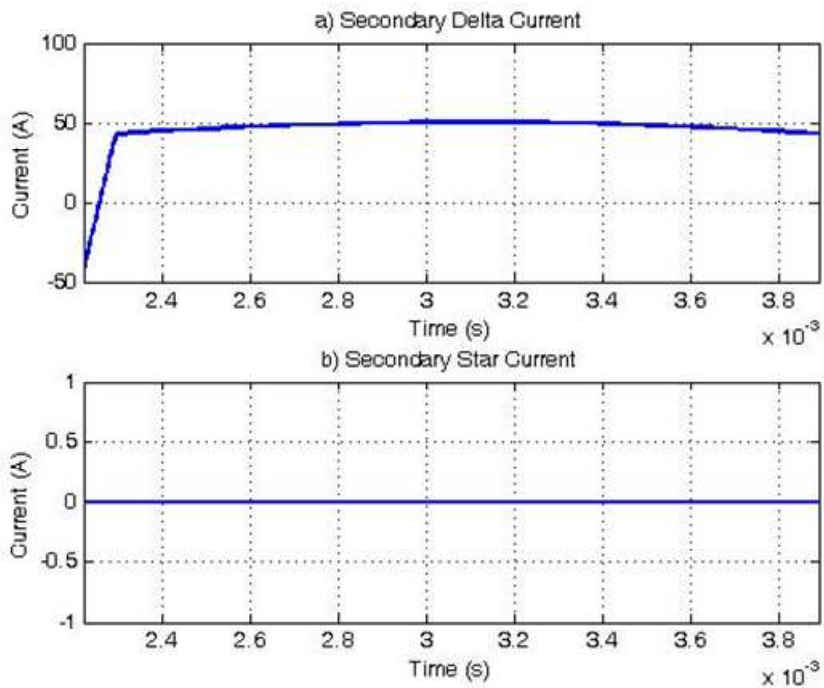Figure 4.22. Tension et courant au primaire du transformateur ($\alpha = 40°$).
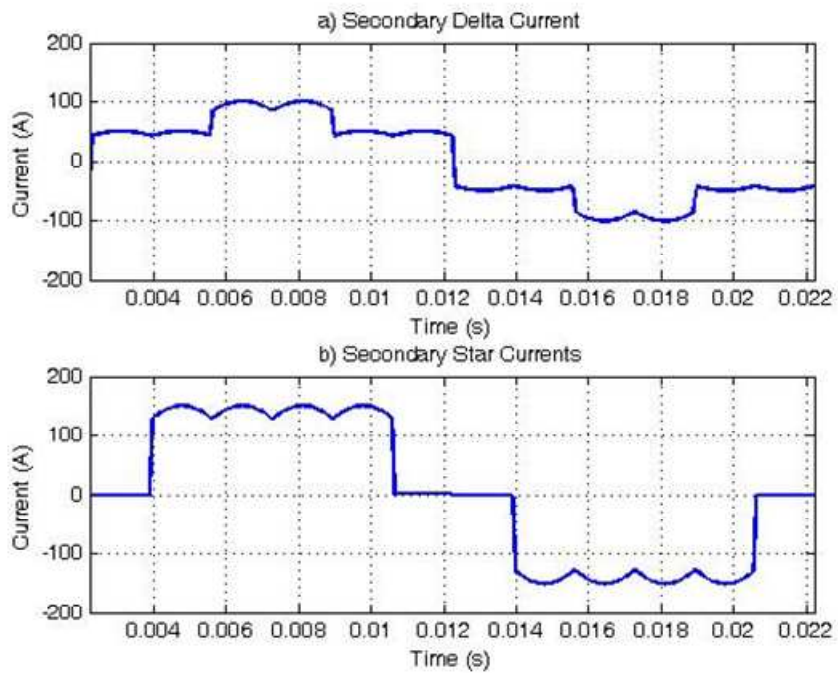
Fig. 4.23. Secondary delta and star currents on the secondary side of transformer ($\alpha = 40°$).

Figure 4.23. Courants dans les enroulements secondaires du transformateur ($\alpha = 40°$).

4.3.7. Analytical features of the developed model

4.3.7.1. DC side average values calculation

The models are developed in the form of equation 4.54 because it has the solution in simple exponential form. With this form of the solution, one can easily obtain the integration of the state variable:

$$\int_{t_1}^{t_2} X(t)dt = \int_{t_1}^{t_2} e^{A \cdot t}dt \cdot X(t_0) = \left(A^{-1} \cdot e^{A \cdot t} \Big|_{t_1}^{t_2} \right) \cdot X(t_0) \tag{4.130}$$

For example, the analytical solution for the average value of i_L is:

$$i_{L,avg} = \frac{1}{T'} \left(\begin{array}{c} \int_{t_0}^{t_c} \begin{bmatrix} 0 & G_3 \end{bmatrix} \cdot e^{A_1 \cdot t} \cdot X_1(t_0) \, dt \\ + \int_{t_c}^{T'} G_3 \cdot e^{A_2 \cdot (t-t_c)} \cdot X_2(t_0 + T_C) \end{array} \right) \tag{4.131}$$

where t_c is the time where ends the commutation process and: $T' = \dfrac{1}{12 \cdot f}$ \qquad (4.132)

So:
$$i_{L,avg} = \frac{1}{T'} \left(\begin{array}{c} \begin{bmatrix} 0 & G_3 \end{bmatrix} \cdot A_1^{-1} \left(e^{A_1 \cdot t_c} - I \right) \cdot X_1(t_0) \\ + G_3 \cdot A_2^{-1} \left(e^{A_2 \cdot T' - t_c} - I \right) \cdot X_2(t_0 + T_C) \end{array} \right) \tag{4.133}$$

In the same manner, the analytical solution for the average value of v_C is:

$$v_{C,avg} = \frac{1}{T'} \left(\begin{array}{c} \begin{bmatrix} 0 & G_4 \end{bmatrix} \cdot A_1^{-1} \left(e^{A_1 \cdot t_c} - I \right) \cdot X(t_0) \\ + G_4 \cdot A_2^{-1} \left(e^{A_2 \cdot T - t_c} - I \right) \cdot X_2(t_0 + T_C) \end{array} \right) \tag{4.134}$$

Applied equation 4.131 and 4.134 to the model described in 4.91, 4.92, 4.110 and 4.111 with the data for the converter given in Annex 3, the analytical average value of the DC side on the study interval of $\dfrac{\pi}{6}$ can be found. On Fig. 4.24 and 4.25 are the average value of current i_L and voltage v_C at 0 degree firing angle. Since the fundamental frequency of the DC side is 12 times greater than the AC side, the steady state period of the DC side is completed within the study interval $\pi/6$.

The result can be repeatedly appended together to form the operation along 2π which is the 1 cycle period of the AC side, as shown in 4.26 and 4.27.
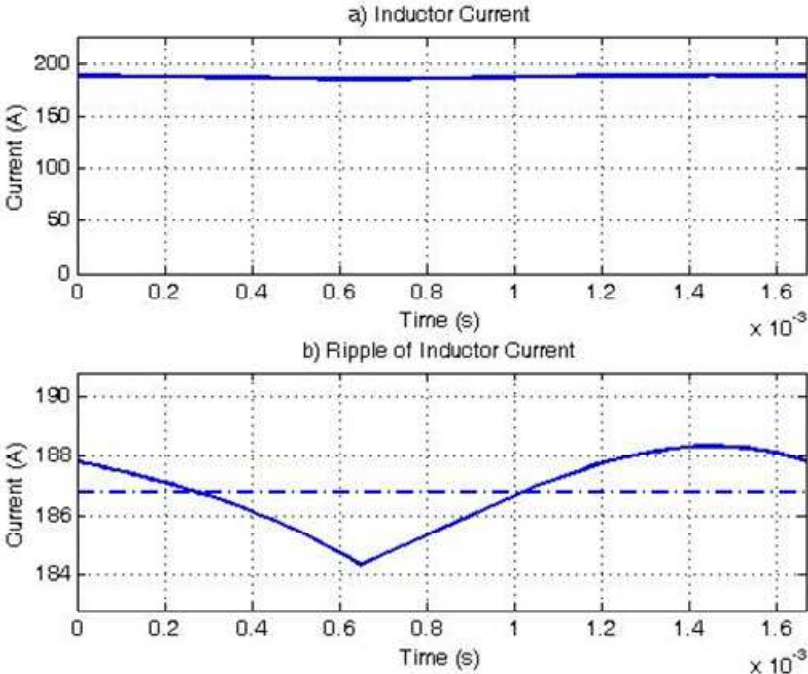
Fig. 4.24. Inductor current and its average value for the studied interval of $\pi/6$ at $\alpha = 0°$.

Figure 4.24. Courant dans l'inductance et valeur moyenne sur l'intervalle d'étude de $\pi/6$ pour $\alpha = 0°$.
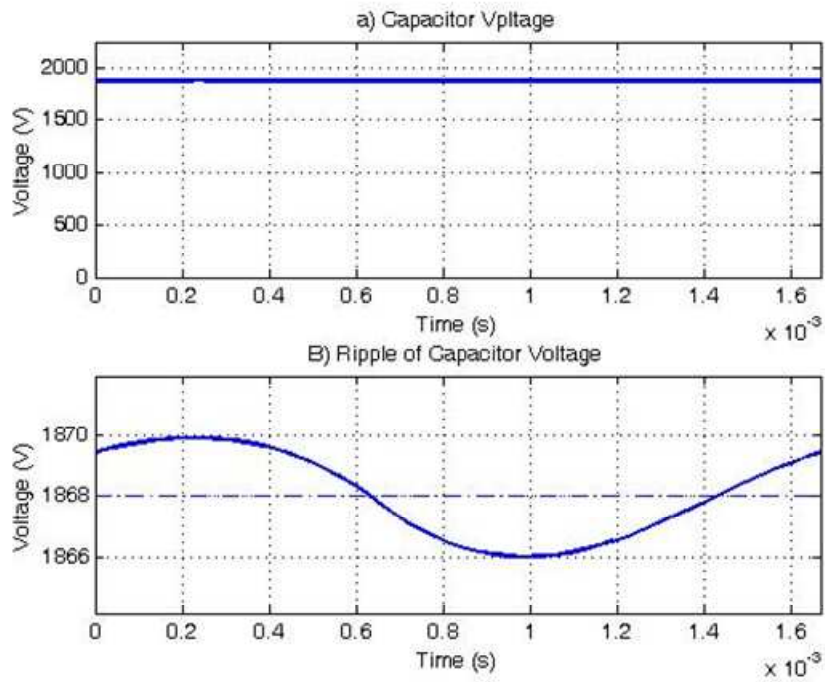
Fig. 4.25. Capacitor voltage and its average value for the studied interval of $\pi/6$ at $\alpha = 0°$.

Figure 4.25. Tension aux bornes de la capacité et valeur moyenne sur l'intervalle d'étude de $\pi/6$ pour $\alpha = 0°$.

Fig. 4.26. Inductor current and its average value for a period at $\alpha = 0°$.

Figure 4.26. Courant dans l'inductance et valeur moyenne sur une période pour $\alpha = 0°$.

Fig. 4.27. Capacitor voltage and its average value for a period at $\alpha = 0°$.

Figure 4.27. Tension aux bornes de la capacité et valeur moyenne sur une période pour

$\alpha = 0°$.

In the same manner, in Fig. 4.28 and 4.29 are shown the inductor current and capacitor voltage on the study interval of $\pi/6$ at the firing angle of 40 degree. And the whole AC period is shown in Fig. 4.30 and 4.31.
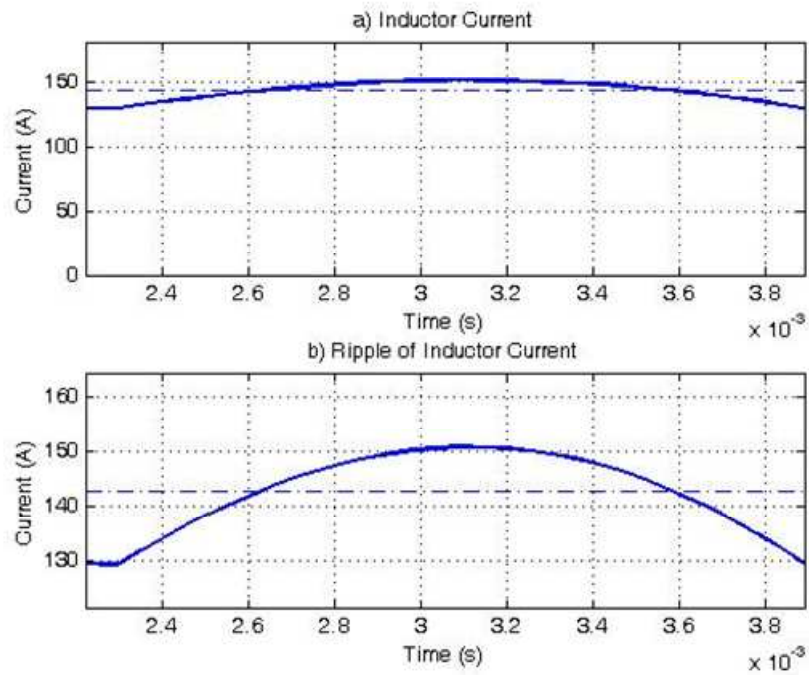
Fig. 4.28. Inductor current and its average value for the studied interval of $\pi/6$ at $\alpha = 40°$.

Figure 4.28. Courant dans l'inductance et valeur moyenne sur l'intervalle d'étude de $\pi/6$ pour $\alpha = 40°$.
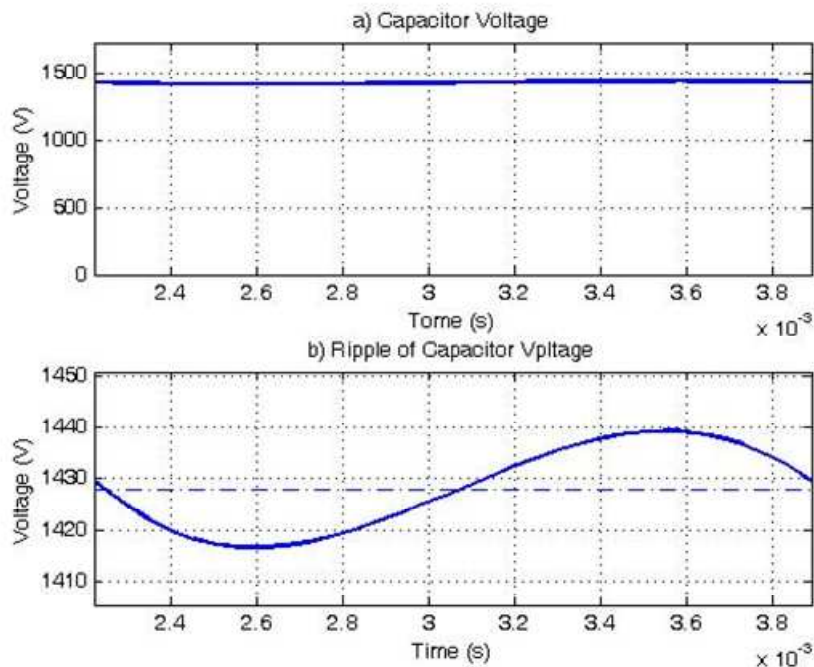
Fig. 4.29. Capacitor voltage and its average value for the studied interval of $\pi/6$ at $\alpha = 40°$.

Figure 4.29. Tension aux bornes de la capacité et valeur moyenne sur l'intervalle d'étude de $\pi/6$ pour $\alpha = 40°$.
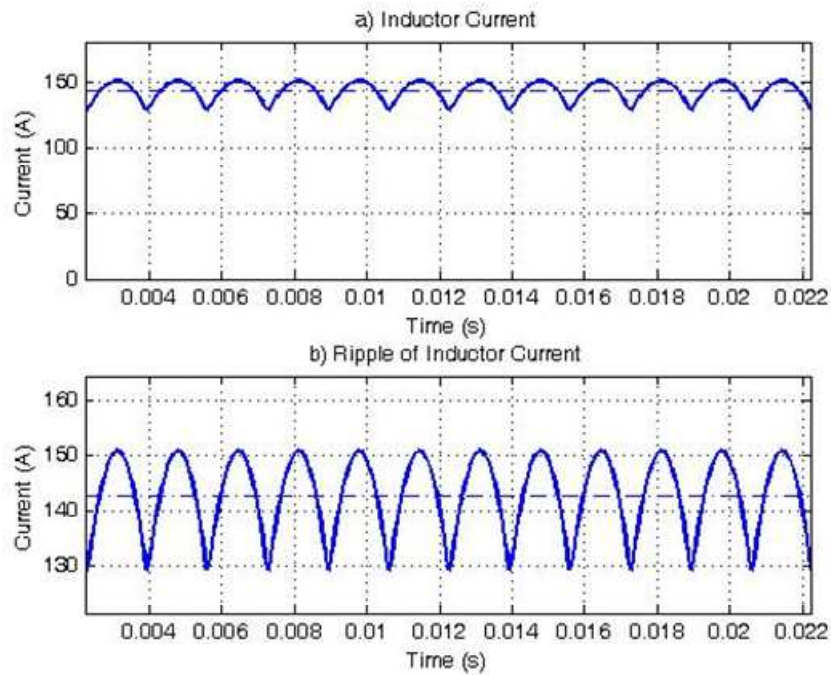
Fig. 4.30. Inductor current and its average value for a period at $\alpha = 40°$.

Figure 4.30. Courant dans l'inductance et valeur moyenne sur une période pour $\alpha = 40°$.

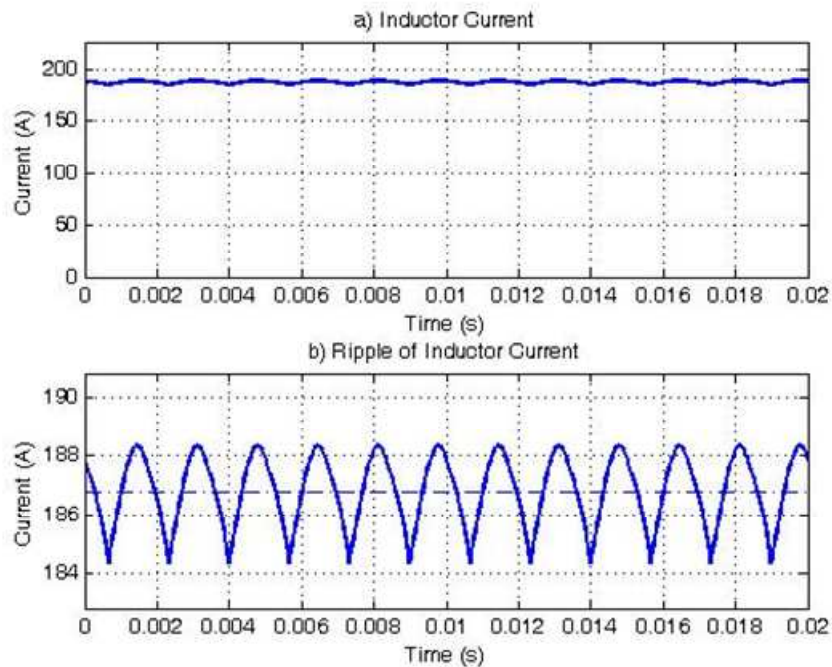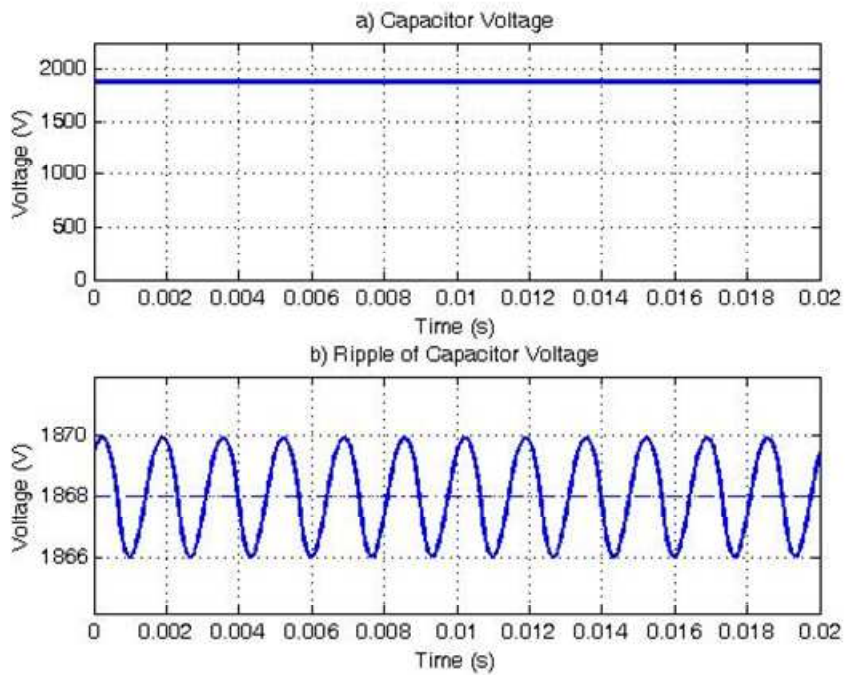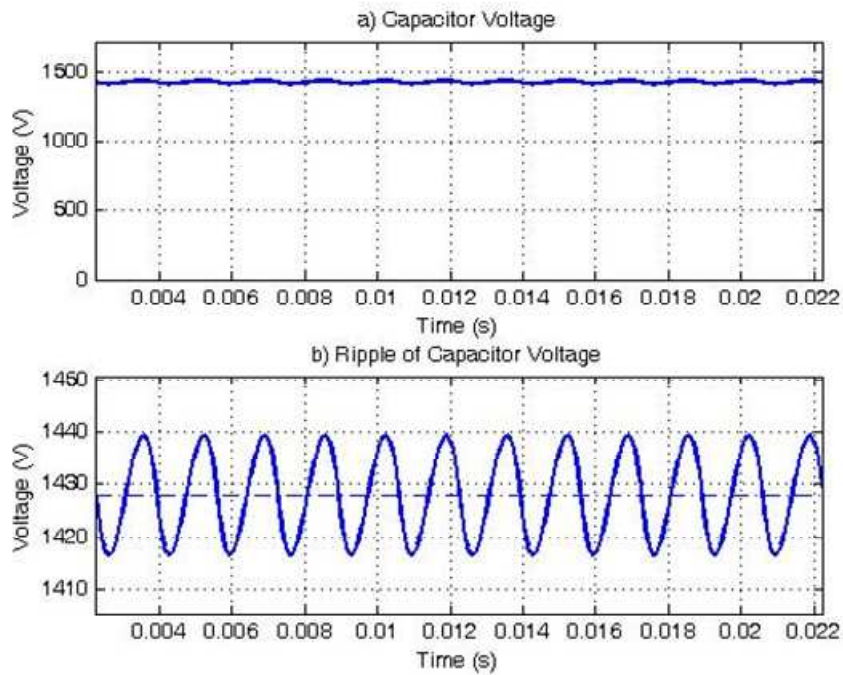
Fig. 4.31. Capacitor voltage and its average value for a period at $\alpha = 40°$.

Figure 4.31. Tension aux bornes de la capacité et valeur moyenne sur une période pour

$\alpha = 40°$.

4.3.7.2. Fourier analysis

According the Fourier theory, any periodic waveform can be decomposed into Fourier series as:

$$f(t) = c_0 + \sum_{h=1}^{\infty}\left(c_h \cdot e^{j(h \cdot \omega_0 \cdot t)} + c_{-h} \cdot e^{-j(h \cdot \omega_0 \cdot t)}\right) = \sum_{h=-\infty}^{\infty}\left(c_h \cdot e^{j(h \cdot \omega_0 \cdot t)}\right) \qquad (4.135)$$

where c_h is Fourier coefficient:

$$c_h = \frac{1}{T}\int_0^T f(t) \cdot e^{-j(h \cdot \omega_0 \cdot t)} dt, \qquad \text{for} \quad h = 0, \pm 1, \pm 2, \dots \qquad (4.136)$$

Applied equation 4.136 to the developed model results in:

$$c_h^{i_L} = \frac{1}{T'}\left(\begin{array}{c} \int_0^{T_C} [0 \quad G_3] \cdot e^{A_1 \cdot t} \cdot X_1(t_0) \cdot e^{-j(h \cdot \omega \cdot t)} dt \\[2mm] + \int_{T_C}^{T'} G_3 \cdot e^{A_2(t-T_C)} \cdot X_2(t_0+T_C) \cdot e^{-j(h \cdot \omega \cdot t)} dt \end{array}\right) \qquad (4.137)$$

Since $e^{-j(h \cdot \omega \cdot t)}$ is scalar, it can be moved inside to multiply with the term $e^{A \cdot t}$ and the analytical solution for Fourier coefficient of i_L is:

$$c_h^{i_L} = \frac{1}{T'}\left(\begin{array}{l} [0 \quad G_3] \cdot (A_1 - I \cdot j \cdot h \cdot \omega)^{-1} \cdot \left(e^{(A_1 - I \cdot j \cdot h \cdot \omega)T_C} - I\right) \cdot X_1(t_0) \\[2mm] + G_3 \cdot (A_2 - I \cdot j \cdot h \cdot \omega)^{-1} \cdot \left(e^{(A_2(T'-T_C) - I \cdot j \cdot h \cdot \omega T')} - I \cdot e^{(-j \cdot h \cdot \omega \cdot T_C)}\right) \cdot X_2(t_0+T_C) \end{array}\right) \quad (4.138)$$

The analytical solution for Fourier coefficient of v_C is:

$$c_h^{v_C} = \frac{1}{T'}\left(\begin{array}{l} [0 \quad G_4] \cdot (A_1 - I \cdot j \cdot h \cdot \omega)^{-1} \cdot \left(e^{(A_1 - I \cdot j \cdot h \cdot \omega)T_C} - I\right) \cdot X_1(t_0) \\[2mm] + G_4 \cdot (A_2 - I \cdot j \cdot h \cdot \omega)^{-1} \cdot \left(e^{(A_2(T'-T_C) - I \cdot j \cdot h \cdot \omega T')} - I \cdot e^{(-j \cdot h \cdot \omega \cdot T_C)}\right) \cdot X_2(t_0+T_C) \end{array}\right) \quad (4.139)$$

To proceed on primary current, the model gives the waveform only 1/12 of period long and the whole period can be obtained by rotation process, then the equation for Fourier coefficients are also involved with the rotational process. The equation for Fourier coefficient of the primary current is:

$$c_h^{\overline{i^P}} = \frac{1}{T}\sum_{n=0}^{11}\left(\begin{array}{l} \displaystyle\int_{t_0}^{t_0+T_C} R(n)\cdot\begin{bmatrix} 0 & G_1 \\ 0 & G_2 \end{bmatrix}\cdot e^{A_1\cdot t}\cdot X_1(t_0)\cdot e^{-j(h\cdot\omega\cdot t)}dt \\[4mm] +\displaystyle\int_{t_0+T_C}^{t_0+T'} R(n)\cdot\begin{bmatrix} G_1 \\ G_2 \end{bmatrix}\cdot e^{A_2(t-T_C)}\cdot X_2(t_0+T_C)\cdot e^{-j(h\cdot\omega\cdot t)}dt \end{array}\right) \tag{4.140}$$

and the result is:

$$c_h^{\overline{i^P}} = \frac{1}{T}\sum_{n=0}^{11}\left(\begin{array}{l} R(n)\cdot\begin{bmatrix} 0 & G_1 \\ 0 & G_2 \end{bmatrix}\cdot(A_1-j\cdot h\cdot\omega)^{-1}\cdot e^{(A_1-j\cdot h\cdot\omega)\cdot t}\cdot X_1(t_0)\Big|_{t_0}^{t_0+T_C} \\[4mm] +R(n)\cdot\begin{bmatrix} G_1 \\ G_2 \end{bmatrix}\cdot(A_2-j\cdot h\cdot\omega)^{-1}\cdot e^{(A_2-j\cdot h\cdot\omega)\cdot t}\cdot X_2(t_0+T_C)\Big|_{t_0+T_C}^{t_0+T'} \end{array}\right) \tag{4.141}$$

where R(n) is the rotational matrix:

$$R(n) = \begin{bmatrix} e^{j\frac{n\cdot\pi}{6}} & 0 \\[2mm] 0 & e^{-j\frac{n\cdot\pi}{6}} \end{bmatrix} \tag{4.142}$$

Equation 4.139 works properly as long as the order of Fourier coefficient, h, is higher than 1. However, the singular matrix problem occurs when trying to calculate the Fourier coefficient at fundamental frequency.

4.3.7.3. Fourier coefficient of the primary current at the fundamental frequency

The Fourier coefficient of the primary current at the higher order frequency, i.e. $h>1$, can be obtained by equation 4.141. However, we encounter a singular matrix problem when trying to evaluate Fourier coefficient at the fundamental frequency. We then have to split the model back into the general form shown in equation 4.53, and then, integrate it for the analytical result of primary currents. In this form, the analytical solution of primary currents can be used to perform Fourier analysis at the fundamental frequency, and include all other frequency order, without singular matrix problem. Models during the commutation and normal operation in general form was respectively shown in equations 4.87 and 4.106. The time solution of the primary current for the whole period can be found by:

$$\overline{i^p}(t) = \begin{cases} \text{for } t_0 \le t - nT' < t_0 + T_C; \\[2mm] R(n) \cdot \begin{bmatrix} 0 & G_1 \\ 0 & G_2 \end{bmatrix} \cdot \left(e^{a_1(t\text{-}nT'\text{-}t_0)} \cdot x_1(t_0) + \int\limits_{t_0}^{t\text{-}nT'} e^{a_1(t-\tau)} \cdot b_1 \cdot \begin{bmatrix} e^{j \cdot \omega \cdot \tau} \\ e^{-j \cdot \omega \cdot \tau} \end{bmatrix} \cdot d\tau \right) \\[5mm] \text{for } (t_0 + T_C) \le t - nT' < t_0 + T'; \\[2mm] R(n) \cdot \begin{bmatrix} G_1 \\ G_2 \end{bmatrix} \cdot \left(e^{a_2(t\text{-}nT'\text{-}(t_0+T_C))} \cdot x_2(t_0 + T_C) + \int\limits_{(t_0+T_C)}^{t\text{-}nT'} e^{a_2(t-\tau)} \cdot b_2 \cdot \begin{bmatrix} e^{j \cdot \omega \cdot \tau} \\ e^{-j \cdot \omega \cdot \tau} \end{bmatrix} \cdot d\tau \right) \end{cases} \quad (4.143)$$

where $n = 0, 1, \ldots, 11$

To avoid the matrix integration let us consider:

$$\int e^{a(t-\tau)} \cdot b \cdot \begin{bmatrix} e^{j \cdot \omega \cdot \tau} \\ e^{-j \cdot \omega \cdot \tau} \end{bmatrix} \cdot d\tau = \int e^{a(t-\tau)} \cdot b \cdot \left(e^{j \cdot \omega \cdot \tau} \begin{bmatrix} 1 \\ 0 \end{bmatrix} + e^{-j \cdot \omega \cdot \tau} \begin{bmatrix} 0 \\ 1 \end{bmatrix} \right) \cdot d\tau$$

$$= \int e^{a(t-\tau+j \cdot \omega \cdot \tau)} \cdot b \cdot \begin{bmatrix} 1 \\ 0 \end{bmatrix} \cdot d\tau + \int e^{a(t-\tau-j \cdot \omega \cdot \tau)} \cdot b \cdot \begin{bmatrix} 0 \\ 1 \end{bmatrix} \cdot d\tau \quad (4.144)$$

By applying the manipulation technique previously used to equation 4.141, the integration result can be obtained as follows:

$$\overline{i^p}(t) = \begin{cases} \text{for } t_0 \le t - nT' < t_0 + T_C; \\[2mm] R(n) \cdot \begin{bmatrix} 0 & G_1 \\ 0 & G_2 \end{bmatrix} \cdot \begin{pmatrix} e^{a_1(t\text{-}nT'\text{-}t_0)} \cdot x_1(t_0) \\[2mm] + e^{a_1(t\text{-}nT')} \cdot (-a_1 + j \cdot \omega)^{-1} \cdot e^{(-a_1+j \cdot \omega) \cdot \tau} \cdot b_1 \cdot \begin{bmatrix} 1 \\ 0 \end{bmatrix} \Big|_{t_0}^{t\text{-}nT'} \\[2mm] + e^{a_1(t\text{-}nT')} \cdot (-a_1 - j \cdot \omega)^{-1} \cdot e^{(-a_1-j \cdot \omega) \cdot \tau} \cdot b_1 \cdot \begin{bmatrix} 0 \\ 1 \end{bmatrix} \Big|_{t_0}^{t\text{-}nT'} \end{pmatrix} \\[6mm] \text{for } (t_0 + T_C) \le t - nT' < t_0 + T'; \\[2mm] R(n) \cdot \begin{bmatrix} G_1 \\ G_2 \end{bmatrix} \cdot \begin{pmatrix} e^{a_2(t\text{-}nT'\text{-}(t_0+T_C))} \cdot x_2(t_0 + T_C) \\[2mm] + e^{a_2(t\text{-}nT')} \cdot (-a_2 + j \cdot \omega)^{-1} \cdot e^{(-a_2+j \cdot \omega) \cdot \tau} \cdot b_2 \cdot \begin{bmatrix} 1 \\ 0 \end{bmatrix} \Big|_{t_0+T_C}^{t\text{-}nT'} \\[2mm] + e^{a_2(t\text{-}nT')} \cdot (-a_2 - j \cdot \omega)^{-1} \cdot e^{(-a_2-j \cdot \omega) \cdot \tau} \cdot b_2 \cdot \begin{bmatrix} 0 \\ 1 \end{bmatrix} \Big|_{t_0+T_C}^{t\text{-}nT'} \end{pmatrix} \end{cases} \quad (4.145)$$

where n = 0,1,...,11.

Substitute the upper and lower integration boundary result in the time solution of the primary current as follow:

$$
\overline{i^p}(t) = \begin{cases}
\text{for } t_0 \leq t-nT' < t_0 + T_C; \\[2mm]
R(n) \cdot \begin{bmatrix} 0 & G_1 \\ 0 & G_2 \end{bmatrix} \cdot \left(\begin{aligned}
& e^{a_1(t\text{-}nT'\text{-}t_0)} \cdot x_1(t_0) \\
& + e^{a_1(t\text{-}nT')} \cdot (-a_1 + j\cdot\omega)^{-1} \cdot e^{(-a_1+j\cdot\omega)\cdot(t\text{-}nT')} \cdot b_1 \cdot \begin{bmatrix} 1 \\ 0 \end{bmatrix} \\
& - e^{a_1(t\text{-}nT')} \cdot (-a_1 + j\cdot\omega)^{-1} \cdot e^{(-a_1+j\cdot\omega)\cdot t_0} \cdot b_1 \cdot \begin{bmatrix} 1 \\ 0 \end{bmatrix} \\
& + e^{a_1(t\text{-}nT')} \cdot (-a_1 - j\cdot\omega)^{-1} \cdot e^{(-a_1-j\cdot\omega)\cdot(t\text{-}nT')} \cdot b_1 \cdot \begin{bmatrix} 0 \\ 1 \end{bmatrix} \\
& - e^{a_1(t\text{-}nT')} \cdot (-a_1 - j\cdot\omega)^{-1} \cdot e^{(-a_1-j\cdot\omega)\cdot t_0} \cdot b_1 \cdot\cdot \begin{bmatrix} 0 \\ 1 \end{bmatrix}
\end{aligned} \right) \\[10mm]
\text{for } (t_0 + T_C) \leq t-nT' < t_0 + T'; \\[2mm]
R(n) \cdot \begin{bmatrix} G_1 \\ G_2 \end{bmatrix} \cdot \left(\begin{aligned}
& e^{a_2(t\text{-}nT'\text{-}(t_0+T_C))} \cdot x_2(t_0 + T_C) \\
& + e^{a_2(t\text{-}nT')} \cdot (-a_2 + j\cdot\omega)^{-1} \cdot e^{(-a_2+j\cdot\omega)\cdot(t\text{-}nT')} \cdot b_2 \cdot \begin{bmatrix} 1 \\ 0 \end{bmatrix} \\
& - e^{a_2(t\text{-}nT')} \cdot (-a_2 + j\cdot\omega)^{-1} \cdot e^{(-a_2+j\cdot\omega)\cdot(t_0+T_C)} \cdot b_2 \cdot \begin{bmatrix} 1 \\ 0 \end{bmatrix} \\
& + e^{a_2(t\text{-}nT')} \cdot (-a_2 - j\cdot\omega)^{-1} \cdot e^{(-a_2-j\cdot\omega)\cdot(t\text{-}nT')} \cdot b_2 \cdot \begin{bmatrix} 0 \\ 1 \end{bmatrix} \\
& - e^{a_2(t\text{-}nT')} \cdot (-a_2 - j\cdot\omega)^{-1} \cdot e^{(-a_2-j\cdot\omega)\cdot(t_0+T_C)} \cdot b_2 \cdot \begin{bmatrix} 0 \\ 1 \end{bmatrix}
\end{aligned} \right)
\end{cases}
\tag{4.146}
$$

Then, according to equation 4.136, the Fourier coefficient at the fundamental frequency of the primary current can be found as follow:

$$
\begin{aligned}
c_h^{\bar{i^p}} = \frac{1}{T} \sum_{n=0}^{11} \Bigg(& R(n) \cdot \begin{bmatrix} 0 & G_1 \\ 0 & G_2 \end{bmatrix} \cdot \left(\begin{aligned}
& e^{-j(\omega \cdot t)} \left(a_1 - j\cdot\omega\right)^{-1} \cdot e^{a_1\left(t-(t_0+nT')\right)} x_1(t_0) \Big|_{n\cdot T'}^{n\cdot T'+T_C} \\
& + \left(-a_1 + j\cdot\omega\right)^{-1} \cdot e^{-j(\omega\cdot n\cdot T')} \cdot t \cdot b_1 \cdot \begin{bmatrix} 1 \\ 0 \end{bmatrix} \Big|_{n\cdot T'}^{n\cdot T'+T_C} \\
& - \left(-a_1 + j\cdot\omega\right)^{-1} \cdot \left(a_1 - j\cdot\omega\right)^{-1} \cdot e^{a_1\left(t-(t_0+nT')\right)} \cdot e^{-j\cdot\omega(t-t_0)} \cdot b_1 \cdot \begin{bmatrix} 1 \\ 0 \end{bmatrix} \Big|_{n\cdot T'}^{n\cdot T'+T_C} \\
& + \left(-a_1 - j\cdot\omega\right)^{-1} \cdot \left(-2\cdot j\cdot\omega\right)^{-1} \cdot e^{-j\cdot\omega\cdot t} \cdot e^{-j\cdot\omega(t-n\cdot T')} \cdot b_1 \cdot \begin{bmatrix} 0 \\ 1 \end{bmatrix} \Big|_{n\cdot T'}^{n\cdot T'+T_C} \\
& - \left(-a_1 - j\cdot\omega\right)^{-1} \cdot \left(a_1 - j\cdot\omega\right)^{-1} \cdot e^{-j\cdot\omega(t+t_0)} \cdot e^{a_1\left(t-(t_0+nT')\right)} \cdot b_1 \cdot \begin{bmatrix} 0 \\ 1 \end{bmatrix} \Big|_{n\cdot T'}^{n\cdot T'+T_C}
\end{aligned} \right) \\
& + R(n) \cdot \begin{bmatrix} G_1 \\ G_2 \end{bmatrix} \cdot \left(\begin{aligned}
& e^{-j\cdot\omega\cdot t} \cdot e^{a_2\left(t-(t_0+nT'+T_C)\right)} \cdot x_2(t_0+T_C) \Big|_{n\cdot T'+T_C}^{n\cdot T'+T'} \\
& + \left(-a_2 + j\cdot\omega\right)^{-1} \cdot e^{-j\cdot\omega\cdot n\cdot T'} \cdot t \cdot b_2 \cdot \begin{bmatrix} 1 \\ 0 \end{bmatrix} \Big|_{n\cdot T'+T_C}^{n\cdot T'+T'} \\
& - \left(-a_2 + j\cdot\omega\right)^{-1} \cdot \left(a_2 - j\cdot\omega\right)^{-1} \cdot e^{-j\cdot\omega\left(t-(t_0+T_C)\right)} \cdot e^{a_2\left(t-(t_0+n\cdot T'+T_C)\right)} \cdot b_2 \cdot \begin{bmatrix} 1 \\ 0 \end{bmatrix} \Big|_{n\cdot T'+T_C}^{n\cdot T'+T'} \\
& + \left(-a_2 - j\cdot\omega\right)^{-1} \cdot \left(-2\cdot j\cdot\omega\right)^{-1} \cdot e^{-j\cdot\omega\cdot t} \cdot e^{-j\cdot\omega(t-nT')} \cdot b_2 \cdot \begin{bmatrix} 0 \\ 1 \end{bmatrix} \Big|_{n\cdot T'+T_C}^{n\cdot T'+T'} \\
& - \left(-a_2 - j\cdot\omega\right)^{-1} \cdot \left(a_2 - j\cdot\omega\right)^{-1} \cdot e^{-j\cdot\omega(t_0+T_C)} \cdot e^{a_2\left(t-(t_0+n\cdot T'+T_C)\right)} \cdot b_2 \cdot \begin{bmatrix} 0 \\ 1 \end{bmatrix} \Big|_{n\cdot T'+T_C}^{n\cdot T'+T'}
\end{aligned} \right) \Bigg)
\end{aligned}
\tag{4.147}
$$

Then the complete Fourier analysis of primary current can be performed by using equations 4.147 for fundamental frequency and 4.141 for higher orders.

4.3.7.4. Example of Fourier analysis

For the two simulation examples given before, the results of the analytical Fourier analysis of the primary current for AC side, inductor current and capacitor voltage for DC side are shown in Fig. 4.26 and 4.27 at the firing angle of 0 degree and in Fig. 4.30 and 4.31 at the firing angle of 40 degrees.

The reducing harmonics from converters by 12-pulse converter are shown in Fig. 4.32 to 4.37. The analytical Fourier analysis of the total waveform confirms that the twelve pulse converter gives harmonic currents of the following order $k\cdot12 \pm 1$ where $k = 1, 2, 3...$

Thus the characteristic harmonics from a twelve pulse converter are 11, 13, 23, 25... and this connection has effectively eliminated the six pulse harmonics. These harmonic current have maximum theoretical magnitude which varies as follows, $I_n = I_n/n$. In fact the magnitudes of the harmonic currents vary as a function of DC current as well as the firing angle and the overlap angle of the converter.
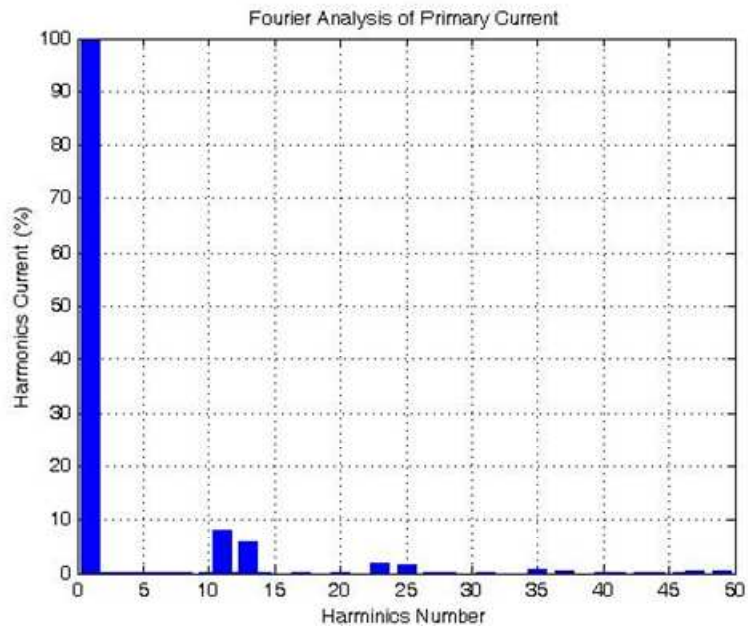
Fig. 4.32. Harmonics spectrum of primary current at $\alpha = 0°$.

Figure 4.32. Spectre harmonique du courant primaire pour $\alpha = 0°$.

Fig. 4.33. Harmonics spectrum of inductor current at $\alpha = 0°$.

Figure 4.33. Spectre harmonique du courant dans l'inductance pour $\alpha = 0°$.

Fig. 4.34. Harmonics spectrum of capacitor voltage at $\alpha = 0°$.

Figure 4.34. Spectre harmonique de la tension capacité pour $\alpha = 0°$.

Fig. 4.35. Harmonics spectrum of primary current at $\alpha = 40°$.

Figure 4.35. Spectre harmonique du courant primaire pour $\alpha = 40°$.
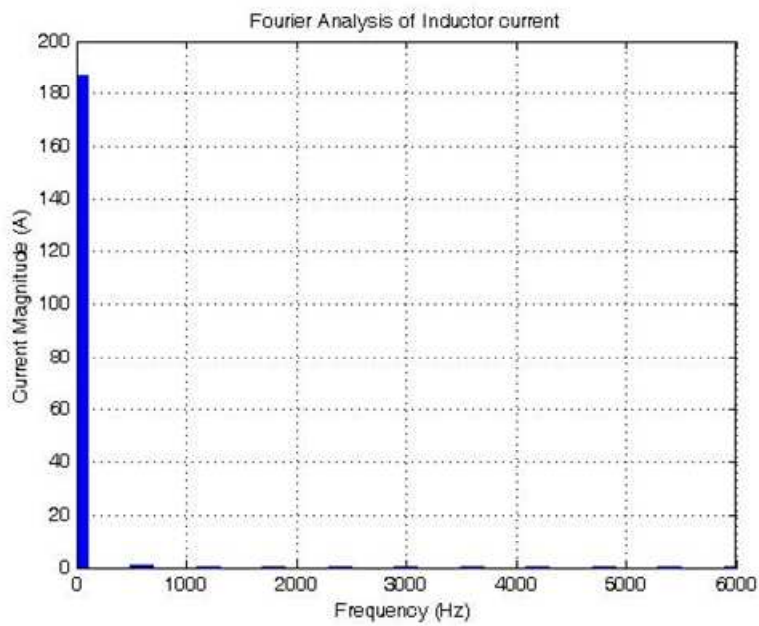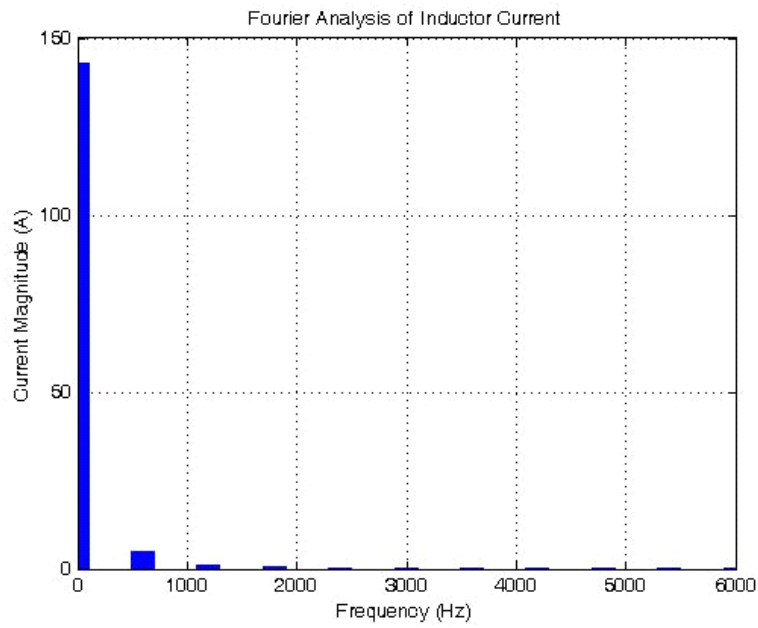
Fig. 4.36. Harmonics spectrum of inductor current at $\alpha = 40°$.

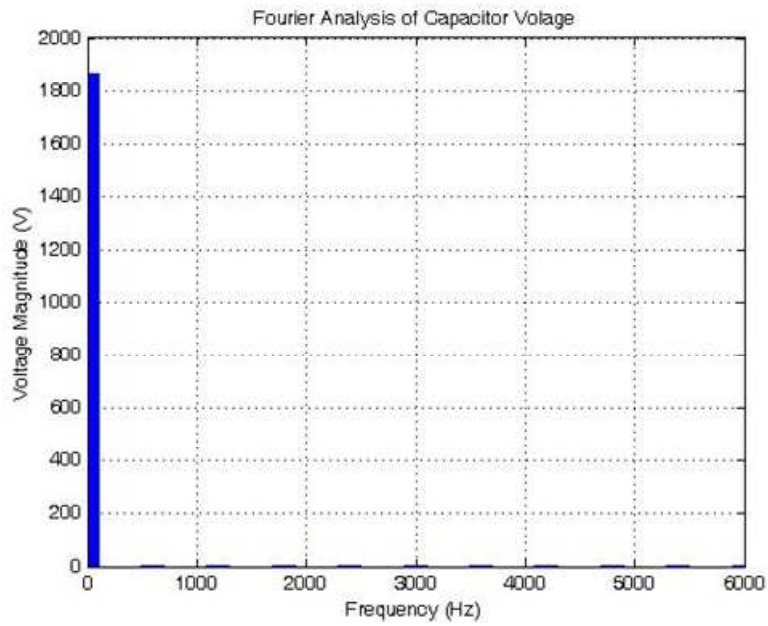Figure 4.36. Spectre harmonique du courant dans l'inductance pour $\alpha = 40°$.
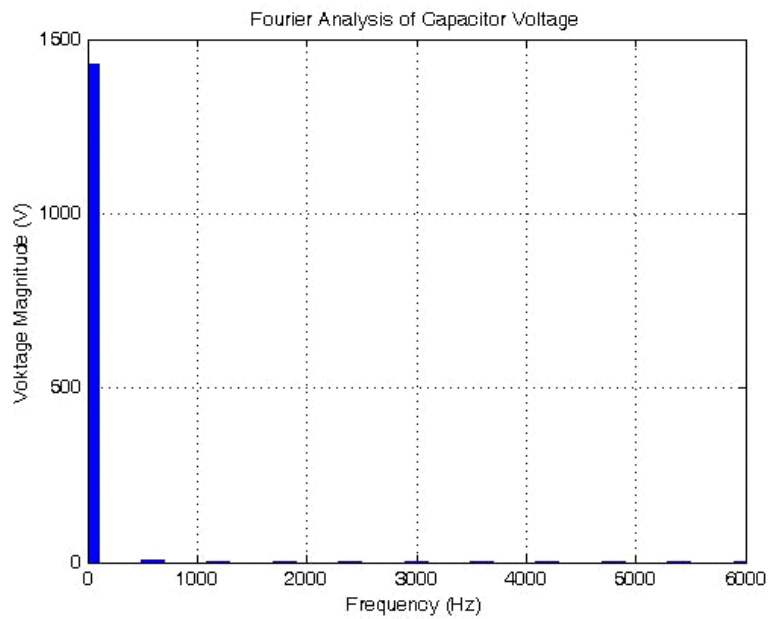
Fig. 4.37. Harmonics spectrum of capacitor voltage at $\alpha = 40°$.

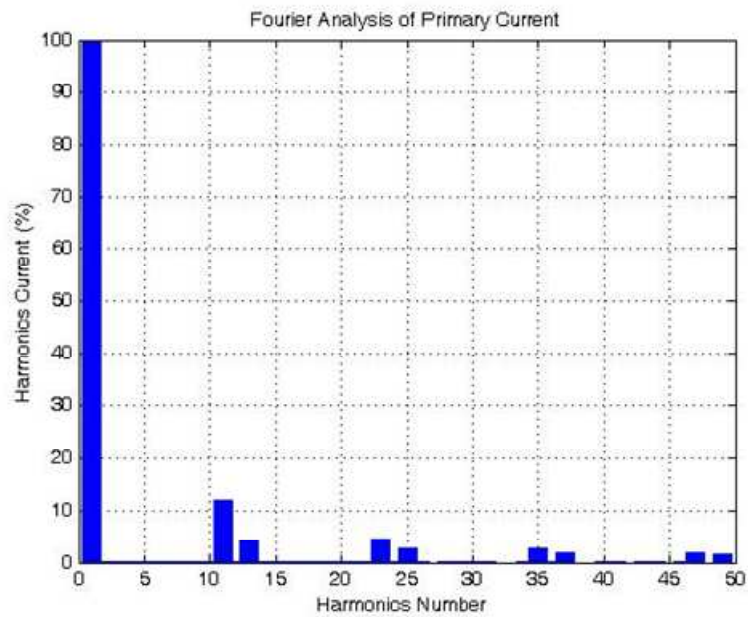Figure 4.37. Spectre harmonique de la tension capacité pour $\alpha = 40°$.

4.4. Conclusion

Multipulse converters are widely used in industry since they provide a simple and effective method to reduce harmonics from the systems. A new tool for studying the steady state operation and the harmonics of the 12-pulse converter has been developed.

The basic concept is based on the symmetry of trajectories of waveforms on the complex plane. To develop a switched model of the 12-pulse converter, 24 of the different instance models are needed to be developed where half of them are for normal conductions and the other half are for commutation processes. The developed model is in complex. There are only two instance models needed by the symmetrical property. One of them is the model during commutation and the other one is the model of normal conduction. These two models are sufficient to provide a segment of the waveforms and the whole period waveforms can be obtained by a rotational process.

The new model is developed in an exponential form of state equations. This form has advantages in both accuracy and speed of simulation. The model in this form can also give results in analytical form, for example, a Fourier analysis of the waveforms, an average value, a root mean square value, etc.

Since the goal is to study the steady state operation, numerical techniques based on the Newton-Raphson method can be used to find the initial vector and the sequences duration for steady state operation. As a result, the simulation in transient state is skipped and the simulation speed is increased.

In conclusion, the model presented in this chapter is not serving just as a tool for studying the harmonics in the 12-pulse converter system, but it also demonstrates a good method that can be adapted to another circuit which operates periodically.

Conclusion

The main company in charge of production and transmission of electricity in Thailand is the EGAT (Electricity Generating Authority of Thailand). EGAT is a state company in charge of production and transmission of electricity within the country. EGAT has a production capacity of about 28 000 MW for an annual production of 117 000 GWh. However, only 59 % of the production capacity comes from EGAT power plants. Others come from private producers or foreign countries.

EGAT is also responsible for the transmission of electricity. A 28 000 km network covers the country with three voltage levels 500, 230 and 115 kV. The network is interconnected with the neighboring countries. The main connections are with Laos (115 and 230 kV) and Malaysia (115 and 132 kV, 300 kV in HVDC). A 500 HVDC connection is in project between Thailand and China.

The Thailand-Malaysia HVDC interconnection system was begun in 1997. The 300/600 MW grid interconnection system allows both countries bi-directional control for the energy exchange and improving their reliability. The system was designed to be bipolar; however, in the first stage it is a monopolar configuration with metallic return which can be extended into the bipolar configuration later. The power converter unit consists of two three-phase 6-pulse converter bridges connected in series to form a 12-pulse converter unit. The EGAT-TNB thyristor converters have 48 thyristors connected in series in each valve. In the complete 12-pulse converter, the number of thyristors is 576. This power converter produces also harmonic problems to the AC sides of the systems.

There are mainly three options for handling with the harmonic problems which are using phase shifting transformers, passive filters, and active filters. Passive filter is a simple method to reduce harmonics from systems, but it suppresses only a tuned harmonic order, i.e., multiple passive filter are required for multiple order harmonic reduction.

Active filters are constructed from the power electronic converters and energy storage devices. The principle of the active filter is to generate the inverse harmonic waveform to

cancel the existing harmonic in the systems. In this thesis, the prototype of a shunt active filter has been developed. After connected the prototype to a 6 pulse converter with resistive load which operates at 6 kW, it can reduce THD_i of the converter from 29.5% to 3.2%. Active filter is the effective method for harmonic reduction; however, the capability of the switching devices used in the converter prevents them to be used in medium or high power systems.

Since shifting fundamental current for $\pi/6$ degree can cause some of their higher harmonics shifted inversely, phase shifting transformers is an interesting option for harmonic mitigation in medium and high power systems. The twelve pulse system is the selected system in the Thailand-Malaysia HVDC interconnection project.

To study, in particular, the harmonics generated from the twelve pulse system, a method to model in steady state multipulse converters has been developed in this thesis. Using symmetrical properties, one has shown that the study of the converter can be reduced to a short period corresponding to two elementary converter sequences. The study leads to an exact solution of the problem and gives the possibility to incorporate the effect of both the commutation process of the thyristors and the load in the calculation of the harmonics which significantly affects the characteristics of the systems.

Annex 1

Example of calculation of a voltage drop

Let consider the example given on Fig. A.1.1, where a motor starts 15 times per hour on a low voltage network [19].

For a base value of 100 MVA of the system, one can calculate the per unit impedance of the high voltage system in the form of power:

$$Z_{pu(high)} = j \cdot \frac{MVA_{base}}{MVA_{high}} = j \cdot \frac{100}{4000} = j \cdot 0.025 \tag{A1.1}$$

The per unit impedance of the power transformer is in the form:

$$Z_{trans(power)} = \frac{MVA_{base}}{MVA} \cdot \frac{R + j \cdot X}{|Z|} \tag{A1.2}$$

$$Z_{trans(power)} = \frac{60}{100} \cdot \frac{100}{100} \cdot \frac{1 + j \cdot 30}{\sqrt{1 + 30^2}} = 0.020 + j \cdot 0.600 \tag{A1.3}$$

The per unit impedance of the feeder is:

$$Z_{feed} = \frac{MVA}{(kV)^2} \cdot Z \tag{A1.4}$$

$$Z_{feed} = \frac{100}{11^2} \cdot (0.28 + j \cdot 0.34) = 0.0231 + j \cdot 0.281 \tag{A1.5}$$

The per unit impedance of the distribution transformer is obtained from equation A1.2:

$$Z_{trans(distr)} = \frac{5}{100} \cdot \frac{100}{1} \cdot \frac{1 + j \cdot 5}{\sqrt{1 + 5^2}} = 0.981 + j \cdot 4.903 \tag{A1.6}$$
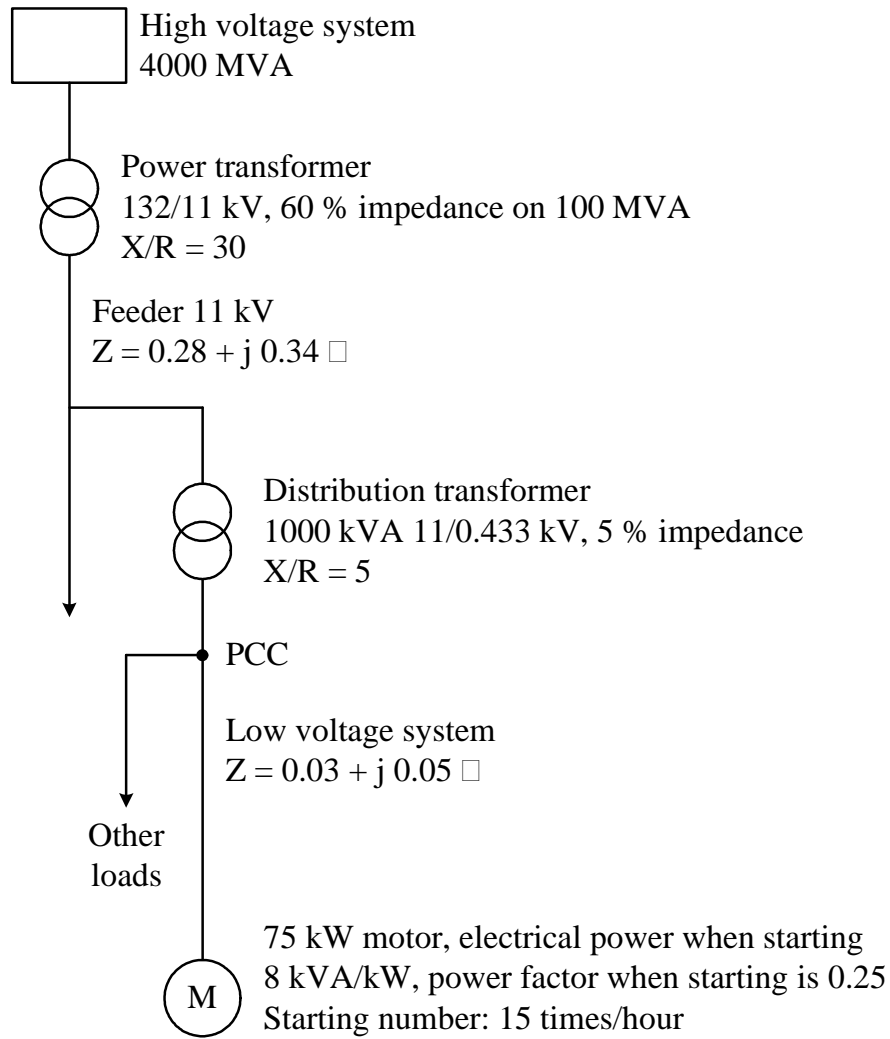
Fig. A1.1. Motor connected on the main.

Figure A1.1. Schéma de connexion au réseau du moteur.

The total per unit impedance at the point of common coupling from equations A1.1, A1.3, A1.5 and A1.6 is:

$$Z_1 = Z_{pu(high)} + Z_{trans(power)} + Z_{feed} + Z_{trans(distr)} = 1.232 + j \cdot 5.809 \qquad (A1.7)$$

The short circuit power (fault level) at the point of common coupling is calculated by equation A1.1. The absolute value of the per unit impedance is in the form:

$$|Z_1| = \frac{MVA_{base}}{MVA_{sc}} \qquad (A1.8)$$

So that the short circuit power is:

$$MVA_{sc} = \frac{100}{\sqrt{1.232^2 + 5.809^2}} = 16.8 \, MVA \tag{A1.9}$$

The ratio of operating power of the motor to the short circuit at the point of common coupling is expressed as:

$$\frac{MVA_{mot}}{MVA_{sc}} = \frac{8 \, kVA/kW}{16.8 \, MVA} \cdot \frac{75 \, kW}{1000} = 0.0357 \tag{A1.10}$$

The fluctuation causes by the motor is over 0.03 [19], therefore, the connection of the motor into the system must pass the evaluation of voltage fluctuation at the point of common coupling according to Fig. 1.7.

The per unit impedance when starting the motor is:

$$Z_{mot} = \frac{100 \, MVA}{8 \, kVA/kW} \cdot \frac{1000}{75 \, kW} \cdot (0.25 + j \cdot 0.9682) = 41.667 + j \cdot 161.367 \tag{A1.11}$$

The per unit impedance of the low voltage system can be obtained from equation (A1.4):

$$Z_{pu(low)} = \frac{100}{0.433^2} \cdot (0.03 + j \cdot 0.05) = 16.001 + j \cdot 26.668 \tag{A1.12}$$

The total per unit impedance at the point of common coupling of the low voltage system is:

$$Z_2 = Z_{mot} + Z_{pu(low)} = 57.668 + j \cdot 188.035 \tag{A1.13}$$

The sum of the total per unit impedances at the point of common coupling for the whole system is:

$$Z_{tot} = Z_1 + Z_2 = 58.900 + j \cdot 193.844 \tag{A1.14}$$

The percentage of voltage while starting the motor at the point of common coupling is:

$$V_{mot} = \left| \frac{Z_2}{Z_{tot}} \right| \cdot 100\% = \frac{\sqrt{57.668^2 + 188.035^2}}{\sqrt{58.900^2 + 193.844^2}} \cdot 100 = 97.08\% \tag{A1.15}$$

So that the voltage change at the point of common coupling is as follows:

$$\frac{\Delta V}{V} = 100\% - 97.08\% = 2.92\% \qquad \text{(A1.16)}$$

In this case, from graph number 2 (Pst = 1.0) in Fig. 1.7, the highest voltage change which is acceptable at the rate of 15 times/hour is equal to 4.2 %. Then, the obtained value of 2.9 % allows the motor to be connected to the system.

On the contrary, for example, an equipment connected to the system which causes the highest voltage change of 2 % at the rate of 12 times/hour, from graph number 2 (Pst = 1.0) in Fig. 1.7, the highest voltage change which is acceptable at the rate of 12 times/hour is equal to 4.5 %.

Therefore, the ratio of the actual voltage change to the highest voltage change at the rate of 12 times/hour (1st-source) and 15 times/hour (2nd-source) can be calculated as follows:

$$R_1 = \frac{2}{4.5} = 0.44 \qquad \text{(A1.17)}$$

and:

$$R_2 = \frac{2.92}{4.2} = 0.69 \qquad \text{(A1.18)}$$

When R_i is the ratio of voltage change which generated from i-sources to the highest voltage change according to the graph number 2 (Pst = 1.0) in Fig. 1.7.

The value of "m" depends on the characteristic of voltage fluctuation source. For example, $m = 2$ has to be used for electrical equipments which often tend to have simultaneous operation [19].

From the guideline at $m = 2$, the calculated value from equation A1.19 must be less than 1:

$$\sqrt[m]{R_1^m + R_2^m + ... + R_N^m} < 1 \qquad \text{(A1.19)}$$

Therefore:

$$\sqrt[m]{R_1^m + R_2^m + ... + R_N^m} = \sqrt{0.44^2 + 0.69^2} = 0.81 \tag{A1.20}$$

As the obtained value is less than 1, the motor can be connected to the network.

<div align="right">

Annex 2

</div>

Calculation of the DC voltage of 6-pulse converter

Let consider the commutation process for 3-pulse converter (Fig. A2.1).
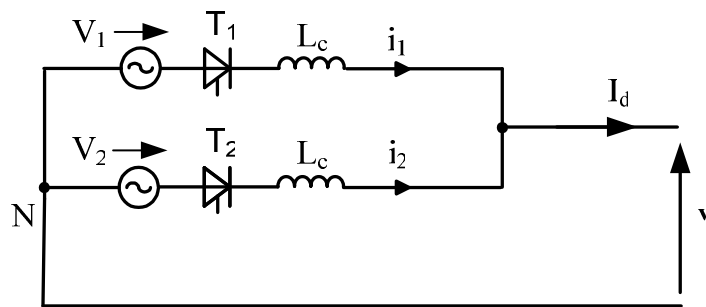
Fig. A2.1. 3-pulse converter circuit, commutation process.

Figure A2.1. Redresseur d'indice de pulsation 3, phénomène de commutation.

If we consider the voltage under the form of:

$$v_n = V \cdot \sqrt{2} \cdot \sin\left(\omega t - (n-1) \cdot \frac{2\pi}{3}\right) \qquad (A2.1)$$

where n is the phase number ($n = 1, \ 2, \ 3$).

The commutation angle for phase 2 is defined from the angle $\dfrac{5\pi}{6} + \alpha$ (Fig. A2.2). On this figure, α is the firing angle and μ is the commutation duration (overlap angle).
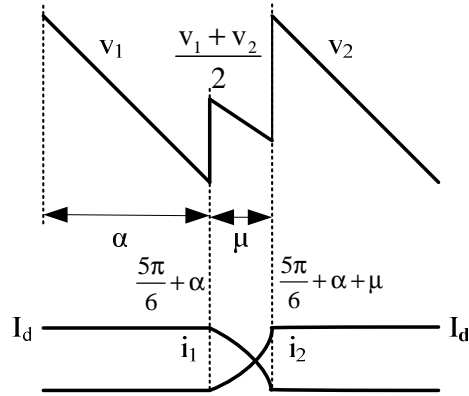
Fig. A2.2. Commutation process from phase 1 to phase 2.

Figure A2.2. Commutation de la phase 1 sur la phase 2.

During the commutation process, as the current I_d is supposed to be constant:

$$2 \cdot L_c \cdot \frac{di_2}{dt} = v_2 - v_1 \tag{A2.2}$$

The DC voltage is defined as:

$$
\begin{aligned}
V_d &= \frac{3}{2\pi} \cdot \int\limits_{\frac{5\pi}{6}+\alpha}^{\frac{5\pi}{6}+\alpha+\frac{2\pi}{3}} v(\omega t) d\omega t \\
&= \frac{3}{2\pi} \cdot \left[\int\limits_{\frac{5\pi}{6}+\alpha}^{\frac{5\pi}{6}+\alpha+\mu} \frac{v_1 + v_2}{2}\, d\omega t + \int\limits_{\frac{5\pi}{6}+\alpha+\mu}^{\frac{5\pi}{6}+\alpha+\frac{2\pi}{3}} v_2\, d\omega t \right] \\
&= \frac{3}{2\pi} \cdot \int\limits_{\frac{5\pi}{6}+\alpha}^{\frac{5\pi}{6}+\alpha+\frac{2\pi}{3}} v_2\, d\omega t + \frac{3}{2\pi} \cdot \int\limits_{\frac{5\pi}{6}+\alpha}^{\frac{5\pi}{6}+\alpha+\mu} \frac{v_1 - v_2}{2}\, d\omega t
\end{aligned}
\tag{A2.3}
$$

the first term of this DC voltage being:

$$
\begin{aligned}
\frac{3}{2\pi} \cdot \int\limits_{\frac{5\pi}{6}+\alpha}^{\frac{5\pi}{6}+\alpha+\frac{2\pi}{3}} v_2\, d\omega t &= \frac{3}{2\pi} \cdot \int\limits_{\frac{5\pi}{6}+\alpha}^{\frac{5\pi}{6}+\alpha+\frac{2\pi}{3}} V \cdot \sqrt{2} \cdot \sin\left(\omega t - \frac{2\pi}{3}\right) d\omega t \\
&= \frac{3\sqrt{6}}{2\pi} \cdot V \cdot \cos\alpha
\end{aligned}
\tag{A2.4}
$$

- 184 -

and the second:

$$\frac{3}{2\pi} \cdot \int_{\frac{5\pi}{6}+\alpha}^{\frac{5\pi}{6}+\alpha+\mu} \frac{v_1 - v_2}{2} \ d\omega t = \frac{3}{2\pi} \cdot \int_{\frac{5\pi}{6}+\alpha}^{\frac{5\pi}{6}+\alpha+\mu} -L_c \frac{di_2}{dt} \ d\omega t$$

$$= -\frac{3 \cdot L_c \cdot \omega}{2\pi} \cdot I_d$$

(A2.5)

For a 6-pulse converter, these results have to be double:

$$V_d = V_o \cdot \cos\alpha - R_c \cdot I_d$$

(A2.6)

with:

$$V_o = \frac{3\sqrt{6}}{\pi} \cdot V$$

$$R_c = \frac{3}{\pi} \cdot L_c \cdot \omega$$

(A2.7)

One can also calculate the DC voltage with voltage v_1:

$$V_d = \frac{3}{2\pi} \cdot \int_{\frac{5\pi}{6}+\alpha+\mu-\frac{2\pi}{3}}^{\frac{5\pi}{6}+\alpha+\mu} v(\omega t) d\omega t$$

$$= \frac{3}{2\pi} \cdot \left[\int_{\frac{5\pi}{6}+\alpha+\mu-\frac{2\pi}{3}}^{\frac{5\pi}{6}+\alpha} v_1 \ d\omega t + \int_{\frac{5\pi}{6}+\alpha}^{\frac{5\pi}{6}+\alpha+\mu} \frac{v_1 + v_2}{2} \ d\omega t \right]$$

(A2.8)

$$= \frac{3}{2\pi} \cdot \left[\int_{\frac{5\pi}{6}+\alpha+\mu-\frac{2\pi}{3}}^{\frac{5\pi}{6}+\alpha+\mu} v_1 \ d\omega t + \int_{\frac{5\pi}{6}+\alpha}^{\frac{5\pi}{6}+\alpha+\mu} \frac{v_2 - v_1}{2} \ d\omega t \right]$$

the first term of the DC voltage being:

$$\frac{3}{2\pi} \cdot \int_{\frac{5\pi}{6}+\alpha+\mu-\frac{2\pi}{3}}^{\frac{5\pi}{6}+\alpha+\mu} v_1 \; d\omega t = \frac{3}{2\pi} \cdot \int_{\frac{5\pi}{6}+\alpha+\mu-\frac{2\pi}{3}}^{\frac{5\pi}{6}+\alpha+\mu} V \cdot \sqrt{2} \cdot \sin \omega t \; d\omega t$$

$$= \frac{3\sqrt{6}}{2\pi} \cdot V \cdot \cos(\alpha+\mu)$$

(A2.9)

Then for a 6-pulse converter, the DC voltage can be obtained from:

$$V_d = V_o \cdot \cos(\alpha+\mu) + R_c \cdot I_d$$

(A2.10)

Annex 3

Converter parameters for the simulation examples

The parameters for the firing angle $\alpha = 0°$ and $\alpha = 40°$ are shown in Tables A3.1 and A3.2.

Symbol	Descriptions	Values
V_{rms}	Primary voltage (RMS)	220 V
f	Line frequency	50 Hz
k	Transformer gain	2
L_p	Primary winding inductance	50 mH
R_p	Primary resistance	0.02 Ω
σ^D and σ^S	Leakage constant	0.001
L_O	L output	12 mH
r	Parasitic resistance of L_O	0.2 Ω
C_O	C output	220 μF
R_O	R output	10 Ω
α	Firing angle	0 deg

Table A3.1. Parameters for the firing angle $\alpha = 0°$.

Table A3.1. Paramètres pour l'angle d'amorçage $\alpha = 0°$.

Symbol	Descriptions	Values
V_{rms}	Primary voltage (RMS)	220 V
f	Line frequency	50 Hz
k	Transformer gain	2
L_p	Primary winding inductance	50 mH
R_p	Primary resistance	0.02 Ω
σ^D and σ^S	Leakage constant	0.001
L_O	L output	12 mH
r	Parasitic resistance of L_O	0.2 Ω
C_O	C output	220 μF
R_O	R output	10 Ω
α	Firing angle	40 deg

Table A3.2. Parameters for the firing angle $\alpha = 40°$.

Table A3.2. Paramètres pour l'angle d'amorçage $\alpha = 40°$.

References

[1] IEEE
IEEE recommended practices and requirements for harmonic control in electrical power systems.
New York, 1993.

[2] M. P. Bahrman
HVDC transmission overview.
IEEE PES'08, Transmission and Distribution Conference and Exposition, April 2008, pp. 1-4.

[3] M. Pereira, A. Zenkner, A. de Oliveira
Full range active AC filter with multilevel IGBT converter for transmission and distribution systems.
IEEE PES'08, Transmission and Distribution Conference and Exposition, Latin America, 13-15 August 2008, pp. 1-6

[4] W. Zhang, G. Asplund
Active DC filter for HVDC systems.
IEEE Transactions on Computer Applications in Power, vol. 7 (1), 1994, pp. 40-44.

[5] A. Emadi, A. Nasiri, S. B. Bekiarov
Uninterruptible power supplies and active filters.
CRC PRESS, 2005.

[6] D. A. Paice
Power electronics converter harmonics: Multipulse methods for clean power.
IEEE Press, 1996.

[7] W. Kaewmannee, P. Sethakul, B. Davat
Exact analytical study of steady state operating multi-pulse rectifiers.
EECON'27, 27th Electrical Engineering Conference, Khon Khean (Thailand), 11-12 November 2004.

[8] W. Kaewmannee, P. Sethakul, B. Davat
Analytical study of steady state operating of 12-pulse autotransformer rectifier unit.
EECON'28, 28th Electrical Engineering Conference Phuket (Thailand), 21-22 October 2005.

[9] T. Gomez San Romin, J. Romin Ubeda
Regulation in Argentina: Flicker and harmonics.
IEEE Transactions on Power Delivery, vol. 13, n° 3, July 1998, pp. 895-901.

[10] N. Leeprechanon, S. S. Moorthy, C. S. Greacen, P. Vongthanet, A.K. David
EGAT's legacy and the transition towards a competitive electricity market in Thailand.
PowerCon'2000, IEEE Power System Technology International Conference, 2000, vol. 2, pp. 715-720.

[11] B. Direksathapon
Financing Thailand's mega projects. Options in meeting future electricity demand.
Ratchaburi Electricity Generating Holding PCL, Thailand, September 16, 2005.

[12] Electricity Generating Authority of Thailand (EGAT)
Annual Report 2002, 2003, 2004, 2005 and 2006, Bangkok, Thailand.

[13] V. Viravong, D. Phonekeo, J. Mountford, J. Mitsche, S. Yusof, A. Cook
Use of system charges for the proposed Lao PDR national transmission grid.
EMPD'98, IEEE International Conference on Energy Management and Power Delivery, 1998, vol. 2, pp. 443-448.

[14] A. Noosuk, T. Mermork, A. Semjan, M. S. Rahman, A. R. Dawood, S. B. Ismail, R. D. Kurth, S. R. Atmuri
Commissioning experience of the 300 MW Thailand-Malaysia interconnection project.
IEEE Transmission and Distribution Conference, 2002, vol. 2, pp. 1004-1009.

[15] Mohd Halimi Abdullah
Operational performance of the Malaysia-Thailand 300/600 MW HVDC interconnection.
National Power and Energy Conference, Bangi, Malaysia, 2003.

[16] S. Chusanapiputt
The studies of transmission system interconnection between PR China and Thailand.
IEEE Power System Technology International Conference, 2000, vol. 1, pp. 169-172.

[17] Ratchaburi Electricity Generating Public Company
Major shareholders.
Annual Report 2007, Bangkok, Thailand, 2007, pp. 44-45.

[18] The Power System Reliability Improvement Committee (EGAT, PEA and MEA)
Harmonic regulation concerning electricity business and industry.
1st Issue, Bangkok, Thailand, 1998.

[19] The Power system Reliability Improvement Committee (EGAT, PEA and MEA)
Voltage fluctuation regulation concerning electricity business and industry.
1st Issue, Bangkok, Thailand, 1998.

[20] Vijay K. Sood
HVDC and facts controller.
Kluver Academic Pulbishers, New York, 2004.

[21] N. Mohan, T. M. Undeland, W. P. Robbins
      Power electronics.
      John Wiley & Sons, IEEE Press, New York, 1995.

[22] Muhammad H. Rashid, Editor in Chief
      Vijay K. Sood
      HVDC transmission.
      Power Electronics Handbook, Academic Press, California, 2001, pp. 575-597.

[23] EGAT-TNB 300/600 MW HVDC interconnection project
       HVDC guide book.
       Teshmont Consultants Inc., Canada, March 31, 2000.

[24] V. Makkavimarn, T. Saengsuwan
      Modelling of the high voltage direct current transmission system links between
      Thailand-Malaysia using EMTP/ATP program
      IEEE TENCON, 2004, vol. 3, pp. 405-408.

[25] Section of Electrical Power Station Maintenance 3, Department of Transmission System
      Maintenance 3, Electricity Generating Authority of Thailand (EGAT)
      Khong Nage HVDC converter station.
      Presented papers at the Meeting of Department of Southern Operation, Songkla,
      Thailand, April 17, 2003.

[26] Tenaga Nasional Berhad (TNB)
      Corporate profile.
      Tenaga Nasional Berhad Annual Report 2007, Malaysia, 2007, pp. 3.

[27] S. Dreechum, C. Bualek
      Remote control Khlong Ngae HVDC substation.
      IEEE Transmission and Distribution Conference, 2002, vol. 3, pp. 1916-1921.

[28] J. Arrillaga, D. A. Bradley, P. S. Bodger
      Power system harmonics.
      A Wiley-Interscience Publication, Norwich, 1985.

[29] Muhammad H. Rashid, Editor in Chief
      S. Mark Halpin, A. Card
      Power quality.
      Power Electronics Handbook, Academic Press, California, 2001, pp. 817-828.

[30] A. Perez, N. Bravo, M. Anton, F. Eddi
      Harmonics handbook.
       Imprimerie du Pont de Claix, Claix, 2005.

[31] P. T. Krein
      Elements of power electronics.
      Oxford University Press, New York, 1998.

[32] Muhammad H. Rashid, Editor in Chief
L. Moran, J. Dixon
Active filters.
Power Electronics Handbook, Academic Press, California, 2001, pp. 829-851.

[33] H. Akagi
New trends in active power filters for power conditioning.
IEEE Transaction on Industry Application, vol. 32, n° 6, November/December 1996, pp. 1312- 1322.

[34] M. Ei-Hablouk, M.K. Dawish, P. Mehta.
Active power filter: A review.
IEE Proceedings, Electric Power Applications, vol. 147, n° 5, September 2000, pp. 403-413.

[35] J. H. Xu, C. Lott, S. Saadate, B. Davat.
Simulation and experimentation of a voltage source active power filter compensating current harmonics and power factor.
IECON'94, IEEE International Conference on Industrial Electronics Control and Instrumentation, 1994, pp. 411-415.

[36] P. Verdelho, G. D. Marques
An active power filter and unbalanced current compensator.
IEEE Transactions on Industrial Electronics, vol. 44, n° 3, June 1997, pp. 321-328.

[37] H.-H. Khou, S.-N. Yeh, J.-C. Hang.
Novel analytical model for design and implementation of three-phase active power filter controller.
IEE Proceedings, Electric Power Applications, vol. 148, 4, July 2001, pp. 369-383.

[38] J. W. Dixon, S. M. Tepper, L. T. Moran.
Analysis and evaluation of different modulation techniques for active power filters.
APEC94, IEEE Applied Power Electronics Conference, 1994, pp. 894-900.

[39] S. Buso, L. Malesani, P. Mattavlli.
Comparison of current control techniques for active filter applications.
IEEE Transaction on Industrial Electronics, vol. 44, n° 5, October 1998, pp. 722-729.

[40] A. W. Green, J. T. Boys
Hysteresis current-forced three phase voltage-sourced reversible rectifier.
IEE Proceedings, Electric Power Applications, vol. 136, n° 3, May 1989, pp. 113-120.

[41] P.C. Krause, P. C., O. Wasynczuk, S. D. Sudhoff.
Analysis of electric machinery.
2nd ed. New York: IEEE Press, 1995.

[42] H. Akagi, Y. Kanazawa, A. Nabae.
Instantaneous reactive power compensators comprising switching devices without energy storage components.
IEEE Transaction on Industry Application, vol. IA-20, n° 3, May/June, pp. 625-630.

[43] J. Holtz
Pulse width modulation for electronic power conversion.
Proceeding of the IEEE, vol. 82, n° 8, August 1994, pp. 1194-1214.

[44] T. Thomas, K. Haddad, G. Joos, A. Jaafari.
Design and performance of active power filters.
IEEE Industry Applications Magazine, September/October 1998, pp. 38-46.

[45] H.-L. Jou, J.-C. Wu, H.-Y. Chu
New single-phase active power filter.
IEE Proceedings, Electric Power Applications, vol. 141, n° 3, May 1994, pp. 129-134.

[46] N. Bruyant, M. Machmoum, P. Chevrel
Control of a three-phase active power filter with optimized design of the energy storage capacitor.
PESC'98, IEEE Power Electronics Specialists Conference, 1998, vol. 1, pp. 878-883.

[47] S. Somkun, V. Chunkag, P. Sethakul
3-Phase shunt active filter employing DSP for estimating compensated harmonics current.
EECON'26, 26th Electrical Engineering Conference, King Mongkut's Institute of Technology North Bangkok, Thailand, 2003.

[48] Texas Instrument
TMS320F243/F241/C242 DSP controller reference guide.
Texas Instrument, 2000.

[49] S. Somkun, P. Sethakul, V. Chunkag
Simulation of DSP-based control of paralleled boost PFC with minimized current sensors.
ICIT'05, IEEE International Conference on Industrial Technology, Hong-Kong, December 14-18, 2005, FP1-42, 1215-1220.

[50] K. Emadi, M. Ehsani.
Aircraft power systems: technology, state of the art, and future trends.
IEEE Aerospace and Electronic Systems Magazine, January 2000, pp. 28-32.

[51] T. Liang, J Chen, C. Chu, K. Chen.
Analysis of 12 pulse phase control AC/DC converter.
IEEE International Conference on Power Electronics and Drive Systems, July 1999, pp. 779-783.

[52] N. D. Rao, S. I. Sporea, A. Sawma.
      Analysis of resonance problems and harmonic filter design in power factor correction
      capacitor applications.
      IEEE Canadian Conference on Electrical and Computer Engineering, May 1998, pp.
      293-296.

[53] S. M. Sandler, C. Hymowitz
      SPICE circuit handbook.
      McGraw-Hill, New-York, 2006.

[54] R. W. Erickson.
      Fundamentals of power electronics.
      Chapman and Hall, Boston, 1997.

[55] B. Davat
      Power semiconductor converters.
      ELINA project LEONARDO, DG XII, June 2001, ISBN 80-89061-04-4.

[56] P. W. Lehn.
      Exact modeling of the voltage source converter.
      IEEE Transaction on Power Delivery, January 2002, pp. 217-222.

[57] S. C. Chapra, R. P. Canale.
      Numerical methods for engineers.
      McGraw-Hill, New-York, 2002.

AUTORISATION DE SOUTENANCE DE THESE
DU DOCTORAT DE L'INSTITUT NATIONAL
POLYTECHNIQUE DE LORRAINE

o0o

VU LES RAPPORTS ETABLIS PAR :
Monsieur Jean FAUCHER, Professeur, ENSEEIHT, Toulouse

Monsieur Mohamed MACHMOUM, Professeur, Polytech'Nantes, Saint Nazaire

Le Président de l'Institut National Polytechnique de Lorraine, autorise :

Monsieur SETHAKUL Panarit

à soutenir devant un jury de l'INSTITUT NATIONAL POLYTECHNIQUE DE LORRAINE, une thèse intitulée :

« Réseaux électriques et filtrage des harmoniques – Mise en œuvre et méthode d'étude »

NANCY BRABOIS
2, AVENUE DE LA
FORET-DE-HAYE
BOITE POSTALE 3
F - 54501
VANDŒUVRE CEDEX

en vue de l'obtention du titre de :

DOCTEUR DE L'INSTITUT NATIONAL POLYTECHNIQUE DE LORRAINE

Spécialité : **« Génie électrique »**

Fait à Vandoeuvre, le 02 novembre 2009
Le Président de l'I.N.P.L.,
F. LAURENT

_____

Résumé en français
Réseaux électriques et filtrage des harmoniques, mise en œuvre et méthode d'étude

Cette thèse s'intéresse au problème de la qualité de l'énergie électrique sous l'angle particulier des harmoniques, leurs sources, leurs effets et les solutions permettant de les réduire. Deux solutions sont principalement considérées, les convertisseurs à indice de pulsation élevé et les filtres actifs.

Ce travail a été mené en faisant porter l'accent sur le réseau électrique thaïlandais. C'est ainsi qu'une présentation de l'évolution de la façon dont l'électricité est produite, transportée et distribuée en Thaïlande est effectuée avant de décrire les contraintes imposées sur les harmoniques.

Les différents systèmes de liaison à courant continu haute tension (CCHT) actuellement installés dans le monde sont rappelés avant de décrire en détails les différents composants et le contrôle de la liaison 300-600 MW existant entre la Thaïlande et la Malaisie. Après avoir ensuite présenté les différentes solutions envisageables de réduction des harmoniques, un exemple de réalisation, l'une des premières en Thaïlande utilisant un contrôle numérique, est détaillé afin d'illustrer les avantages de ce type de solution.

La thèse se termine sur la présentation d'une méthode originale de modélisation des convertisseurs à indice de pulsation élevé. Cette modélisation repose sur une solution analytique exacte du problème d'état qui est considéré sur le plus petit intervalle permettant, en utilisant des propriétés de symétrie, de reconstruire la période de fonctionnement du dispositif. Le modèle ainsi développé donne des informations sur le fonctionnement du système tant dans les domaines fréquentiel que temporel.

Mots clés
Réseau électrique thaïlandais, qualité de l'électricité, filtrage actif, liaison CCHT, convertisseur m-pulse, modélisation
_____

Résumé en anglais
Electrical networks and harmonics mitigation, development and modelling method

The problem of quality of electrical energy is the main object of this thesis. This problem is considered especially from the point of view of harmonics, sources, effects and solutions to reduce them. Two main solutions are considered, multi-pulse converters and active filters.

This work is developed with a particular emphasis on the Thai electrical network. Then, the production, transmission and distribution system of electricity in Thailand and the harmonics regulations are presented. The different types of HVDC interconnection systems which are installed in the world today are detailed before presenting the 300/600 MW Thailand-Malaysia HVDC interconnection.

After presenting the different possible solutions to avoid harmonics, a realized example, one of the first one developed in Thailand with a numerical control, is detailed to show the advantages of such a solution.

The thesis ends on the presentation of an original modelling method of multi-pulse converters. The model is based on an exact analytical solution of the state problem which is considered on the smallest interval, which can, by using property of symmetry, rebuild the whole period. The result model gives the full information on the operation of the whole device both in time and frequency domains.

Key words: Thai electrical network, power quality, active filter, HVDC link, m-pulse converter, modelling.